

SUPPLEMENT
3RD INTERNATIONAL WORKSHOP ON
WAVE HINDCASTING AND FORECASTING

MONTREAL, QUEBEC
MAY 19 - 22, 1992

This workshop was supported by the
Federal Panel on Energy R&D

Published by:

Environment Canada
Atmospheric Environment Service
4905 Dufferin Street
Downsview, Ontario
M3H 5T4

TABLE OF CONTENTS

Session G: Special Session on the Halloween 1991 East Coast Storm

G-1 A Meteorological Overview of the Halloween Storm of 1991;
 Donald Cameron and George Parkes, Maritimes Weather Centre,
 Bedford, N.S.

G-2 A Sampling of Damage Reports from the Halloween 1991 Storm;
 Ralph Bigio, Canadian Forces Meteorological and Oceanographic
 Centre, Halifax, N.S.

G-3 The Halloween Storm: Data Observations from NDBC Stations;
 David Wei-Chi Wang and Theodore Mettlach, Stennis Space Center,
 MS

**G-4 A Wind Wave Hindcast for the Halloween Northeaster in 1991 in the
 Atlantic Ocean Coastal Waters;** C.L. Vincent, R.E. Jensen, Coastal
 Engineering Research Center, Vicksburg, MS; P.A. Wittmann, Fleet
 Numerical Oceanography Center, Monterey, CA; and H.C. Graber,
 University of Miami, Miami, FL

**G-5 Kinematic Analysis of the Surface Wind Field in the Halloween
 Storm and a Preliminary Spectral Model Wave Hindcast;**
 V.J. Cardone and B. T Callahan, Oceanweather, Inc.,
 Cos Cob, CT

**G-6 A Possible Interpretation of the Climatology of the Halloween
 1991 East Coast Storm;** D.T. Resio and M. Sager, Florida Institute
 of Technology, Melbourne, FL

Rapporteur's Summary Report; Peter C.P. Chandler, Institute of Ocean
 Sciences, Sidney, B. C

List of Participants

Note: Session A-F, P were reported in the Preprint volume.

A METEOROLOGICAL OVERVIEW OF THE HALLOWEEN STORM OF 1991

Donald Cameron and George Parkes

Maritimes Weather Centre
Bedford, Nova Scotia**Abstract**

Between October 26 and November 2 1991 the 500 mb wind pattern over North America, which was initially characterized by long shallow amplitude waves and a strong zonal flow, changed to a flow characterized by large amplitude waves and a strong meridional flow. The potential energy build-up, initially represented by a strong latitudinal gradient of temperature and moisture, was converted into the kinetic energy of a large, slow moving extra-tropical storm. The absorption of moisture previously associated with Hurricane Grace then enhanced the intensity of the storm. Subsequently, the system re-acquired tropical characteristics and became classified as a new hurricane.

Discussion

The upper circulation of late October 1991 was dominated by a broad trough over the western United States and a broad flat ridge over eastern North America (Figure 1). This pattern began to change on October 26. A short wave trough descended into and sharpened the longer wave trough over the western United States. Intense ridging followed just to the west of the Great Lakes on October 27 and a sharpening trough began to dig across New England and the Maritimes on October 28.

At 12Z October 28, this 500 millibar trough stretched from Labrador to Maine (Figure 2). The trough then continued to dig southwards and became a slow moving cut off low on October 30 (Figure 3). This upper feature governed the motion of the surface low after October 29, causing it to move counter clockwise in a large circle. The upper low position at 12Z November 1 is shown in Figure 4 .

Figure 5 and 6 show the surface analysis and GOES photo at 12Z October 28. The intense ridging aloft was reflected at the surface by an anticyclone over Quebec which had built to a central pressure of 1046 millibars. The short wave trough supported a low pressure centre over eastern Nova Scotia. A cold front had just moved off the east coast. A sharp contrast of temperature and moisture existed across this front; dew points in the warm air ranged from 16° to 21° Celsius, while representative cold air values over Labrador were as low as -11° Celsius. Strong to gale force northeasterlies had already spread across the Gulf of St. Lawrence and the Gulf of Maine.

Map 1 shows the positions of the weather buoys over the Gulf of Maine and off the Eastern Canadian Seaboard. Appendix 1 details the measurement procedures of buoys 44137 through 44141.

At 18Z October 28, the Nova Scotia low passed to the north of buoy 44139 and subsequently weakened. Northeast gales reached buoy 44139 at 00Z October 29 (Figure 7) and peak winds remained near or over 40 knots during the following 36 hours, with a maximum of 58 knots at 12Z October 29. The wind direction at 44139 slowly veered towards easterly during the period. The significant wave height reached a maximum of 10.5 metres at 17Z October 29 and thereafter diminished very slowly.

A newly developed low pressure system, which passed just south of buoy 44137 at 18Z October 28, was nearing buoy 44141 at 00z October 29 (Figure 8). Peak wind at buoy 44137 backed to northerly at 19Z and began a steady increase to reach 40 knots at 04Z October 29 (Figure 9). The peak wind remained over 40 knots for the next 27 hours and the wind direction slowly veered towards easterly. A period of 6 hours with easterly peak winds exceeding 60 knots occurred between 02Z and 07Z October 30. Wave heights at buoy 44137 increased steadily. The significant wave height exceeded 14 metres during a 9 hour period between 02Z and 11Z October 30. The highest significant wave height was 17.4 metres at 0355Z October 30. The maximum wave height reached 30.7 metres at 0355Z and 30.6 metres at 0555Z October 30. These values represent the highest wave heights ever measured on the Scotian Shelf.

The low passed buoy 44141 and then reformed further to the south. Peak wind at buoy 44141 increased to south southeast at over 35 knots late on October 28 as the low approached (Figure 10). The wind then diminished as the centre passed and veered to northerly at 04Z October 29. Northeast winds increased quickly. A 24 hour period was experienced where peak winds at buoy 44141 exceeded 40 knots. A 10 hour period of peak winds exceeding 60 knots was experienced between 21Z October 29 and 06Z October 30. Wind direction veered gradually to easterly. At 0055Z October 30, the significant wave heights and the maximum wave heights peaked at 15.2 metres and 28.5 metres respectively.

The cold front encountered Hurricane Grace after 12Z October 29 (Figure 11) and the hurricane circulation weakened quickly as can be seen in the GOES satellite photographs from 12Z, 15Z and 18Z Oct 29 (Figures 12 , 13 and 14).

A new circulation is visible on the GOES visible photographs at 18Z at 38° N 60° W and an extra-tropical low pressure centre is placed at this location. Moisture previously associated with Hurricane Grace moved quickly north-northeastwards (Figures 15 and 16). As it

passed 39° N near 00Z, the new circulation intensified and became more clearly visible on the IR photographs (Figure 17). It was within a few hours of this time that winds and wave heights at buoys 44137 and 44141 reached their maximums; and it is believed that the low pressure system was reaching its maximum intensity at this time. The central pressure of the low reached approximately 975 mb between 00Z and 12Z October 30 (Figures 18 and 19). The upper centre continued to dig southwards. At 00Z October 30, it was located to the southwest of the surface centre. The surface low therefore rotated northwestwards under its influence and subsequently turned southwards (Figures 20 and 21) describing a large counter-clockwise loop.

The low passed southeast of Cape Cod on October 31. Northerly gales at buoy 44011 persisted between 21Z Oct 28 and 22Z Oct 30 (Figure 22); peak winds reached or exceeded 60 knots between 15Z and 18Z October 30, as the low approached from the east. Significant wave heights increased steadily to reach 12 metres at 16Z October 31 with many reports of peak period 17 to 20 seconds.

Northerly gales persisted at buoy 44008 between 12Z October 28 and 03Z October 31 (Figure 23); and peak winds exceeded 60 knots for a few hours near 00Z October 31, as the centre of the low passed to the east. Winds subsequently dropped quickly. The significant wave height reached 9.6 metres at 00Z Oct 31.

At 00Z Oct 31 coastal buoys 44007 and 44013 reported significant wave heights and peak periods of 6.8 metres, 20 seconds and 7.7 metres, 17 seconds respectively (Figures 24 and 25).

Figures 26 and 27 detail the effects of the storm at buoys 44138 and 44140 respectively.

The loop to the south took the storm over sea surface temperatures which exceeded 24° Celsius (Figure 28). Convection near the centre increased. At 12Z November 1, the National Hurricane Centre declared that the system had reached tropical storm strength (Figures 29 and 30). Continued intensification took place. At 00Z November 2, the storm was investigated by a NOAA reconnaissance aircraft and was declared by the National Hurricane Centre to be of hurricane strength (Figures 31 and 32).

As the hurricane passed north of latitude 40° N early on November 2, it encountered the much colder waters of the continental shelf and began to weaken rapidly (Figure 33). By the time it reached the Nova Scotia coast near Halifax at 14Z, its maximum sustained winds had diminished to near 40 knots (Figure 34).

Storm Surges on the Canadian Coast

Map 2 shows the tide gauge sites maintained by the Canadian Hydrographic Service along the Atlantic coast of Nova Scotia.

Storm surge may be defined as the difference between the observed water level and the predicted astronomical tide. Figures 35 -38 show the observed waters levels, predicted astronomical tides and storm surge profiles for four sites during the Halloween Storm. Storm surge heights ranged from near 50 cm at North Sydney, 60 cm at Point Tupper and 70 cm at Halifax, to one metre at Yarmouth.

When the surge component due to isostatic pressure response is subtracted, the resulting surge due to other factors (wind and wave setup) can be examined. Residual surges for two sites are shown in Figures 39 -40 . In these diagrams, the theoretical SSP curves assume an isostatic pressure response. Since pressure was relatively high during this period along the Nova Scotia coast, the maximum residual storm surge rises to 78 cm at Halifax and to 105 cm at Yarmouth. The wind barbs shown along the top of these diagrams are standard meteorological convention. The diagram for Halifax shows winds observed from McNabs Island in the approaches to Halifax Harbour, while the Yarmouth diagram shows winds observed at Yarmouth Airport. Times in these diagrams are Atlantic Standard.

The storm surge diagrams show that storm surges were extremely high along the South Shore of Nova Scotia during Oct 29 and Oct 30. Figure 41 shows that wave heights at Shearwater were also very high throughout this period. This combination caused coastal damage and inundation.

Summary

The weather pattern evolved through three broad stages:

1. Oct 28-29: The co-existence of a digging upper trough with several surface waves, and Hurricane Grace. The intensification of the final wave and the absorption of Hurricane Grace followed on October 29.
2. Oct 30-31: The intense extra-tropical low rotated counter-clockwise around its upper centre then began to weaken.
3. Nov 1-2: An unnamed hurricane formed in the centre of the extra-tropical low and then moved northwards and weakened. Its remains passed across Nova Scotia on November 2.

Appendix 1

A network of ship shaped buoys 6 metres in length and bearing the numbers 44137 through 44141 is shown in Figure 4 .

The buoys have anemometers at approximately 5 metres above the sea surface. Wind samples are taken every two seconds during the 10 minutes prior to observation time. The numeric average of these samples is reported as the average wind. The highest 10 second sample window over the 10 minute period is reported as the peak wind. It is the experience at Maritimes Weather Centre that the peak wind speed, not the average wind speed, most closely resembles the wind likely to be reported by a ship of opportunity at the same location.

The Buoys have Columbia Research or Datawell heave sensors with a range of plus or minus 15 metres. A collection is made of 256 heave samples at one second intervals, and this is then broken up into 8 spectral bands by Fourier analysis. This procedure is repeated 8 times, which gives a 35 minute process. The results are converted into a significant wave height for output on the hourly report which is completed at 5 minutes before the hour. The peak period and the maximum wave height are also reported. The maximum wave height is twice the highest wave amplitude (i.e. twice the zero-crossing to peak plus or minus height) during the sampling interval.



Figure 2. CMC 500 millibar Analysis Oct. 26 1991 12Z

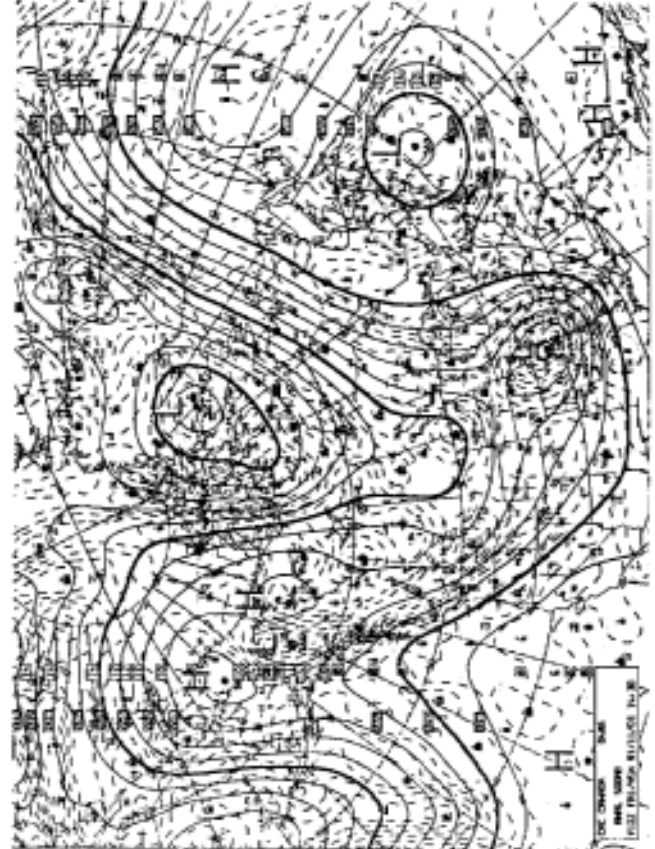


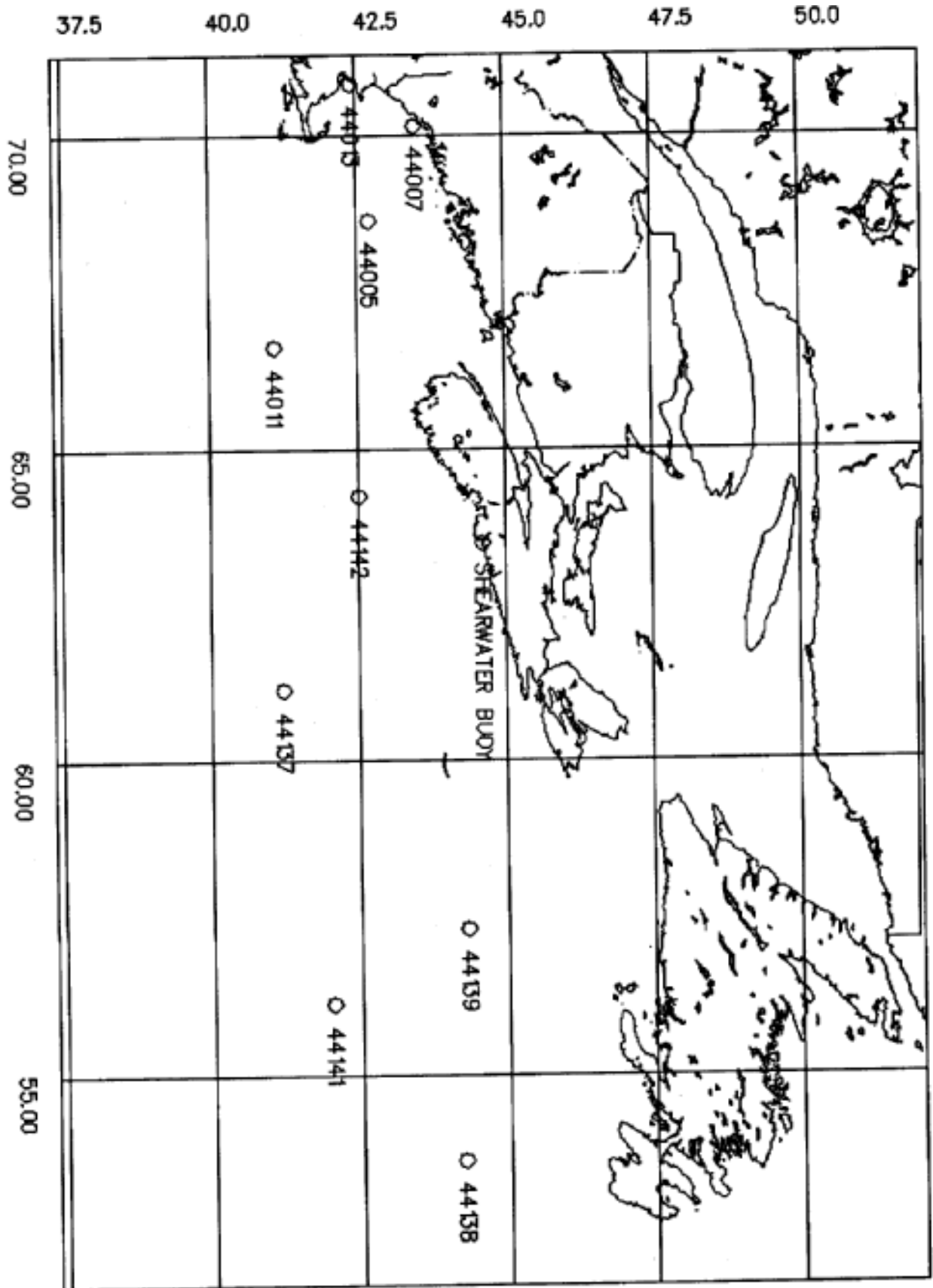
Figure 4. CMC 500 millibar Analysis Nov. 01 1991 12Z

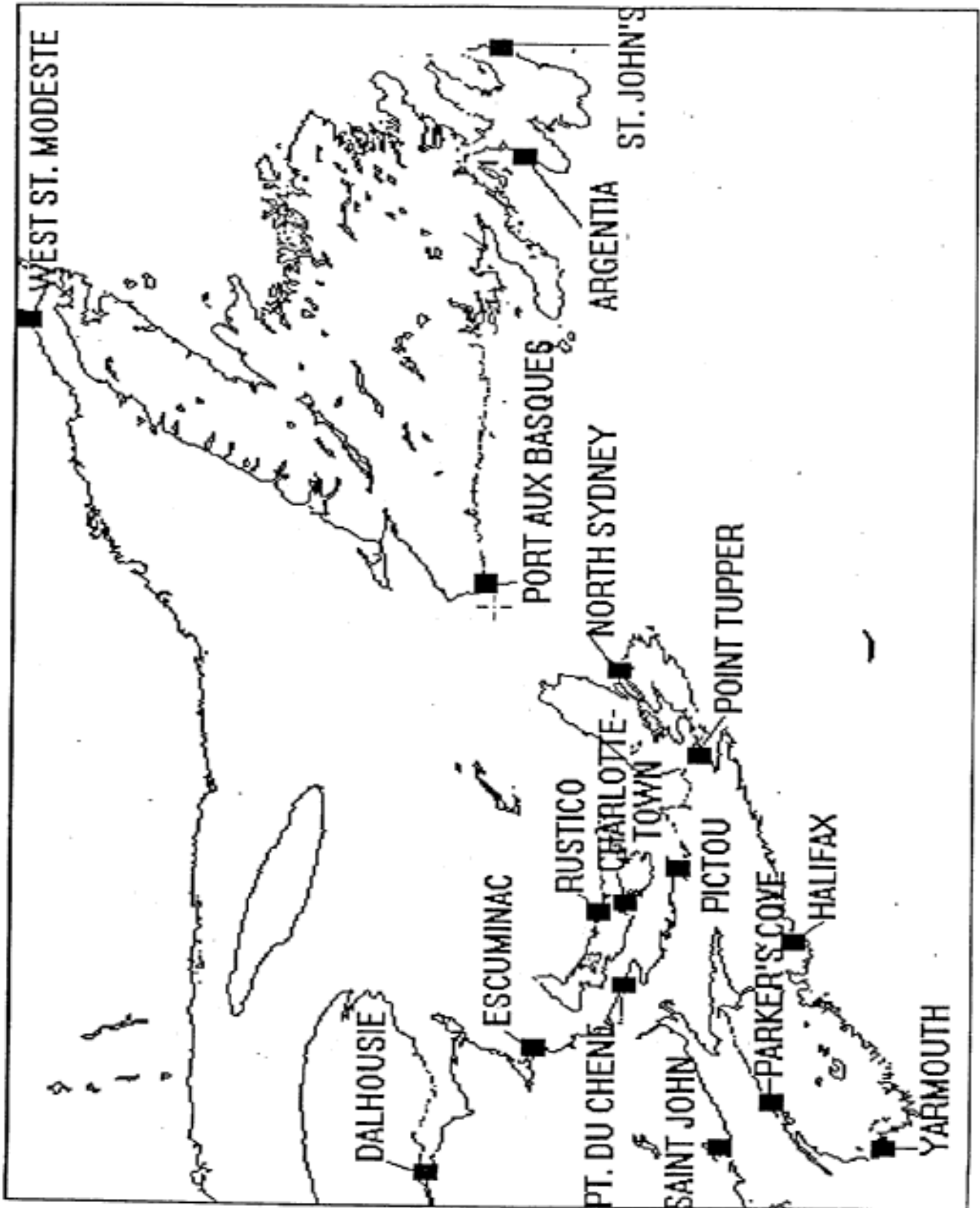


Figure 1. CMC 500 millibar Analysis Oct. 26 1991 00Z



Figure 3. CMC 500 millibar Analysis Oct. 30 1991 00Z





Map 2. Tide gauge sites on the Atlantic coast.

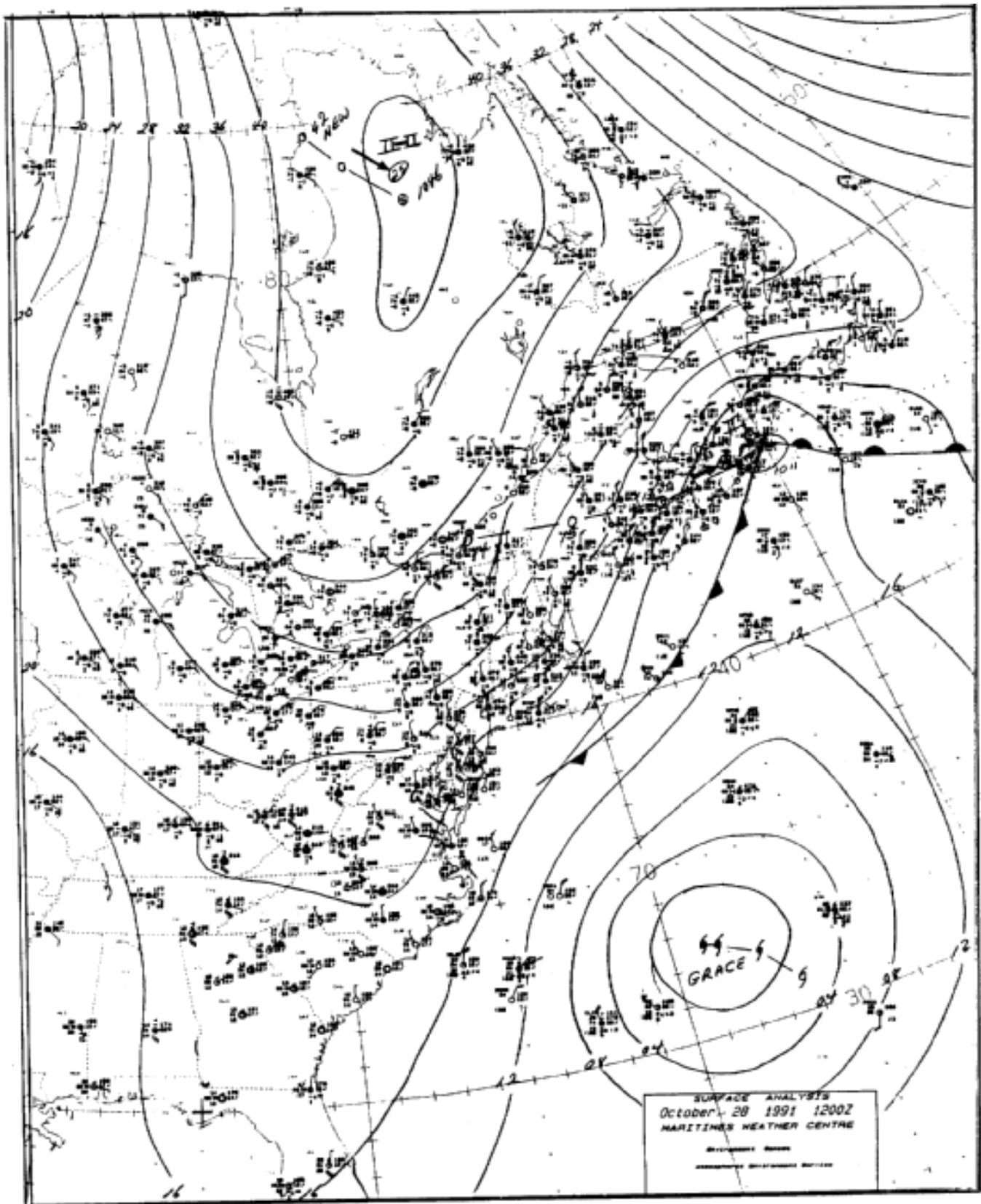


Figure 5. Maritimes Weather Centre surface analysis 1200Z October 28, 1991

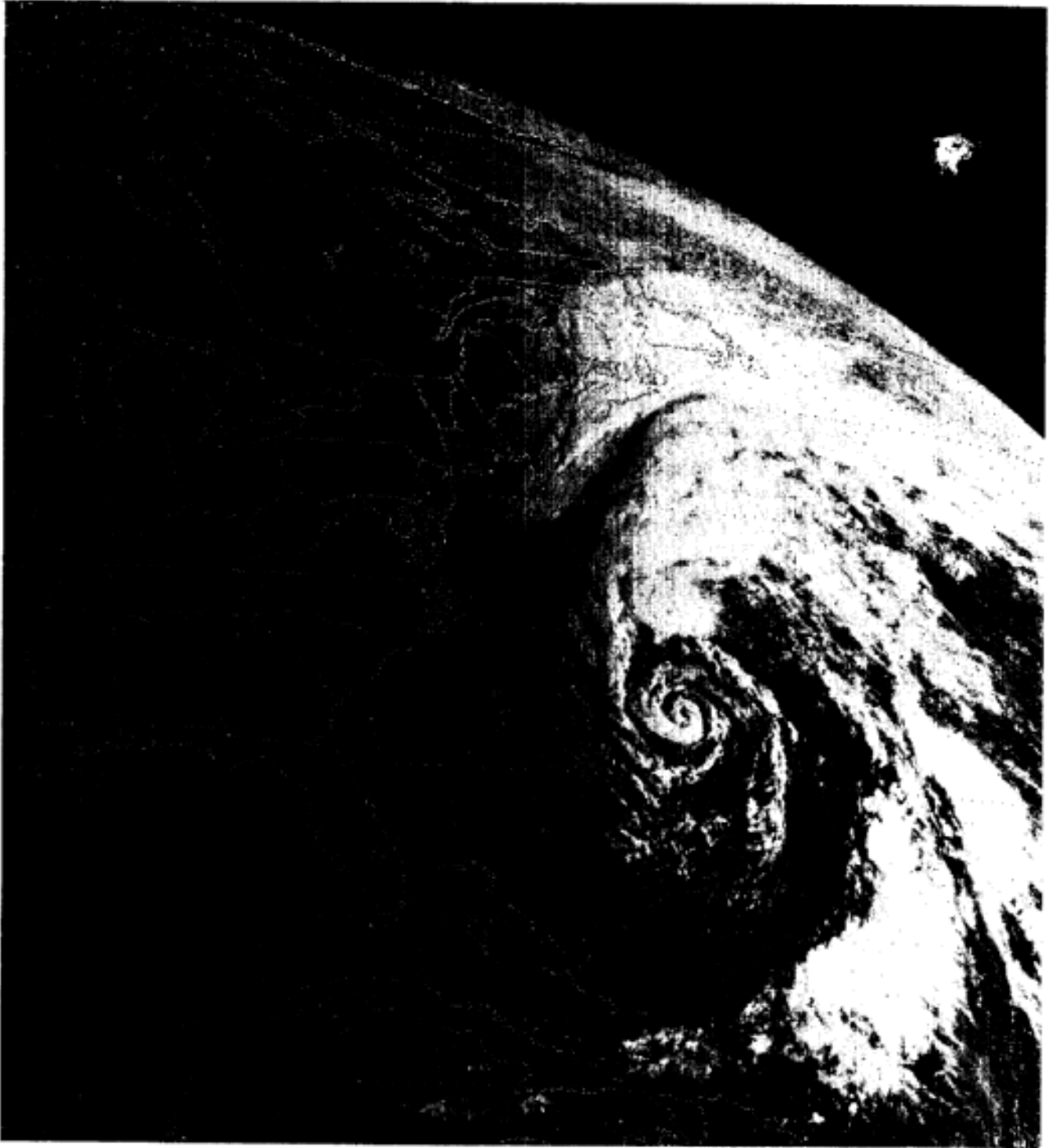
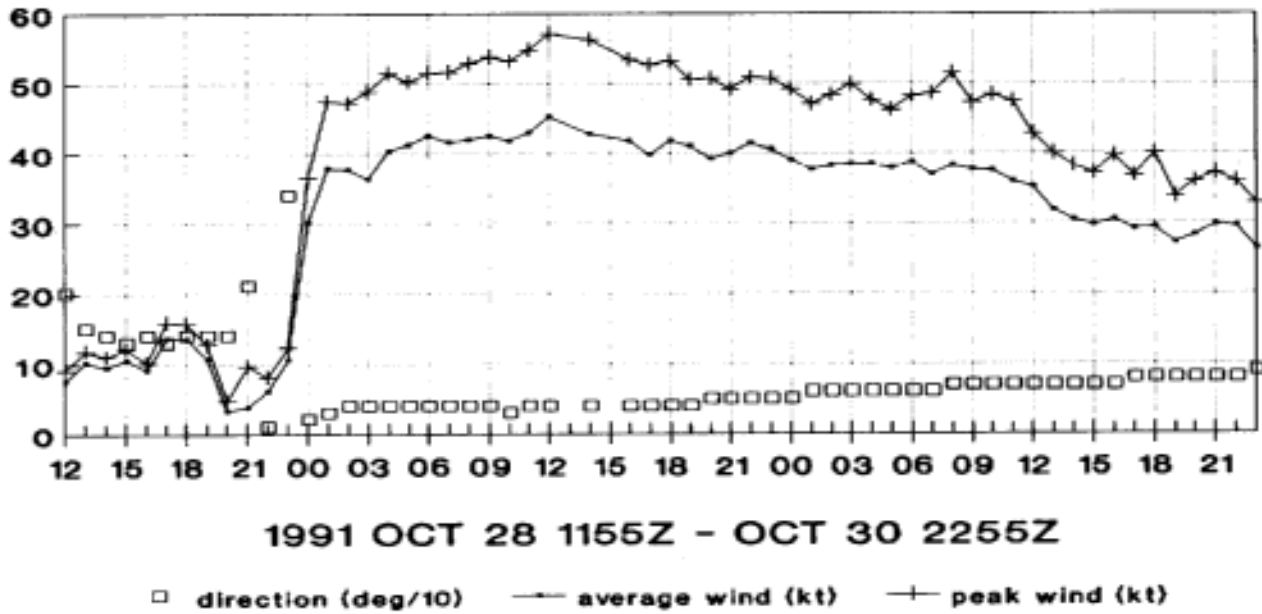


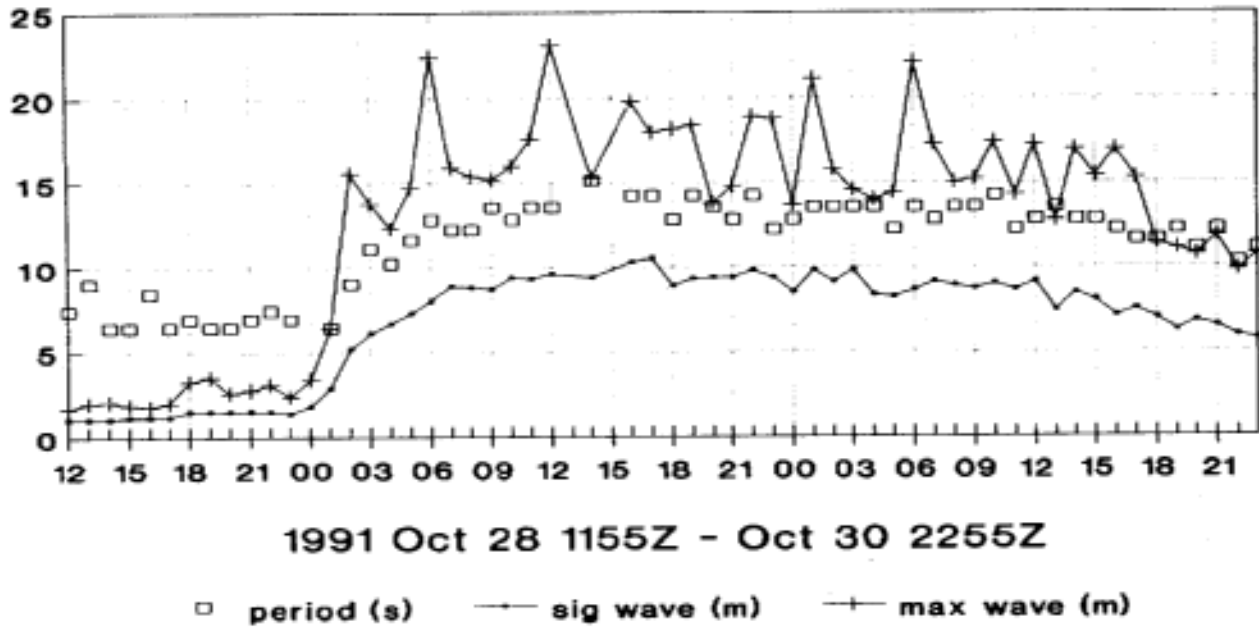
Figure 6. GOES visible photo 12:04Z October 28, 1991. The cloud band extending from Nova Scotia to the south of Cape Cod is caused by a cold front. The circulation associated with Hurricane Grace is centered near 32°N 69°W.

44139 WIND



2913Z 2915Z misg

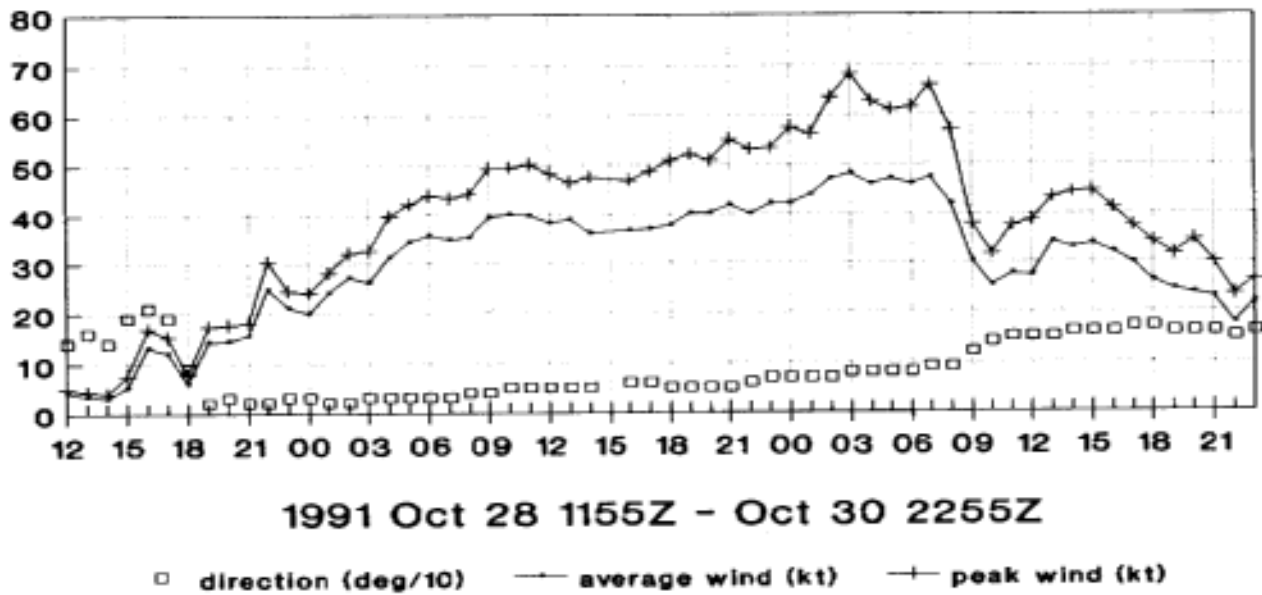
44139 WAVE HEIGHT/PERIOD



2913Z 2915Z misg

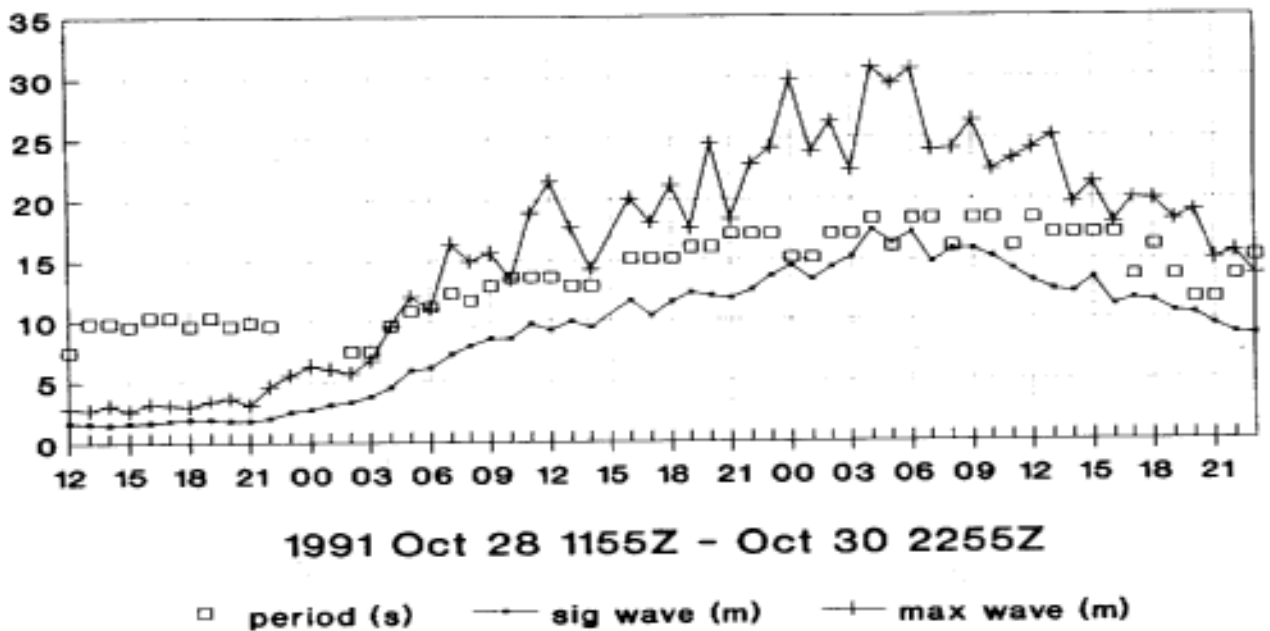
Figure 7. Buoy wind and wave measurements for 44139.

44137 WIND



2915Z misg

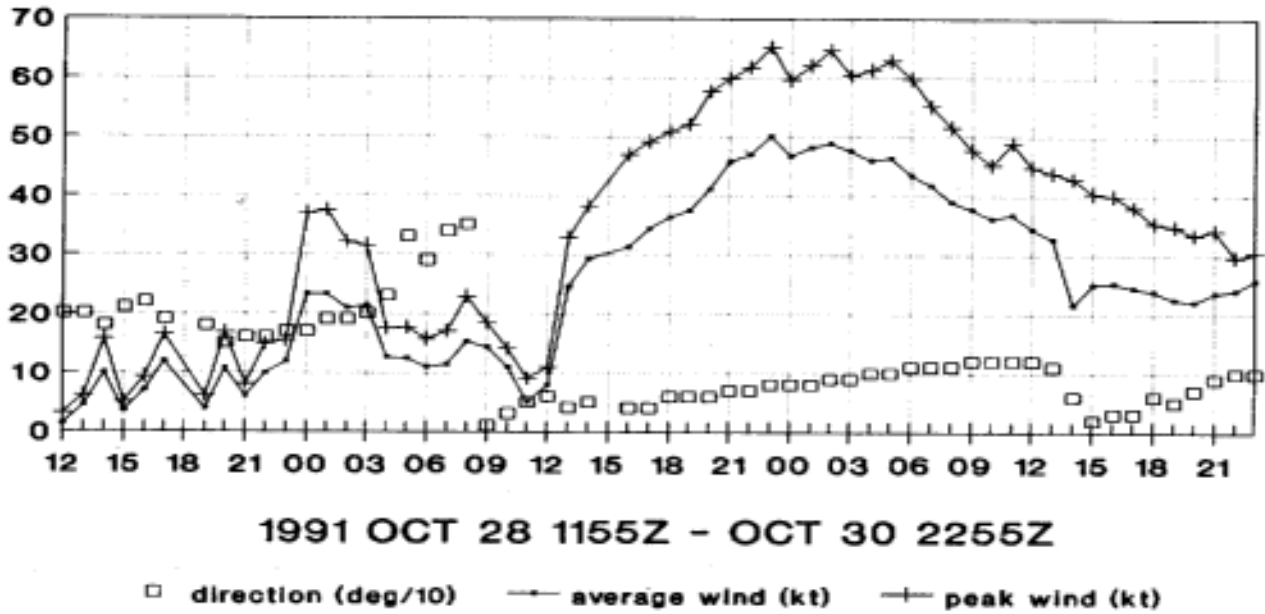
44137 WAVE HEIGHT/PERIOD



2915Z misg

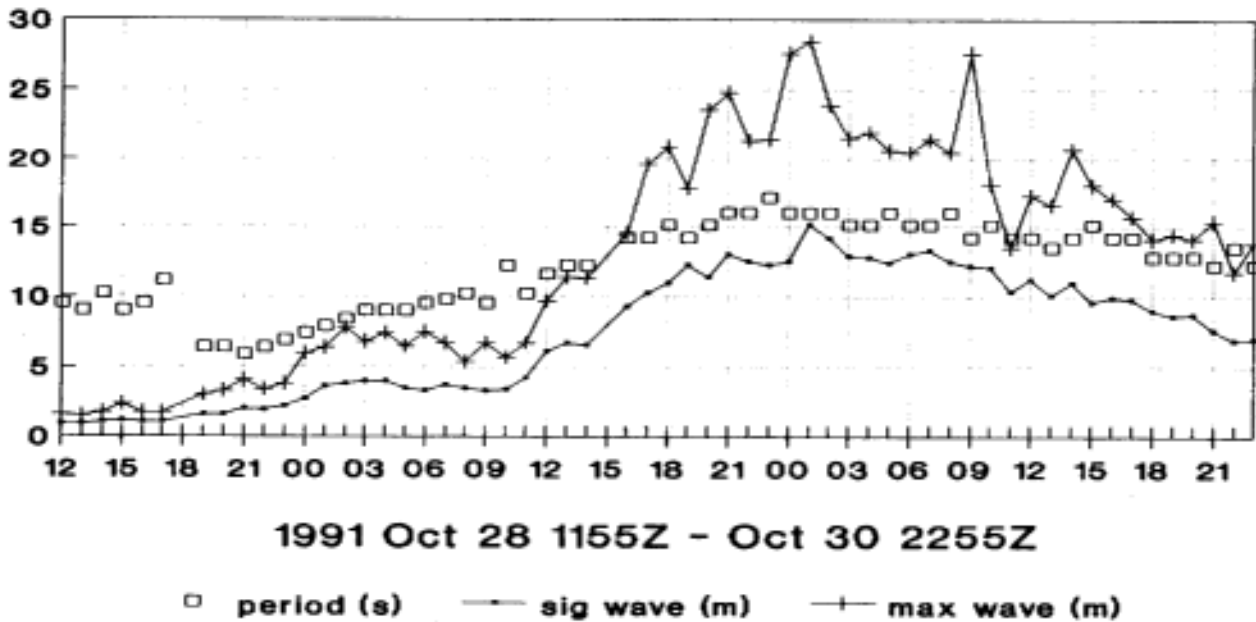
Figure 9. Buoy wind and wave measurements for 44137.

44141 WIND



2818Z 2915Z misg

44141 WAVE HEIGHT/PERIOD



2818Z 2915Z misg

Figure 10. Buoy wind and wave measurements for 44141.

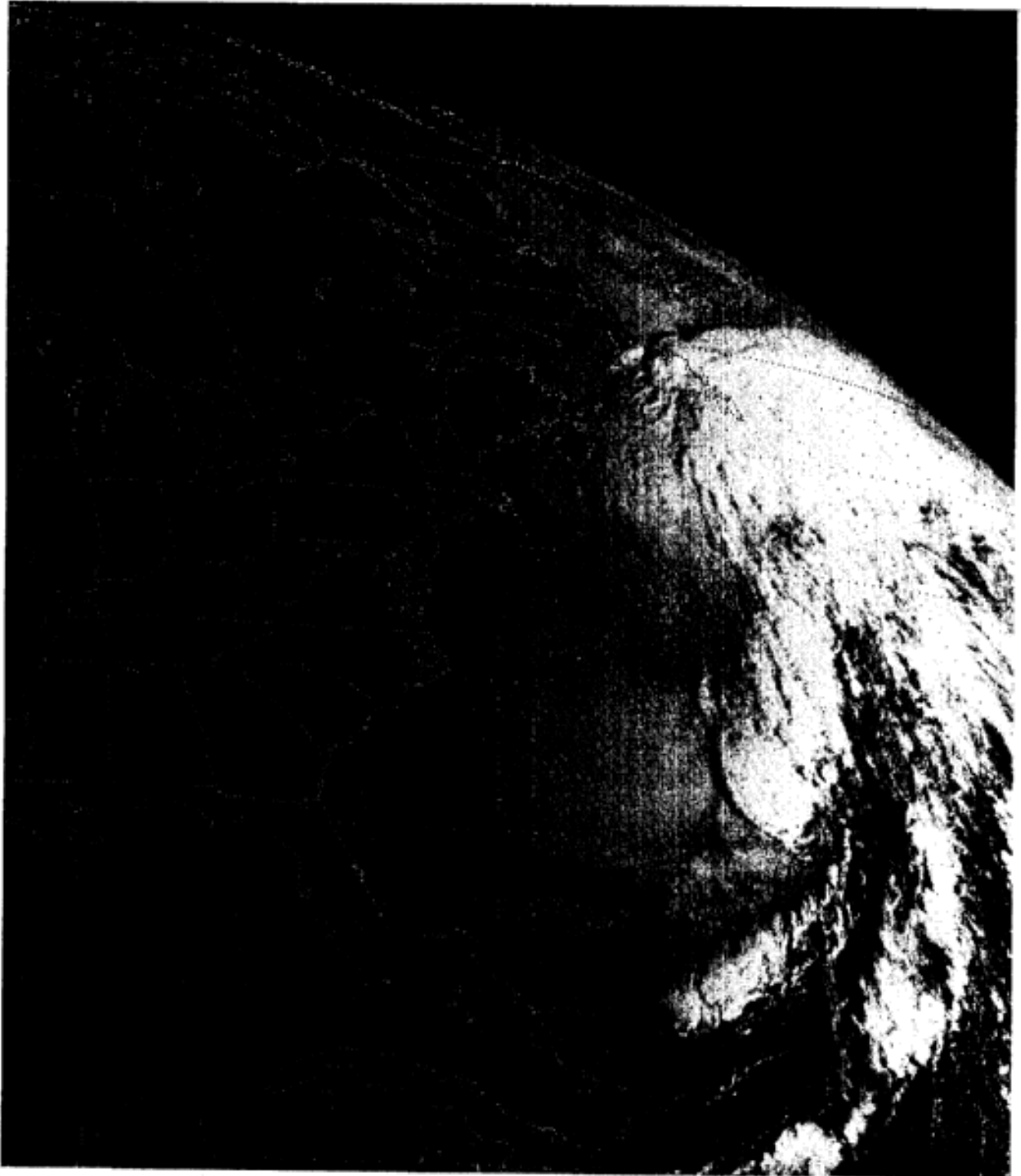


Figure 12. GOES visible imagery 12:04Z October 29, 1991.



Figure 13. GOES visible imagery 15:03Z October 29, 1991.

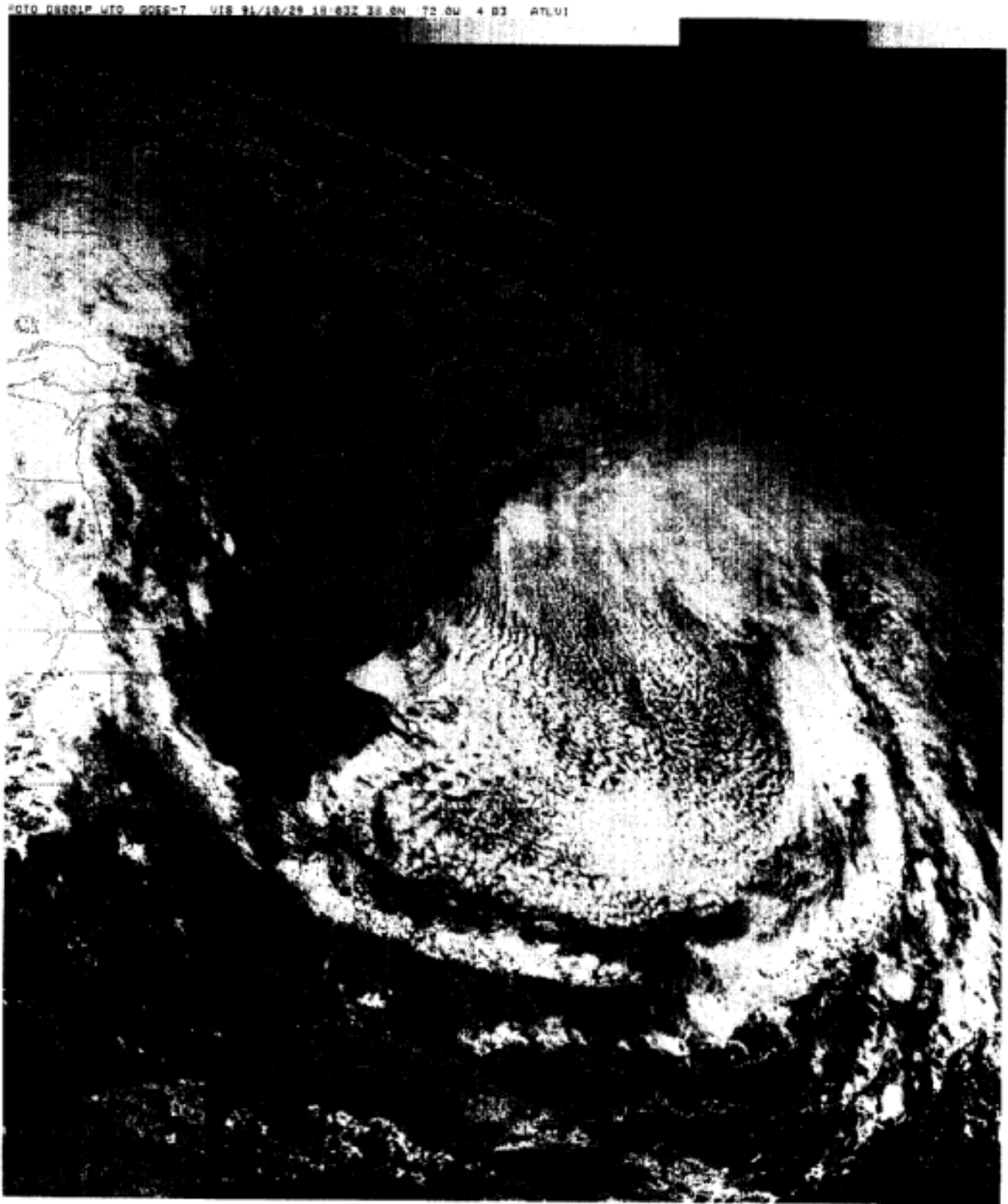


Figure 14. GOES visible imagery 18:03Z October 29, 1991.

PHOTO DHE00P WTD GOES-T 11V 01/10/29 18:03Z 70 0N 72 0W 4 AF ATLIR

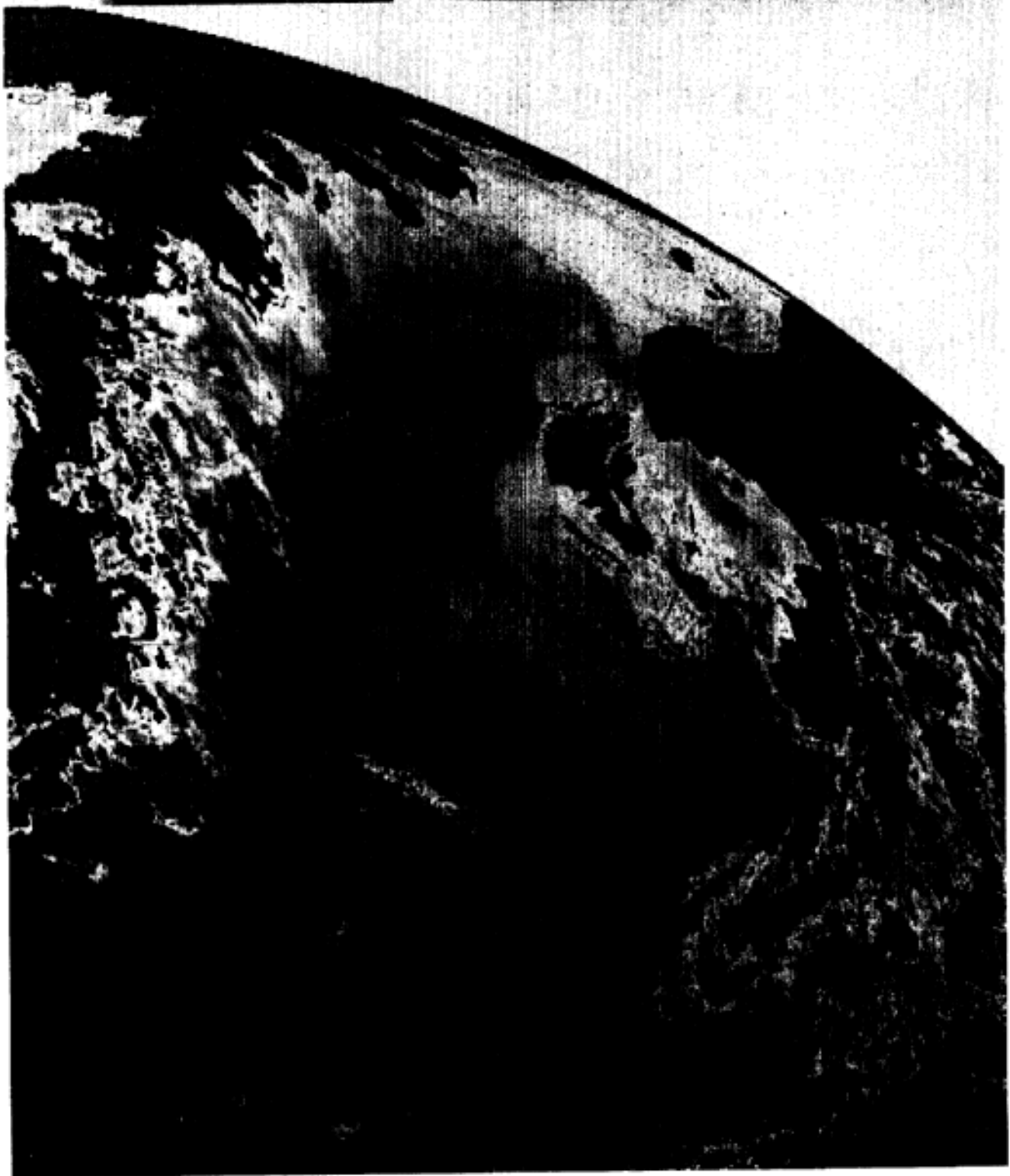


Figure 15. GOES IR imagery 18:03Z October 29, 1991.



Figure 16. GOES IR imagery 21:03Z October 29, 1991.

PGO DB000P MTO GOES-7 11N 91/10/30 00:03Z 28.1N 72.0W 4 AF AT-IR



Figure 17. GOES IR imagery 00:03Z October 30, 1991.

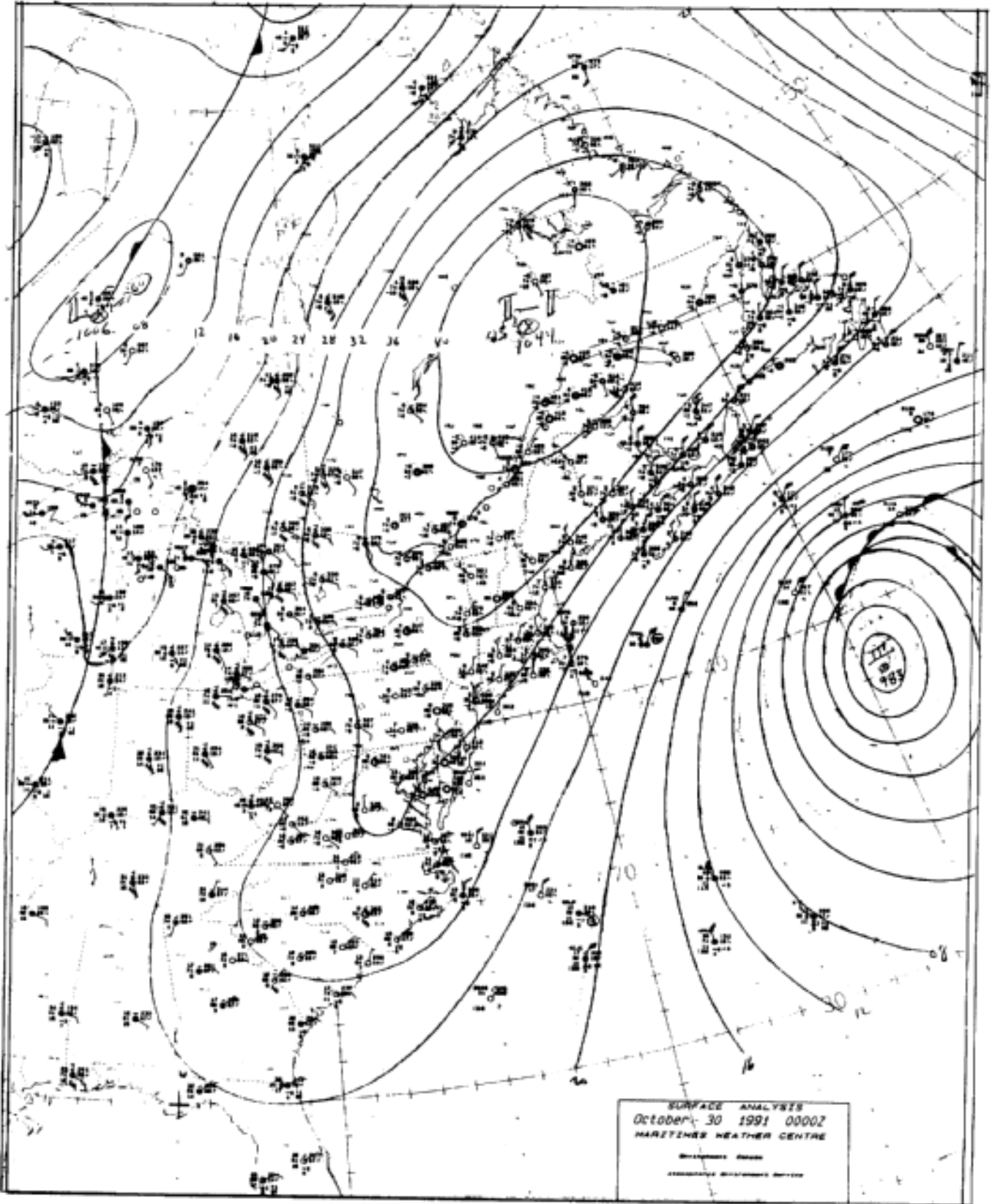


Figure 18. Maritimes Weather Centre surface analysis 0000Z October 30, 1991

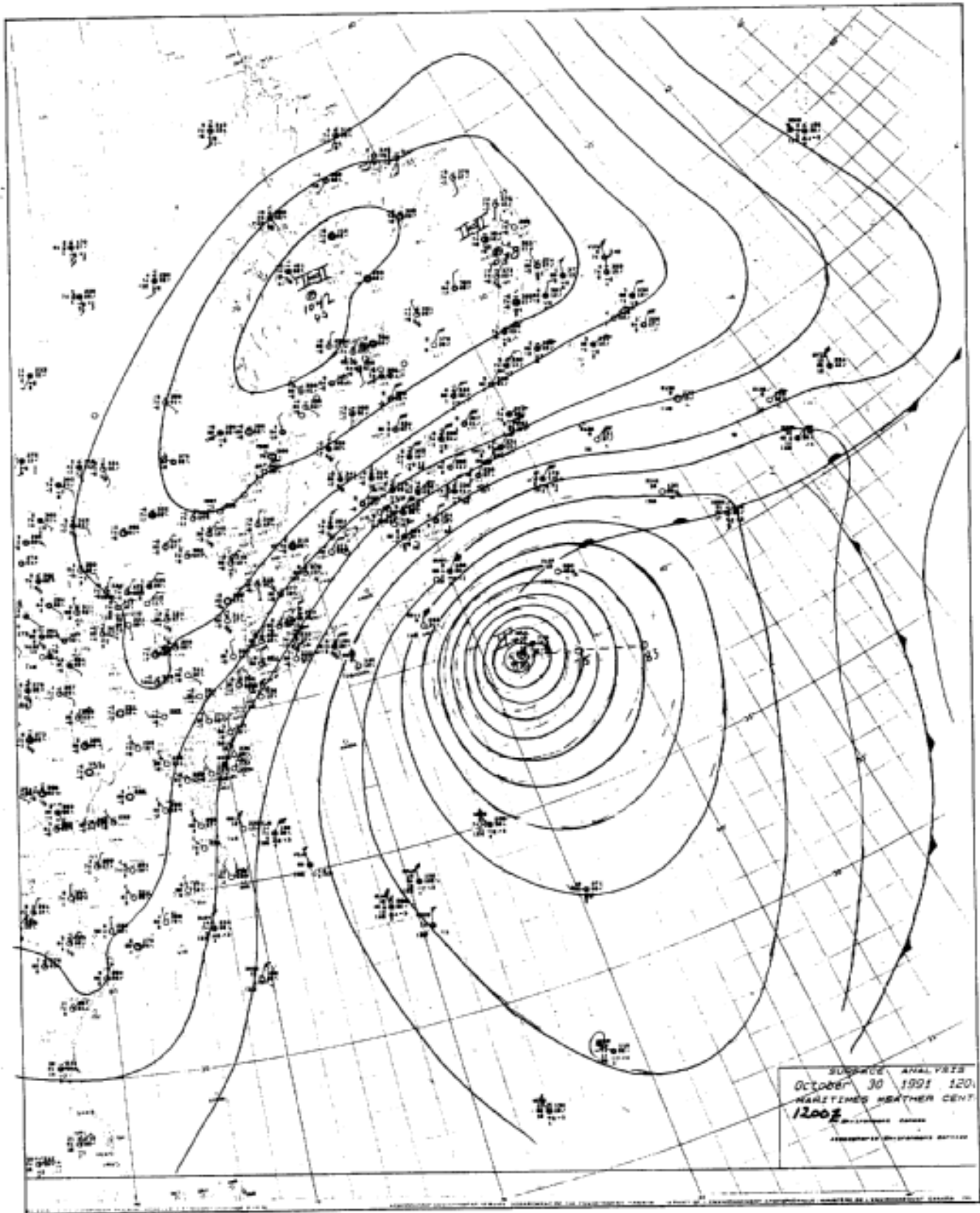


Figure 19. Maritimes Weather Centre surface analysis 1200Z October 30, 1991

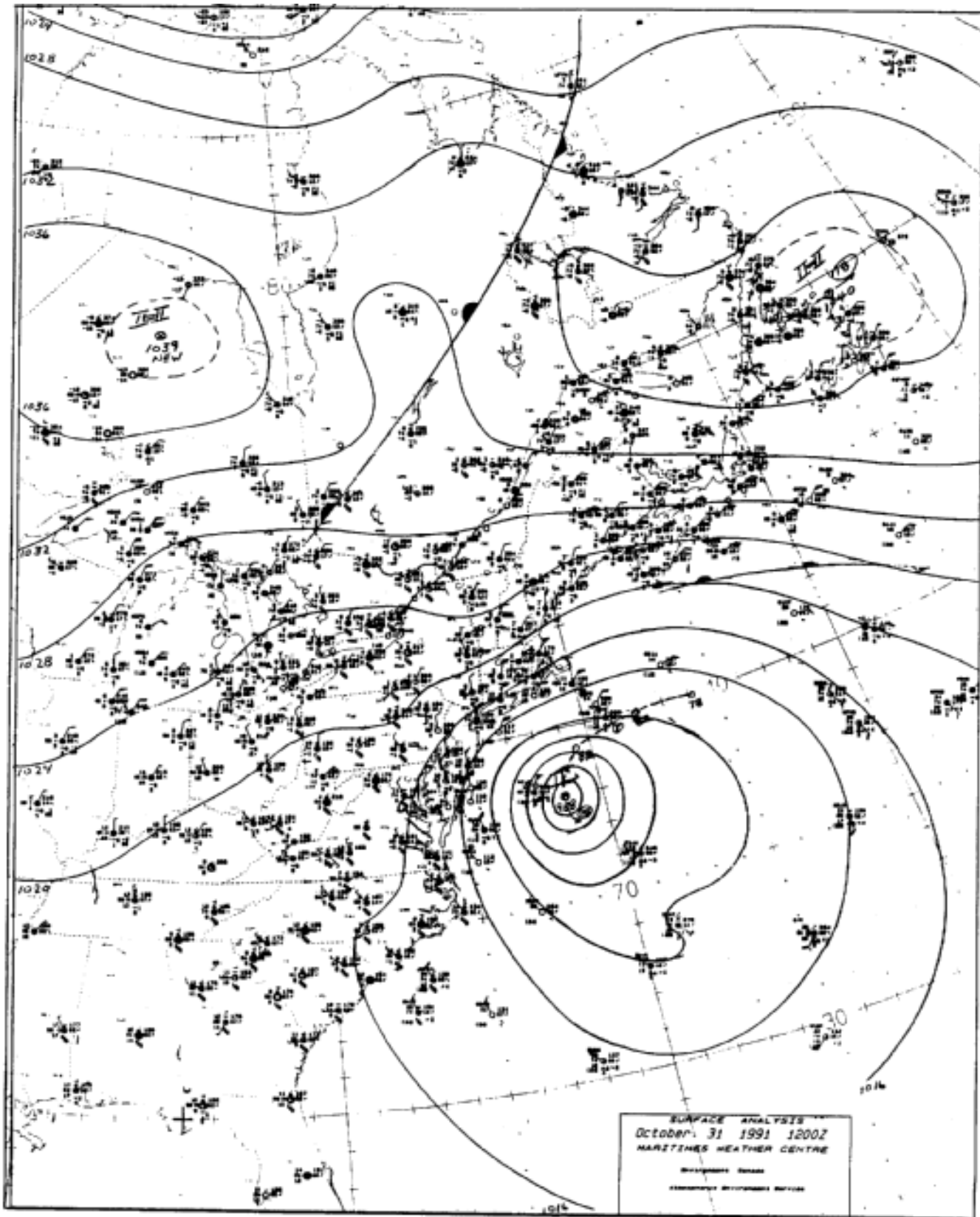


Figure 20. Maritimes Weather Centre surface analysis 1200Z October 31, 1991

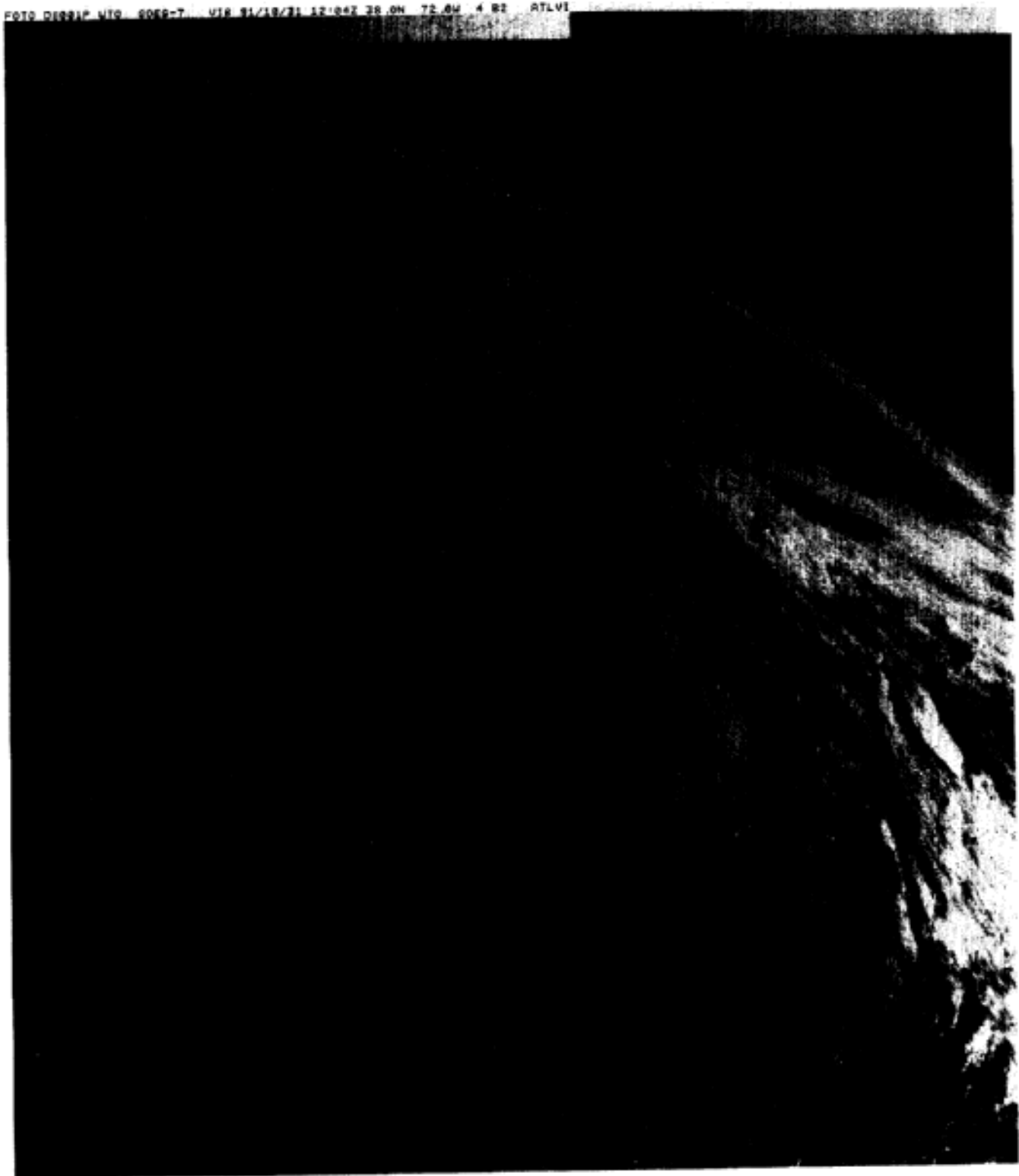
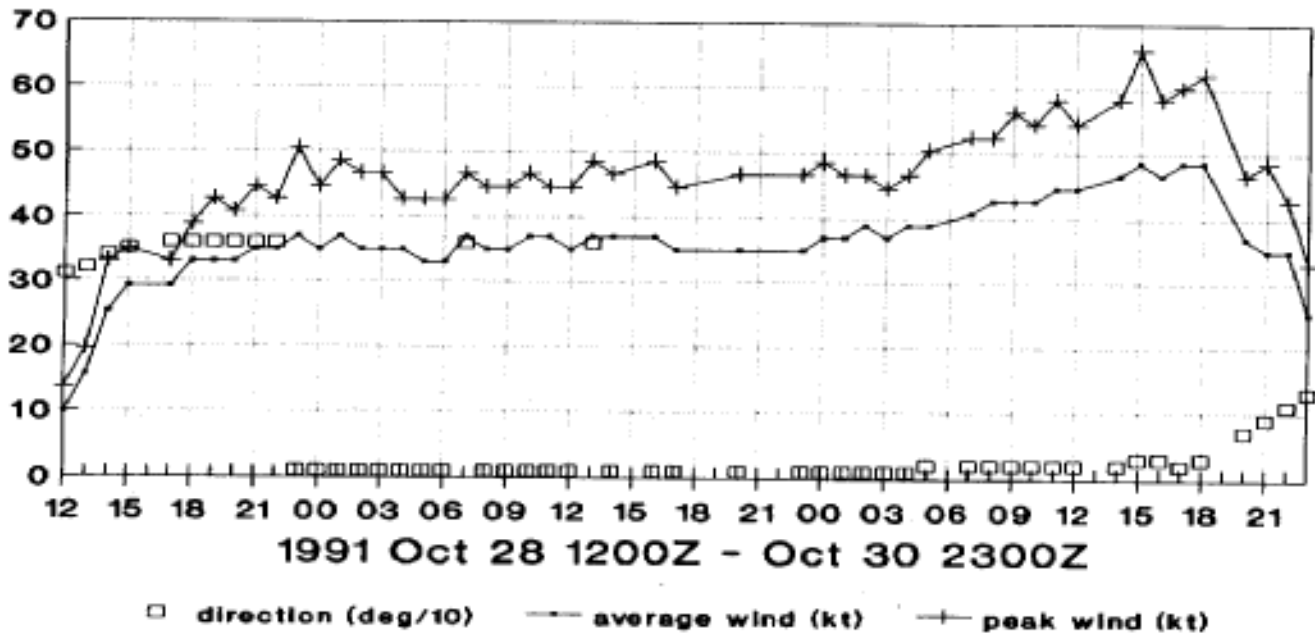


Figure 21. GOES visible imagery 12:04Z October 31, 1991.

44011 WIND



44011 WAVE HEIGHT/PERIOD

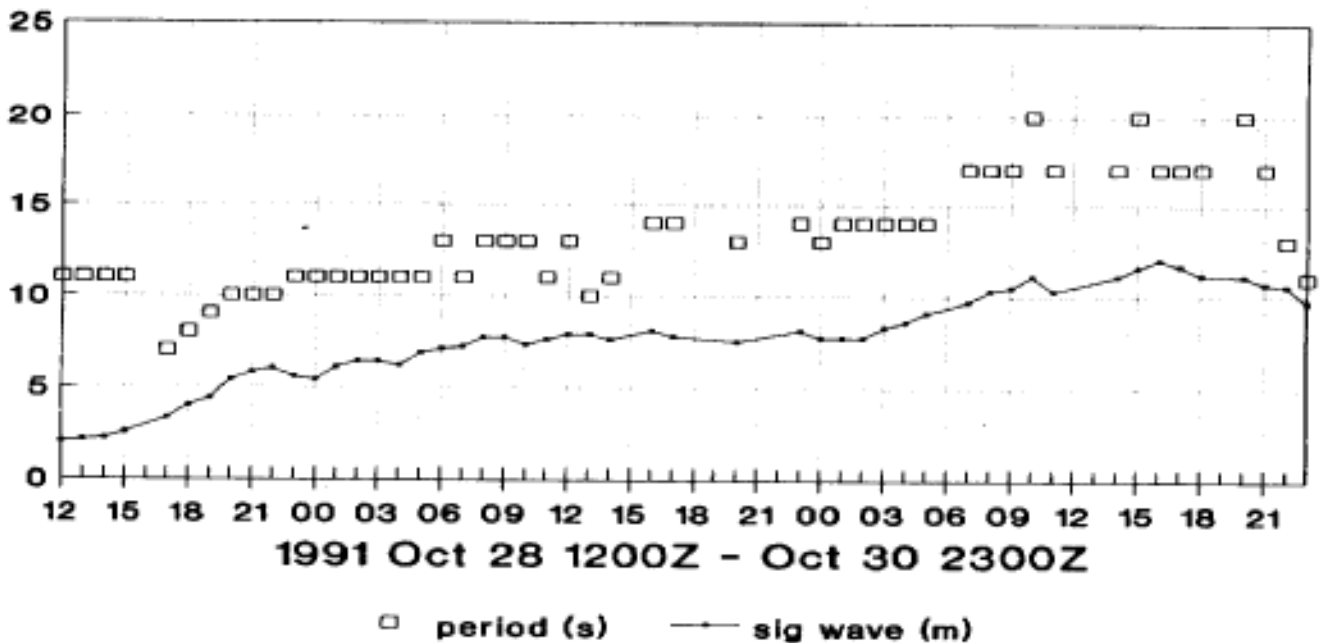
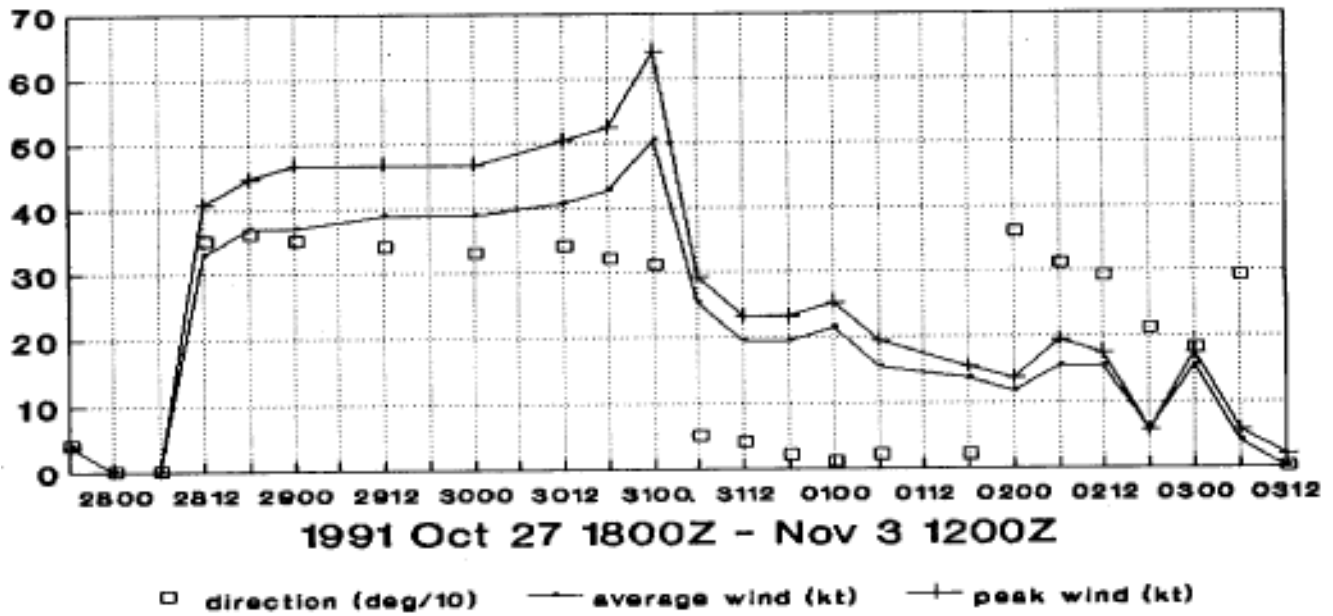


Figure 22. Buoy wind and wave measurements for 44011.

44008 WIND



44008 WAVE HEIGHT/PERIOD

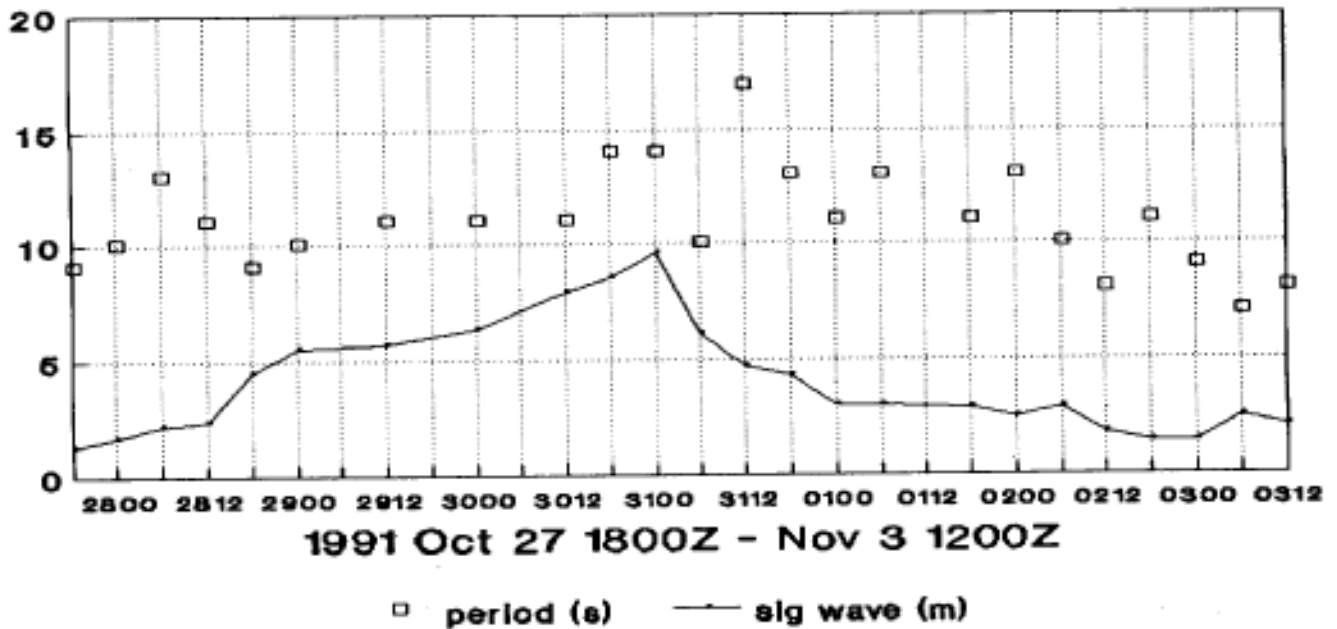
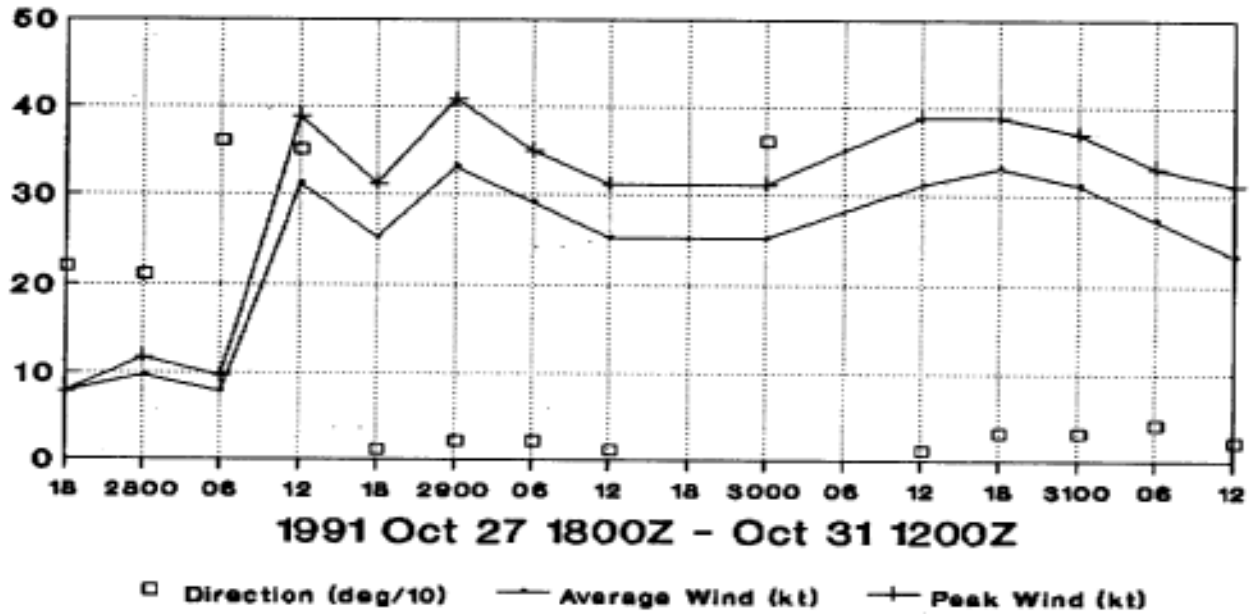


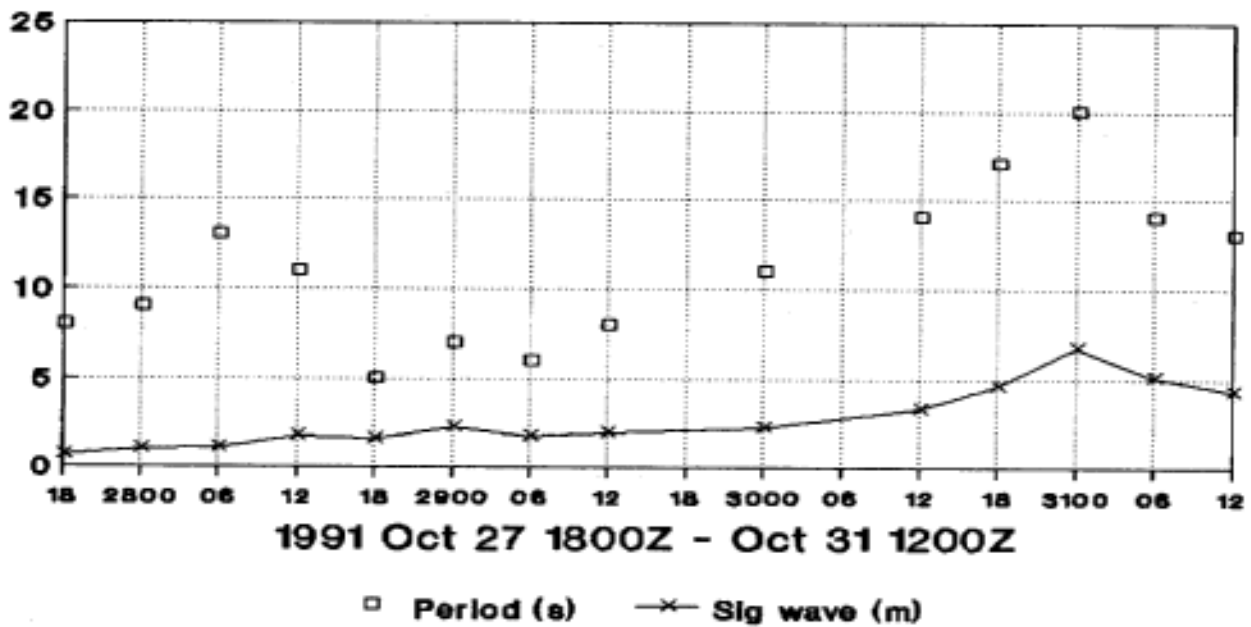
Figure 23. Buoy wind and wave measurements for 44008.

44007 WIND



2918Z 3006Z misg

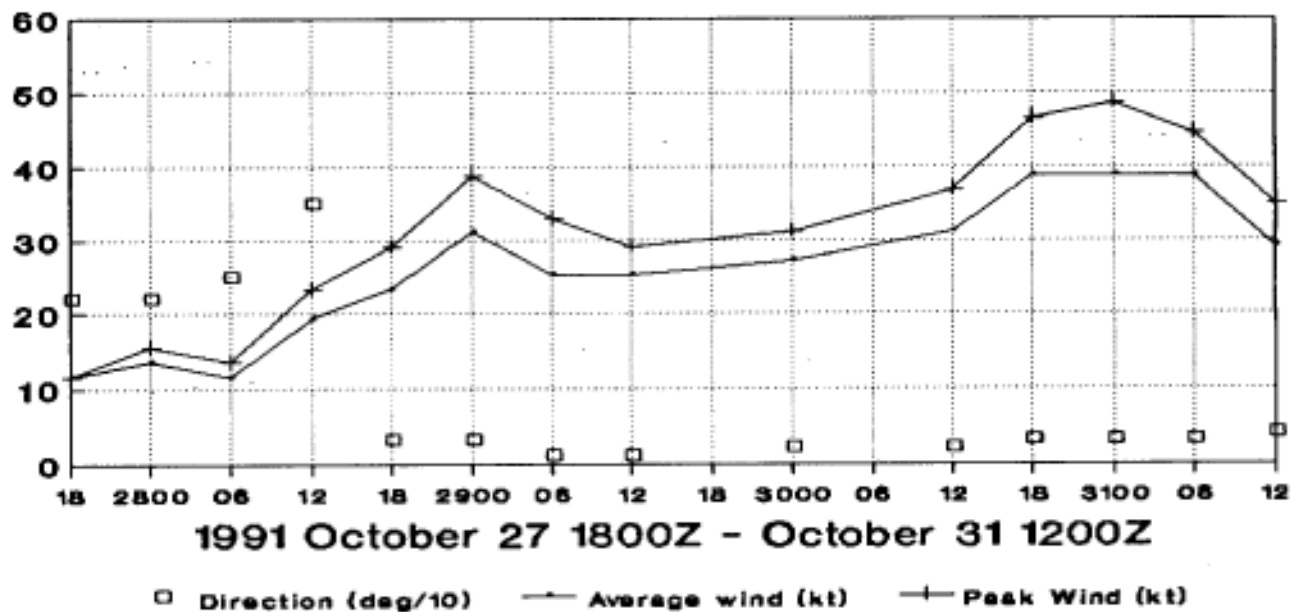
44007 WAVE HEIGHT/PERIOD



2918Z 3006Z misg

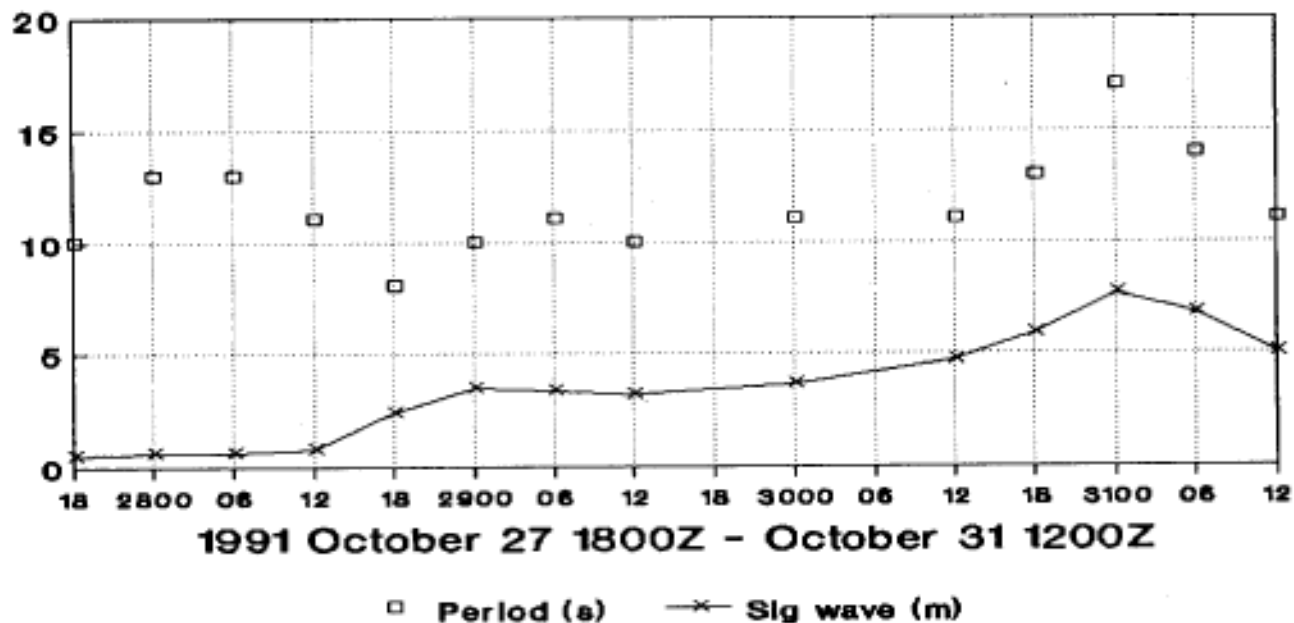
Figure 24. Buoy wind and wave measurements for 44007.

44013 WIND



2918Z 3006Z misg

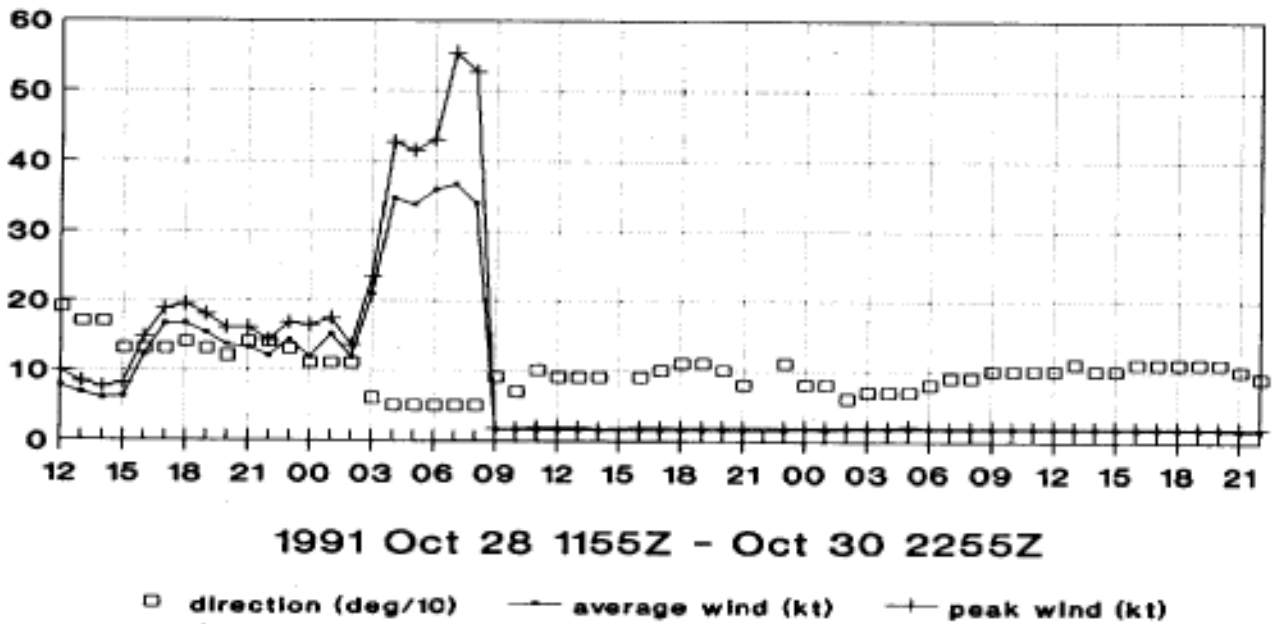
44013 WAVE HEIGHT/PERIOD



2918Z 3006Z misg

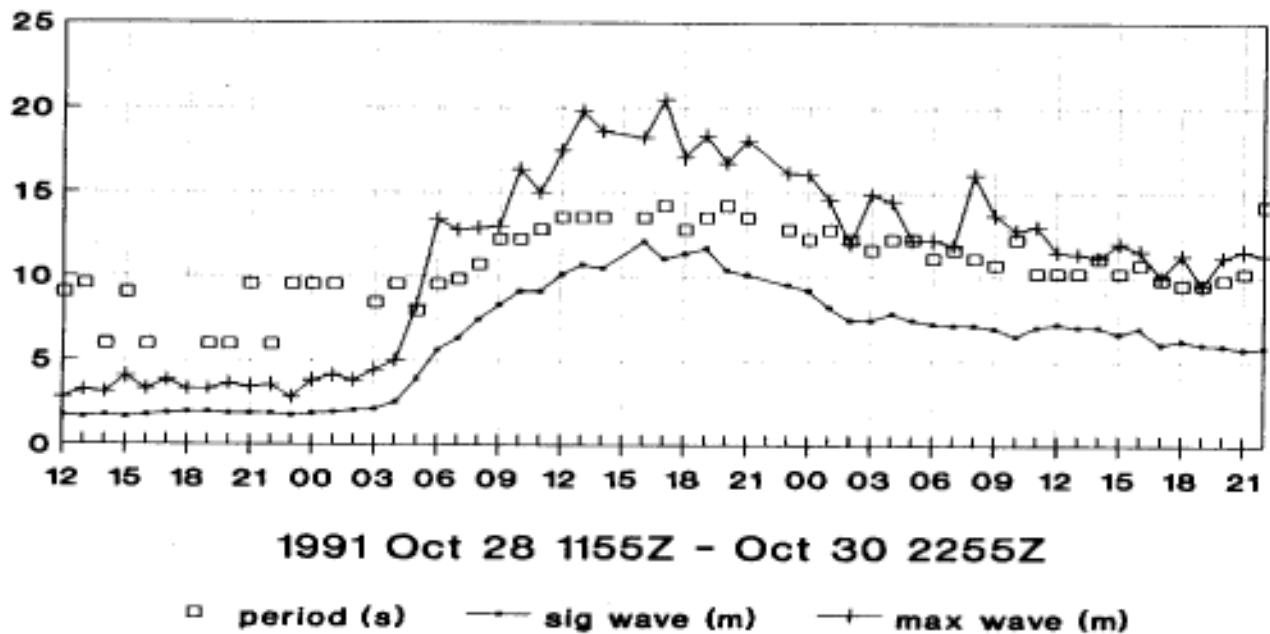
Figure 25. Buoy wind and wave measurements for 44013.

44138 WIND



2915Z 2922Z misg

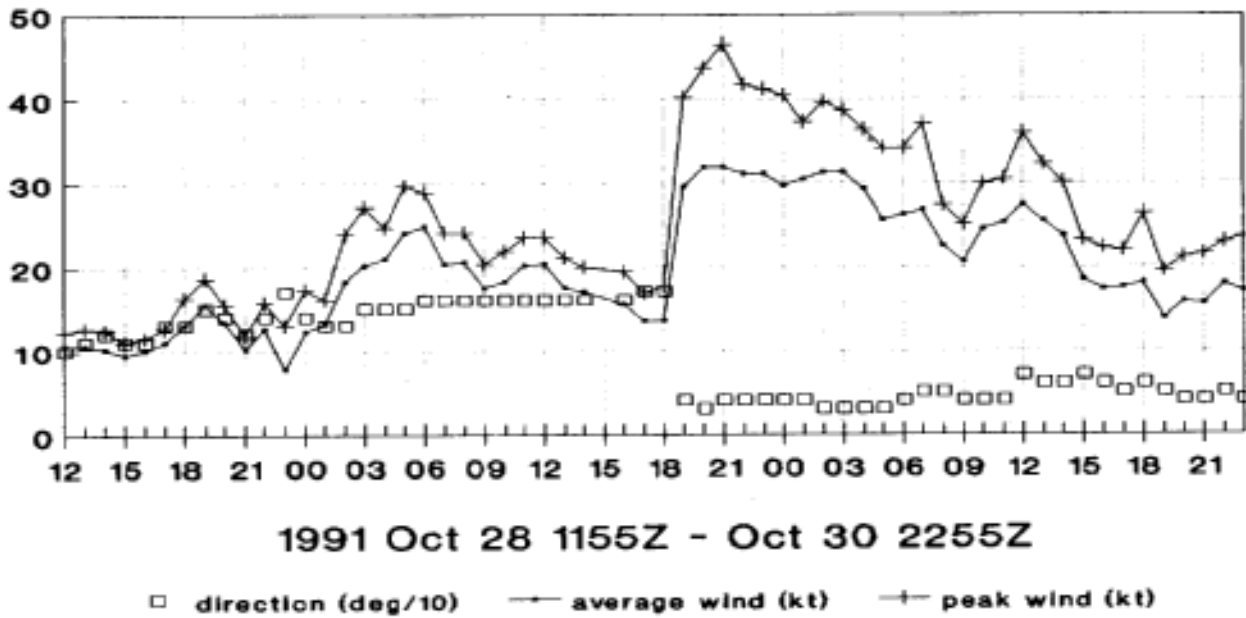
44138 WAVE HEIGHT/PERIOD



2915Z 2922Z misg

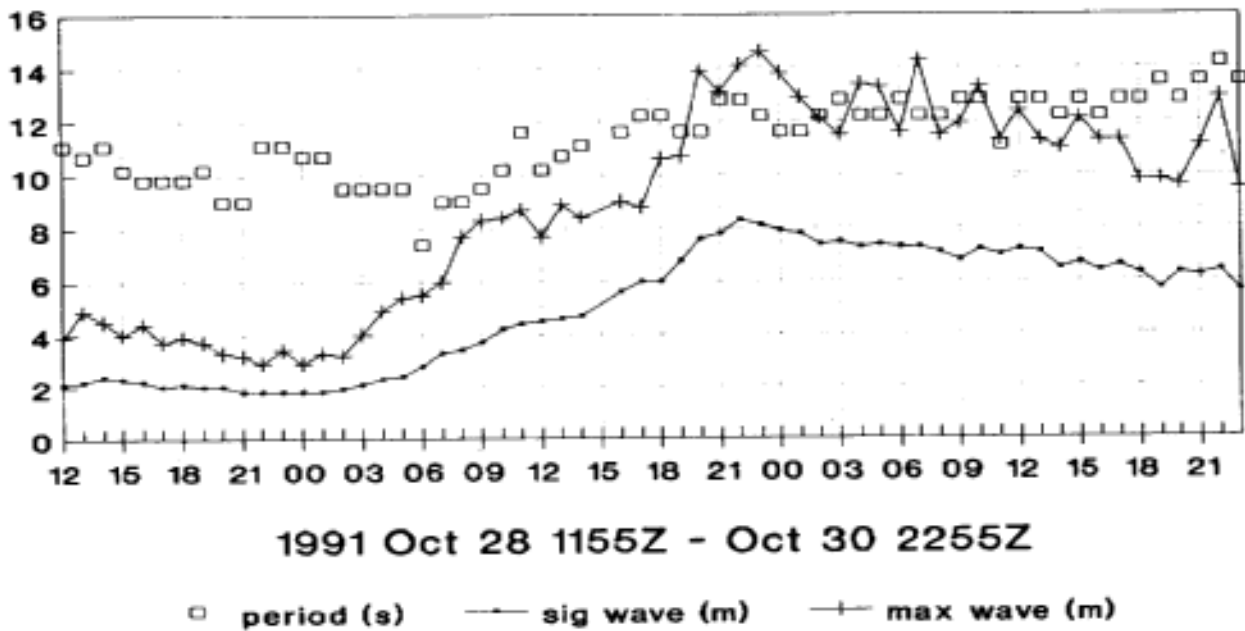
Figure 26. Buoy wind and wave measurements for 44138.

44140 WIND



2915Z misg

44140 WAVE HEIGHT/PERIOD



2915Z misg

Figure 27. Buoy wind and wave measurements for 44140.

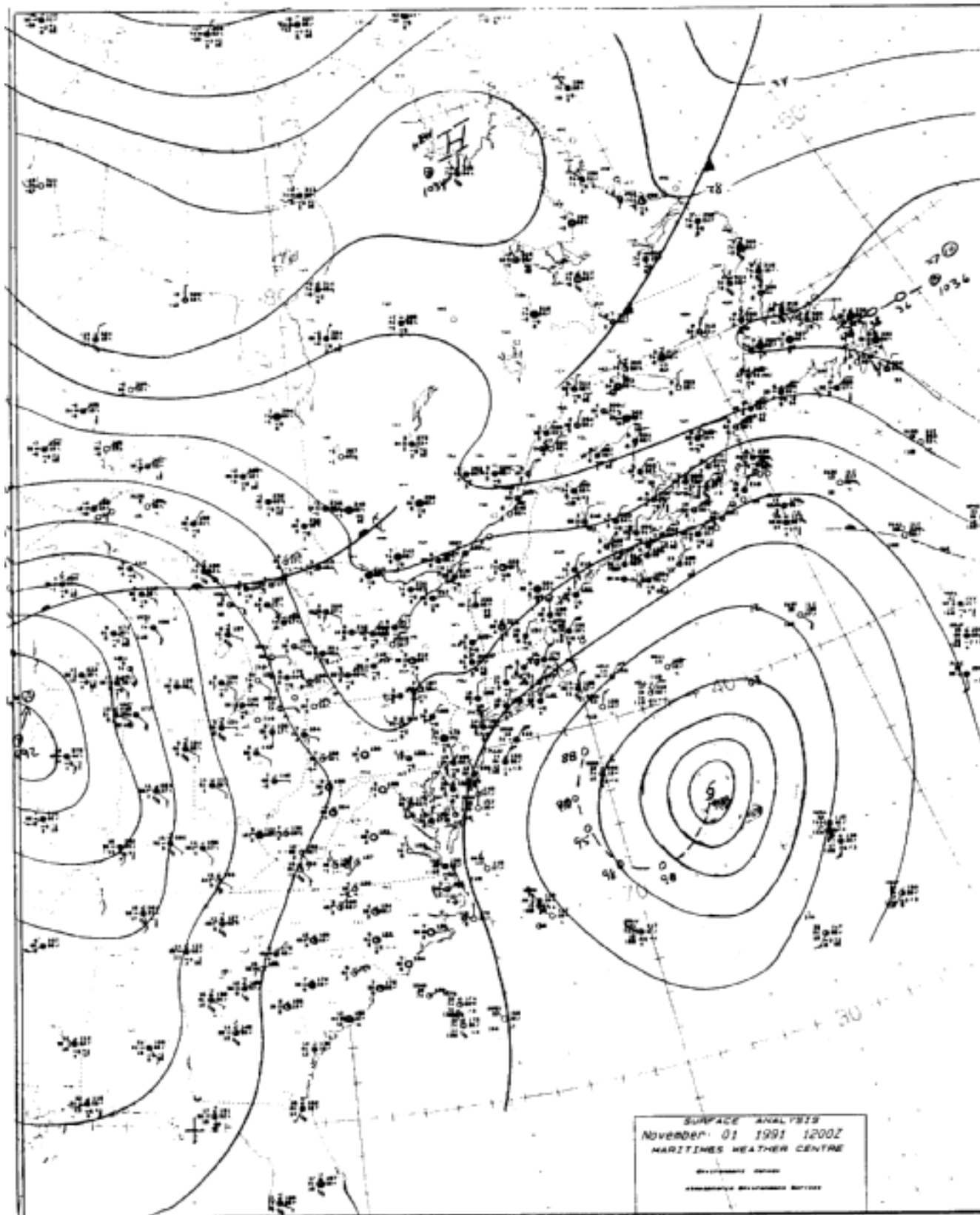


Figure 29. Maritimes Weather Centre surface analysis 1200Z November 1, 1991

FOTO DIBBIP WTC GOES-7 VIS 91/11/01 12:04Z 38.0N 72.0W 4 8Z ATLVI

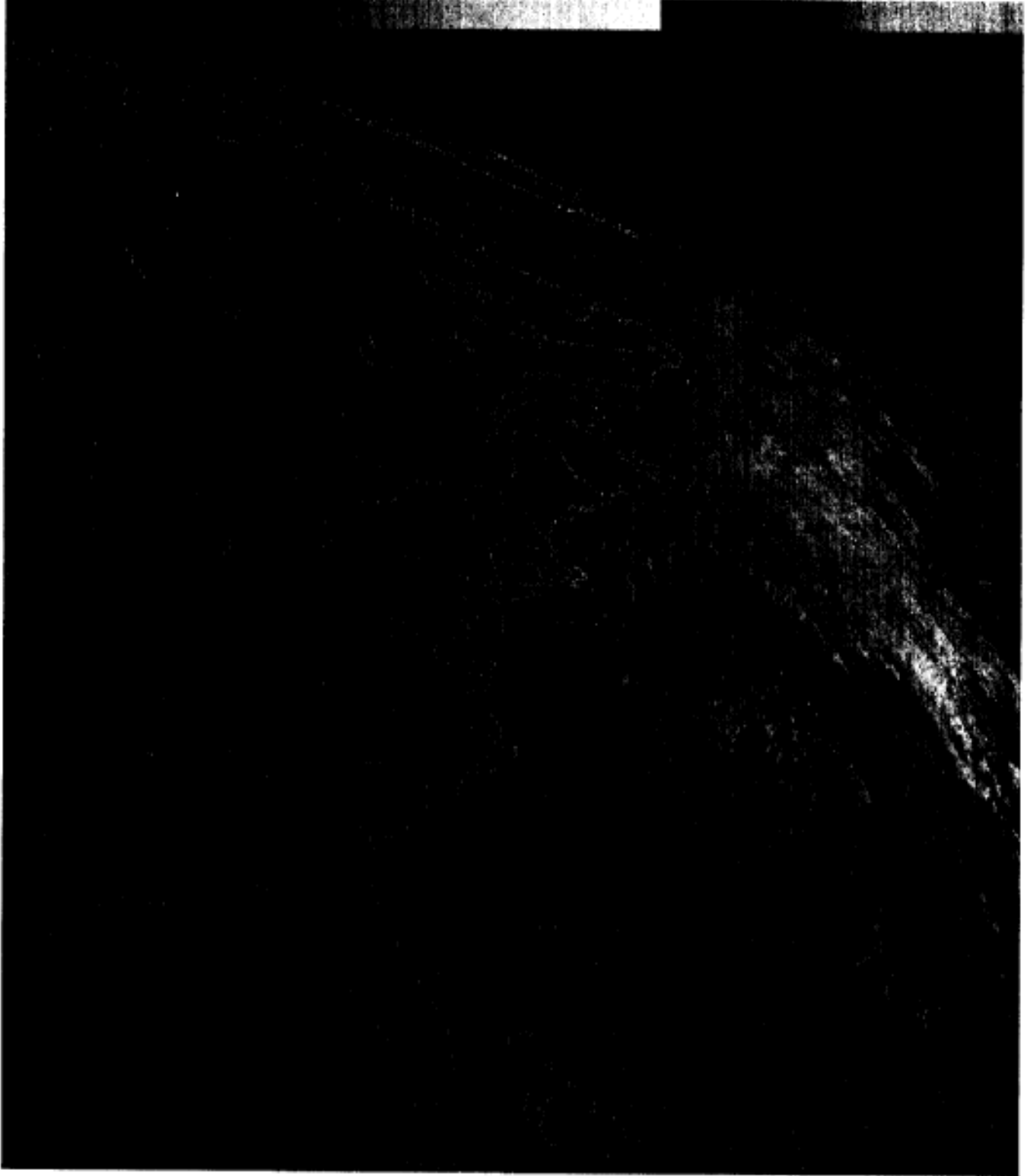


Figure 30. GOES visible imagery 12:04Z November 1, 1991.

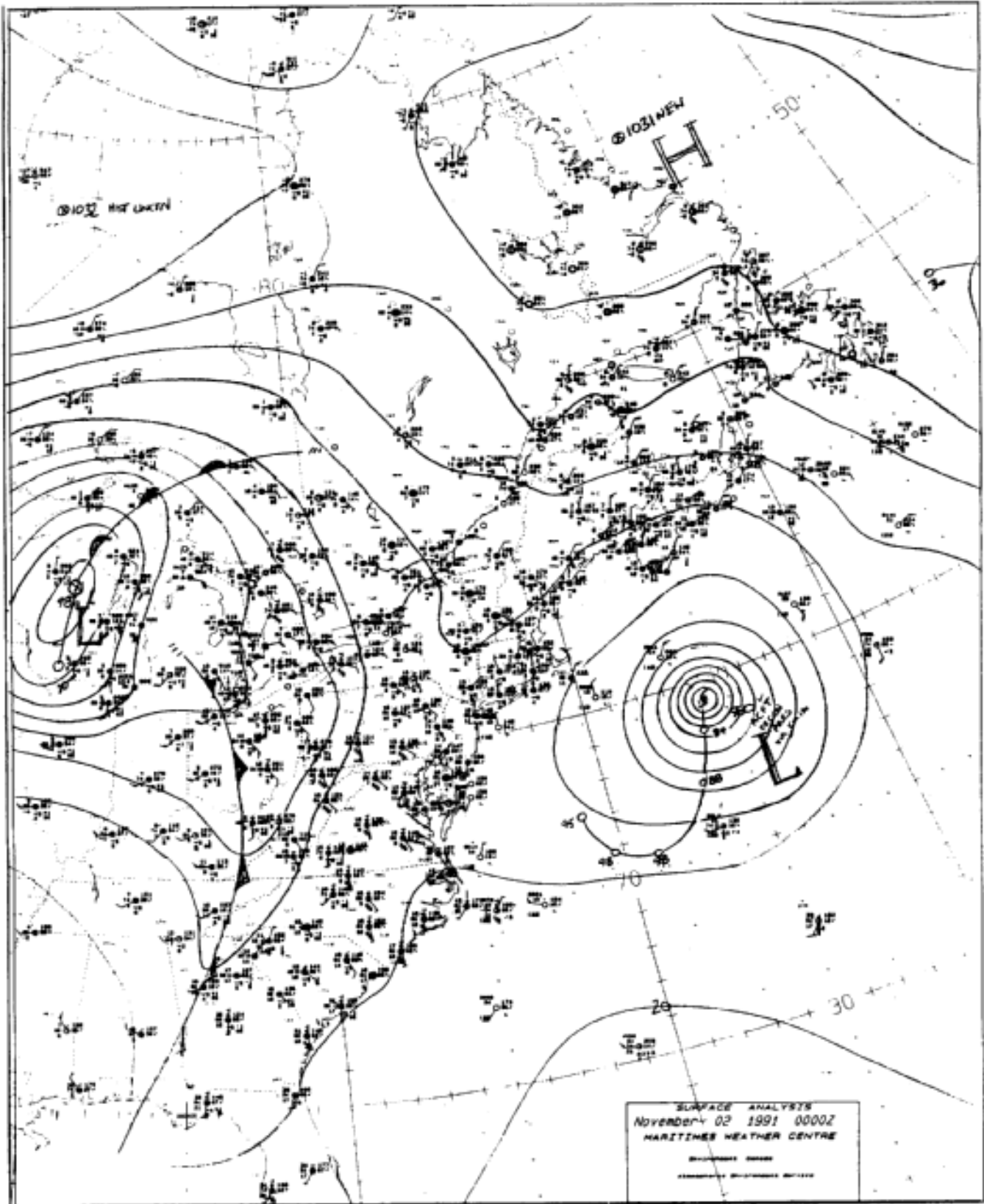


Figure 31. Maritimes Weather Centre surface analysis 0000Z November 2, 1991

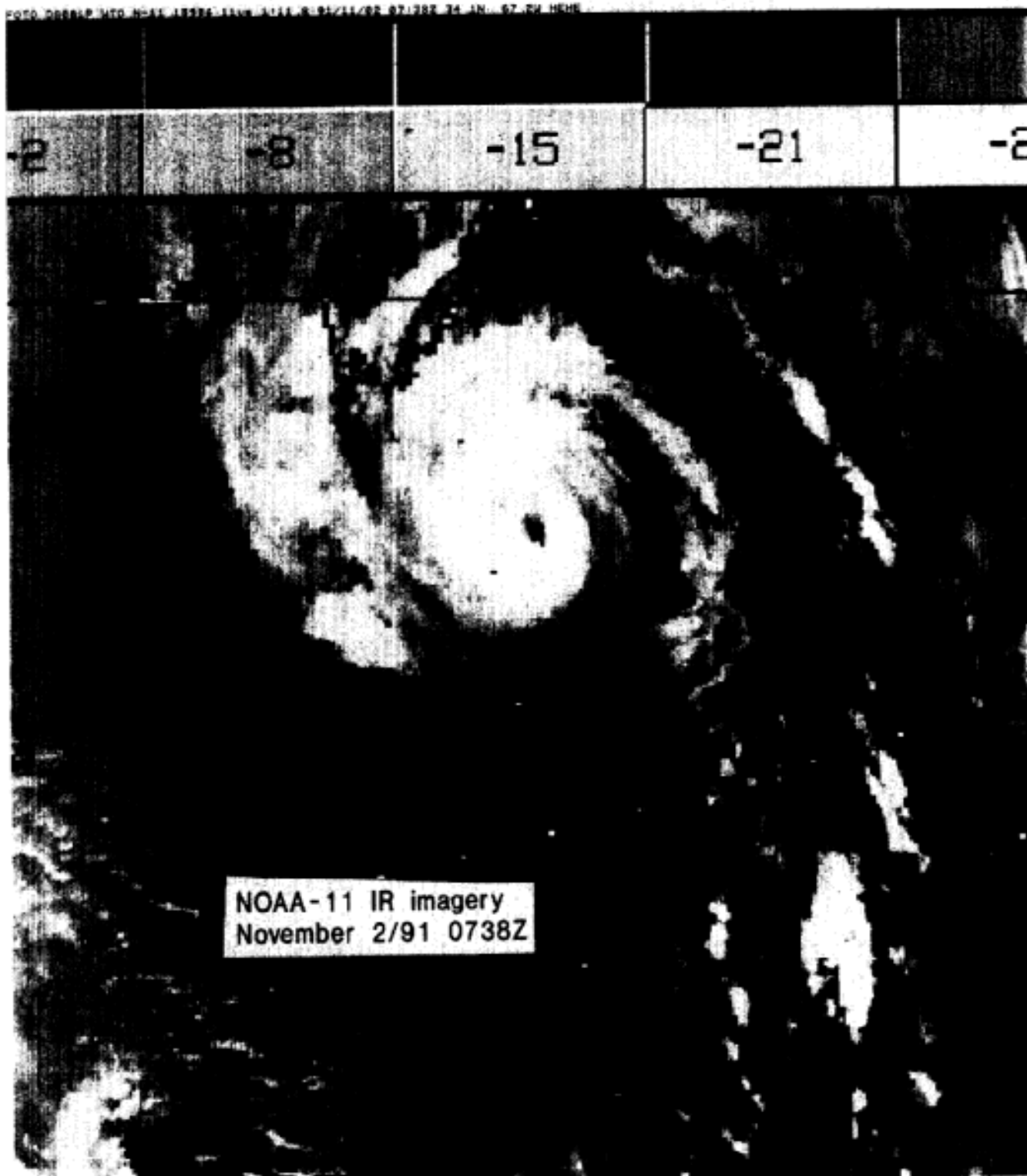


Figure 33. NOAA-11 IR imagery 07:38Z November 2, 1991.

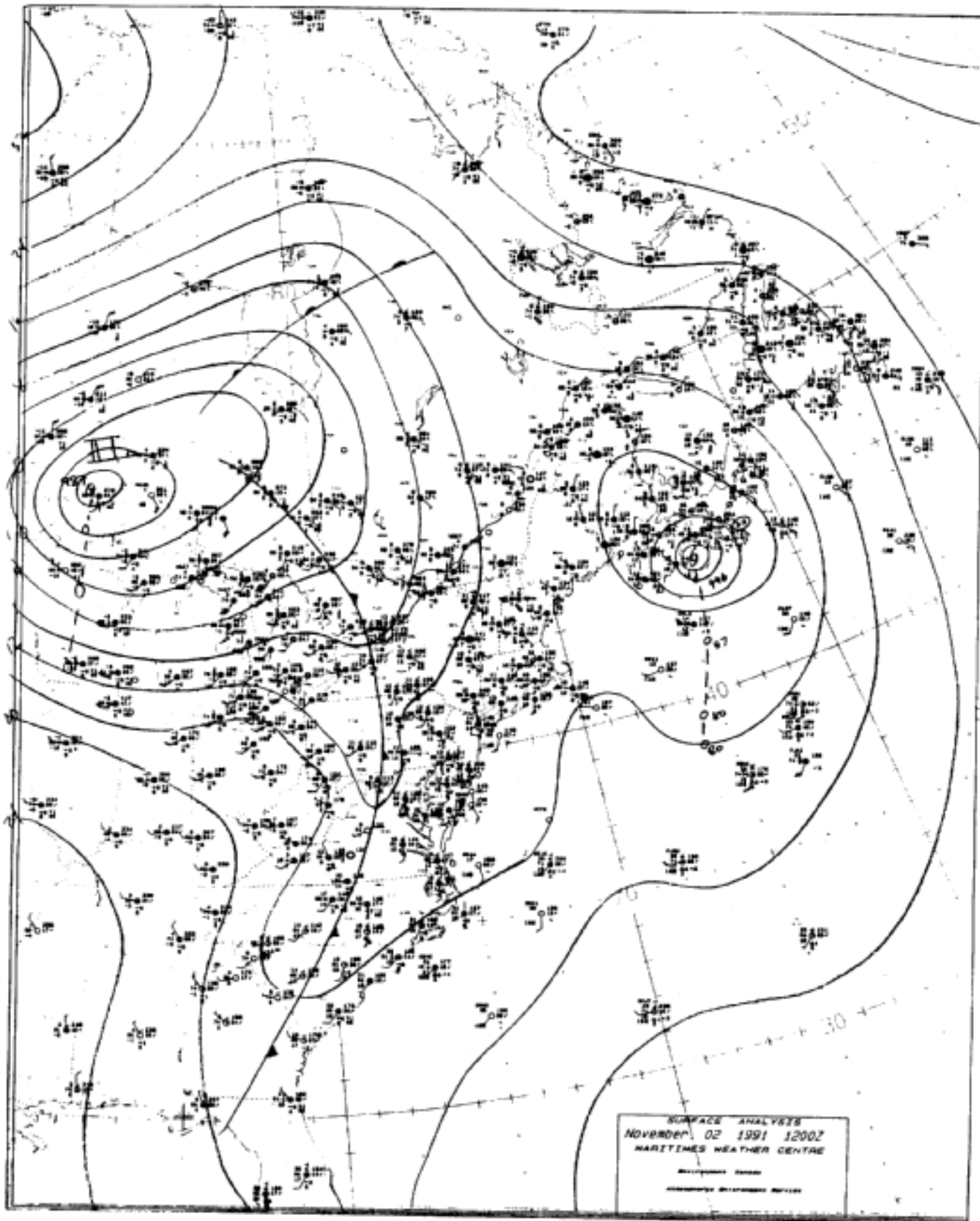


Figure 34. Maritimes Weather Centre surface analysis 1200Z November 2, 1991

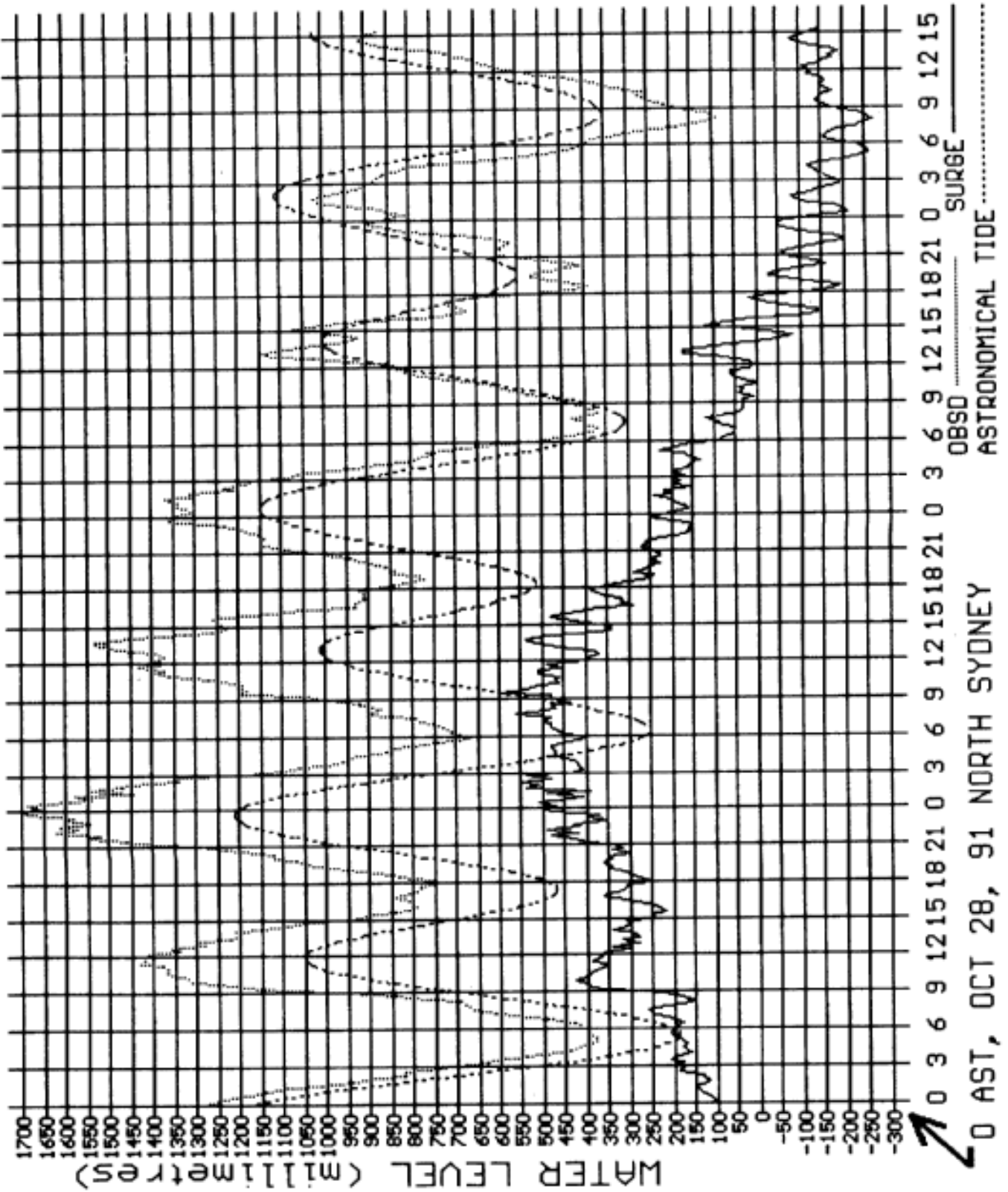


Figure 35. Water level at North Sydney.

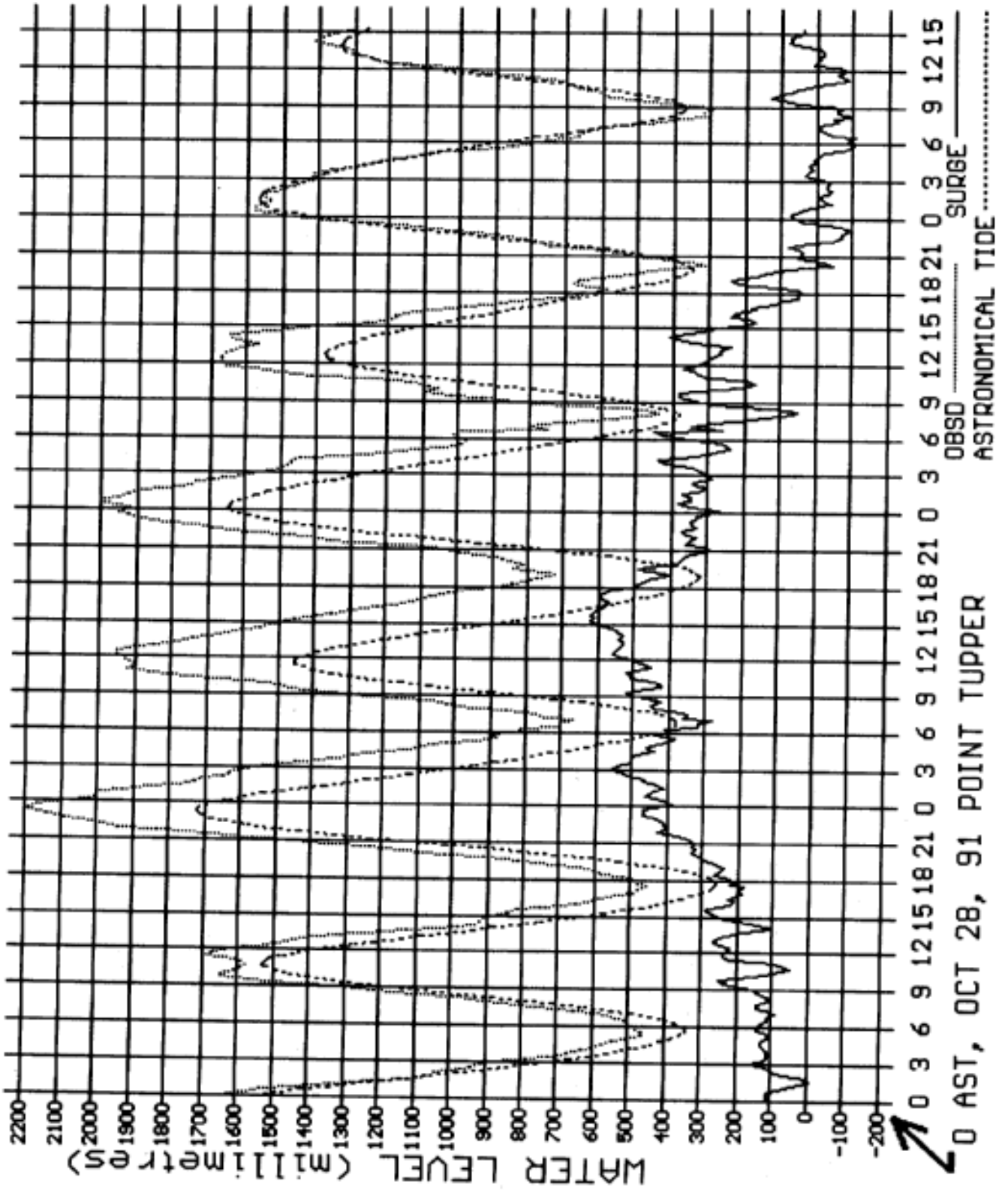


Figure 36. Water level at Point Tupper.

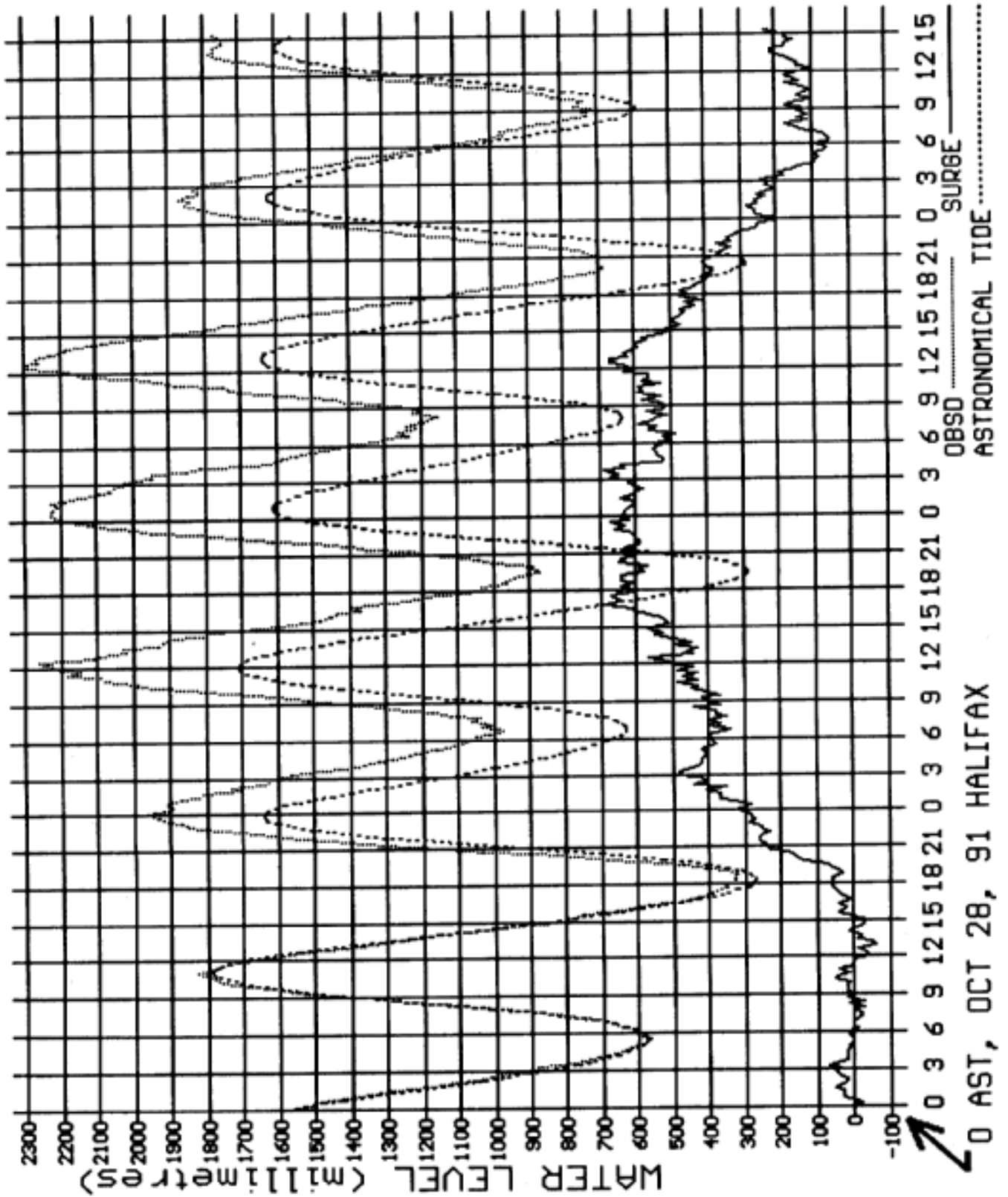


Figure 37. Water level at Halifax.

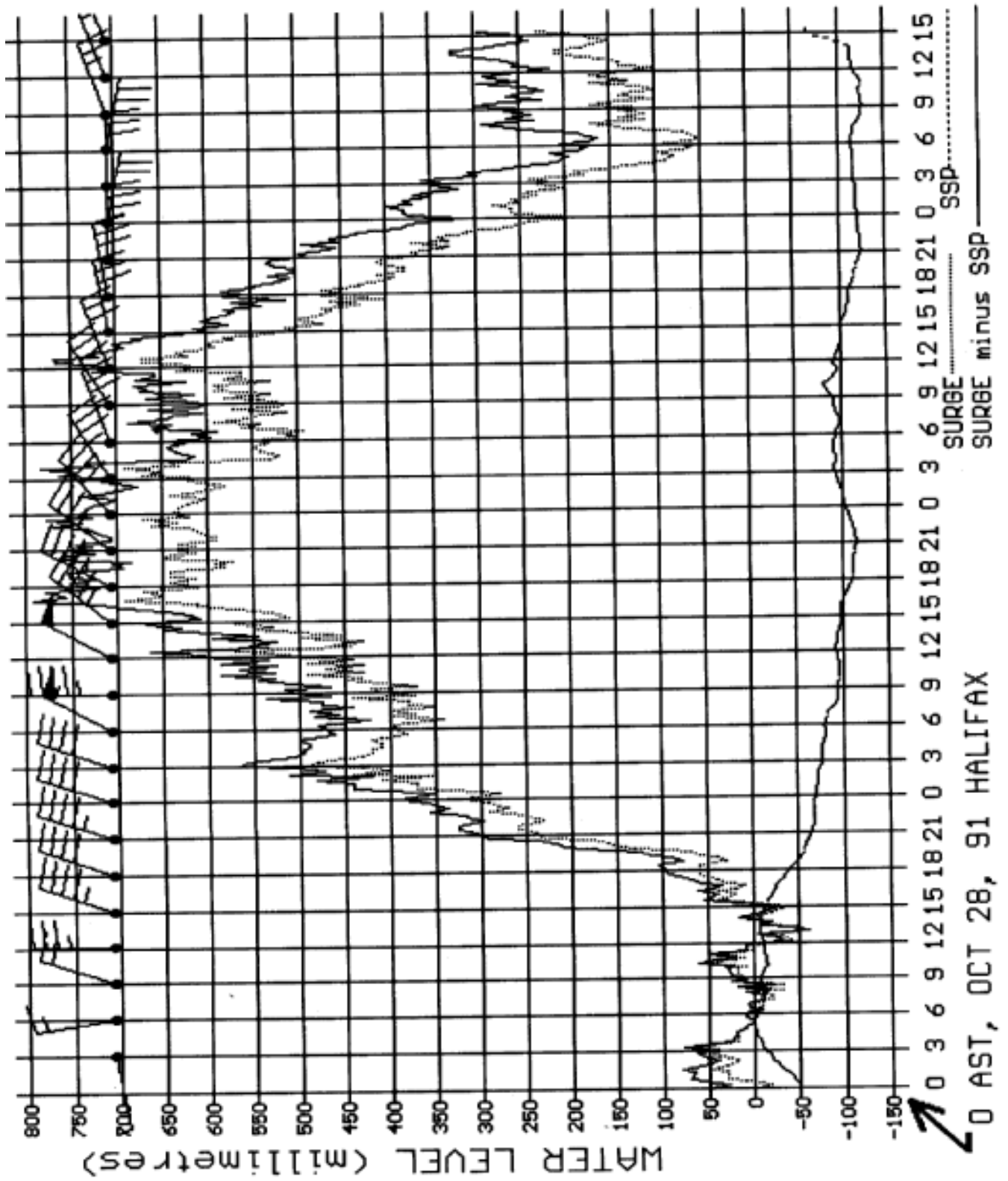


Figure 39. Residual surge at Halifax.

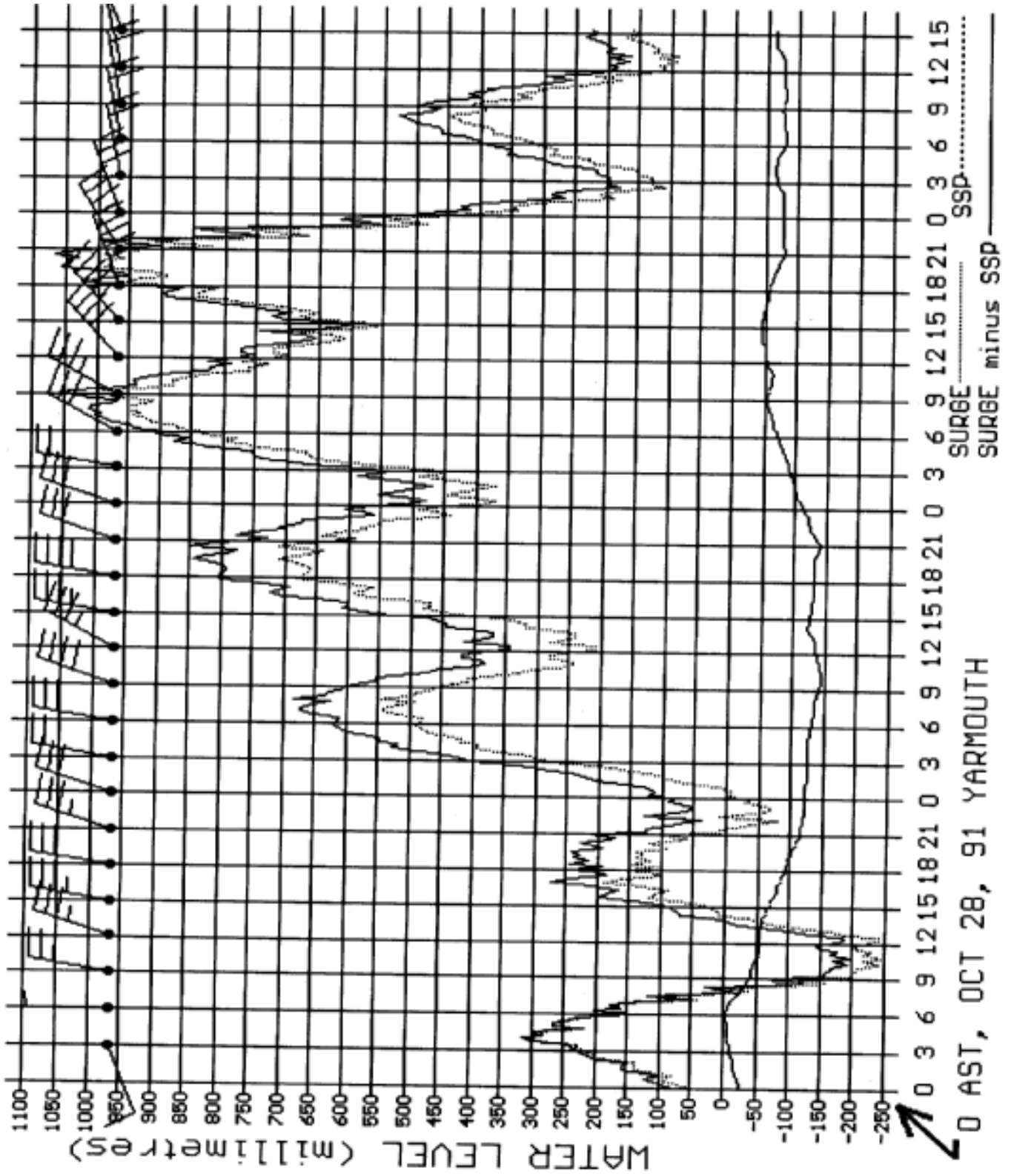


Figure 40. Residual surge at Yarmouth.

Shearwater Waverider

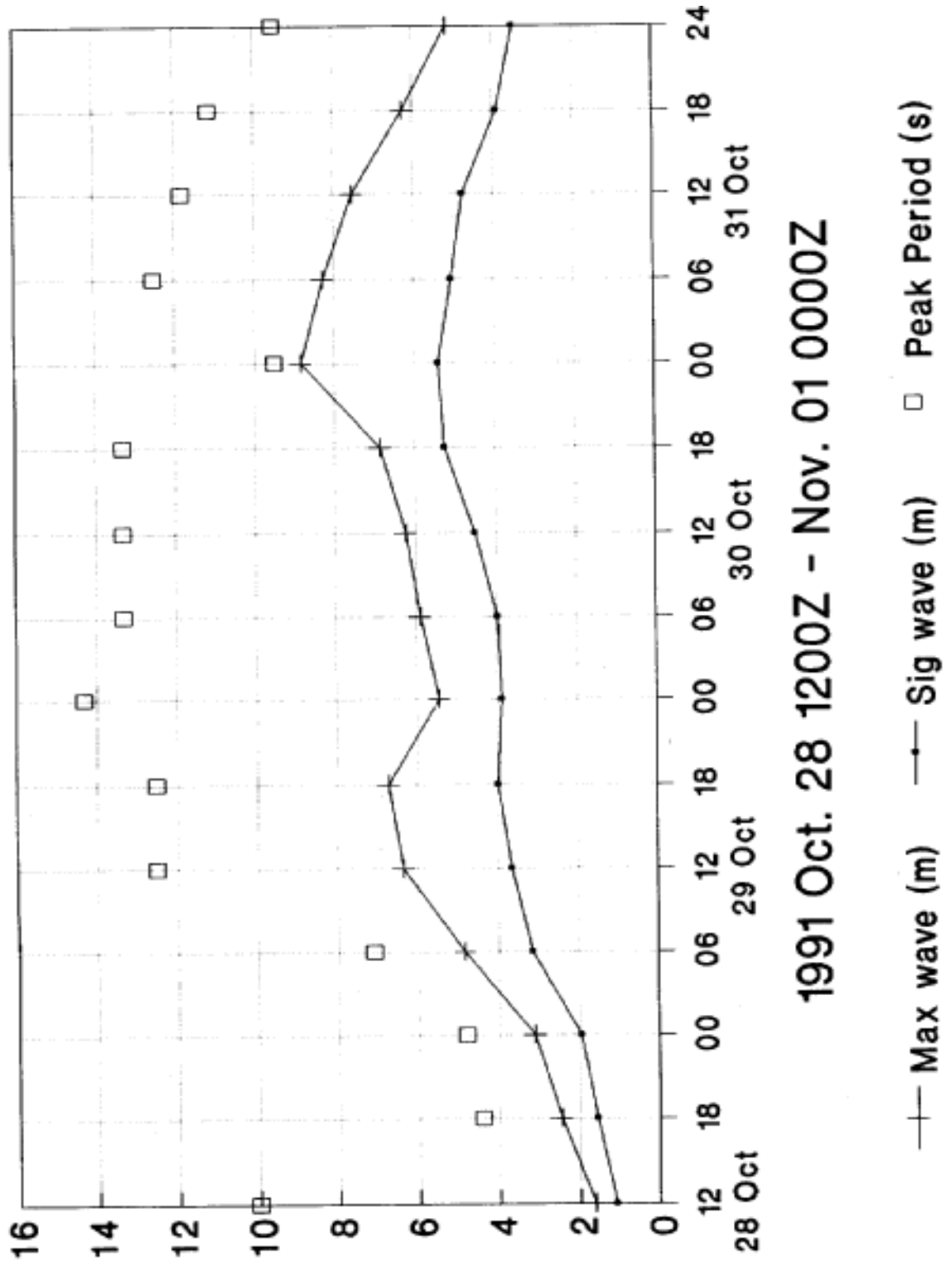


Figure 41. Waverider measurements at Shearwater.

A SAMPLING OF DAMAGE REPORTS FROM
THE HALLOWE'EN 1991 STORM

R. Bigio

Canadian Forces Meteorological and Oceanographic Centre
Halifax, N.S.

INTRODUCTION

The Hallowe'en 1991 storm caused widespread damage along most of the East coast from Newfoundland to Florida. Many boats, wharves, and seaside properties were damaged or destroyed. At least one aircraft went down. Many beaches suffered extreme erosion. Many coastal roads were flooded, damaged, or littered with debris.

The damage inflicted by this storm fell into three broad categories - incidents well offshore, incidents along the coast, and incidents inland. The largest group, by far, was incidents along the coast.

OFFSHORE INCIDENTS

There were four incidents which took place well offshore. Their locations are shown in Figure 1 . Three of these took place near Canadian offshore buoys. The locations of these buoys are shown in Figure 2 . Data from these buoys are plotted in Figures 3 to 11 to show the conditions which likely caused these incidents. The Appendix gives a brief discussion of the buoy anemometers.

Anne Kristine

The first offshore incident was the loss of the *Anne Kristine*. She was a 123-year old, 29 metre long, topsail schooner en route from New York to the West Indies. On the 28th she was about 650 kilometres southeast of Long Island. (See Figure 1 .) Late that morning, she began taking on water in high winds and heavy seas. The newspaper account reported 50 knot winds and nine metre seas, although METOC Centre analyses suggest that these values represent peak wind and maximum wave. That night, the crew was rescued safely after pumps proved unable to cope. She is believed to have sunk later that night.

This incident began during the early stages of the storm. At that time, Hurricane Grace was just west of Bermuda, and the low further north had not yet begun to deepen rapidly.

Eishin Maru

The *Eishin Maru* was a Japanese 50-metre trawler with 21 crewmen and a Canadian fisheries observer on board. On the 30th at 1022Z she called

for assistance. High waves had smashed the windows in her wheelhouse and the resulting flooding disabled her engine and helm. At that time she was near 42N 60W (see Figure 1) where METOC Centre analyses showed significant wave height near 12 metres, and winds near 50 knots. On-scene rescue units said the wind reached 70 knots at times. Such conditions made it impossible to get a tow-line to her. Fortunately, the crew was able to regain control after boarding up the wheelhouse windows. She arrived in Halifax late the next night under her own power.

Buoy 44137 was close to where the *Eishin Maru* was damaged. On figures 3 -5 , the thick vertical line marks the time at which this incident began. This buoy recorded maximum winds over 25 metres/second and maximum waves over 20 metres for many hours just before this incident. It also reported four occurrences of maximum wave near 30 metres.

Zarah

The *Zarah* was a 180-metre bulk carrier. On the 30th at about 0800Z she also requested assistance. She had lost power after high seas had flooded her engine room. She was then near 42N 57W (see Figure 1) where she had experienced much the same conditions as the *Eishin Maru*. But as with the *Eishin Maru*, the crew was able to regain control, and she later arrived in Halifax under her own power.

Buoy 44141 was very close to where the *Zarah* ran into difficulty. On Figures 6 -8 , the thick vertical line marks the time when this incident began. This buoy also recorded maximum wind over 25 metres/second and maximum waves over 20 metres for many hours just prior to this incident.

Andrea Gayle

The *Andrea Gayle* was a U.S. swordfishing boat with a crew of six. On the 31st, at 0039Z, she was reported overdue. In the ensuing search, debris from this vessel was found at Sable Island. The crew was presumed drowned. It was not determined where she was when she went down, though her normal fishing ground is near 44N 56W (see Figure 1). According to METOC Centre analyses, significant wave height there peaked near ten metres late on the 29th. In terms of lives lost, this was the costliest single incident resulting from this storm.

Buoy 44139 was close to the *Andrea Gayle's* fishing grounds. On Figures 9 -11 , the thick vertical line marks the time at which she was reported overdue. Data from this buoy show that conditions were slowly subsiding on the 30th. But they also show that for many hours on the 29th and 30th, maximum winds were over 25 metres/second and maximum waves were over 15 metres.

INLAND INCIDENTS

Because there was so much damage along the coast, there was little coverage by the news media of inland damage. The *New York Times* of Nov 01 went so far as to summarize the situation with the subheadline "Flooding and chaos along the coast, while inland all is calm". The few items which were reported usually referred to trees or power lines being blown down, or to roofs being blown off.

Power interruptions of various lengths were reported from many areas. The *New York Times* reported that, on Long Island, 22,000 customers were without power for several hours, and that shorter disruptions affected smaller areas. In Nova Scotia there were 26 interruptions on the 30th and 31st. Of these, 23 were caused by the storm - four were due to high winds and 19 were from salt contamination of insulators. (Apparently, in strong onshore winds, salt spray coats insulators, causing short-circuits.)

Most of the inland incidents were not serious enough to make the news, but did lead to insurance claims. One adjustor in Dartmouth, Nova Scotia processed several storm-related claims for damage to fences and siding, and one claim for a house fire. It was unclear whether the storm had caused the fire, but it was clear that the strength and direction of the wind made it impossible for firefighters to control the fire. That house was a total loss.

COASTAL INCIDENTS

The greatest impact from the storm was felt along the coast. Damage was widespread and some areas were devastated. Dozens of boats broke loose from their moorings and were sunk or washed ashore. Ferry schedules were disrupted. At North Sydney N.S., one ferry could not dock for two days, while another snapped three of its mooring lines. Elsewhere, 22 of 24 scheduled crossings from Nova Scotia to Prince Edward Island were cancelled.

Newfoundland

In southeastern Newfoundland several boats were swamped or sunk by 40 to 50 knot winds and high waves. On the 29th, the *St John's waverider* recorded significant wave height near six metres and maximum wave height near nine metres. This storm also produced the season's first significant snowfall for Newfoundland. On the 28th, *St John's* reported 11.6 centimetres of snow, setting a new record for the date. *Gander* reported a similar snowfall.

Magdalen Islands

In the Gulf of St Lawrence, significant wave height built to over five metres on the 29th. This damaged three of four sections of a steel

walkway at a docking facility on the Magdalen Islands. Waves twisted some members of the steel frame - seriously weakening the structure. They had been designed to withstand winds to 51 m/s and waves to 3 in above maximum high water. An engineering report says 5-6 in waves caused the damage and recommends that these structures be redesigned accordingly.

Nova Scotia

At Arichat on Cape Breton Island a lobster plant suffered over \$100K in damage from this storm. In the afternoon of the 30th, when workers went home for the day, all was well. The following morning, when workers arrived, they found part of their beach and driveway washed away, and their intake pipes ripped off the bottom of the bay. The plant is located in a cove along a coastline which runs east and west. The location of the plant is shown on a coarse scale map in Figure 12 , and on a finer scale in Figure 13 .

The beach in front of the plant was reinforced with rocks up to 50 centimetres in diameter. At the east end of the plant, an area several metres wide and a few metres deep was washed away.

The water intake system consisted of two lines - each 30 centimetres in diameter. One line was about 500 metres long and extended to a depth of about 20 metres. The other was about 1100 metres long, and extended to a depth of 75 metres. They extended almost straight southward through the cove. Figure 14 shows the layout of these pipes. (Note that figure 14 shows two shallow intake pipes - in reality there is only one.) Each pipe was held down by concrete weights. These weights weigh about 100 kilograms each, and are spaced at 1.5 metre intervals where the water depth is less than ten metres, and at 3 metre intervals in deeper water. At the end of each line is a 1300 kilogram weight which also supports the intake screen. Wave action during the night tore the pipes loose from their weights and left the pipes floating at the surface. Fortunately, the lines continued to operate, so no lobsters were lost.

There is a waverider about nine kilometres offshore, just outside of Halifax Harbour. Reports from this buoy during this storm are shown in Figure 15 . Wave heights at this buoy peaked at about the same time as this lobster plant suffered its damage.

There is a tide gauge at Point Tupper - about 24 kilometres west of the lobster plant. It showed a storm surge (see Figure 16) which peaked at about 60 centimetres on the 29th. But the water level was back to normal by the afternoon of the 30th. At North Sydney, (see Figure 17) the surge also peaked at about 60 centimetres above normal, but the peak and the return to normal were about six hours

earlier than at Point Tupper. Thus the damage here was inflicted by waves and not by surge.

R.B. Taylor of the Bedford Institute of Oceanography surveyed some beaches after this storm and documented some significant changes. In one case, a seven metre high shore cliff at the southern tip of Nova Scotia was cut back as much as 8.5 metres between September 18 and November 26 1991. He believes there is sufficient evidence to show that most of this erosion was the result of the Hallowe'en storm.

New England

U.S. President Bush's summer home at Kennebunkport Maine was severely damaged. This incident was reported nationwide in Canada and the USA. Photographs showed debris strewn about the property. Film showed walls caved in, furniture tossed about, and a pier badly damaged. More than 100 seaside homes in Maine were damaged. There were similar reports from throughout coastal New England.

Nantucket

Nantucket Island has the distinction of having been completely exposed to everything this storm could offer. A report in *The Globe and Mail* said that four houses were "punched into kindling", and that many others were flooded or had verandahs, doors, and windows smashed. Several boats were pushed onto lawns. The wind on the 30th reached 68 knots. Waves eroded almost six metres of a cliff at Sankaty Head on the eastern side of the island (see Figure 18). Part of the road along the narrow neck of land to Great Point was washed away making an island of what had been a peninsula.

Long Island

The *New York Times* reported that there was massive beach erosion on Long Island, with the eastern and southern shores having been hardest hit. It reported that, at Westhampton Beach, tides were well above normal and that many houses were destroyed or damaged. It described the damage this way:

... the storm destroyed 18 homes and severely damaged 10 others. Some were swept out to sea, while others were whipped into scattered piles of lumber with furnishings half buried in the sand. Tides eight feet above normal deposited several feet of sand in 50 homes, and 100 others were left precariously tottering on wave-battered stilts.

The U.S. Coast Guard took part in many rescues at sea. In one mission, a USCG helicopter went down about 100 kilometres southeast of Long Island. Four of the five crewmen were rescued, but the fate of the

fifth was not reported. They had been returning from an unsuccessful attempt to rescue a lone sailor who had been adrift more than 300 kilometres south of Nantucket. That sailor was later rescued by a merchant vessel.

New Jersey

Atlantic City's famous boardwalk was damaged when the storm tide there crested almost three metres above mean high water. This was the second highest tide ever recorded there, and was within about seven centimetres of the record. Shore communities were evacuated and the governor declared a limited state of emergency in coastal counties.

Virginia and North Carolina

As was the case further north, many beaches, piers, beach homes, and coastal roads were damaged or destroyed.

South Carolina and Georgia

There were no damage reports for this section of the coast. This was because the damaging waves were coming from the northeast. This section of coast was sheltered from these waves by Cape Hatteras.

Figure 19 shows a portion of the METOC Centre Combined Wave Analysis the day most of the damage was done. It clearly shows the sheltering effect.

Florida

Florida, however, was not sheltered from the damaging waves. *The Miami Herald* of November 01 reported that most of a concrete pier near West Palm Beach had "crumbled". Surf reached four to five metres in many areas. The road which links the Florida keys with the mainland was closed. Coastal roads along almost the entire east coast of Florida were flooded or littered with debris. Beaches were washed away and sea walls were damaged.

SUMMARY

This storm was very unusual. It lasted five days and caused severe damage to coastal areas from Nova Scotia to Florida. Its effects were also felt in Newfoundland and the Gulf of St Lawrence. Most of the damage was caused by storm surges and exceptionally high waves - wind did most of the rest.

In the Winter 1992 edition of *MARINER'S WEATHER LOG*, Dolan and Davis discuss storms like this one. They offer a rating system by which extratropical storms could be classified. On the Dolan/Davis Scale, this storm earned the highest possible rating - Class 5. In the 42 years of their study, they found only seven storms which reached this intensity.

APPENDIX

A brief note with respect to the buoy anemometers:

There are two anemometers on each buoy - both about five metres above the water line. Data from both are plotted to check for consistency. On the plots, Mean1, Max1, and Dir1 refer to the primary instrument, while Mean2, Max2, and Dir2 refer to the backup.

For 44137, there appears to have been a problem. Although the two anemometers give almost identical wind speeds, their directions differ by about 30 degrees. (See Figure 3 .) The consistency of this difference suggests a simple calibration problem. Such an error has no impact on this report, but would be very important to anyone trying to reconstruct the storm's wind field.

REFERENCE

Dolan, R., and R. E. Davis, 1992; Rating Northeasters, MARINER!S WEATHER LOG Vol. 36, No. 1.

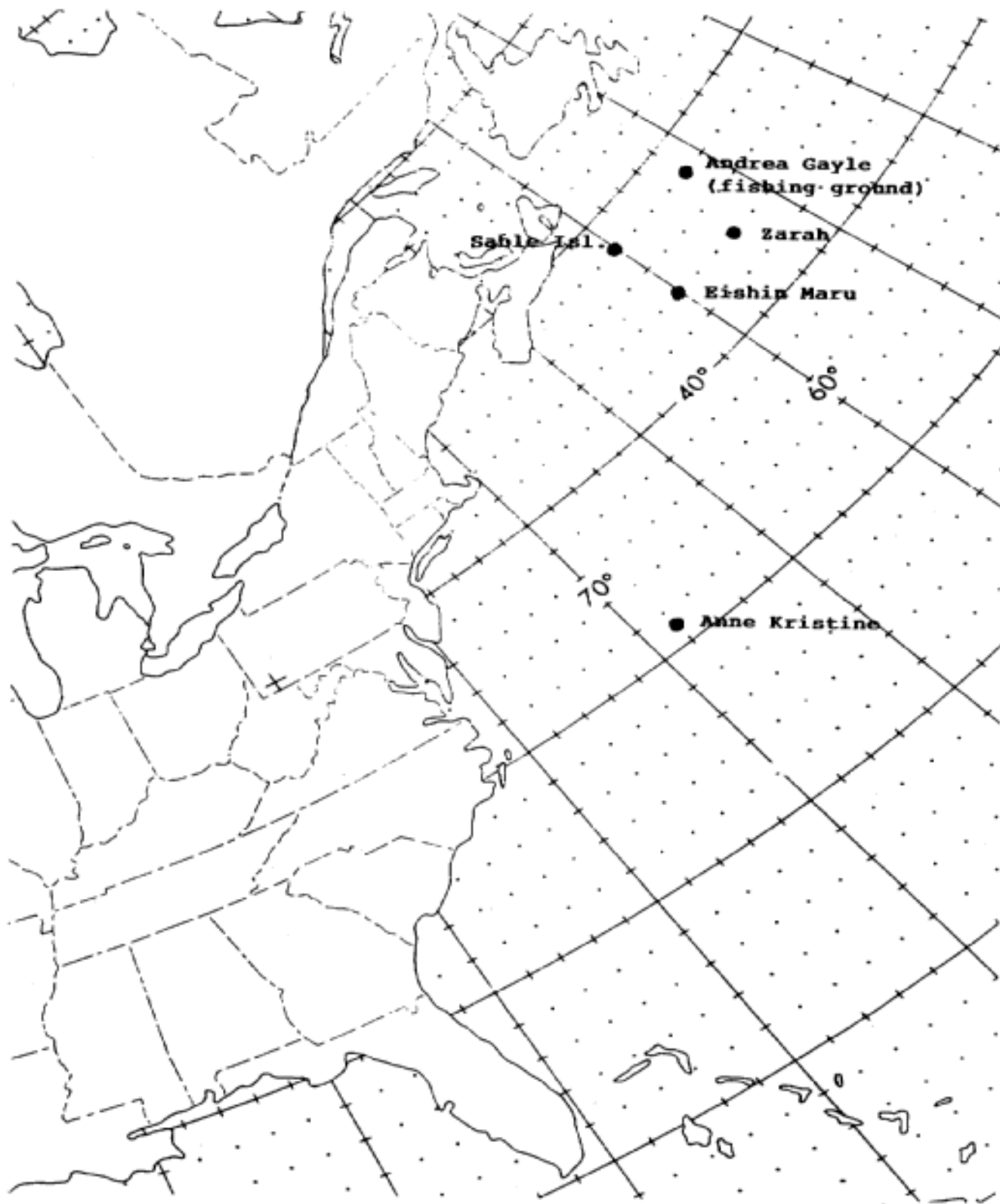


Figure 1. Locations of offshore incidents.

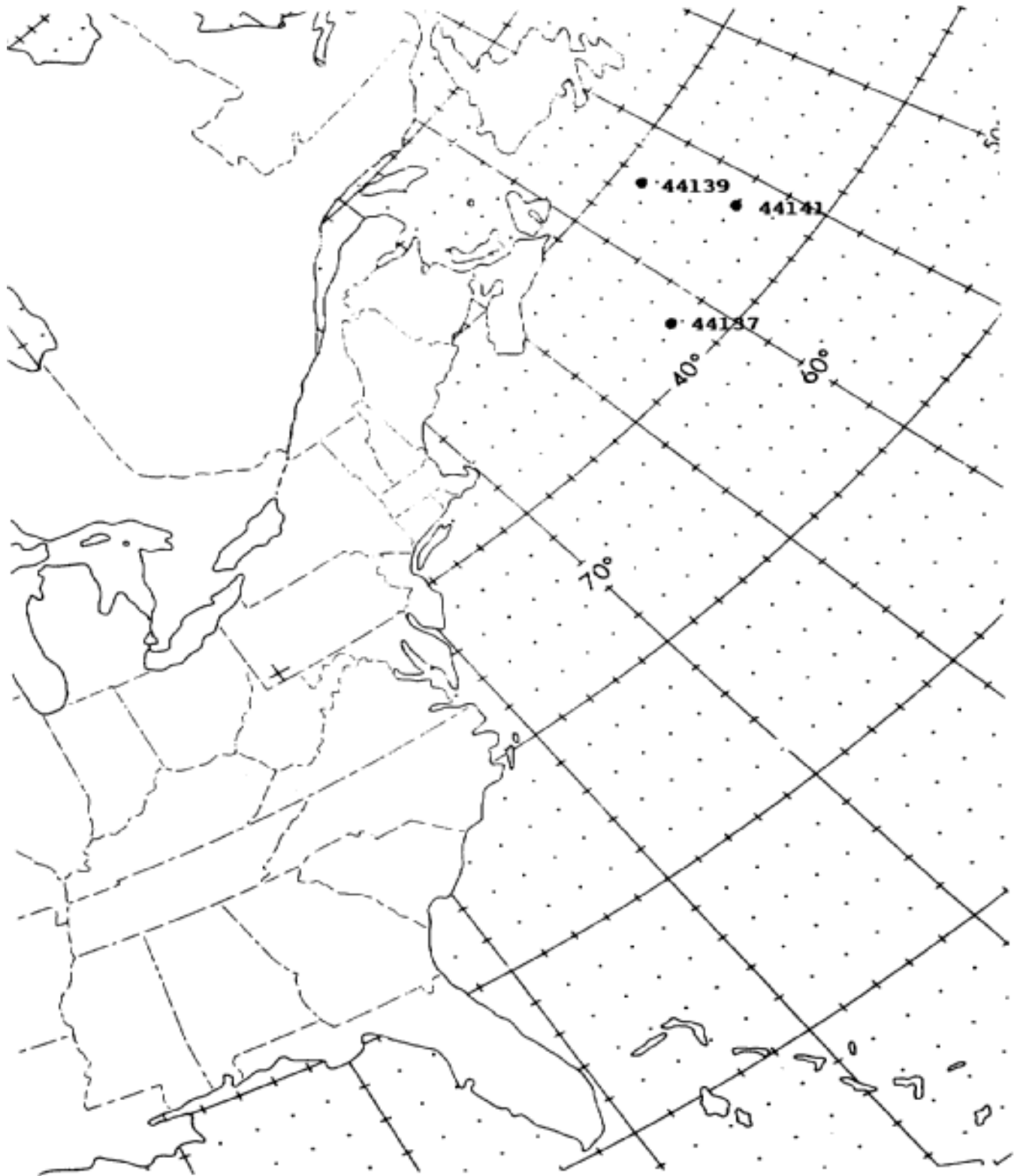
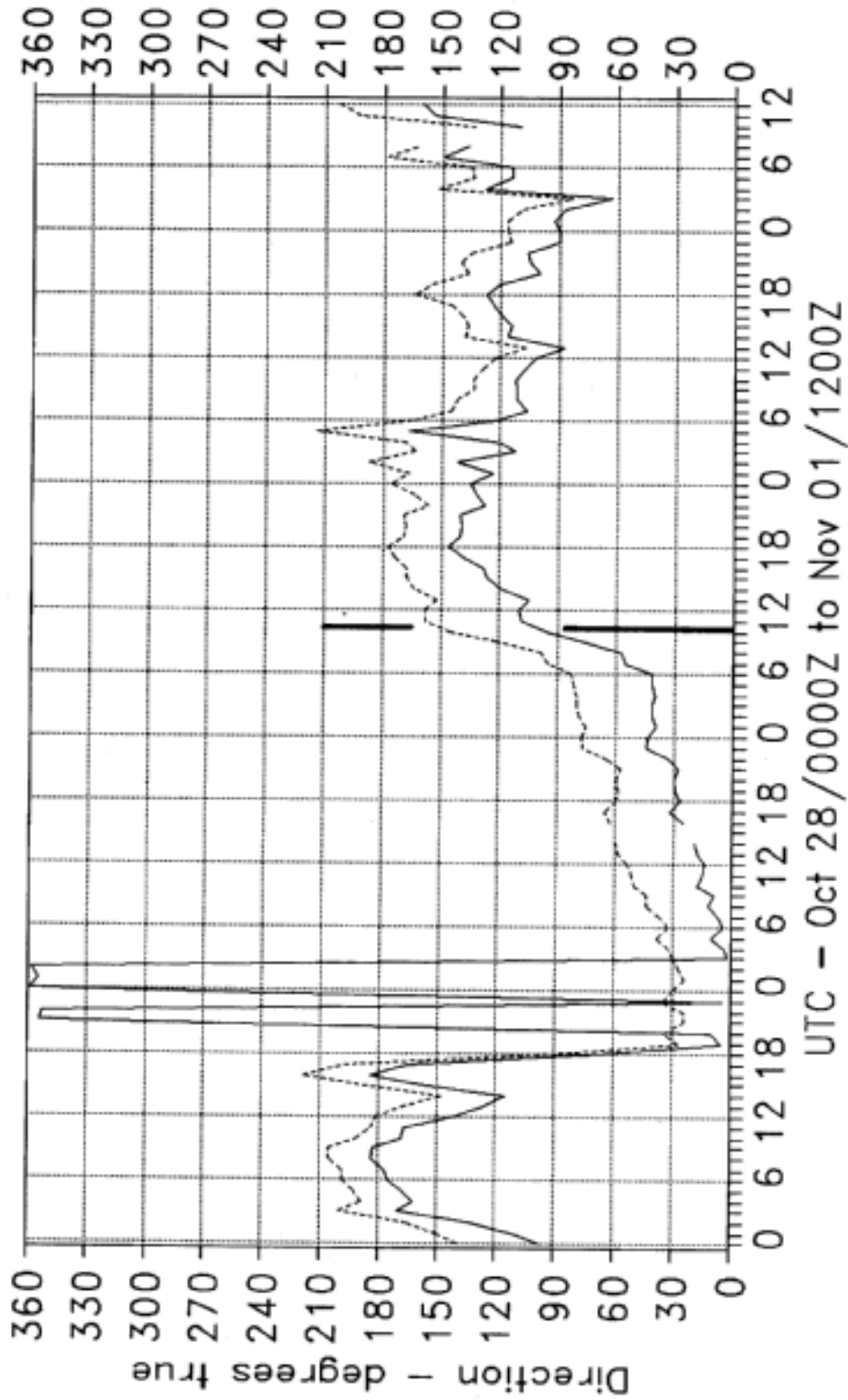


Figure 2. Canadian buoys near the offshore incidents.

Figure 3. Buoy 44137 - Wind direction
Hallowe'en Storm 1991



Dir1 Dir2

Figure 4. Buoy 44137 – Wind speed
Hallowe'en Storm 1991

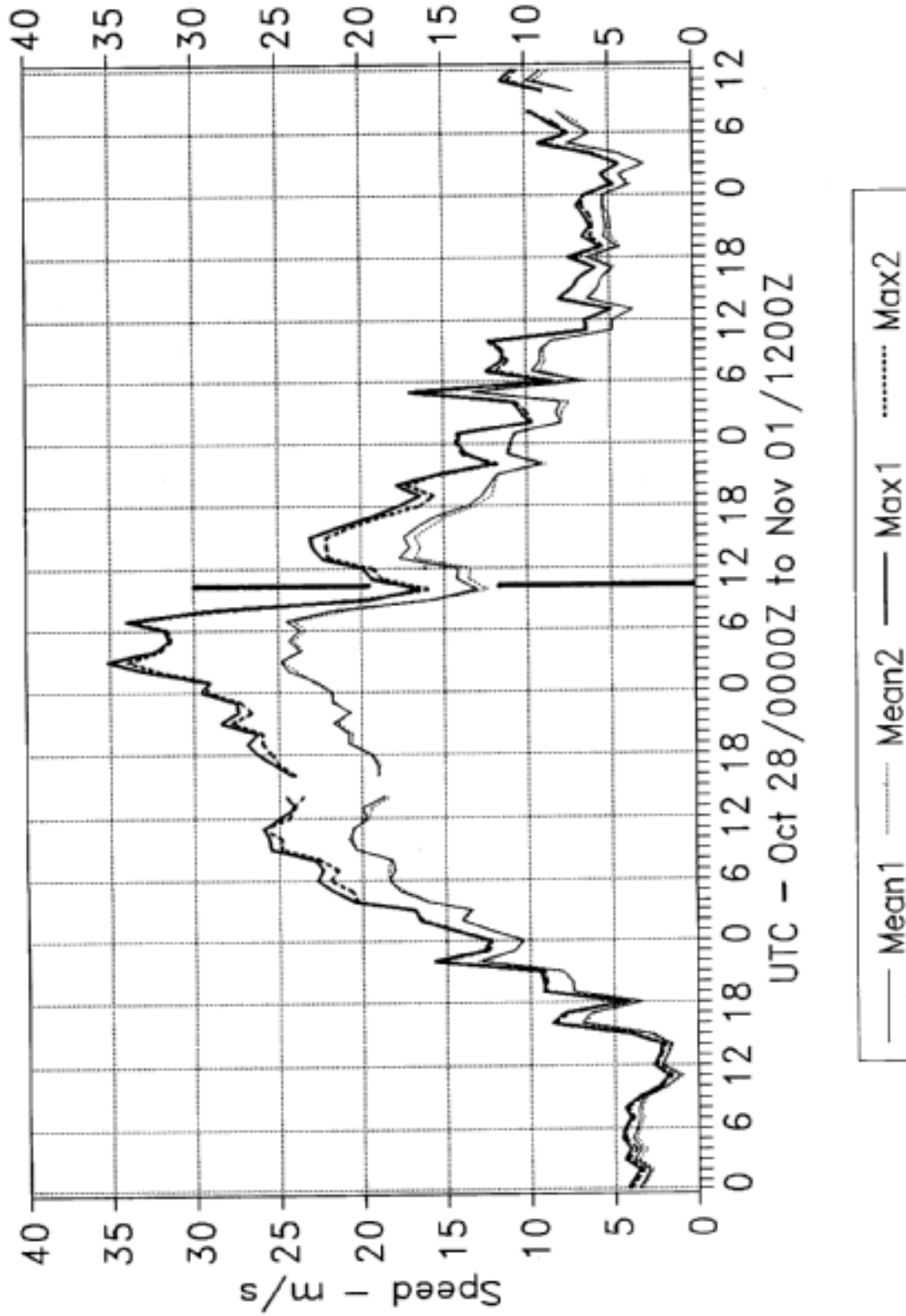


Figure 5. Buoy 44137 - Wave data
Hallowe'en Storm 1991

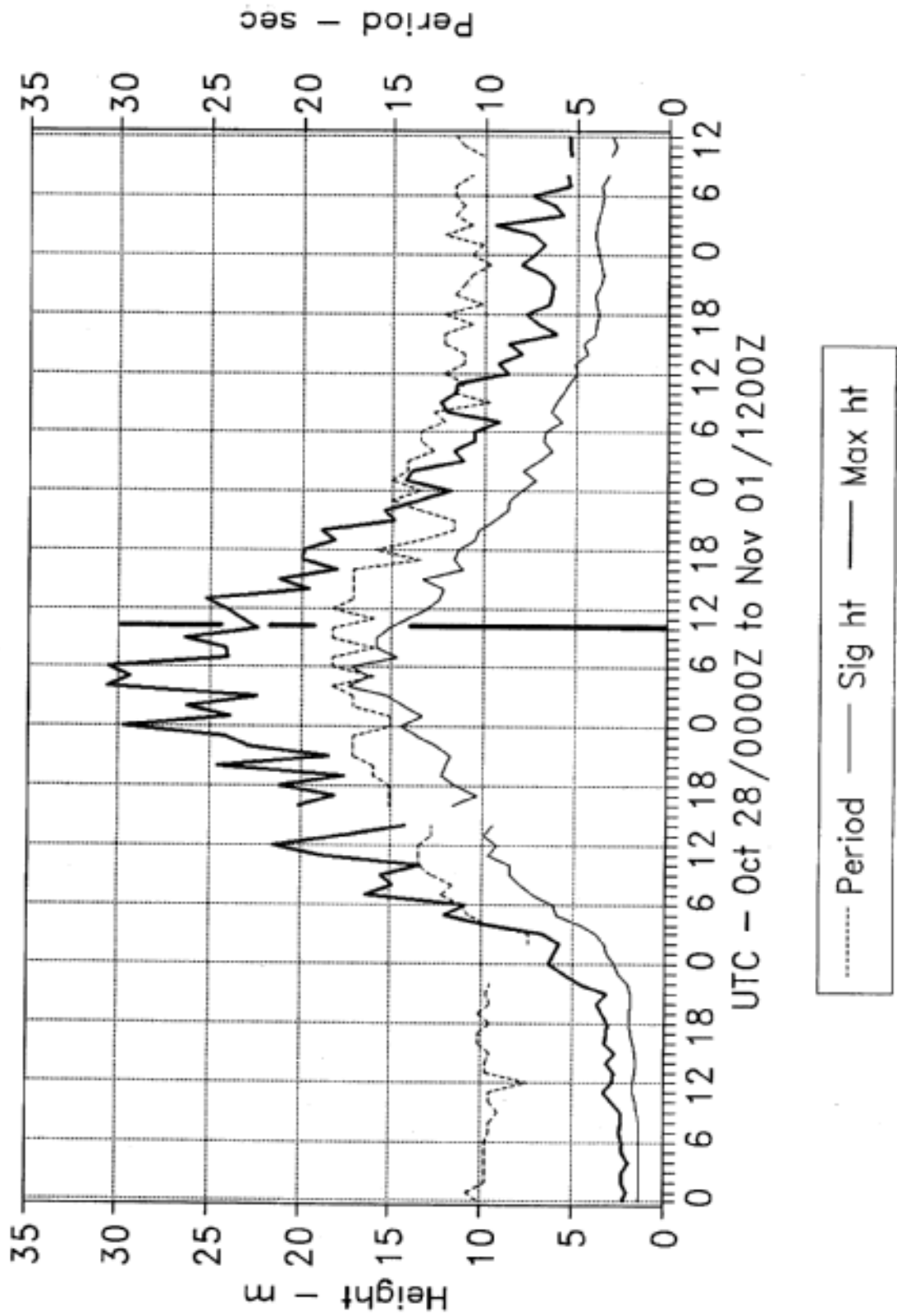


Figure 7. Buoy 44141 – Wind speed
Hallowe'en Storm 1991

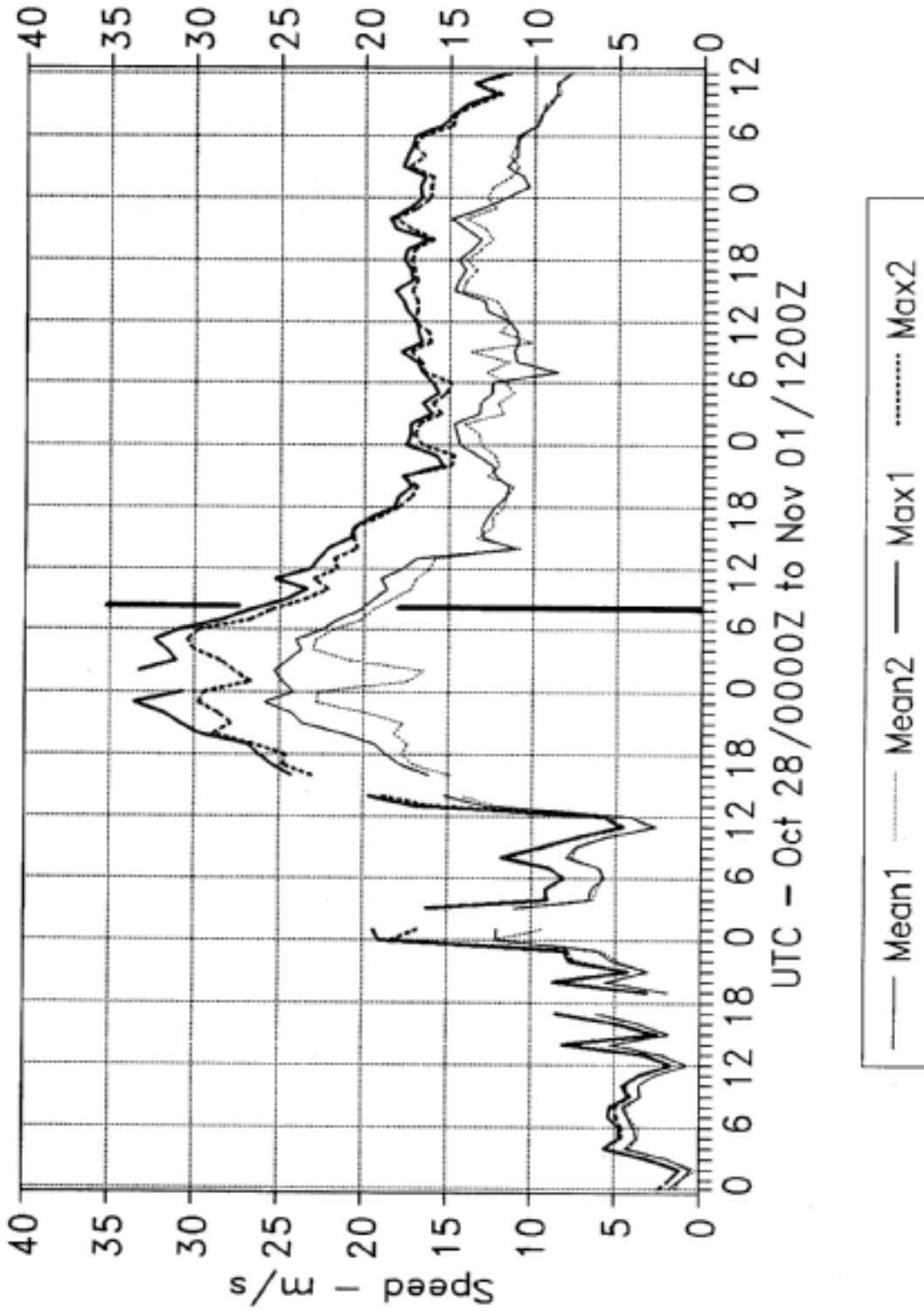


Figure 8. Buoy 44141 - Wave data
Hallowe'en Storm 1991

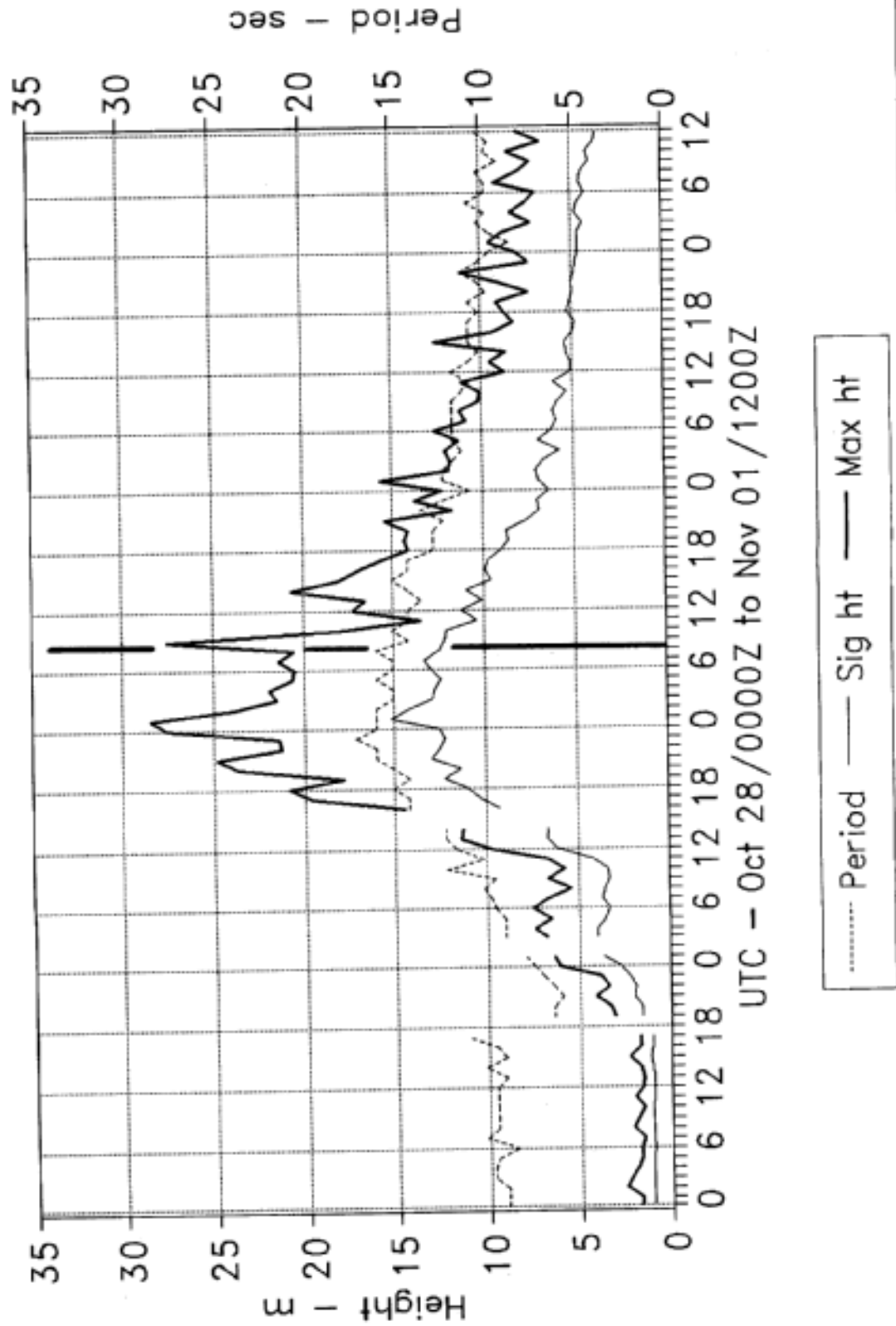


Figure 10. Buoy 44139 – Wind speed
Hallowe'en Storm 1991

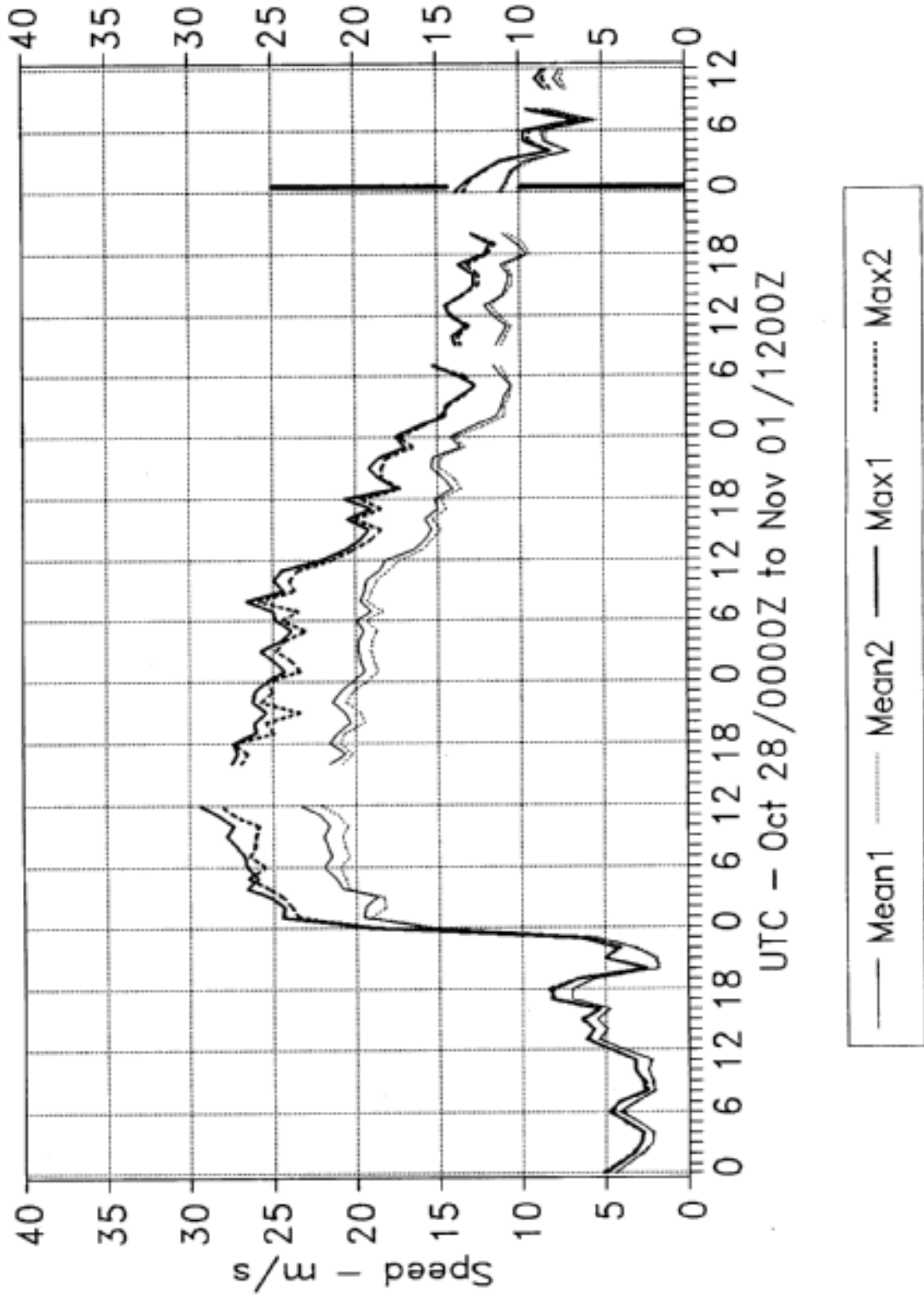
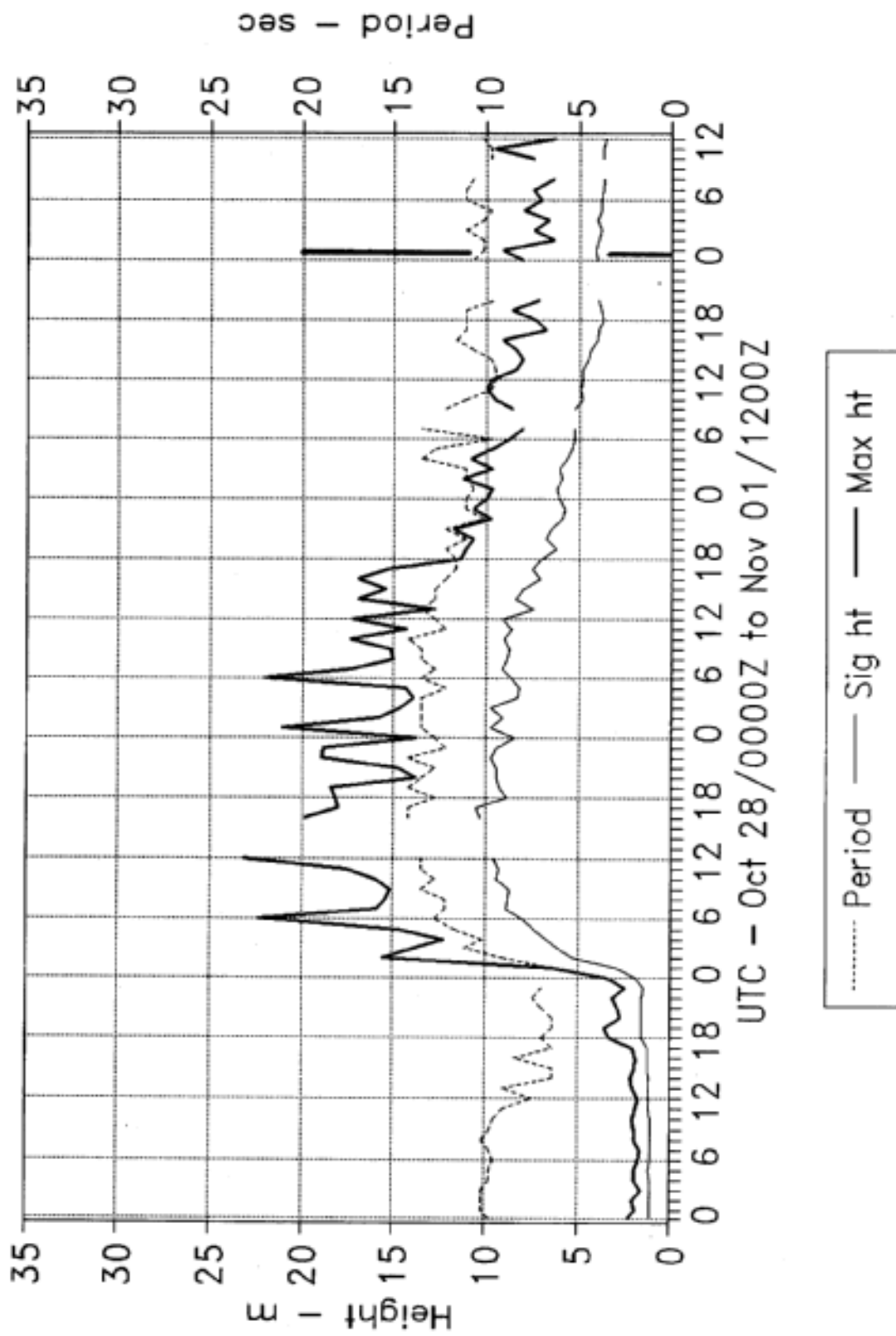


Figure 11. Buoy 44139 – Wave data
Hallowe'en Storm 1991



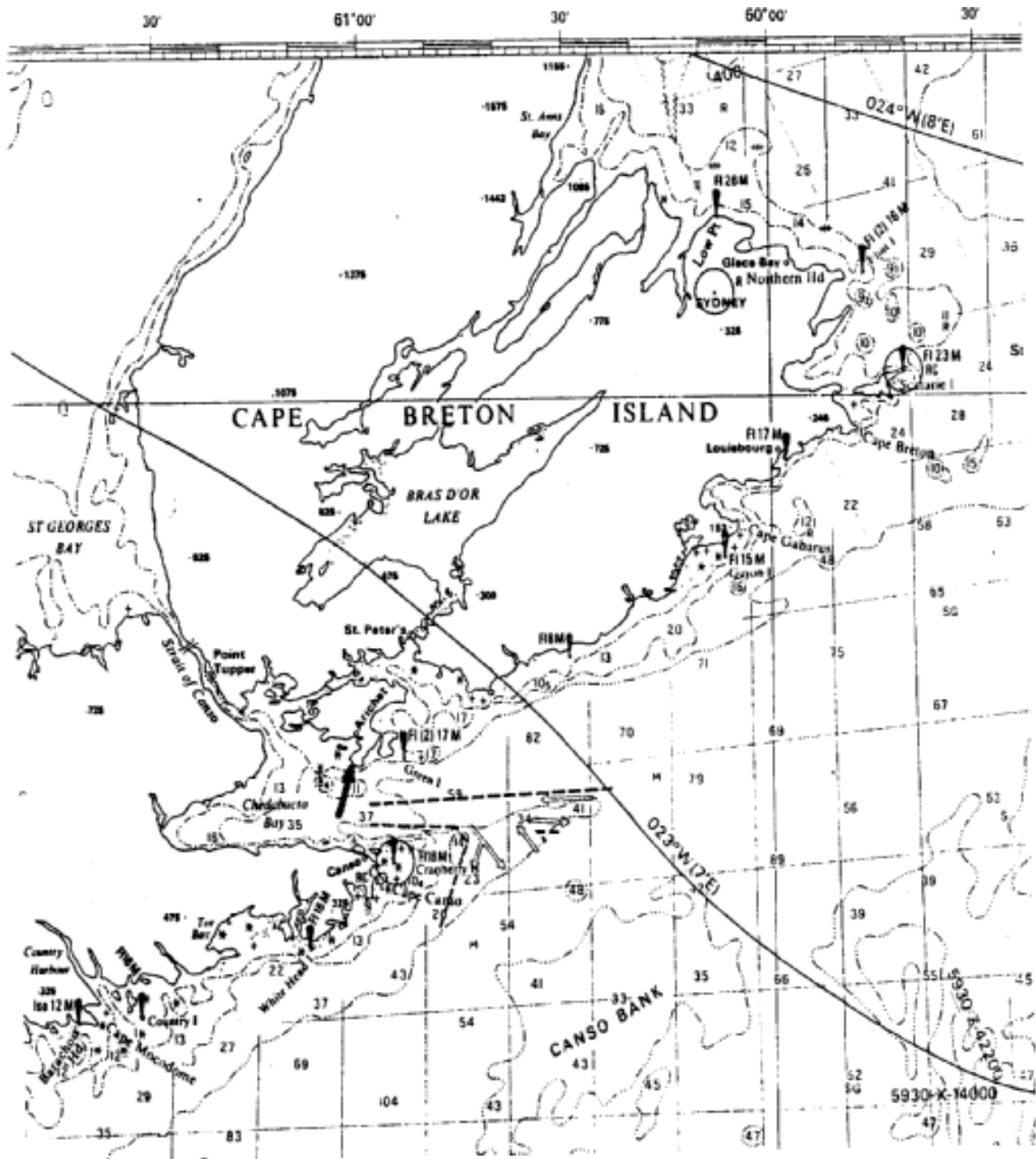


Figure 12. Arrow shows location of lobster plant.

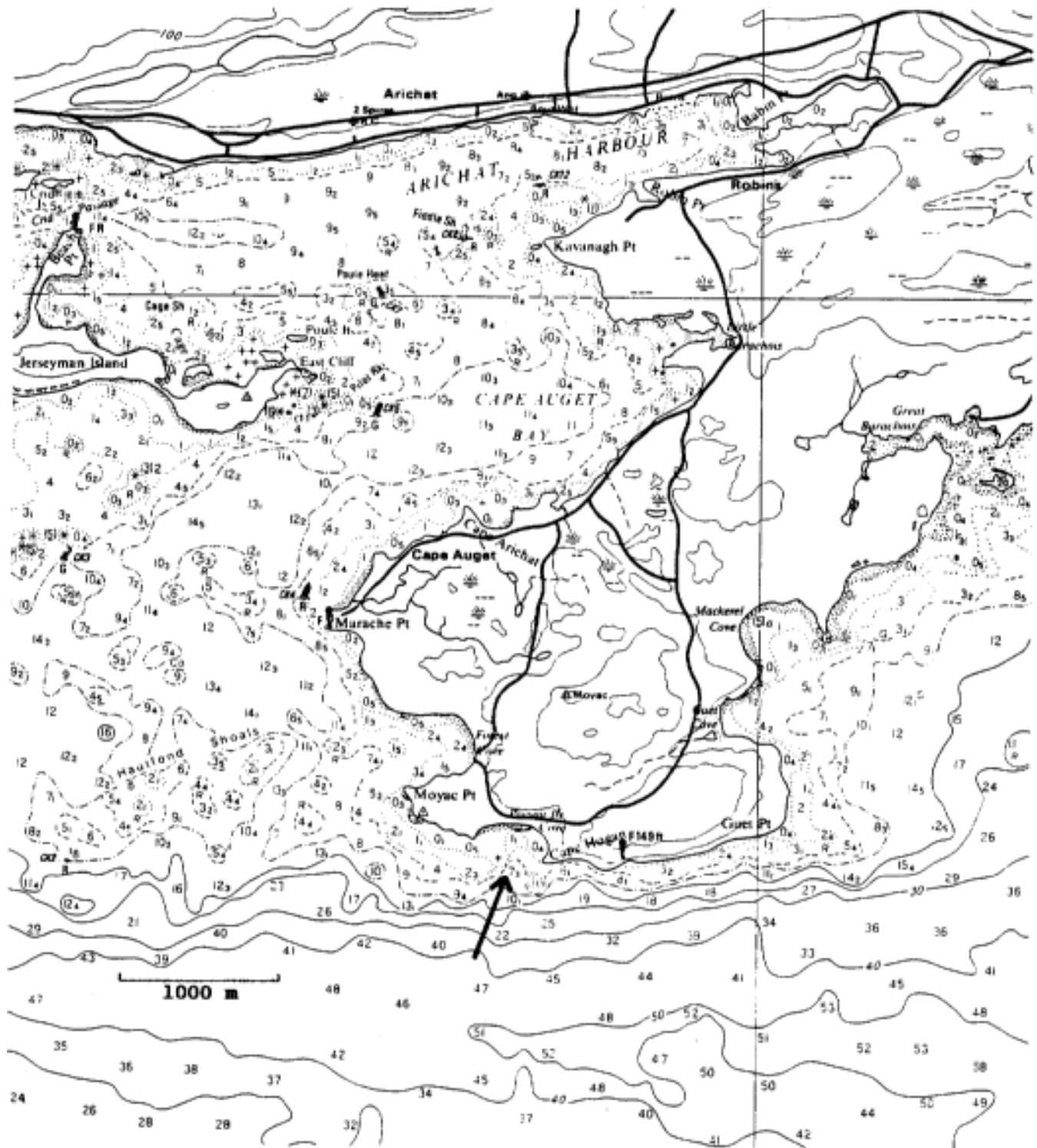


Figure 13. Plant is at Presque'ile Cove at the point where the road comes closest to the shore. Arrow indicates Presqu'ile Cove.

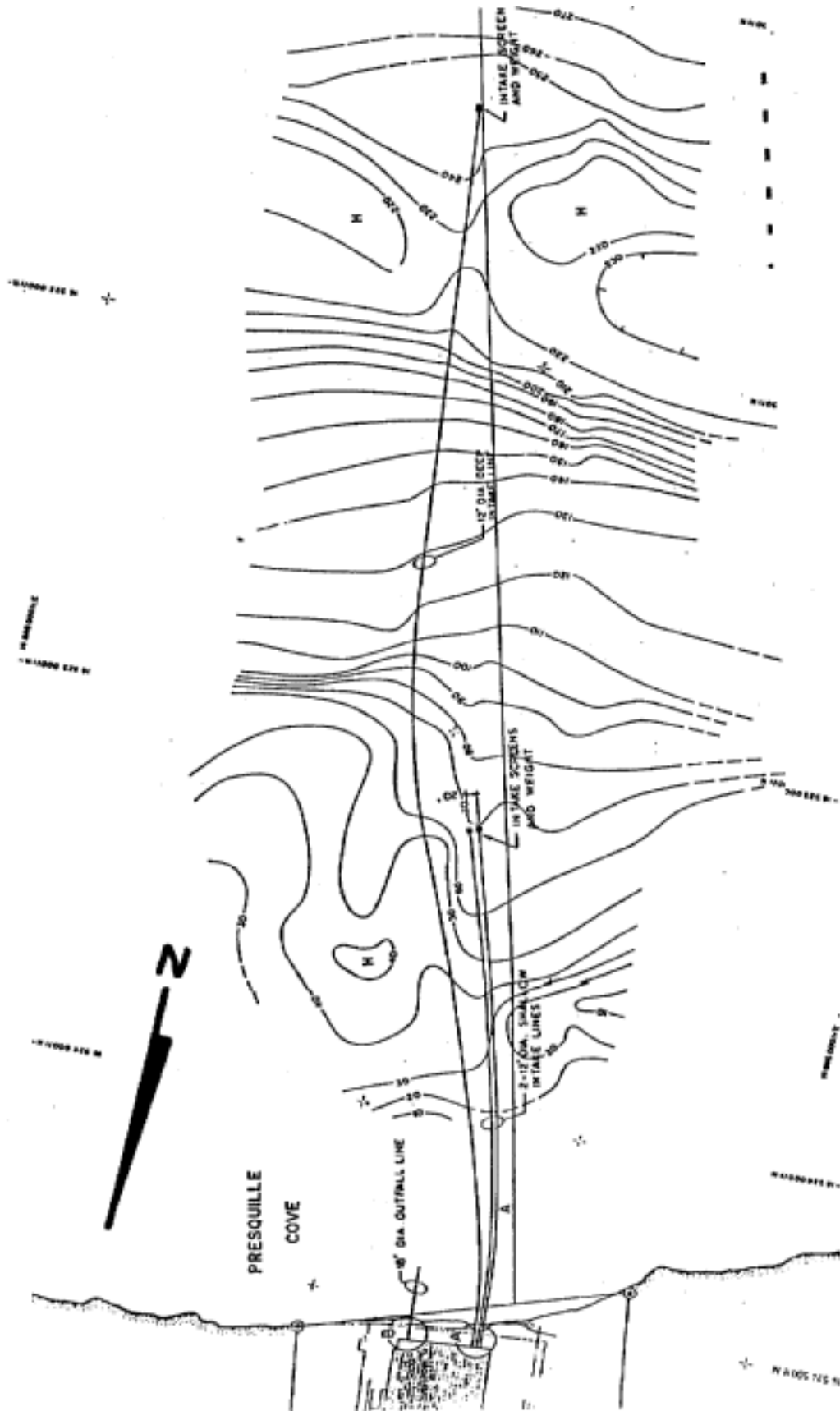


Figure 14. Intake lines at Arichat lobster plant. Depths in feet.

Figure 15. Shearwater Waverider Buoy data for Oct 28 to Nov 02 1991.

Buoy is located at 44.489N 63.416W.
(9 km ESE of Chebucto Head)

Depth is 56.7 metres.

Date	Time GMT	Max Height	Sig Height	Peak Period	Average Period
Oct	28 0603	1.79	1.23	9.5	5.2
	28 1133	1.62	1.09	10.0	5.1
	28 1810	2.45	1.55	4.4	4.3
	29 0615	4.84	3.16	7.1	6.3
	29 1134	6.36	3.66	12.5	7.1
	29 1737	6.73	3.99	12.5	7.2
	30 0555	5.90	3.96	13.3	8.1
	30 1203	6.24	4.52	13.3	8.8
	30 1736	6.88	5.27	13.3	8.7
	30 2336	8.84	5.41	9.5	8.2
	31 0610	8.27	5.07	12.5	8.5
	31 1131	7.53	4.77	11.8	8.7
	31 1733	6.27	3.91	11.1	7.6
	31 2333	5.15	3.48	9.5	7.0
Nov	01 0633	4.21	2.54	11.1	6.5
	01 1212	4.63	2.75	11.8	6.8
	02 0535	3.32	2.15	10.0	6.9
	02 1216	3.12	2.10	8.3	6.0
	02 1556	7.45	5.01	10.0	8.2
	02 1808	5.70	3.90	9.5	7.9
	02 2329	3.64	2.56	10.5	7.3

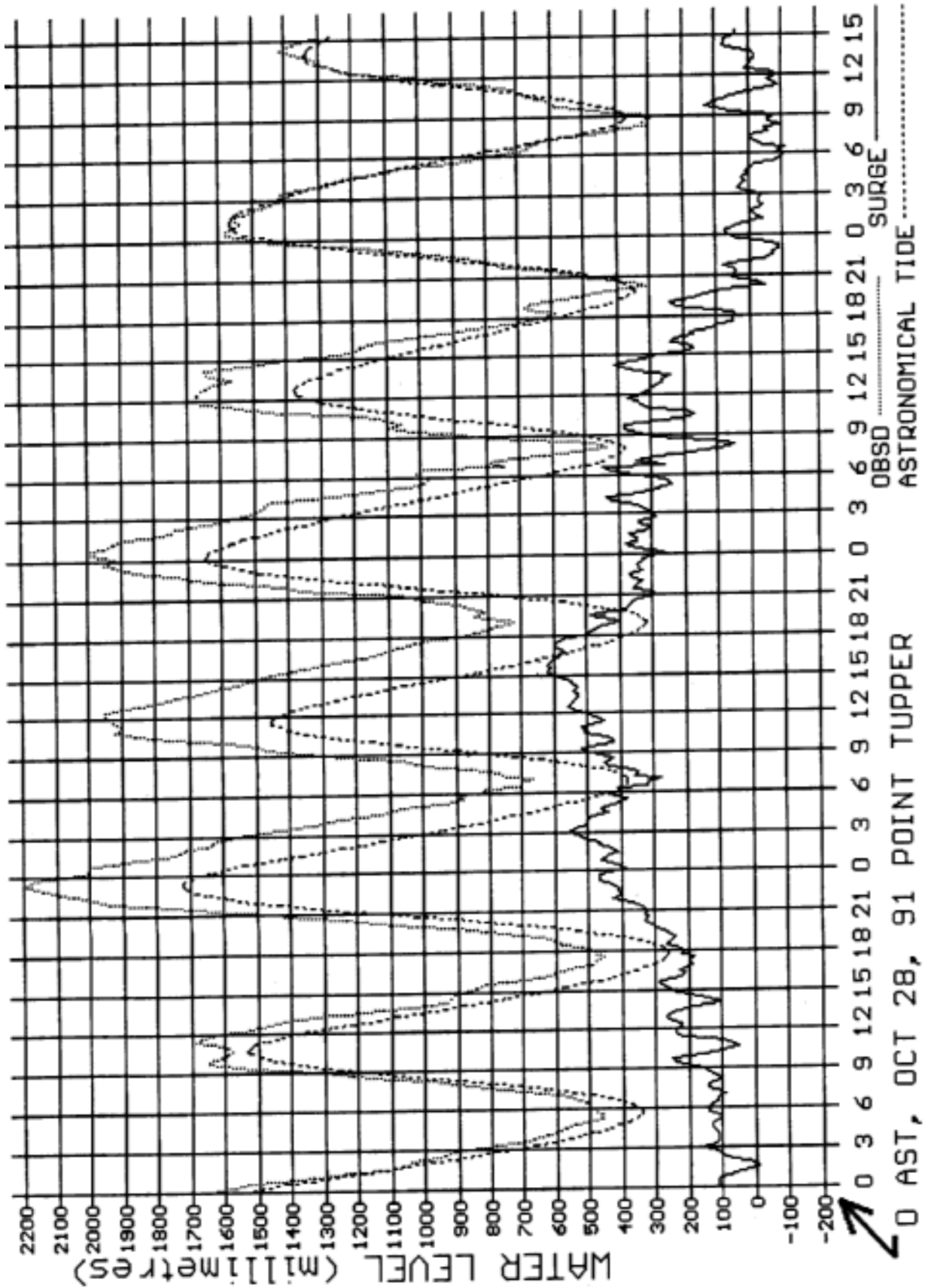


Figure 16. Tide gauge data for Point Tupper, N.S. All times are AST.

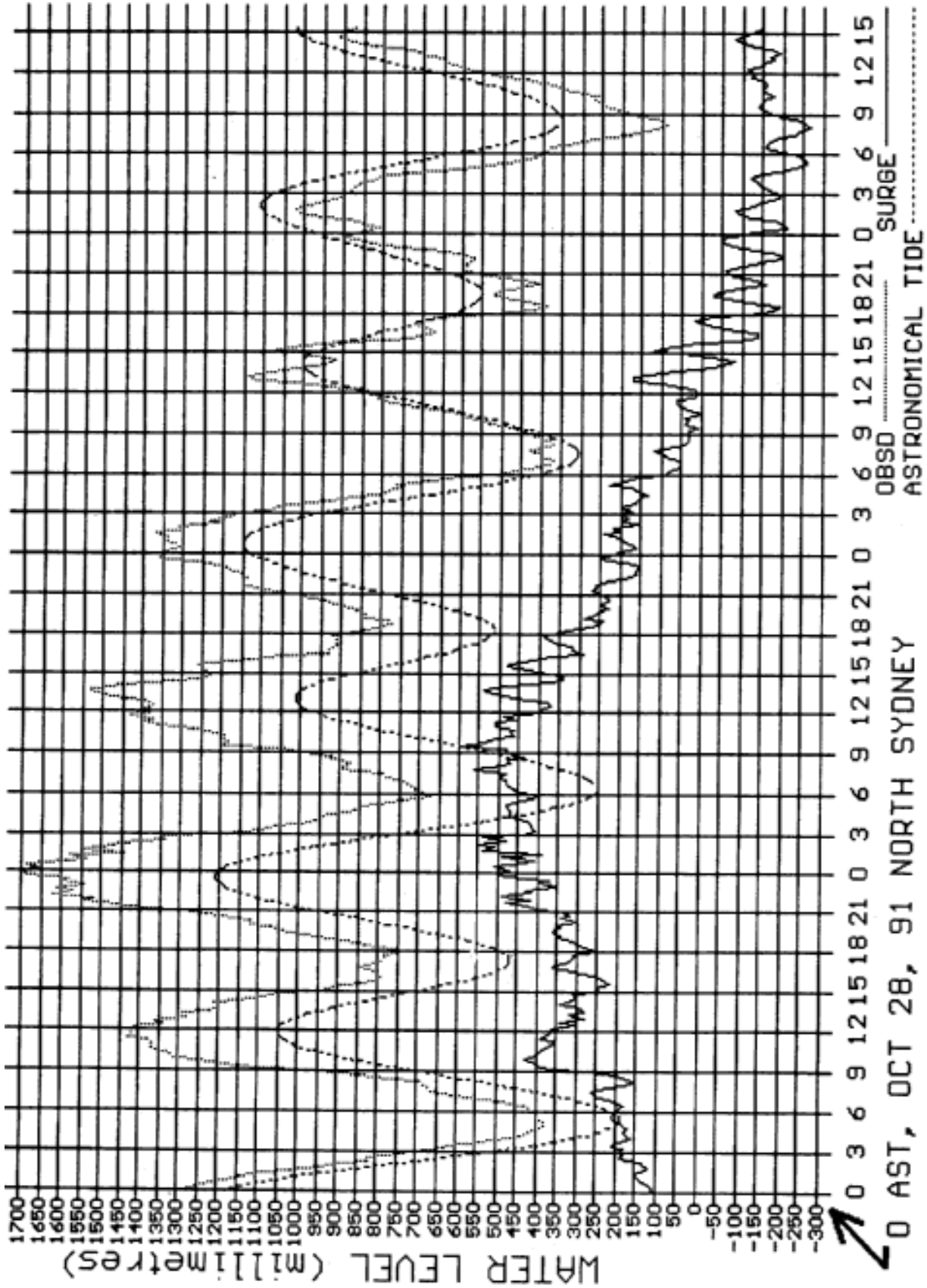


Figure 17. Tide gauge data for North Sydney, N.S. All times are AST.

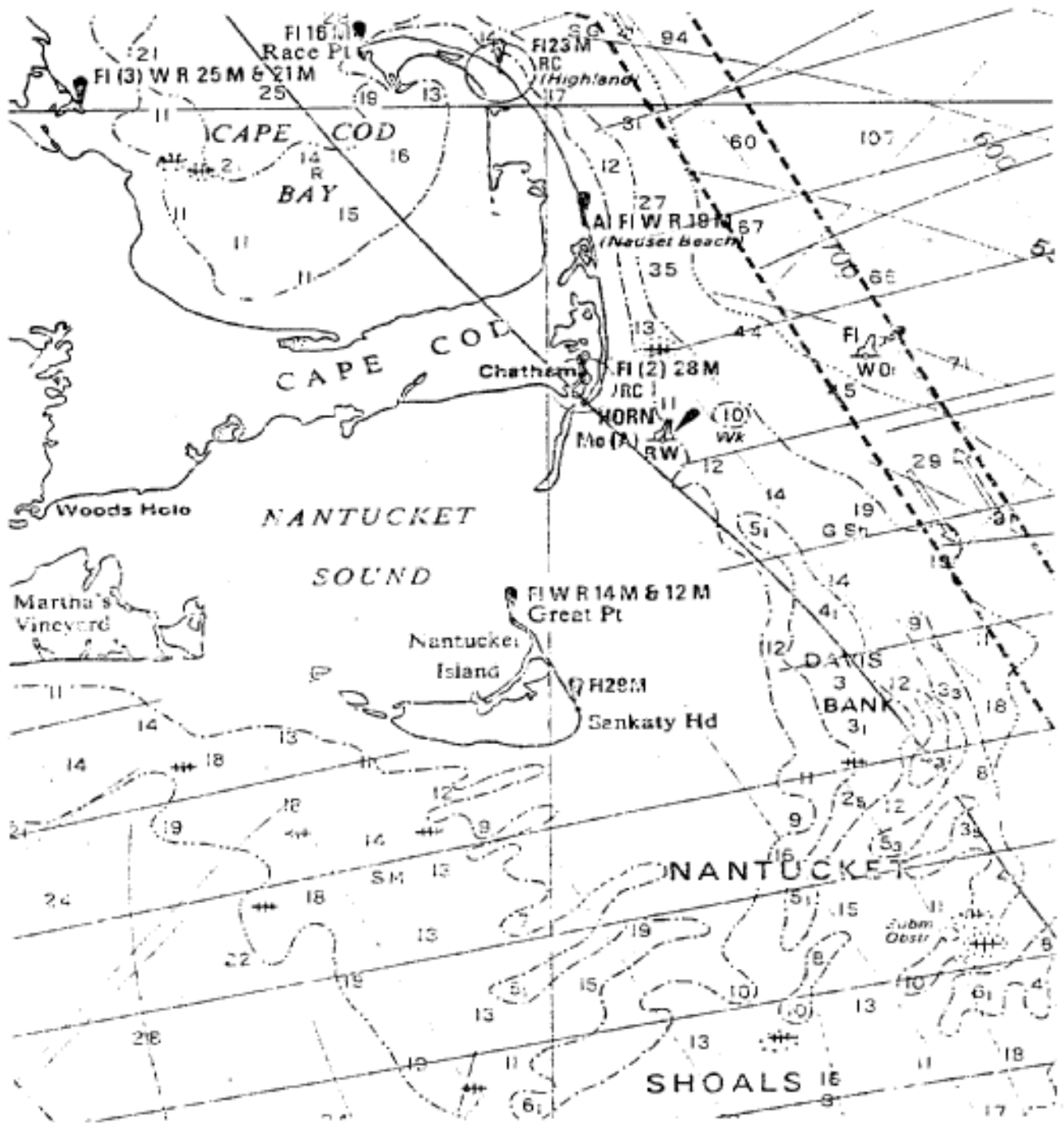


Figure 18. Nantucket Island.

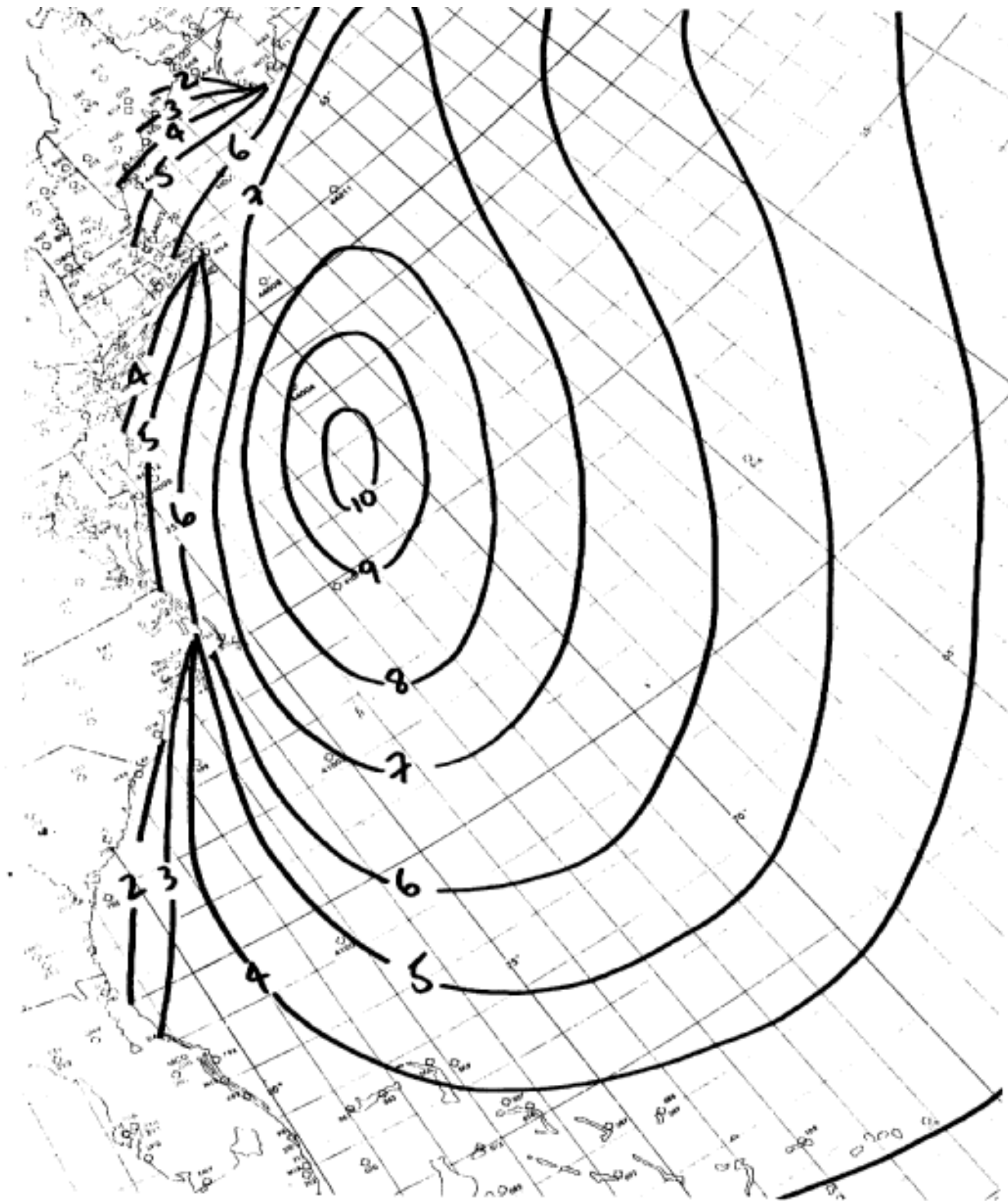


Figure 19. METOC Centre Combined Wave analysis - 911031.1200Z
Height in metres.

THE HALLOWEEN STORM: DATA OBSERVATIONS FROM NDBC STATIONS

David Wei-Chi Wang and Theodore Mettlach

Computer Sciences Corporation
Stennis Space Center, Mississippi 39529-6000

ABSTRACT

In late October 1991, an extratropical storm developed off the Atlantic coast of North America. The strong, northeasterly winds from this storm persisted for two continuous days across a fetch of more than 1800 kilometers and generated high-height, long-period waves that caused widespread damage along the U.S. east coast from Maine to Florida. The National Data Buoy Center operates moored buoy and land stations located along and offshore the U.S. east coast that reported hourly waves and other marine environmental data during the storm. This study documents the storm data from 16 of these stations to provide a very extensive field observation of the storm-generated severe seas. This data set will also be valuable for the development of wave hindcast and forecast models for years to come.

1. INTRODUCTION

Northeasters, extratropical storms that occur off the northeast coast of the United States, are a major threat to marine navigation, offshore operations, beaches, and coastal structures. Although extratropical storms are generally less powerful than hurricanes with respect to wind strength, the longer duration of such storms over a longer fetch can generate waves that exceed those from hurricanes. In March 1962, the severe seas generated by the Ash Wednesday Storm pounded the U.S. east coast for 5 days and caused tremendous damage to coastal communities.

In the last 20 years, efforts have been made to develop numerical wave models for use in storm watch/warning systems that can forecast storm-generated severe seas. Extreme waves by past severe storms were also simulated by wave hindcast models to provide design criteria for offshore and coastal structures. One of the important factors in the successful development of numerical models is verification and calibration using field measurement data. But, extensive field measurements during severe seas are rare due to the difficulties in data collection. Often, even when the data were available, they came from an insufficient number of stations that could not adequately cover the entire wave field. Extensive data collection through a network of reliable automated stations is an essential element for advancing the development of wave hindcast and forecast models.

Since 1975, the National Data Buoy Center (NDBC) has expended much effort toward long-term and regular marine environmental data

acquisition. Currently, there are more than 100 stations located along the east and west coasts of the United States, in the Gulf of Mexico, and in the Great Lakes. Environmental data from these stations are sampled hourly and distributed to users in near real time. Long-term, regular data collection from the NDBC network of stations has provided essential information about severe storms. This information has been used in many studies (Wang et al. (1989), Wang and Carolan (1991), and Graber et al. (1991)).

In late October 1991, the most powerful northeaster in the last 50 years developed off the Atlantic coast of North America. Severe seas generated by the storm pounded the east coast from Nova Scotia to Florida for a period of 72 hours. The maximum reported significant wave height reached 12 meters. Widespread beach erosion, street floodings, and the destruction of several coastal structures and ocean front properties (including the summer house of the President of the United States) gained much public attention. The severity of the storm and the extremely severe seas generated by the storm present a very interesting and important case for the verification and calibration of wave hindcast and forecast models.

This paper documents the hourly wave and meteorological data collected from 16 NDBC stations located along and offshore the U.S. east coast. This data set provides a detailed and complete field observation of the storm and its impact on the ocean.

2. THE EVOLUTION OF THE STORM

Detailed descriptions of the evolution of the October 1991 storm are given by Dolan and Davis (1992) and Pusch and Avila (1992). On October 28, a cold front extended from a weak 1012-hPa low, located 300 kilometers east of Nova Scotia, southwestward to the Carolinas. There was a massive anticyclone over northern Labrador generating north winds, with speeds of 5 to 10 m/sec along the coast from Maine to the Carolinas, pushing the cold front into the Atlantic. Hurricane Grace was west of Bermuda and was moving north-northeastward. Figures 1 (a) through 1(d) show four mean sea level pressure analyses by the U.S. National Weather Service on October 28, 29, 30, and 31, respectively.

By the next day, the Nova Scotia low had deepened from 1012 hPa to 988 hPa and had moved southeastward to near 40°N., 55°W., a position very near the axis of the Gulf Stream. The anticyclone had moved eastward across Labrador, and Hurricane Grace had merged with the cold front well north of Bermuda. A pressure gradient between the Labrador high and the west Atlantic cold front produced gale- to storm-force winds over a continuous, 1800-km fetch from Newfoundland to the Florida Straits.

By October 30, Hurricane Grace had merged with the other low at a location 750 km south of Halifax, Nova Scotia. The combined energy of

the two systems produced a vigorous, 972-hPa, storm-force low with maximum sustained winds of 30 m/sec. As the Canadian high moved southeast, strong winds persisted from Nova Scotia to Florida for the second day.

After reaching maximum intensity, the low moved southwestward, then southward, and then weakened. As it moved over the warm waters of the Gulf Stream convection increased, and the system began taking on the characteristics of a subtropical cyclone. The movement of this low is shown in Figure 2 . On November 1, the storm became a subtropical storm, and on November 2 it was observed by Air Force Reserve Unit aircraft to have all the characteristics of a hurricane; but, by this time, most of the coastal damage from severe seas had already occurred.

3. DATA MEASUREMENT SYSTEM

Table 1 lists information about the NDBC network in place during the storm. There were both moored buoys and automated headland stations. The headland stations are called Coastal-Marine Automated Network (C-MAN) stations. Table 1 identifies moored buoy and headland stations located along and offshore the entire stretch of the U.S. east coast, while Figure 2 is a location map of all these stations and the track of the storm.

Stations 44007, 44013, 44025, 44012, 44009, 41008, and 41009 are located nearshore along the coast; stations 44011, 44008, and 44014 are located offshore on the edge of continental shelf; and stations 41001, 41002, and 41010 are located offshore in deep water. The three C-MAN stations are located at light stations: Diamond Shoals lighthouse, North Carolina (Station DSLN7); Ambrose lighthouse, New York (Station ALSN6); and Chesapeake Bay lighthouse, Virginia (Station CHLV2).

Each station was equipped with a wave measurement system and a meteorological measurement system. Data were collected hourly and then relayed through the Geostationary Operational Environmental Satellite (GOES) to NDBC for further data processing and quality control.

The wave measurement system on the moored buoys used an accelerometer to record buoy heave motion. An NDBC onboard Wave Data Analyzer computes the wave spectral data from the time series of buoy motion. The details of the NDBC wave measurement system and data processing technique are described by Steele et al. (1990). Two stations (44014 and 44025), sponsored by the U.S. Army, Coastal Engineering Research Center (CERC), provided the directional wave data. Directional wave data are estimated from records of the buoy's heave, pitch, and roll motions based on the approach proposed by Longuet-Higgins et al.

with the peak of wave spectrum (peak wave period), wind speed, wind direction, air temperature, water temperature, and barometric pressure at the time of maximum significant wave heights. The approximate water depth at each station is also given. As seen in the table, the largest significant wave height during the storm from all the stations was 12 meters at station 44011, which is located about 280 kilometers east of Cape Cod, Massachusetts, in the continental shelf waters of Georges Bank. The maximum reported significant wave heights from those offshore stations exceeded 5 meters with the peak wave periods ranging from 16.7 seconds to 25 seconds. The relatively low pressures at stations 44011 and 44008 were 996.6 hPa and 994.4 hPa, respectively, which indicate a close proximity to the storm center.

Table 2. Observed wave and meteorological data by NDBC stations during the storm.

Station	Hs	Tp	Wspd	Wdir	Atmp	Wtmp	Barp	Time	Depth
44007	6.92	14.29	14.67	28	7.7	9.8	1021.0	31/0200	47
44013	9.06	16.67	21.99	29	8.6	11.0	1014.9	31/0200	30
44011	12.00	16.67	26.26	26	9.8	13.6	996.6	30/1600	88
44008	9.56	12.50	25.34	291	11.0	12.8	994.4	30/2300	60
ASLN6	3.11	12.50	15.54	51	11.1	14.6	1012.8	31/0900	25
44025	5.05	11.11	17.78	25	12.4	15.2	1010.1	31/1000	40
44012	4.72	25.00	12.31	14	15.6	15.6	1012.5	31/0002	24
44009	4.81	14.29	14.40	20	12.2	15.7	1011.0	31/1200	18
CHLV2	4.03	20.00	9.43	339	16.0	17.1	1013.5	31/0500	12
44014	8.05	16.67	10.51	328	15.7	14.8	1012.7	31/0300	48
DSL7	6.82	16.67	8.57	320	14.3		1012.0	31/1000	16
41001	8.13	20.00	12.50	336	17.3	23.7	1009.7	31/0000	4206
41002	7.94	20.00	8.07	340	20.5	24.1	1012.4	31/0900	3658
41008	2.86	7.69	12.40	60	21.9	22.7	1023.6	30/0500	18
41010	5.18	20.00	3.60	305	23.4	26.1	1016.9	31/1830	833
41009	5.56	20.00	2.36	318	21.5	25.8	1018.0	31/1830	41

Hs: maximum significant wave height in meters Wtmp: sea surface water temperature in °C
 Tp: peak wave period in seconds Barp: sea surface barometric pressure in hPa
 Wspd: wind speed at 10-meter height in m/sec Time: day and UTC hour of the Hs
 Wdir: wind direction in degrees Depth: water depth in meters
 Atmp: sea surface air temperature in °C *: sensor failure

In the present study, the data from four stations are selected for further analysis. Data from the two offshore stations represent conditions in the northern (station 44011) and southern (station 41010) portions of the NDBC network. Data from the two nearshore stations (stations 44013 and 44014) give the representative wave field in the nearshore area where significant coastal damage was reported.

4.1 STATION 44011

Figures 3 (a) through 3(f) show the data measured at station 44011 from October 27 to November 3, 1991. This station was moored about 280 kilometers east of Cape Cod, Massachusetts, in a water depth of about 88 meters. As seen in Figure 3 (b), as the cold front passed on October 28, the wind speed increased rapidly from about 2 m/sec to about 20 m/sec, with the wind direction (see Figure 3 (e)) shifting from about 320 degrees (northwest) to about 10 degrees (north). In the meantime, the significant wave height (see Figure 3 (a)) increased from less than 2 meters to about 6 meters. In the next 24 hours (October 29), the significant wave height gradually increased to about 8 meters, while wind speed and wind direction remained nearly constant at about 20 m/sec and around 10 degrees, respectively. Also, during this period the air temperature (see Figure 3 (f)) gradually dropped from about 15°C to about 6°C. In the early hours of October 30, the wind gradually shifted to the northeast with the wind speeds increasing to greater than 25 m/sec and the barometric pressure (see Figure 3 (c)) gradually decreasing to 990.50 hPa. Strong northeasterly winds further increased the significant wave height to the maximum of 12 meters at 1600 UTC, October 30, with a peak wave period of 16.7 seconds. During that hour, the wind speed was 26.4 m/sec and the wind direction was 24 degrees. The 12 meter significant wave height was the largest significant wave height reported from all the stations during the storm. After the peak, the wind speed decreased significantly, while the wind direction shifted to east. During the next 24 hours, the significant wave height gradually decreased to about 4 meters. Through the course of these 8 days, the water temperature decreased gradually from approximately 14°C to 11°C.

4.2 STATION 41010

Figures 4 (a) through (f) show the data measurements from station 41010, which is located 290 kilometers east of Cape Canaveral, Florida, in a water depth of 833 meters. The data from this station provide representative observations of the effects of the storm along the southern portion of the U.S. east coast. As can be seen in Figure 4 (a), before the easterly wind increased to 13 m/sec on October 29, the waves were predominantly long-period swell with a significant wave height around 2.7 meters and a peak wave period of about 12.5 seconds. On October 29, the significant wave height gradually increased from about 2.7 meters to 4 meters. The wind then started to decrease in the early hours of October 30 as the wind direction shifted counterclockwise from east to northwest. However, the significant wave height increased to 5 meters with a 20-second peak period. The increase in sea state was due to the arrival of long-period swells, which were observed earlier at other stations to the north (stations 44011, 44008, 41001, and 41002).

4.3 STATION 44013

Figures 5 (a) through 5(f) show the data measurements from station 44013, which is located outside Boston Harbor in a water depth of 30 meters. Data reported from this station provided a field observation of sea state in this nearshore region during the storm. As seen in Figure 5 (a), on October 28 the significant wave height started to increase from less than 1 meter to about 3.5 meters in about 15 hours. The dramatic increase of significant wave height was due to the increase of wind (see Figures 5 (b) and 5 (e)) which shifted from southwest at 5 m/sec to northeast at about 15 m/sec, as the cold front passed. A similar shift in wind direction occurred along the entire northeast coast, setting up long fetch for wind-wave growth. For the next 96 hours the wind direction remained between 10 to 30 degrees. The wind speed gradually increased to 22 m/sec in the early hours of October 31, as the significant wave height increased to 9 meters with a 20-second peak period. These high-height, long-period waves caused significant beach erosion and damage to ocean-front properties. The air temperature (see Figure 5 (f)) started to drop from 19.1°C at 2100 UTC of October 27 down to 3.5°C at 1200 UTC of October 29, as the barometric pressure (see Figure 5 (c)) increased from 1017 hPa to 1034 hPa.

4.4 STATION 44014

Figures 6 (a) through 6(f) show the data measurements from station 44014, located about 80 kilometers east of Virginia Beach, Virginia, in a water depth of 48 meters. In addition to the nondirectional wave measurements, this station also provided directional wave measurements.

The wind speed (see Figure 6 (b)) started to increase significantly on October 28 from 8 m/sec to 15 m/sec over a 12-hour period, while the wind direction remained from the north (see Figure 6 (e)). In the meantime, the significant wave height (see Figure 6 (a)) gradually increased from 2.5 meters to 4.3 meters. It is noted that the changes in wind speed on October 28 were also observed by the three stations discussed above and are related to the development of a cold front as described in Section 2 . The significant wave height remained at about 4.5 meters for the next 36 hours as the wind speed varied from 12 m/sec to 14 m/sec and the wind direction shifted to northwest. At 1000 UTC of October 30, 1991, the significant wave height began to increase from 4.5 meters to 8 meters by the early hours of October 31, 1991. It is noted that as the significant wave height reached 8 meters the wind speed decreased to 10 m/sec with the wind direction shift to the more fetch-limited direction of northwest. It is apparent that the

severe seas were due to the arrival of long-period swell observed earlier at stations 44011, 44013, and 41 01 0 as discussed previously.

Figures 7 (a) and 7(b) show the directional wave data at 0200 and 0300 UTC, October 31, when the significant wave height reached 8.05 meters and the peak period exceeded 17 seconds. The directional wave data show that the wave directions at higher frequencies aligned with the local wind directions (about 330 degrees). The direction of lower frequency waves was about 75 degrees. This direction is inconsistent with the placement of the storm but can be explained by refraction of long-period waves in shallow water. Before reaching this station, 20-second wave energy may have been significantly refracted as it traveled over the continental shelf.

5. DISCUSSION

This large data base consists of wave and meteorological data produced under storm conditions. Several interesting observational results are presented for further discussion.

5.1 THE HIGH-HEIGHT, LONG-PERIOD SWELL

As shown in Table 2 , high-height, long-period swell significantly raised the sea state along the Florida coast (stations 41009 and 41010), while the local winds were very mild. These swells were generated by nearly continuous northeasterly gale- to storm-force winds that blew from west of the storm center to Cape Hatteras. These swells propagated southwestward and caused serious beach erosion and property damage along the U.S. east coast.

Figures 8 (a) and 8(b) show time series plots of the wave energy at frequencies of 0.05 and 0.06 Hz (20 seconds and 16.7 seconds) from stations 44011, 44008, 41001, 41002, and 41010. These offshore stations covered the area from Georges Bank to Cape Canaveral, Florida. As can be seen, the wave energy appeared at station 44011 with a high level of energy (the energy peak at 0.06 Hz was about 200 m^2/Hz), which was at least 250 percent of that value measured from other stations. Station 44011 is located about 1700 km northeast of station 41010. It takes about 31 hours for wave energy at 0.05 Hz to travel between these two stations with a traveling speed of about 56 kilometers/hour. This 31-hour time period agrees well with the time lag shown on the time series plot of 0.05 Hz wave energy at stations 44011 and 41010. This indicates that the high-height, long-period swell was probably from the northeast, and is consistent with the weather condition shown from the surface synoptic chart (Figure 2). It is noted that the wave direction of 0.05-Hz energy at station 44014 (Figure 7) was about 75 degrees, but the waves may have been significantly refracted due to the rather shallow water depth (48 meters).

5.2 GROWTH OF WIND-WAVE IN THE PRESENCE OF SWELL

Due to the effects of Hurricane Grace, the wave field at station 44011 was predominated by the long-period, southeasterly swells generated from the northern and northeastern sides of the hurricane before the rapid increase of local wind on October 28. As the local wind speed began to rapidly increase in the direction of about 10 degrees, an interesting case of wind-wave evolution in the presence of swell became evident.

Figures 9 (a) through 9(c) show the time series of significant wave height, wind speed, and wind direction at station 44011 from 0300 UTC to 2300 UTC, October 28, 1991. In the 10 hours (1100 UTC to 2100 UTC), the wind speed rapidly increased from 2 to 20 m/sec, the wind direction shifted to the north, and the significant wave height increased from 2 meters to 6 meters.

Figure 9 (d) shows the evolution of hourly wave spectrum from 1100 UTC to 2100 UTC of October 28. The wave energy increase began at the high-frequency end of the spectrum and moved to lower frequencies in time, due to the combined effects of the input of wind energy, the resonant nonlinear interactions, and wave breaking.

Before the wind-generated energy appeared at the high frequency end of the spectrum, the slope in the higher frequency ranges of swell-dominated spectra (0.10 to 0.35 Hz) was about -5. The wind-generated energy started to increase at the high frequency end at a much higher level than those of swell-dominated spectra and gradually moved into the lower frequency portion of the wave spectrum, while a slope of -5 at high frequency end generally remained. The effect of the presence of swell on the wave evolution process has been demonstrated from laboratory data (Donelan, 1987). This data set provides a field observation about wave spectrum evolution under the influence of strong swells, which could be an interesting subject for further study.

5.3 EFFECTS OF BOTTOM FRICTION

Due to the wavelength of the long-period swell, energy dissipation due to bottom friction affected the waves at most of the buoy and C-MAN stations. A 20-second wave will "feel" the bottom at a water depth less than 300 meters, which is greater than the depth of water at all but the three deep-water stations: 41001, 41002, and 41010. Hence, the proper estimation of the energy dissipation due to bottom friction plays a key role for successfully modeling waves observed from NDBC nearshore stations during the storm. Station CHLV2 (water depth of 12 meters) was located 86 km west of station 44014 (water depth of 48 meters). The long period swell passed by station 44014 before arriving

at station CHLV2. Figures 10 (a) and 10(b) show the time series of wave energy at 0.05 Hz and 0.06 Hz for stations 44014 and CHLV2. As seen in the figures, energy dissipation due to bottom friction caused the wave energy of the long-period swell measured at station CHLV2 to be much less than that measured at station 44014. Figure 10 (c) shows the wave spectra from station 44014 and CHLV2 at 0300 UTC on October 31. The significant wave heights were 8.05 meters and 3.90 meters for stations 44014 and CHLV2, respectively. The significant energy dissipation was evident in the frequencies ranging from 0.04 Hz to 0.11 Hz.

5.4 EFFECT OF THE GULF STREAM

The Gulf Stream played an important role in several aspects of the storm. Figure 11 depicts the position of the Gulf Stream on October 30. As a large body of warm water it supplied the energy for the transition of the storm into a subtropical cyclone on November 1. In addition, the strong currents of the Stream interacted with storm swell that can affect the wave environment both in offshore and in nearshore regions (Lai and Bales, 1986, and Holthuihsen and Tolman, 1991).

Three stations (41001, 41002 and 41010) were located east of the Gulf Stream. The remaining stations were located between the Gulf Stream and the US. east coast. Based on the time series of wave energy at 0.06 Hz at stations 44008, 44014, and 41001 (see Figure 12 (a)), wave energy peak at 0.06 Hz measured at station 41001 (October 31) south of the Gulf Stream was about 80 percent of those measured at station 44008 and 44014 located north of the Gulf Stream. It is noted that wave energy at 0.06 Hz measured at stations 41001 on October 27 and 29 was much higher than that at stations 44008 and 44014. Figure 12 (b) shows the time series of wave energy at 0.06 Hz for stations 41010 (located outside the Gulf Stream in deep water) and 41009 (located between the Gulf Stream and Florida's coast). As seen in the figure, the differences between the wave energy at stations 41010 and 41009 are small. From the above two examples, the effects of the Gulf Stream on wave energy change seem to be insignificant.

5.5 COASTLINE SHELTERING EFFECT

Station 41008 is located nearshore east of Jacksonville, Florida, in a water depth of 18 meters. The high-height, long-period swells that significantly affected two stations to the south (stations 41009 and 41010) did not significantly affect station 41008 (Table 2). Figure 13 shows the time series of 0.05 Hz wave energy from stations 41008 and 41009. As can be seen, the 20-second swell arrived at station 410,09 with a magnitude 20 times larger than those at station 41008.

The significant difference could well be due to coastline sheltering provided by Cape Hatteras, North Carolina. It was also reported that, due to coastline sheltering provided by Cape Canaveral, beach erosion and coastal structure damage in Cocoa Beach, Florida, were not severe. However, further south severe beach erosions and structure damages were reported. The NDBC C-MAN station located on a pier at Lake Worth, Florida, was destroyed by wave action.

The above discussions illustrate that to model storm waves in the nearshore area along the U.S. east coast, there are various factors that must be properly considered.

6. SUMMARY

Wave and marine environmental data were collected from 16 NDBC stations during the strongest northeaster in 50 years. This data set provides an extensive field observation of the storm-generated severe seas along the U.S. east coast from Maine to Florida. The study documents the data and presents a preliminary analysis of the wave conditions present during the storm.

Several interesting observations were briefly presented to show the propagation of long-period swell, the bottom friction effect, the wind-wave evolution under the effect of swell, the effect of the Gulf Stream, and coastline sheltering.

This data set presents a good effort by NDBC to provide field observations from a network of stations during a severe storm. The field verification and calibration of numerical wave models using this data set will undoubtedly advance the development of wave hindcast and forecast models for years to come.

7. ACKNOWLEDGEMENTS

The authors would like to thank Dr. G. Hamilton (NDBC Data Systems Division Chief) for encouraging and supporting this study. Special thanks also go to Mr. Sam Houston (AOML Hurricane Research Division, Florida) for providing much useful information regarding the storm. Dr. P. Lin and Mr. B. Douglas (Coastal Technology Corporation, Florida), and Dr. J. Maa (Virginia Institute of Marine Science) kindly provided us with the information about beach erosion in the coastal areas. The valuable comments from the CSC Review Committee were also appreciated.

8. REFERENCES

Brown, H. and R. Gustavson, 1990: "Infrared Laser Wave Height Sensor," Proc. Marine Instrumentation'90, San Diego, CA.

Dolan, R. and R.E. Davis, 1992: "Rating Northeasters," Mariners

Weather Log, Winter 1992.

- Donelan, M.A., 1987: "The Effect of Swell on the Growth of Wind Waves," Johns Hopkins APL, Technical Digest, Vol 8, No. 1.
- Graber, H.C., Garuso, M.J. and R.E. Jensen, 1991: "Surface Wave Simulations During the October Storm in SWADE," Proc. MTS'91, Nov., New Orleans, LA.
- Gilhousen, D.B., 1987: "A Field Evaluation of NDBC Moored Buoy Winds," J. of Atmospheric and Oceanic Technology, Vol. 4, No. 1, pp. 94-104.
- Holthuijsen, L.H. and H.L. Tolman, 1991: "Effects of the Gulf Stream on Ocean Waves," J. Geophysical Res., Vol. 96, No. C7, pp. 12755-12771, July 15, 1991.
- Lai, R.J., and S.L. Bales, 1986: "Effect of the Gulf Stream on Nearshore Wave Climate," Proc. Coastal Engineering Conf., pp. 451-465.
- Longuet-Higgins, M.S., D.E. Cartwright, and N.D. Smith, 1963: "Observation of the Directional Spectrum of Sea Waves Using the Motions of a Floating Buoy," in Ocean Wave Spectra, Prentice-Hall.
- Michelena, E.D., and J.F. Holmes, 1986: "The Meteorological and Oceanographic Sensors used by the National Data Buoy Center," Proc. MDS'86 Marine Data Systems International Symposium, New Orleans, LA pp. 596-601.
- Pusch, R.J., and L.A. Avila, 1992: "Atlantic Hurricane Season of 1991," Monthly Weather Review (in press) Steele, K.E., D.W. Wang, C.C. Teng, and N. Lang, 1990: "Directional Wave Measurement with NDBC 3-Meter Discus Buoys," NDBC report No. 1804-01.05,
- Wang, D.W., and R. Carolan, 1991: "Estimation of Swell Direction by a Small Discus Buoy in High Seas," in Proc. of 5th Conference on Meteorological Society. PP. 53-59.
- Wang, D.W., C.C. Teng, and K.E. Steele, 1989: "Buoy Directional Wave Observations in High Seas," in Proc. Oceans '89, Seattle, Mar. Technol. Soc. and IEEE, pp. 1416-1420.

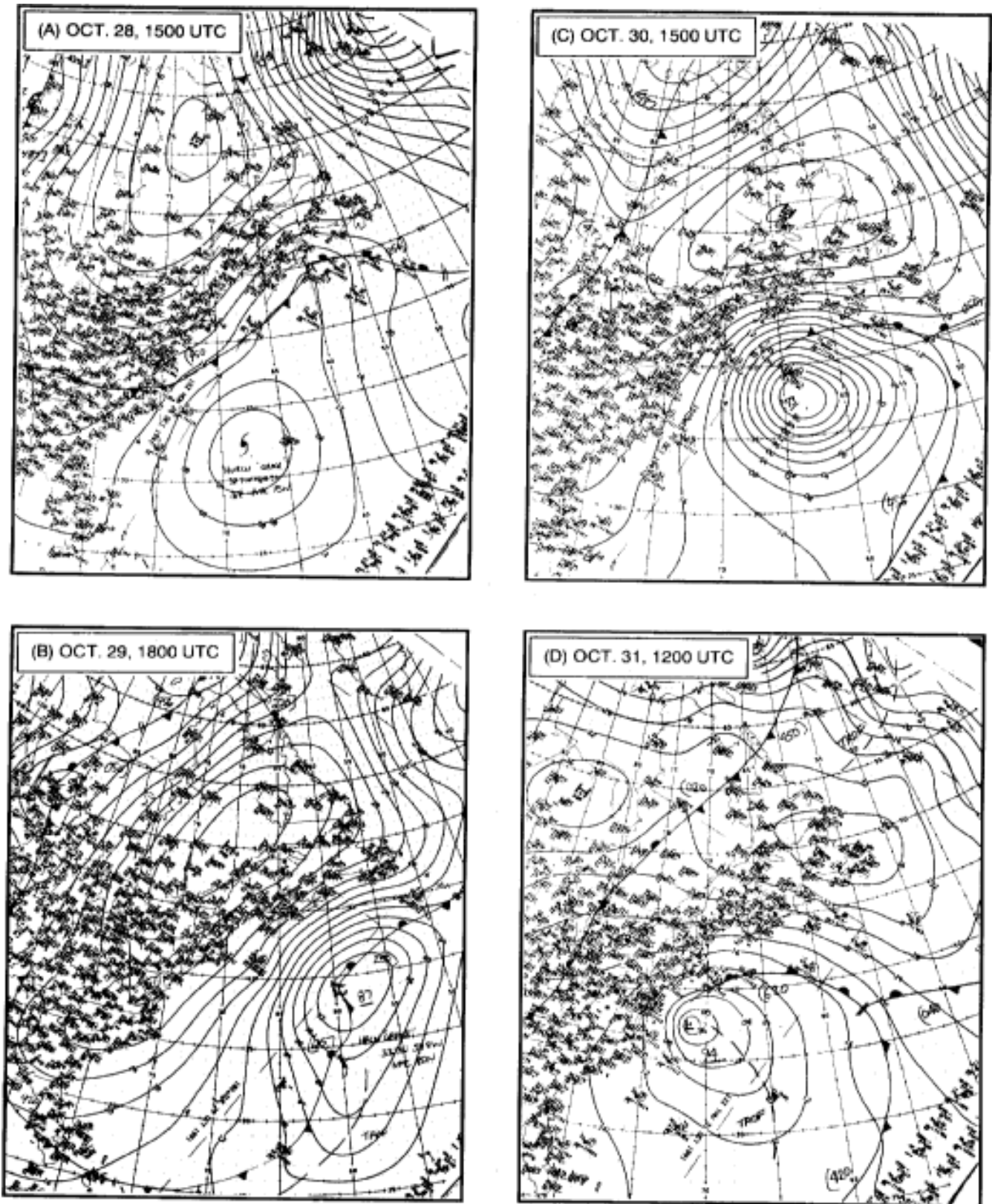


Figure 1. Surface synoptic weather chart.

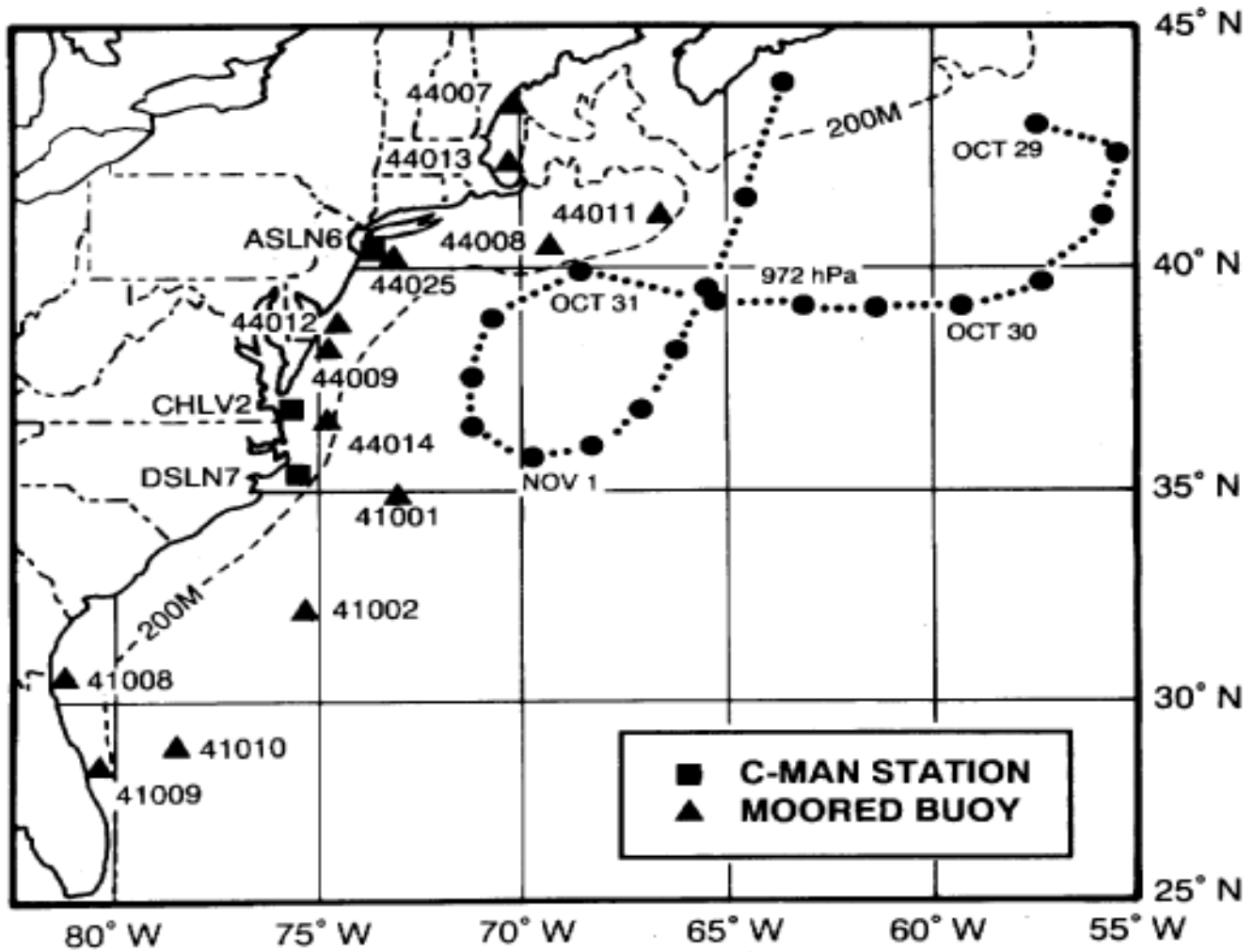


Figure 2. Storm track and locations of East Coast NDBC stations.

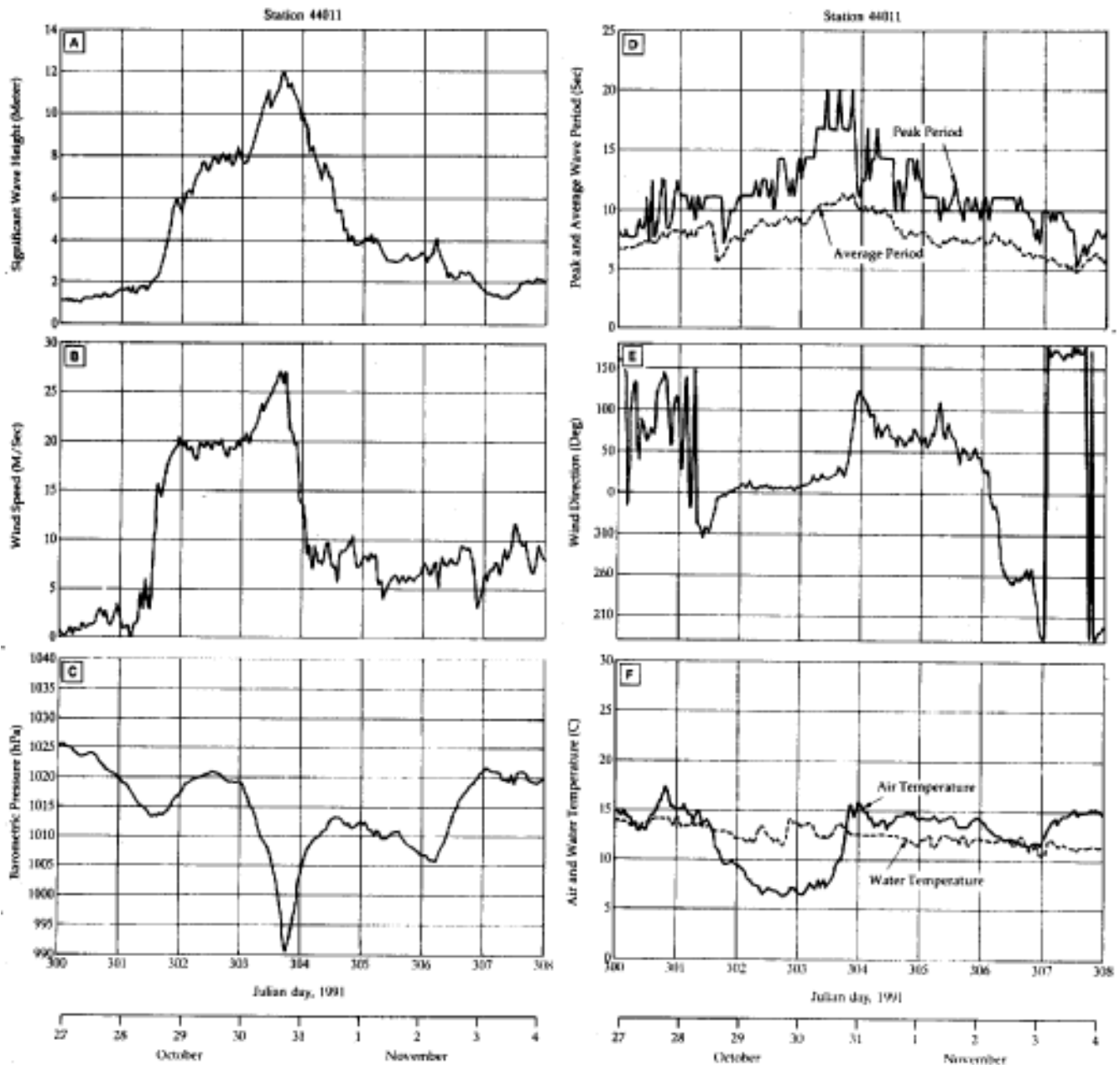


Figure 3. Time series of measured data from station 44011: (a) significant wave height, (b) wind speed, (c) barometric pressure, (d) peak wave period (solid line) and average wave period (dotted line), (e) wind direction, (f) air temperature (solid line) and water temperature (dotted line).

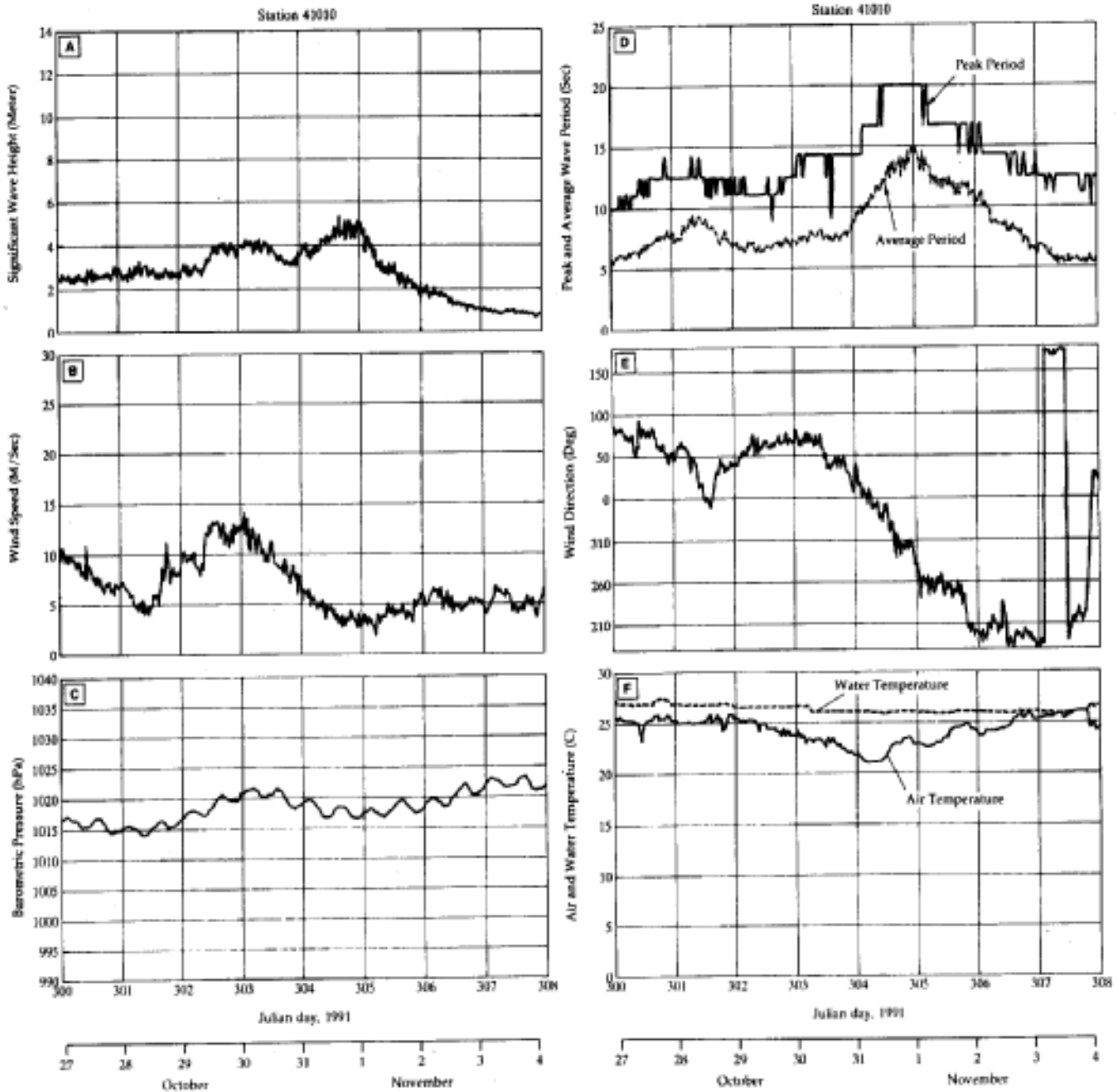


Figure 4. Time series of measured data from station 41010: (a) significant wave height, (b) wind speed, (c) barometric pressure, (d) peak wave period (solid line) and average wave period (dotted line), (e) wind direction, (f) air temperature (solid line) and water temperature (dotted line).

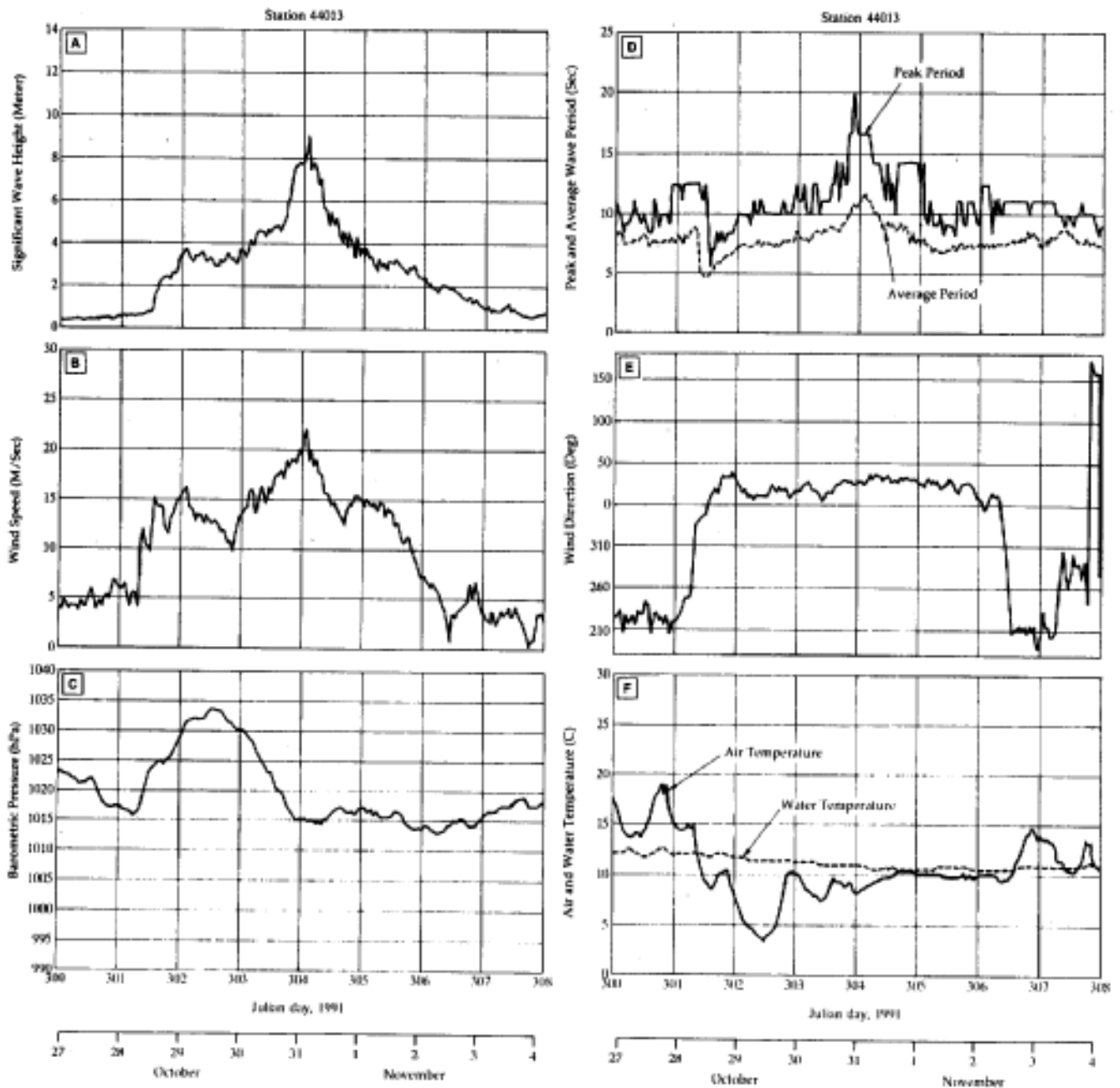


Figure 5. Time series of measured data from station 44013: (a) significant wave height, (b) wind speed, (c) barometric pressure, (d) peak wave period (solid line) and average wave period (dotted line), (e) wind direction, (f) air temperature (solid line) and water temperature (dotted line).

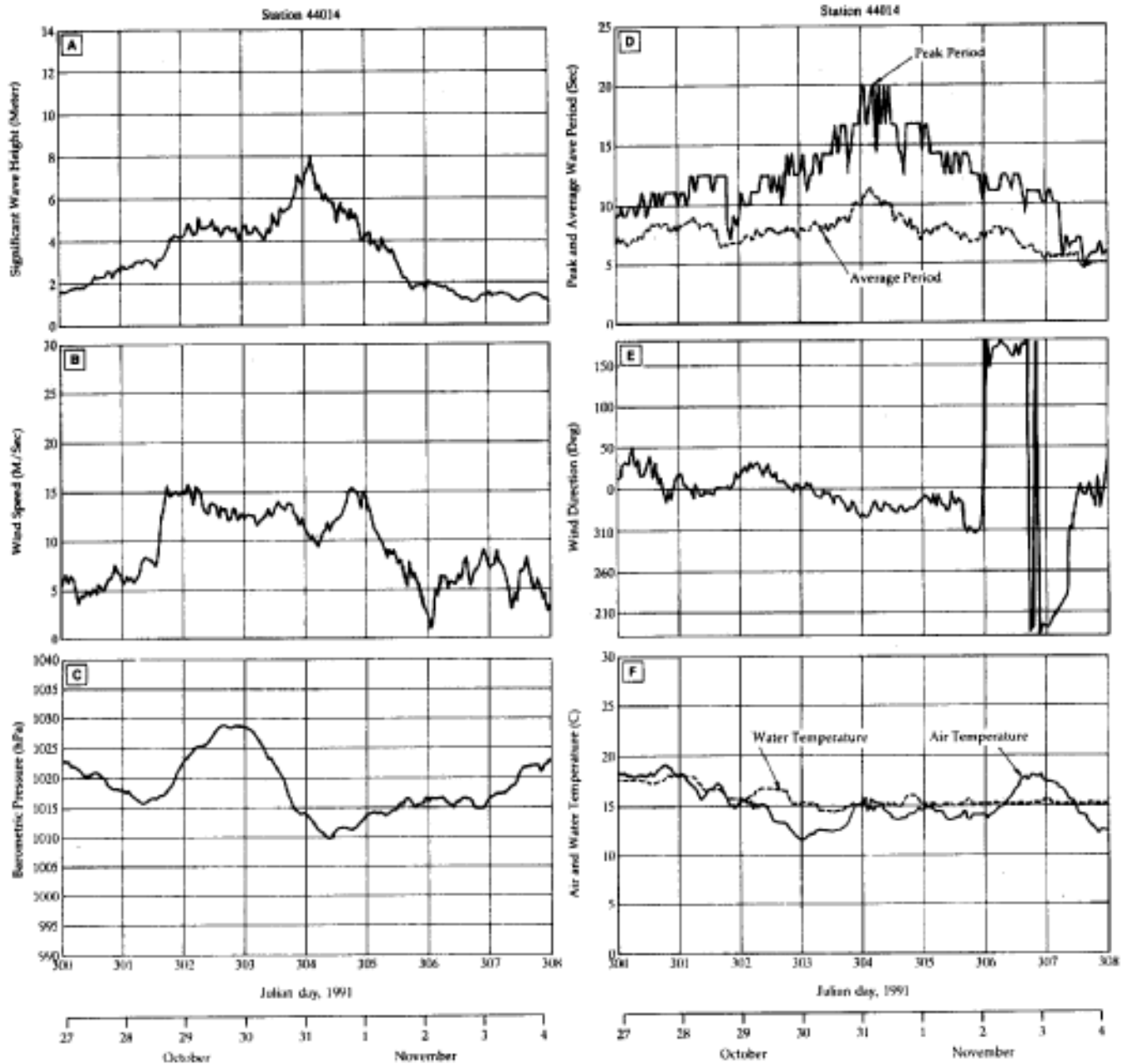


Figure 6. Time series of measured data from station 44014: (a) significant wave height, (b) wind speed, (c) barometric pressure, (d) peak wave period (solid line) and average wave period (dotted line), (e) wind direction, (f) air temperature (solid line) and water temperature (dotted line).

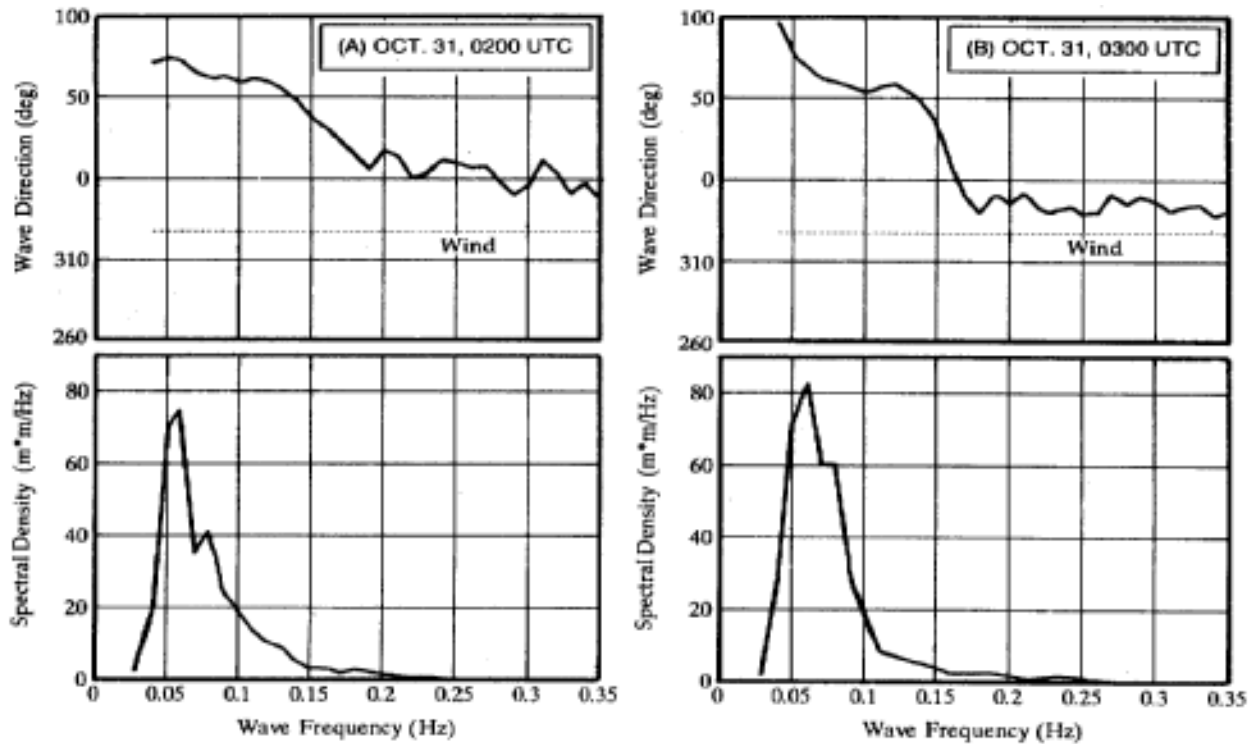


Figure 7. Directional Wave Spectrum from station 44014: (a) at 0200 UTC, Oct. 31, (b) at 0300 UTC, Oct. 31.

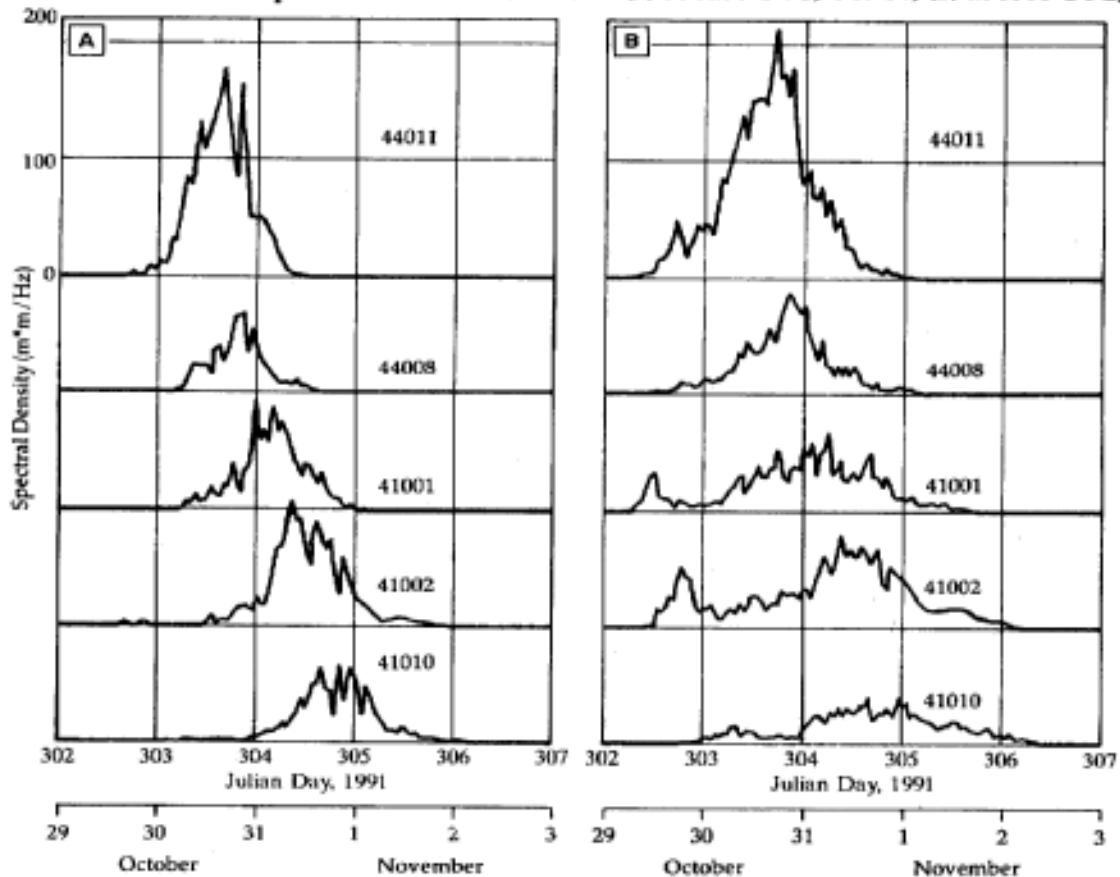


Figure 8. Time series of wave energy from stations 44011, 44008, 41001, 41002, and 41010 at (a) 0.05 Hz, (b) 0.06 Hz.

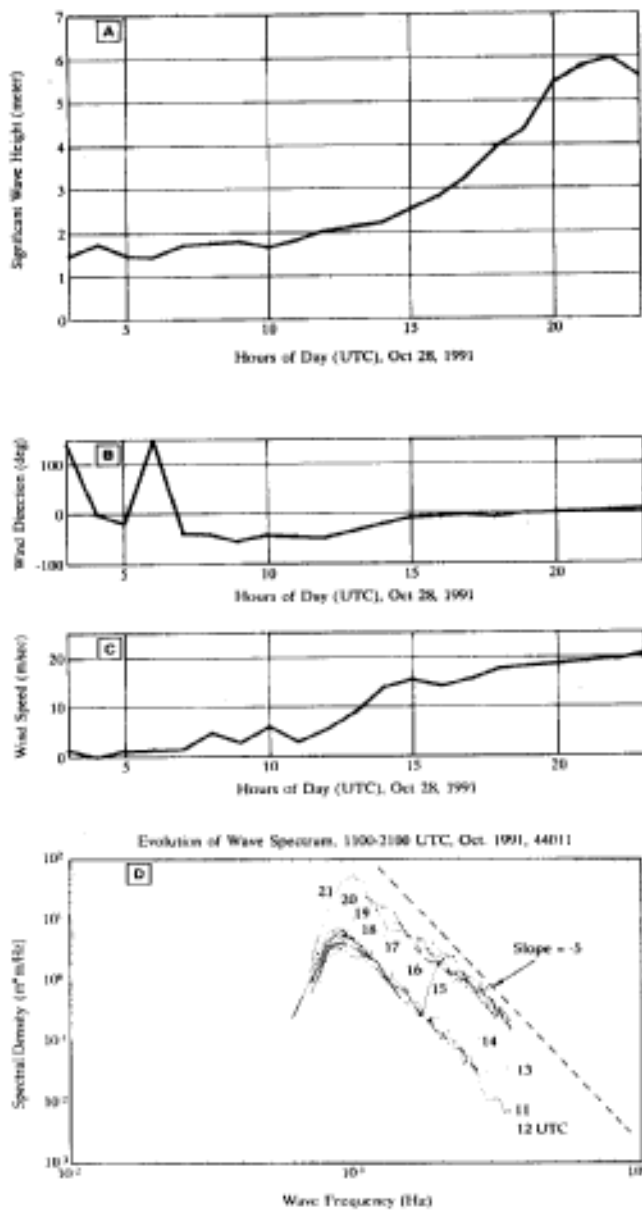


Figure 9. Time series of measured data: (a) significant wave height, (b) wind speed, (c) wind direction; (d) wave spectrum.

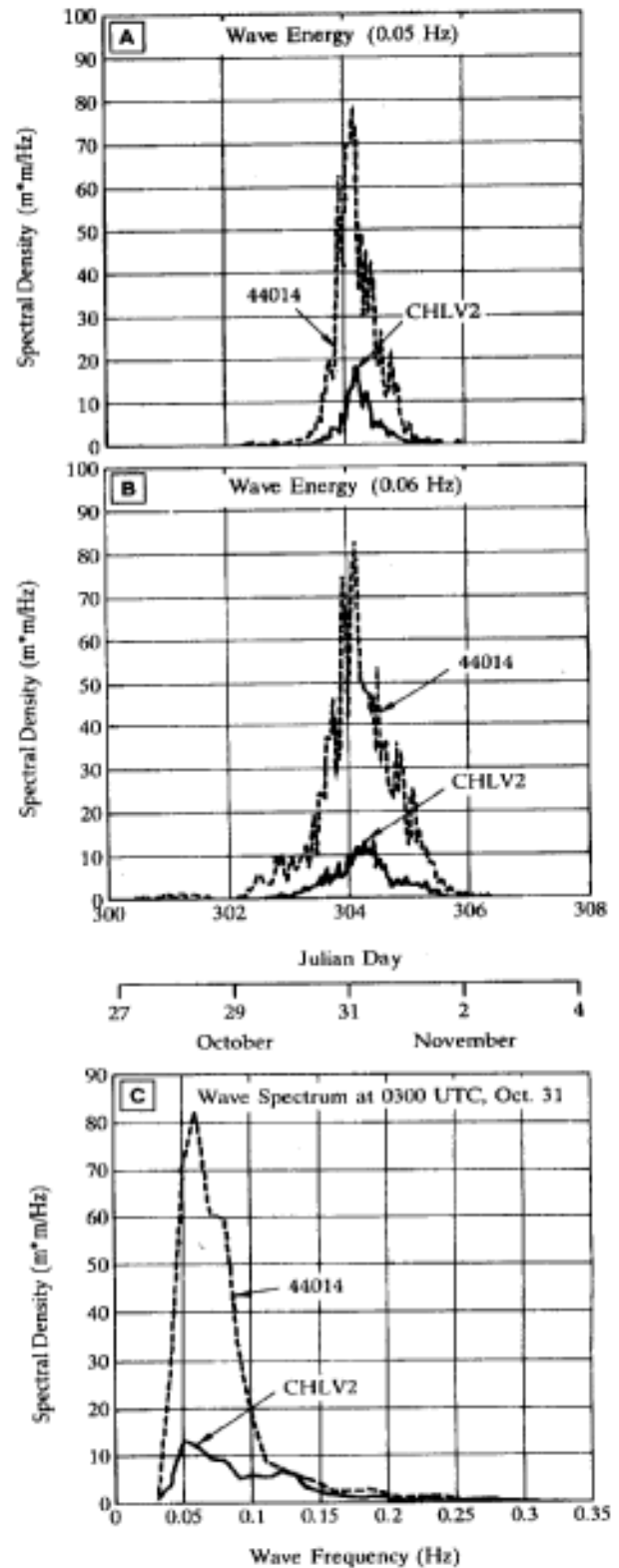


Figure 10. Time series of wave energy and wave spectrum from stations 44014 and CHLV2: (a) at 0.05 Hz, (b) at 0.06 Hz, (c) Wave Spectra at stations 44014 and CHLV2.

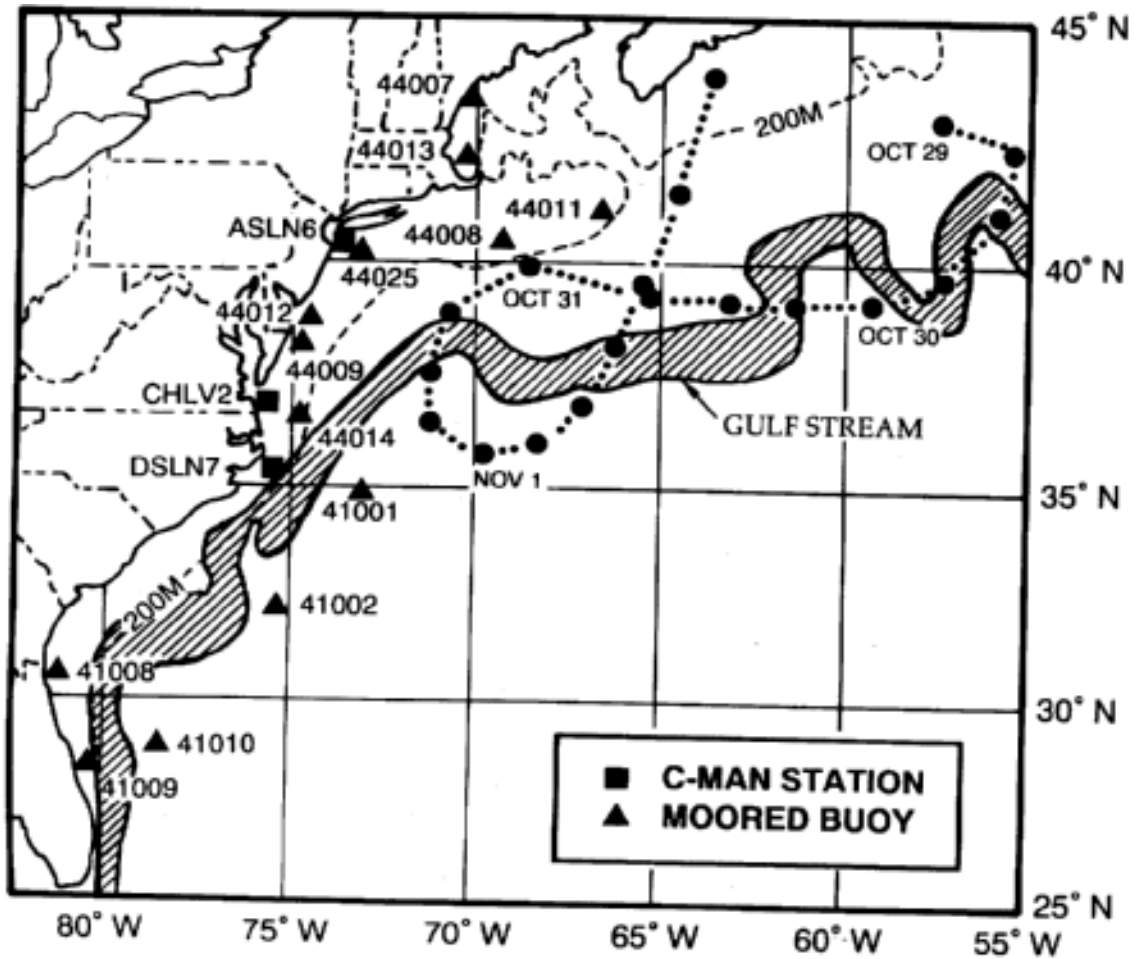


Figure 11. The position of the Gulf Stream on October 30, 1991.

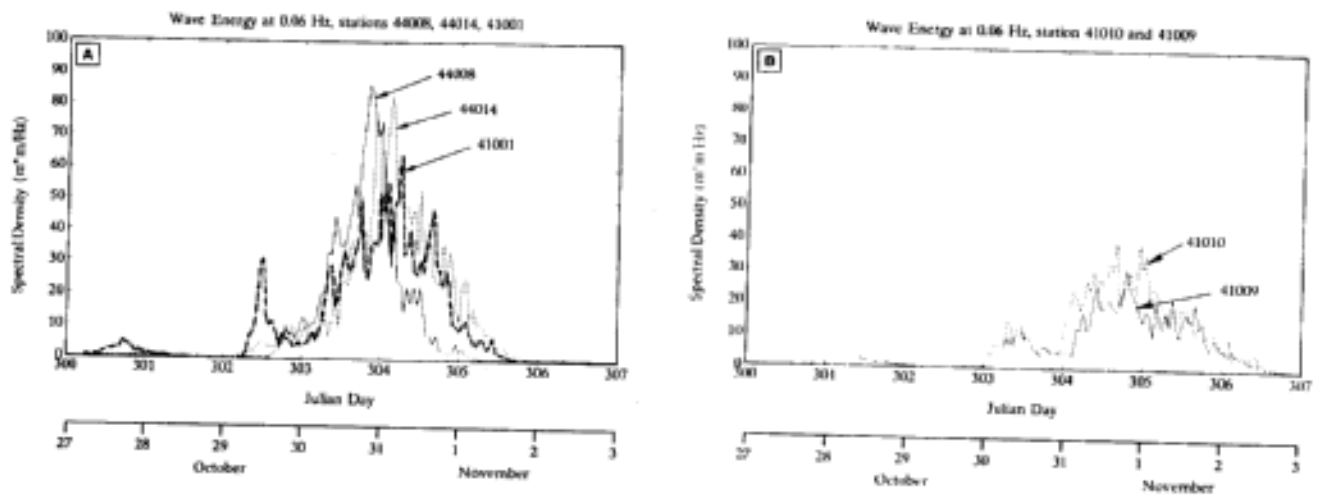


Figure 12. The time series of wave energy at 0.06 Hz: (a) stations 44008, 44014, and 41001, and (b) stations 41009 and 41010.

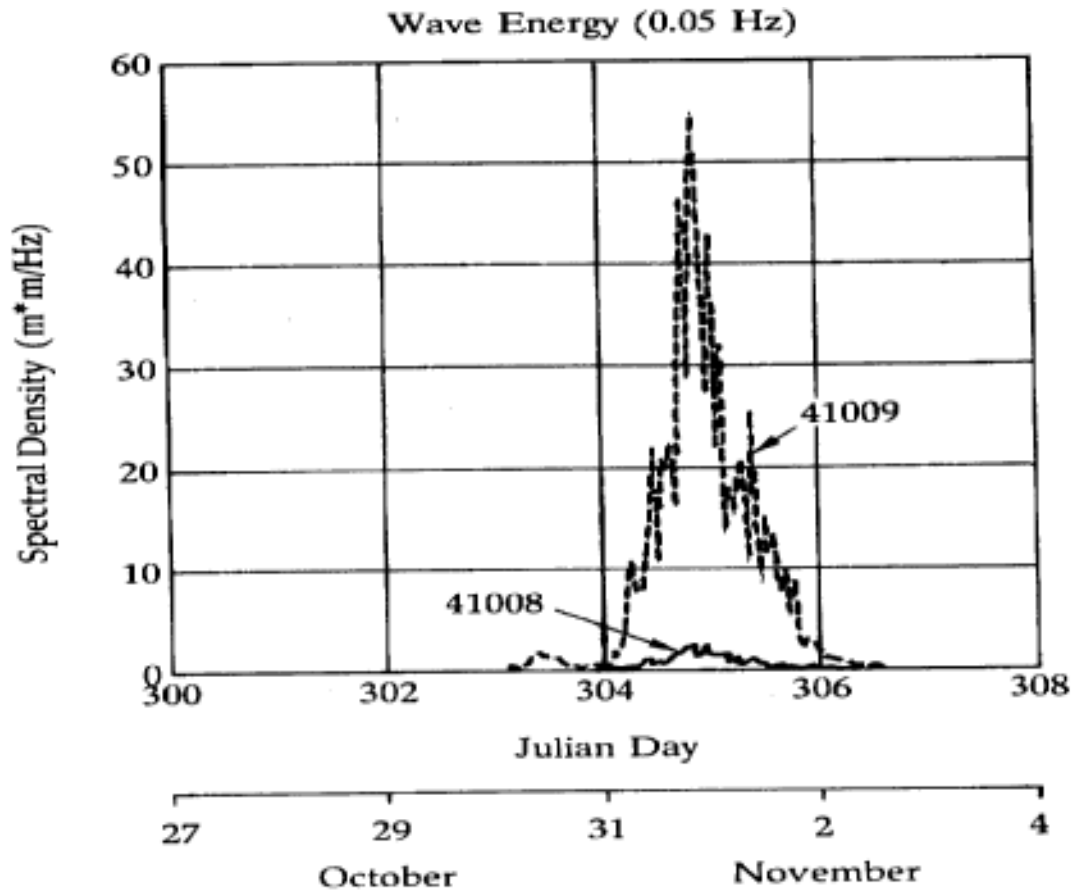


Figure 13. The time series of wave energy at 0.05 Hz from stations 41008 and 41009.

**A WIND WAVE HINDCAST FOR THE HALLOWEEN NORTHEASTER IN 1991
IN THE ATLANTIC OCEAN COASTAL WATERS**

¹C.L. Vincent, ¹R.E. Jensen, ²P.A. Wittmann and ³H.C. Graber

¹USAE Waterways Experiment Station
Coastal Engineering Research Center
Vicksburg, MS 39180-6199

²Fleet Numerical Oceanography Center
Monterey, CA 93943-5005

³Rosenstiel School for Marine and Atmospheric Science
University of Miami
Miami, FL 33149-1098

INTRODUCTION

The northeaster of 28 October to 1 November 1991 off the eastern North American coast, popularly referred to as the Halloween Northeaster, was one of the most severe fall storms in this region in recent years. It was particularly noteworthy in producing measured significant wave heights of 12-17 meters and extremely long wave periods of 20-22 seconds which caused shore damage as far south as Florida. Moreover, the growth and decay of this storm was monitored by an extensive network of wave and wind measuring buoys that stretched southward from the Scotian shelf to the central Florida coast (Wang and Mettlach 1992). Consequently, it is one of the best documented major storms ever recorded on the Atlantic coast.

In meteorological terms, the storm was somewhat unusual. Prior to storm formation, Hurricane Grace was present in the Bermuda region, heading north. With the passage of the cold front on which the storm eventually formed across the Western Atlantic, Hurricane Grace was absorbed into the front and the growing circulation of the extra-tropical system, (Wang and Mettlach 1992). Rather than remaining stationary or moving off to the northeast as would be typical of storms in this region, the northeaster recoiled and moved westward towards the New England and Mid-Atlantic coasts of the U.S.

The Halloween Northeaster provided an excellent opportunity to evaluate the third generation wave forecast model 3GWAM under well-documented extreme wave conditions. This paper presents simulations using two versions of 3GWAM: Cycles 3 and 4. In Cycle 3 the wind forcing has no feed back from the wave field. In Cycle 4 the wind forcing is coupled to the wave field. In this paper the wind forcing were wind stress estimates taken directly from the forecast stream of the U.S. Navy Fleet Numerical Oceanography Center, and no attempt has been made to refine or correct it. Later analysis of the

wind field indicates that in the central area of the storm the initial forecasts overestimated the winds. The storm will be re-hindcast with improved wind fields. Even with the over-forcing of the model, the results provide information about the response of the model and the differences between computations with Cycles 3 and 4.

WAVE MODEL

Cycles 3 and 4 of the model 3GWAM (WAMDIG 198 8, Gunther et al. 1991) were run on a two-level nested grid system (Fig. 1 and 2). The simulations were first made on a 1 x 1 deg grid encompassing the bulk of the North and South Atlantic Oceans. Boundary information was then provided to a regional grid covering the Western Atlantic Ocean from Puerto Rico to Newfoundland on which simulations were made on a 0.25 x 0.25 deg grid. Twenty five logarithmically spaced frequencies beginning at 0.042 Hz and 24 direction bands represented the energy density spectrum. Time steps used in the Atlantic basin simulation was 1200 sec and for the regional grid a time step of 240 sec was assumed.

The transport equation is solved in 3GWAM for the time and spatial change in the spectrum along a great circle path. The source terms in both cycles of 3GWAM are atmospheric input, dissipation, and nonlinear wave-wave interactions. On the regional grid, shoaling and bottom friction were applied for shallow water situations, whereas depth refraction was neglected. The principal difference in Cycle 4 is that the atmospheric input is coupled to the boundary layer following the theory of Janssen (1989, 1991). The adoption of Janssen's theory represents a major change in wave modelling and clear differences between computations in the two cycles should be expected. However, it should be noted that 3GWAM has been well tested and has shown considerable skill in previous applications as shown in Zambresky (1989).

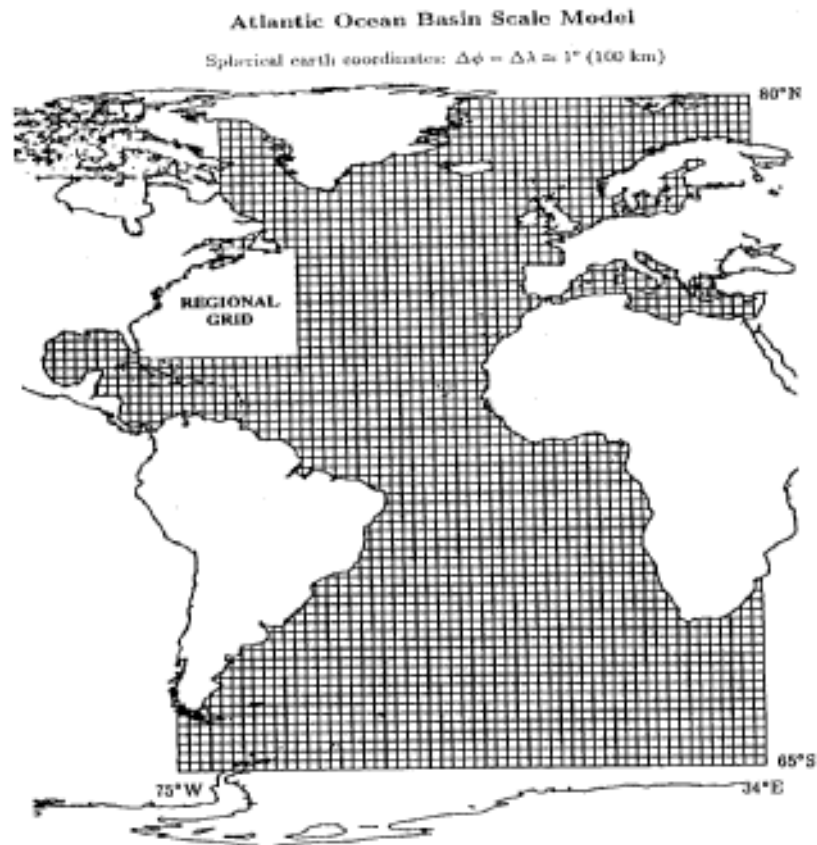


Fig. 1. Atlantic ocean basin grid, note not all grid lines are plotted.

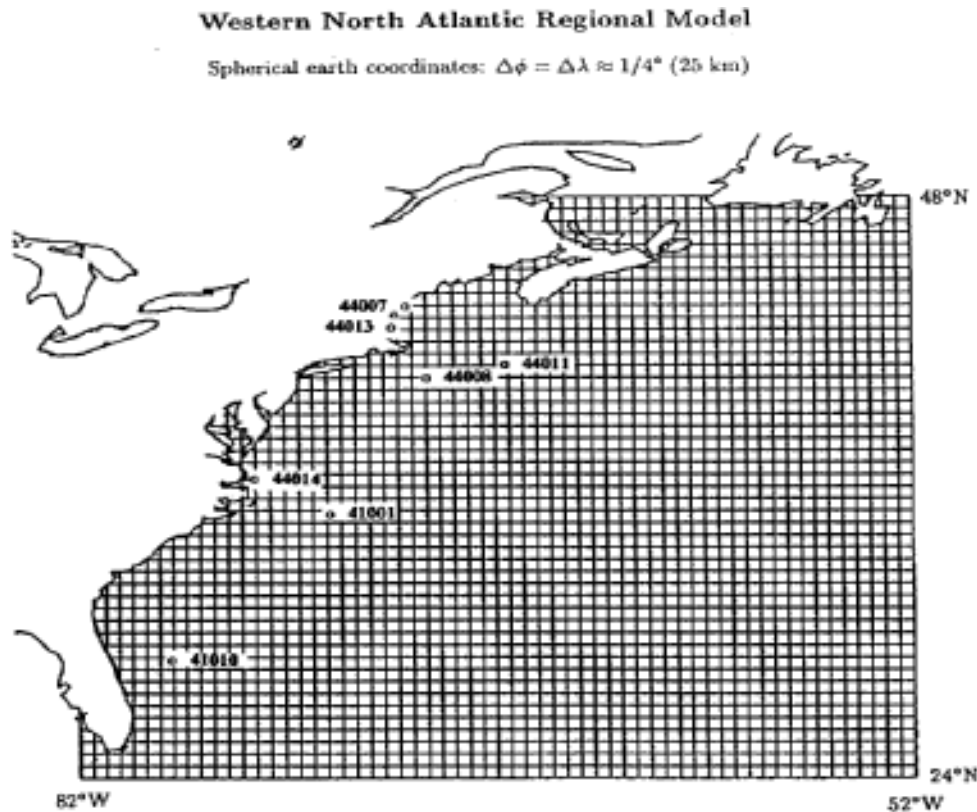


Fig. 2. Regional grid, note not all grid lines are plotted.

WIND DATA

The Fleet Numerical Oceanography Center (FNOC) had archived the wind stress calculations from their global atmospheric model, NOGAPS 3.2 on a 1.25×1.25 deg grid over the Atlantic Ocean directly from their forecast stream for the period 22 October 1991 to 5 November 1991. Generation of the wind stress fields are based on work by Hogan et al., (1991). The stresses are computed using an implicit time-differencing scheme. The mixing length concept used in calculation of the stresses is given by Louis et al. (1982) as a function of the bulk Richardson number. Investigators in the Surface Wave Dynamics Experiment (SWADE) had used the same wind stress forecasts very successfully in forcing Cycle 3 of 3GWAM in the same area for the period of October 1990 to March 1991 (e.g. Jensen et al., 1991 and Graber et al., 1991).

Hurricane Grace, and the Halloween storm passing through the Atlantic coastal area were extremely complex. To capture the wind fields for these rapidly developing intense systems is a difficult task, especially considering the spatial and temporal resolution (2.5 deg and 6 hr) of the standard FNOC products. It mentioned earlier, that the stress fields over-estimate the wind conditions in the

Halloween storm. The degree of this over-estimate has become a topic of this paper. Manual adjustment of the central pressure was performed prior to the objective analysis of the forecast. In general, FNOC uses this method in data sparse areas, and not in regions with numerous measurements. The magnitude and intensity of this particular storm warranted the re-specification of the central pressure, consistent with results obtained from hand analysis of the pressure fields from the National Meteorological Center. By deepening the storm center, the resulting pressure gradients steepen, and thus increase the magnitude of the stress.

Each stress field was updated every 3 hours, and temporally interpolated to a 1 hour time step and held fixed during the wave model simulation. 3GWAM also spatially interpolates the input stress field (1.25 degree resolution) onto the fixed wave model grid. The model then uses a series of algorithms to estimate the coefficient of drag and a friction velocity to drive the wave model. The significant differences between Cycles 3 and 4 lie in these calculations and can be found described in Janssen (1989, 1991). This addition changed the net effect of the energy balance. Balance in the source/sink terms was attained by adjusting the equational form of the dissipation sink.

WAVE DATA

For this paper wave data from National Data Buoy Center buoys were used for comparisons in the wave model. The locations of buoys used for comparison are given in Table 1 . In this paper significant height and peak wave period are used for comparison. In principal, it would also be possible to compare frequency spectra at all and directional spectra at selected buoys. These comparisons will be delayed until a revised wind hindcast is available.

COMPARISON OF MODEL PREDICTIONS AND OBSERVATIONS

Statistical comparisons of the model predictions with the wave observations are summarized for significant height (Table 1) and peak period (Table 2) for the Cycle 4 simulations at eight buoys. The location of these buoys is shown in Figure 2 . In general, the wave height comparisons have a bias of 0.3 m or less, which is small considering the magnitudes in the observed wave heights (means of 1.4-3.1m). Additional statistical results show root mean square errors (RMS) varied from 0.6m to 1.2 m, and correlation coefficients greater than 0.94 except at 41010. This may be due, in part to phasing errors in the initial portion of the simulation that will be shown in the time plots. 3GWAM results are considerably better, further away from the storm track, or in deeper water (e.g. 41001, and 41002, respectively). The peak spectral period statistics are presented in Table 2 . The bias in 3GWAM results, ranges from -2.5 to -0.8 sec

with most model results less than -1.25 sec. The RMS error in period ranges from 1.5-3.8 sec with most between 2.2 and 3.2 sec. The correlation coefficients are greater than 0.6 except at 44013, the shallowest, and most sheltered location. In general, the period statistics are poorer than the height statistics because: the peak frequency in this application is an unstable parameter, and depends more on the resolution of the low frequency portion of the spectrum. 3GWAM and the buoy resolution differ significantly in the low end of the spectrum. Another factor is the model spin-up period in which short waves (relative to longer existing waves) dominate.

The summary statistics are somewhat misleading in that they do not show the clear over-estimate of the main part of the storm that can be seen in the time history plots of wave height (Figs. 3 -8). The model performs reasonably well before and after the maximum of the storm (Julian day 304 in Figs. 3 -8), but at most sites 3GWAM over-predicts the observations near the peak of the storm. Based on what we know at this time, most of the over-prediction is believed to be due to over-estimation of the stresses. Conversion of the modeled wind stress to free air winds (at a 10 m elevation) indicate speeds of 33-39 m/s while the buoy winds were more typically 28 m/s, and about a 28 percent uncertainty. Using simple scaling principles, (Hasselmann et al. 1973), this would translate to a 65 percent uncertainty in wave height estimates, assuming local wind-wave generation. Differences in the model results at 44011 and 44008 (Fig. 3 and 5) support the over-estimation in the stress fields is the primary source of error.

3GWAM Cycle 3 and 4 are compared to the buoy measurements for wave height only. For some buoys (44011, 41001, 41010) the differences between the two cycles are inconsequential. The absolute difference encountered at any particular buoy location did not exceed 1.0m for any given time. The Cycle 3 wave simulation encountered an instability slightly after the peak of the storm, and restricted the comparisons to that point. It is also interesting to note, the phasing of the peak of the storm between Cycle 3 and 4 differ by 2 hours. This is more evident at the southern gage locations. With the uncertainties in the stress fields, no definitive arguments concerning the new source term physics in Cycle 4 can be addressed, and thus, the remainder of the discussion will focus on the results from Cycle 4.

Table 1. NDBC buoy locations and wave height statistics from 3GWAM Cycle 4 simulation.

Station	Latitude	Longitude	Depth (m)	Buoy Mean (m)	Bias (m)	RMS Error (m)	Scatter Index (%)	Correl. Coef
44007	43°31'48"	70°05'24"	47	1.441	1.064	0.825	57.2	0.938
44013	42°22'48"	70°46'48"	30	1.700	0.496	0.561	33.0	0.974
44011	41°04'55"	66°14'49"	88	2.948	0.184	1.047	35.4	0.984
44008	40°30'00"	69°25'39"	60	2.569	0.121	1.229	38.8	0.928
44014	36°34'59"	74°50'01"	48	2.380	0.270	0.902	37.9	0.953
41001	34°55'30"	72°57'05"	4206	3.167	0.288	1.015	39.5	0.977
41002	34°17'42"	75°14'26"	3658	3.139	0.069	0.672	21.4	0.952
41010	28°52'48"	78°31'59"	833	2.456	0.127	0.650	26.4	0.878

Table 1. NDBC buoy locations and wave height statistics from 3GWAM Cycle 4 simulation.

Station	Latitude	Longitude	Depth (m)	Buoy Mean (m)	Bias (m)	RMS Error (m)	Scatter Index (%)	Correl. Coef
44007	43°31'48"	70°05'24"	47	1.441	1.064	0.825	57.2	0.938
44013	42°22'48"	70°46'48"	30	1.700	0.496	0.561	33.0	0.974
44011	41°04'55"	66°14'49"	88	2.948	0.184	1.047	35.4	0.984
44008	40°30'00"	69°25'39"	60	2.569	0.121	1.229	38.8	0.928
44014	36°34'59"	74°50'01"	48	2.380	0.270	0.902	37.9	0.953
41001	34°55'30"	72°57'05"	4206	3.167	0.288	1.015	39.5	0.977
41002	34°17'42"	75°14'26"	3658	3.139	0.069	0.672	21.4	0.952
41010	28°52'48"	78°31'59"	833	2.456	0.127	0.650	26.4	0.878

Table 2. NDBC buoy locations and peak wave period statistics from 3GWAM Cycle 4 simulation.

Station	Latitude	Longitude	Depth (m)	Buoy Mean (sec)	Bias (m)	RMS Error (sec)	Scatter Index	Correl. Coef
44007	43°31'48"	70°05'24"	47	8.893	-0.875	2.695	30.3	0.665
44013	42°22'48"	70°46'48"	30	11.024	-2.594	3.811	34.6	0.359
44011	41°04'55"	66°34'49"	88	10.314	-1.653	2.788	27.0	0.652
44008	40°30'00"	69°25'39"	60	9.599	-1.072	3.195	30.1	0.589
44014	36°34'59"	74°51'01"	48	10.887	-1.248	3.079	28.3	0.634
41001	34°55'30"	72°57'05"	4206	10.581	-0.813	2.872	29.9	0.604
41002	34°17'42"	75°14'26"	3658	10.700	-0.797	2.211	20.7	0.838
41010	28°52'48"	78°31'59"	833	11.398	-1.036	1.561	13.7	0.911

Table 2. NDBC buoy locations and peak wave period statistics from 3GWAM Cycle 4 simulation.

Station	Latitude	Longitude	Depth (m)	Buoy Mean (sec)	Bias (sec)	RMS Error (sec)	Scatter Index (%)	Correl. Coef
44007	43°31'48"	70°05'24"	47	8.893	-0.875	2.695	30.3	0.665
44013	42°22'48"	70°46'48"	30	11.024	-2.594	3.811	34.6	0.359
44011	41°04'55"	66°34'49"	88	10.314	-1.653	2.788	27.0	0.652
44008	40°30'00"	69°25'39"	60	9.599	-1.072	3.195	30.1	0.589
44014	36°34'59"	74°50'01"	48	10.887	-1.248	3.079	28.3	0.634
41001	34°55'30"	72°57'05"	4206	10.581	-0.813	2.872	29.9	0.604
41002	34°17'42"	75°14'26"	3658	10.700	-0.797	2.211	20.7	0.838
41010	28°52'48"	78°31'59"	833	11.398	-1.036	1.561	13.7	0.911

Figs. 3 to 8 provide time histories of observed wave height and that predicted by 3GWAM for the following buoys: 44011 (east of Cape Cod), 44013 (near Boston), 44008 (south of Cape Cod), 44014 (off the Virginia-North Carolina border, but nearshore), 41001 (off Cape Hatteras), and 41010 (off central Florida). In all cases, 3GWAM follows the measurements although the model over-predicts wave heights at the storm peak, by 2-4m. The positive points for this simulation are: the growth, starting at Julian day 302 and then the decay of this storm are modeled quite well. Hence, the FNOC stress fields, although over-estimated at the peak of the storm, do in-fact represent the meteorological conditions, and 3GWAM picks up the structure of the wave climate generated from that storm. Wave heights at 44011 (Fig. 3) increase from 1.5m to 8.0m in about 12 hours. 3GWAM shows a very similar trend. The problem is the stresses begin their over-prediction just after Julian day 302 and continues until day 304. A poor forcing

function, or an inadequate wave model cannot generate these types of results. For an example, the results at 44013 near Boston Harbor and in a very sheltered region (Fig. 4) shows 3GWAM capturing very rapid growth of an initial storm (day 301) slightly over-estimating an initial storm peak at day 302, then following the measurements through the peak and decay of the major storm event. On the down-wind side of the storm, the initial over-estimate is evident at 41001, 44014 and 41010. Again, the initial growth and decay of the storm is well represented.

Figs. 9 to 11 provide time history plots of significant period for selected buoys (44011, 410015 41010). The trends evident at these buoys were typical of all. In initial phases of the simulation the models under-estimate the wave period because the model is in a spin-up phase. In general, as the wave conditions rapidly grow, the model and observed periods come into agreement. The most obvious trend is that in almost all cases the observed periods reach 20 seconds while the modelled periods usually stop at 17-18 seconds, or if they reach 20 seconds, do not remain at that level for the same duration as the observed. Overall, the model peak period estimates follow the trends established in the measurements. This is evident more so during the decay of the storm. Dramatic changes from 10 to 5 second peak periods are clearly evident in the model results around day 306-308. If 3GWAM used frequency bands consistent with the buoy data, improvements would be evident. In general, the model results are, at most, one frequency band from the measurements. This again is attributed to the differences between model and measurements in resolving the low frequency end of the spectrum. It was anticipated Hurricane Grace would be clearly defined in the data sets characterized by an increase in wave heights and long period swell energy. The effects of Grace do not play a significant role in the simulations. The only influence appears to be at the southern gages (41001 and 41010), where there is a distinct peak in the wave height records, while the period results are relatively constant at 15 seconds. We do see the propagation of the swell from the extra-tropical storm from results at 41001 and 41010. The modelled peak period falls short of the measurements in both cases though.

The overall good agreement in periods may in fact be misleading. Since the wave heights in the peak regions of the storm are in general overestimated, one would expect that the wave periods would also be overestimated. If anything at the peak they are under-estimated. One can only speculate that if the model had reproduced the correct wave heights (i.e., lower) the wave periods would also be lower and would significantly under-estimate the conditions observed. This can be checked, to verify the consistency between modeled energy and peak frequency. The model and buoy data sets are scaled according to

nondimensional energy ($\varepsilon = E_o \cdot g^2 / U_{10}^4$, and $v = f_m \cdot U_{10} / g$, where E_o is the total energy, U_{10} is the wind speed at 10m, f_m is the peak frequency, and g is the gravitational acceleration). The results are plotted in Fig. 12a . A large fraction of data points fell to the left of the Pierson-Moskowitz (Pierson and Moskowitz 1964) limit, suggesting fully developed or swell conditions. This plot shows 3GWAM results are consistent with the buoy data in the region of active wave growth (to the right of the P-M limit), and the results follow the formulation established in the JONSWAP data set (Hasselmann et al., 1973). The variation in v versus time is also plotted in Fig 12b . One does see the development of the Halloween Northeaster quite nicely. Beginning at day 301, swell energy is present at 44011, probably from Hurricane Grace. As time progresses, the influence of the extra-tropical cyclone becomes more of a factor. By hour 12 on day 301, local wind-sea persists, throughout the storm period. During the time between day 302 through day 304 (the peak of the storm), 3GWAM results compare favorably to the measurements. There is an overestimate in v prior to the storm peak, but during the major portion of the storm 3GWAM scales consistently with the buoy data. What we do find just after the peak of the storm (day 304 at 00 hours), is the crossing over of the P-M limit for the model and measurements. After day 304, the model results remain in the wind-sea growth stage much longer than the buoy data, although the wave height (Fig. 3) and peak period (Fig. 9) model results track the data.

SUMMARY AND CONCLUSIONS

We have demonstrated that within the context of initial wave hindcasting efforts, the FNOC stress fields simulated much of the complex storm systems during a 10 day period, with one exception. Because of a re-specification of the storm pressure center, the stress fields over-estimated the conditions during the peak of the Halloween Northeaster. Recognizing that the wind fields driving the wave model over-estimated the winds, over-prediction of wave results by both Cycle 3 and Cycle 4 of 3GWAM are expected. It is equally important to model the growth and decay sequences in storm conditions, which Cycle 4 did quite well, all along the Atlantic coast.

Until revised wind fields are available it will not be possible to realistically document model performance. In spite of this restriction, three trends were apparent. First, the Cycle4 version under-estimated peak periods even though the model estimates were biased up to 4 m too high, but in a nondimensional formulation agrees with JONSWAP (Hasselmann, et al., 1973). Second, differences in predictions between Cycles 3 and 4 are insignificant. Thirdly, although the model's peak period under-estimated the buoy data, the nondimensional parameters E and P scaled very well with the

measurements and the JONSWAP parametric formulation. These results are based on two simulations of the Halloween Northeaster. Much was learned from the simulations that will be pursued for some time to come.

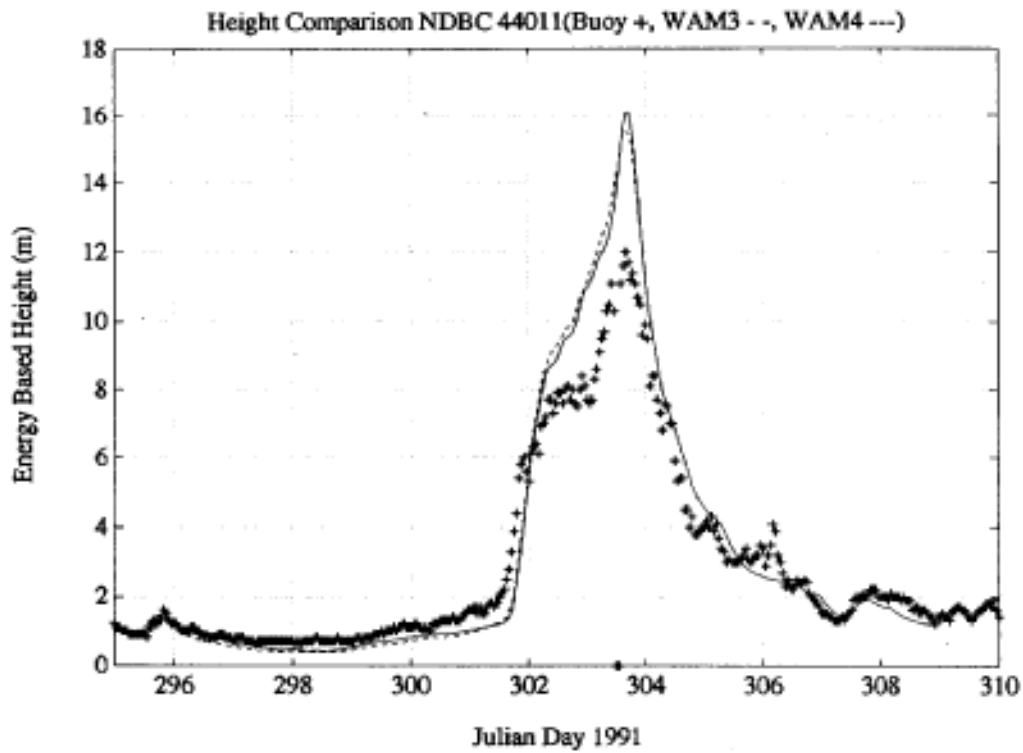


Fig. 3. Energy based wave height results from Cycles 3 and 4 compared to buoy measurements at NDBC 44011.

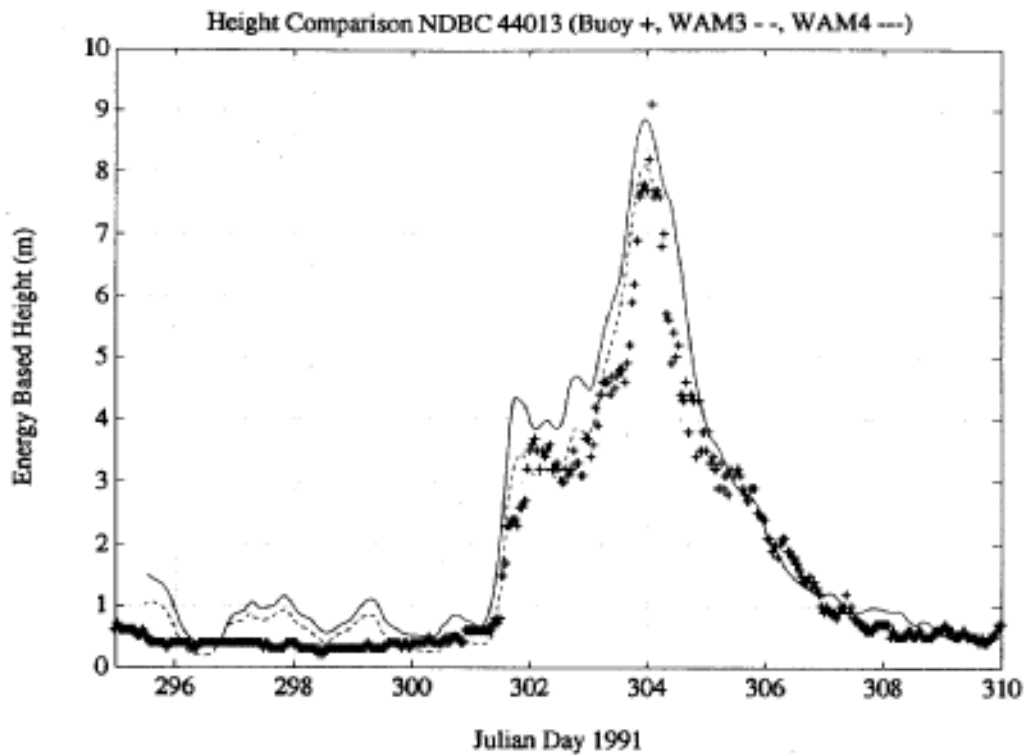


Fig. 4. Energy based wave height results from Cycles 3 and 4 compared to buoy measurements at NDBC 44013.

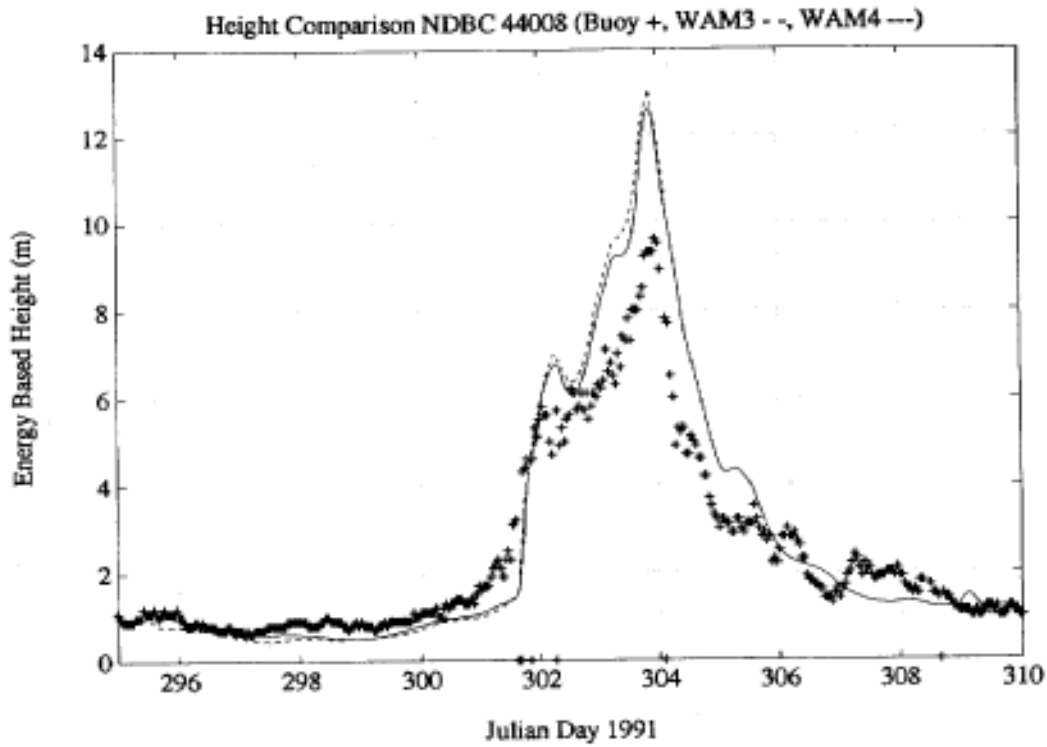


Fig. 5. Energy based wave height results from Cycles 3 and 4 compared to buoy measurements at NDBC 44008.

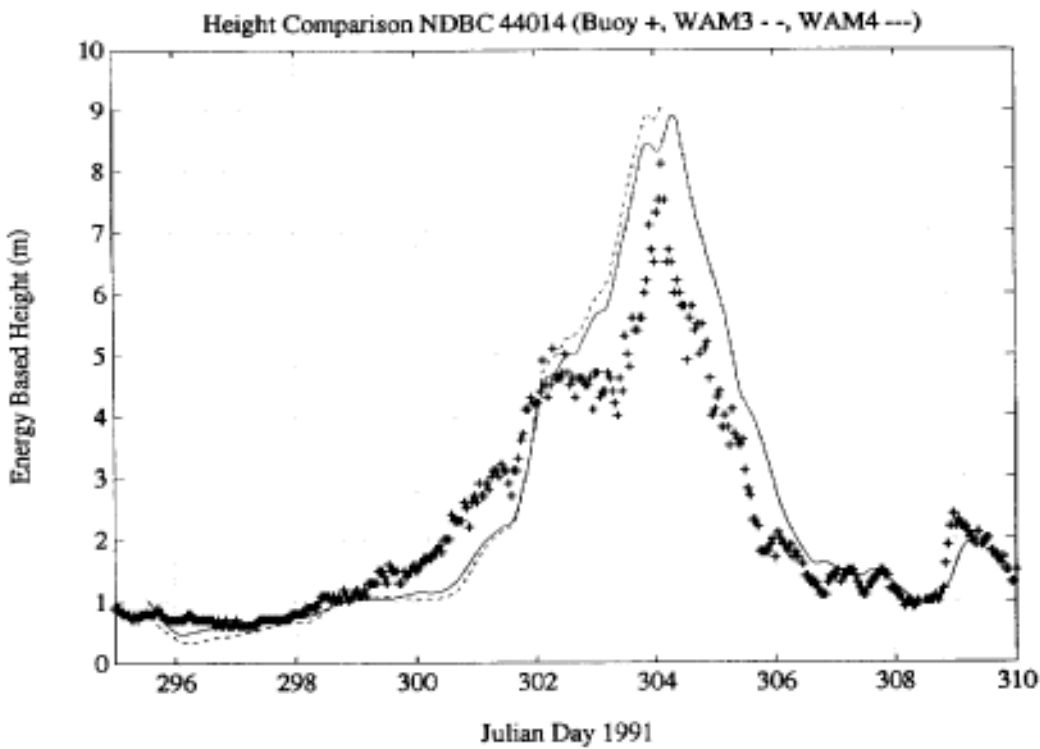


Fig. 6. Energy based wave height results from Cycles 3 and 4 compared to buoy measurements at NDBC 44014.

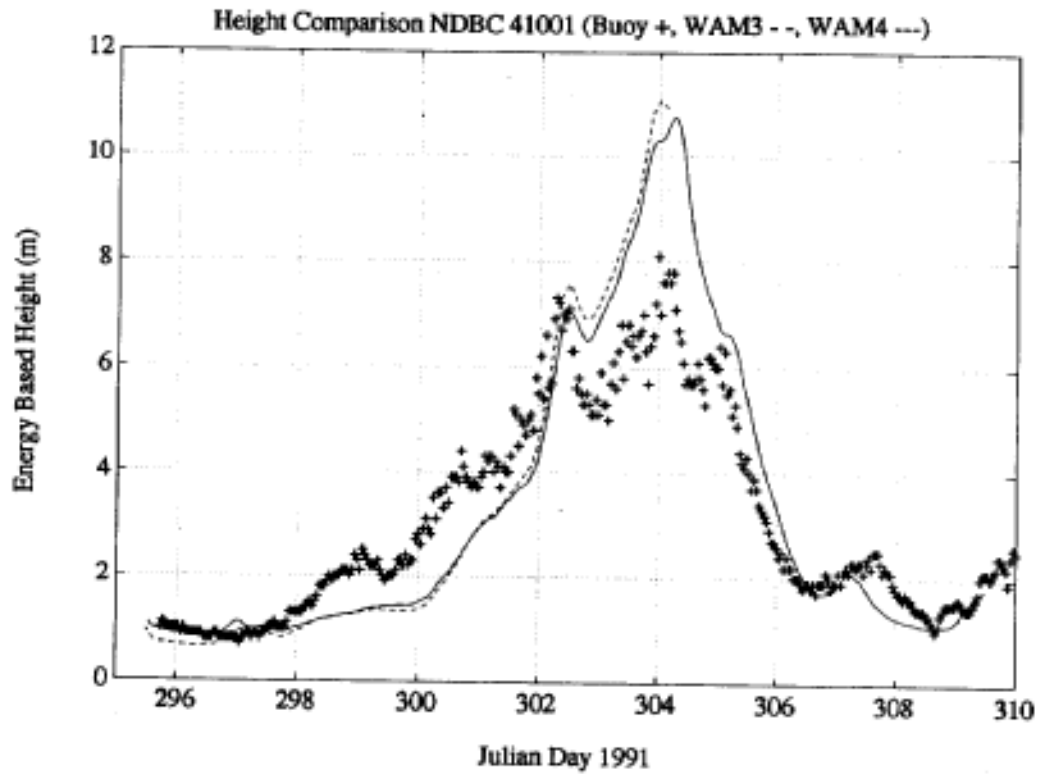


Fig. 7. Energy based wave height results from Cycles 3 and 4 compared to buoy measurements at NDBC 41001.

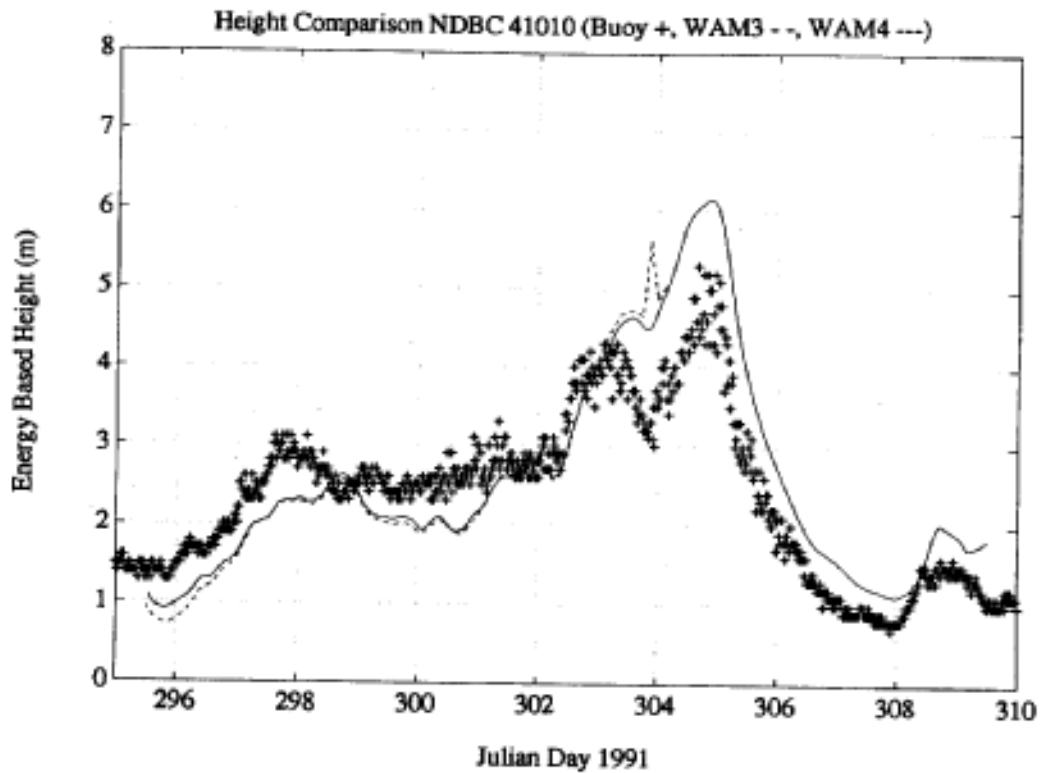


Fig. 8. Energy based wave height results from Cycles 3 and 4 compared to buoy measurements at NDBC 41010.

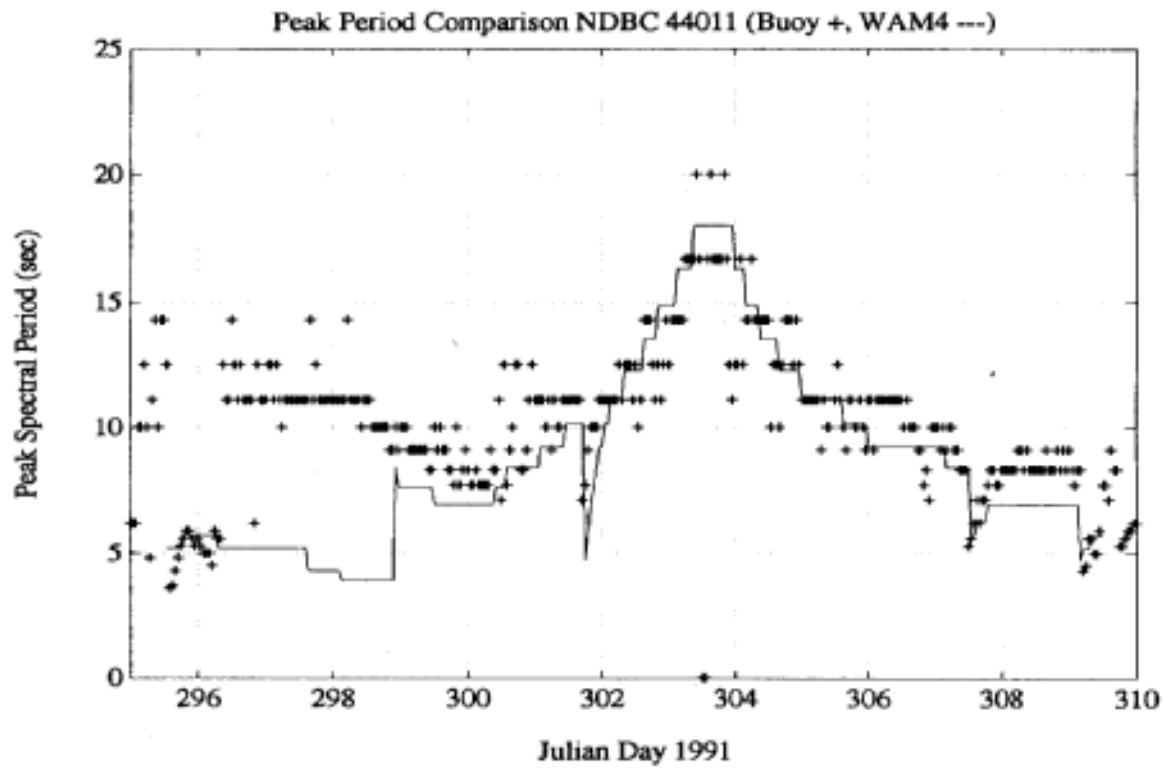


Fig. 9. Peak spectral period results from Cycle 4 compared to buoy measurements at NDBC 44011.

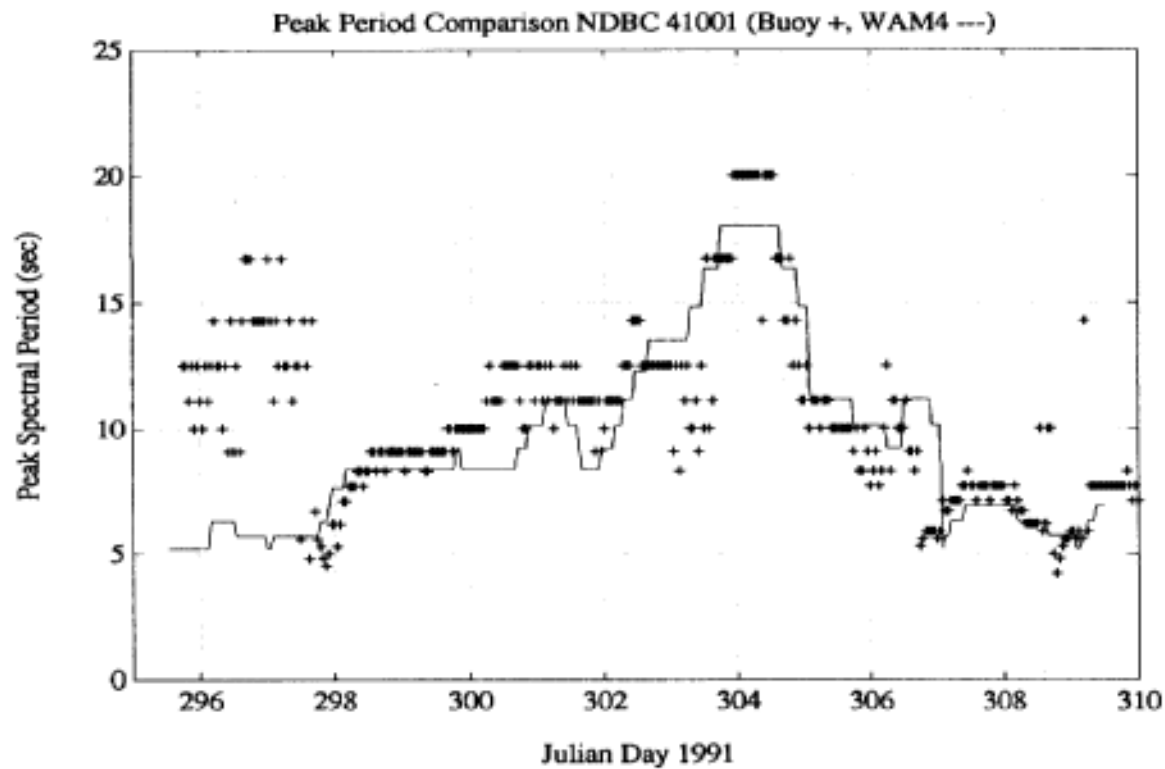


Fig. 10. Peak spectral period results from Cycle 4 compared to buoy measurements at NDBC 41001.

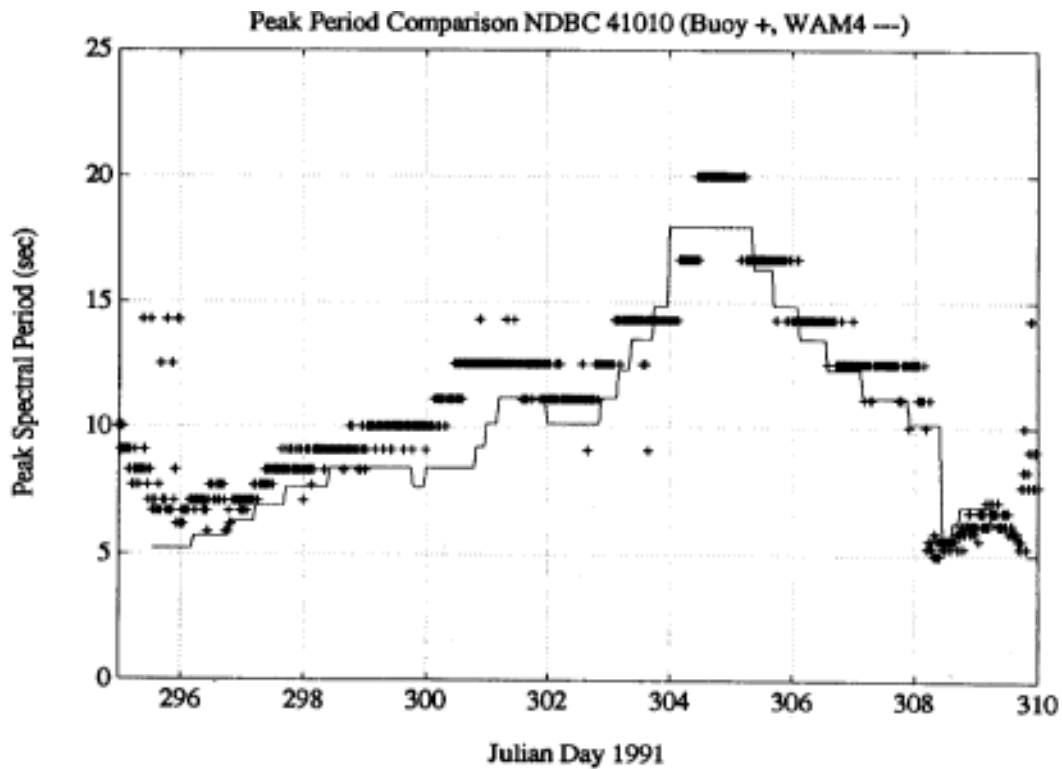


Fig. 11. Peak spectral period results from Cycle 4 compared to buoy measurements at NDBC 41010.

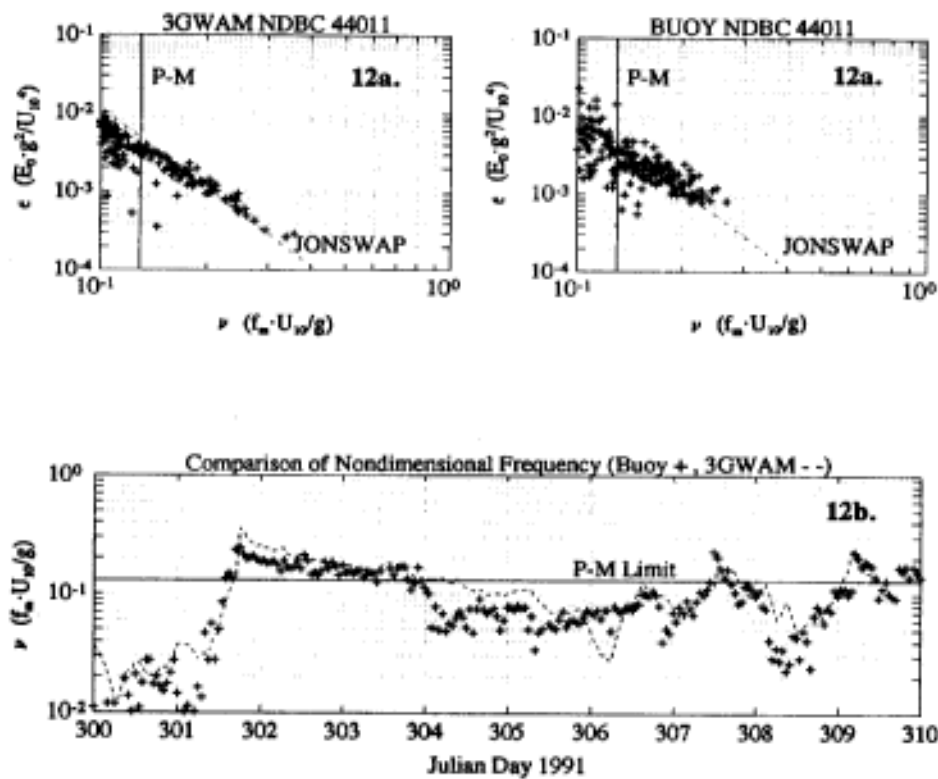


Fig. 12a and b. Nondimensional total energy versus nondimensional peak frequency scaled to U_{10} . Temporal variation in nondimensional peak frequency at NDBC 44011.

ACKNOWLEDGEMENTS

This work was performed as part of the activities of the Upgrading of Discrete Spectral Hindcasting Models work unit of the Coastal Flooding Research Program conducted by the Coastal Engineering Research Center, US Army Engineer Waterways Experiment Station. Permission was granted by the Office, Chief of Engineers to publish this information. Dr. H. C. Graber acknowledges support by ONR Grant No. N00014-09-J-1464. We would like to express our thanks and appreciation the Robin Brody of the Naval Research Laboratory, Monterey for his conscience effort in the generation of the stress fields used in this paper. Additional support from the Fleet Numerical Oceanography Center's Model Support Division is gratefully acknowledged, as well as Mr. Michael Caruso, Woods Hole Oceanographic Institution.

REFERENCES

- Graber H.C., M. J. Caruso and R.E. Jensen, 1991: Surface wave simulations during the October storm in SWADE, *MTS'91 Conference, An Ocean Cooperative: Industry, Government and Academia*, 159-164.
- Gunther, H., S. Hasselmann and P.A.M.E. Janssen, 1991: Wamodel Cycle 4. *Deutsches KlimaRechenZentrum, Technical Report No. 4, 91pp.*
- Hasselmann, K., T.P. Barnett, E. Bouws, H. Carlson, D.E. Cartwright, K. Enke, J.A. Ewing, H. Gienapp, D.E. Hasselmann, P. Krusemann, A. Meerburg, P. Muller, D.J. Olbers, K. Richter, W. Sell and H. Walden, 1973: Measurements of wind-wave growth and swell decay during the Joint North Sea Wave Project (JONSWAP), *Dtsch. Hydrogr. Z.* A12, 95 pp.
- Hogan, T.F. and T.E. Rosmond, 1991: The description of the Navy operational global atmospheric prediction system's spectral forecast model. *Monthly Weather Review*, 119, 1786-1815.
- Janssen, P.A.E.M., 1989: Wave-induced stress and the drag of air flow over sea waves. *J. Phys. Oceanogr.*, 19, 745-754.
- _____, 1991: Quasi-linear theory of wind wave generation applied to wave forecasting. *J. Phys. Oceanogr.*, 21, 1631-1642.
- Jensen, R.E., C.L. Vincent, M.J. Caruso and H.C. Graber, 1991: A wind-wave forecast for the Surface Wave Dynamics Experiment, *MTS'91 Conference, An Ocean Cooperative: Industry, Government and Academia*, 147-153.
- Louis, J.F., M. Tiedtke and J.F. Geleyn, 1982: A short history of the operational PBL-parameterization at ECMWF. Workshop on Planetary Boundary Parameterization, ECMWF, Reading, ENGLAND, 59-79.
- Pierson, W.J., and L. Moskowitz, 1964: A proposed spectral form for fully developed wind seas based on the similarity theory of K.A. Kitaigorodskii, *J. Geophys. Res.*, 89, (C3), 3586-3592.

WAMDIG (The WAM Development and Implementation Group): 1988: The WAM Model - a third generation ocean wave prediction model. *J. Phys. Oceanogr.*, 18, 1775-1810.

Wang, D.W. and T. Mettlach: 1992: The halloween storm: data observations from NDBC stations. *3rd International. Workshop on Wave Hindcasting and Forecasting.*, Environment Canada Atmospheric Environment Service.

Zambresky, L., 1989: A verification study of the global WAM model December 1987 - November 1988. Technical Report No. 63, European Centre for Medium Range Weather Forecasts, 86pp.

**KINEMATIC ANALYSIS OF THE SURFACE WIND FIELD IN THE
HALLOWEEN STORM AND A PRELIMINARY SPECTRAL MODEL WAVE HINDCAST**

V.J. Cardone and B. T. Callahan
Oceanweather, Inc.
Cos Cob, CT.

INTRODUCTION

This study is motivated by a number of unusual properties of this storm. First, from the standpoint of wave modeling, there is the measurement of wave heights of about 30 m (maximum) at buoy 44137, which is located just South of the Scotian Shelf. This sea state exceeds current estimates (e.g. Eid et. al, 1992) of rare return period (100-year) extremes in that area by about 50% Second, given the synoptic evolution of the storm as the complex interaction of an extratropical cyclone (EC) and a hurricane, it is interesting to explore the relationship of this evolution to the extreme sea states. In particular it would be interesting to resolve the contributions of each of these meteorological systems to the total wave field in the area of highest waves. If the tropical system could be shown to contribute significantly, then perhaps the usual approach to estimating extreme wave climates in areas susceptible to both classes of systems from extreme wave distributions developed separately for each class, might have to be modified. Finally, while sea states comparable to those recorded in this storm have been measured before, never have they been observed in an area where it appears possible to develop very accurate wind fields. The recent deployment of buoys by Atmospheric Environment Service (AES) offshore Nova Scotia and Newfoundland provides wind measurements from which (together with all other synoptic marine data) accurate wind fields may be derived by kinematic analysis, and wave measurements which may be used to validate wave models in a wave regime quite different from those normally used to calibrate the component physical mechanisms of such models.

WIND FIELD ANALYSIS METHOD

The objective of the wind field analysis is basically to describe the evolution of the surface wind field over a domain and of spatial and temporal resolution sufficient to hindcast the maximum sea states experienced off the east coasts of the US and Canada. After study of the measured wave data series at each buoy (see e.g. Wang and Mettlach, 1992) the following wind field attributes were adopted:

spatial domain	23 degrees N - 67 degrees N
	30 degrees W - 82 degrees W
grid system	0.5 degrees latitude by 0.5 degrees

	longitude
time step	3-hourly
reference	20m (effective neutral wind speed)
history	0000 UT 25 October - 1800 UT 1 November, 1991

The basic wind field analysis method is described in detail in Cardone (1980). The present practice of this approach is described by Cardone (1992). Briefly, the winds are derived as a blend of surface winds transformed from boundary layer pressure and temperature fields using a marine planetary boundary layer model (MPBL), and winds derived by kinematic analysis. Tedious hand-analysis is employed extensively to derive and maintain continuity of major pressure field and kinematic properties, to reanalyze pressure and temperature fields and for the kinematic analysis itself (refer to Cardone, 1992 for further details).

The principal data sources referred to are:

- NOAA Northern Hemisphere Surface Analysis - Final Analysis
- NOAA National Hurricane Center (NHC) Surface Analysis
- METOC Halifax Surface Analysis
- NOAA NCDC TDF-11 File of Surface Ship Reports
- NOAA and AES buoy observations

The file of ship data contains mainly reports transmitted in real time over the GTS. It is possible that later compilations of historical ship data may yield additional reports near the center of the storm.

The domain of kinematic analysis is restricted to the area shown in Figure 1 , which is a sample analysis at 00 UT 29 October. This area includes the rich networks of both NOAA and AES buoys and several active shipping lanes. It also contains the area within which both Hurricane Grace and the EC evolved and interacted during the period of interest. Kinematic analyses were also restricted in time to the period 12 UT 28 October - 21 UT 31 October.

GENERAL EVOLUTION OF THE WIND FIELD

The main features of the derived wind field are shown in Figure 2 , which displays winds (20 m neutral speeds) at 1 degree intervals (alternate grid points) at 24-hourly intervals between 00 UT 25 October and 00 UT 1 November, 1991. The first map (00 UT 25 October) indicates generally tranquil conditions in the analysis domain and indeed at almost all NOAA and AES buoys significant wave heights (HS) were generally less than 1 meter at this time. At least this extreme wave event evolves in a basin characterized initially by slight background seas and swells. By 00 UT 26 October, Grace is centered

near 25N, 65W. Over the next three days, Grace moved first west-northwestward, then eastward, as an EC developed on the front moving southward from the maritimes.

The wind field for 00 UT 29 October clearly shows the distinct circulations about Grace and the EC. The details of the interaction of Grace and the EC may never be completely resolved since there was no aircraft reconnaissance of Grace after this time. The NHC analyses carried a distinct circulation of Grace until 18 UT 29 October after which NHC considered its circulation absorbed into the EC system. Our kinematic analysis supports the survival of a distinct circulation center of the remnants of Grace until at least 06 UT 30 October. Regardless of the exact evolution of the center, however, there appears little doubt that the tropical system was responsible for the northward penetration of a band of gale force southerlies east of the center and toward the EC frontal boundary. Certainly by 00 UT 31 October, the wind field has simplified into the pattern of an extensive circulation about a single center located just south of Georges Bank.

Figure 3 provides a closer view of the evolution of the wind field during the 24-hour period 12 UT 29 October - 12 UT 30 October. During this period the AES East Coast buoys and the NOAA Georges Bank buoy recorded their peak winds and sea states in this event. For example Table 1 lists the observations from AES buoy 44137. The measured average surface wind (at anemometer height of 5 meters) peaks at 24.8 m/s at 0255 UT 30 October. One hour later the peak HS of 17.4m is measured with associated peak period of 18.3 seconds and maximum wave height of 30.7 m.

Before buoy winds are utilized in the analysis several adjustments are made. At the AES buoys, which use vector averaging for wind, wind speeds are increased by 5% to allow approximately for the negative bias in vector averages (Gilhousen, 1987). Wind speeds at most NOAA buoys are now based upon scalar averaging. At all buoys, both the anemometer height and the thermal stratification are considered to transform the measured wind into the effective neutral 20 m wind. For example, these adjustments transform the highest measured wind speed of 24.8 m/s at 44137 to a maximum effective neutral 20 m wind speed of 30 m/s, which in and of itself is not remarkably high and often found in strong east coast EC systems. Peak winds at the other NOAA and AES buoys were no greater than 30 m/s (20 m neutral) and one objective of this study is to gain understanding of why the Halloween storm wind field generated such extreme sea states.

Figure 3 shows that as the wind field about Grace slowly decayed, the area of strong northeasterlies over the Scotian Shelf and Grand Banks became organized about a central band with maximum speeds

of 30 M/B, which propagated slowly southwestward from the Grand Banks during this 24-hour period, passing directly over 44137 at 03 UT 30 October, then continuing westward with the EC center, passing over Georges Bank buoy 44011 at 12 UT 30 October. There can be little doubt that this wind field feature is primarily responsible for the pattern of generation of extreme sea states in the fetch extending from south of Grand Banks to Scotian Shelf and Georges Bank, from which emanated the extreme swells measured by the US East Coast buoys and observed along East Coast beaches on 31 October. However, our modeled wind field also suggest that the area from Scotian Shelf eastward to western Grand Banks, was susceptible to receive southerly swells generated in the strong southerlies east of Grace and its remnants.

COMPARISON OF MEASURED AND MODELED WINDS

Figure 4 compares modeled and measured winds (at 20 m) at NOAA buoys 44001 and 44011 and at AES buoys 44137 and 44139. These are typical of similar comparisons made at all buoy and C-MAN stations. Where hourly observations are available, they are smoothed to 3-hourly averages using a 1/4-1/2-1/4 weighting of the hourly observation in the three-hour window.

At buoy 41001, east of Cape Hatteras, winds varied slightly in speed and direction over the 4-day period 28-31 October and did not exceed about 20 m/s. At 44011, on Georges Bank, the influence of the approach and passage of the EC is more evident. As expected, agreement between modeled and buoy winds is better during the period of kinematic analysis than before or after, in part, of course, because the buoy winds were referred to in the kinematic analysis process. The same may be said of the comparison at the AES buoys 44137 and 44139. Indeed great care was taken to provide unbiased wind fields, though agreement between kinematic analysis and buoy winds was not forced artificially through the introduction of sub-synoptic scale variations (as such agreement is often obtained in objective fitting schemes).

Figure 5 gives scatter plots between MPBL and measured (adjusted) wind speeds (5a) and between kinematic and measured (adjusted) wind speeds (5b). The MPBL wind speeds exhibit a positive bias of about 2.4 m/s and rms error of 4.0 m/s. The positive bias is unusually large for this particular MPBL model analysis and may be caused by limitations, in this strongly cyclonic regime, of approximating trajectory curvature by isobar curvature. The scatter, however, is fairly typical of marine boundary layer winds. The kinematic winds exhibit much lower bias and lower scatter (Fig. 5b) than the MPBL winds.

WAVE HINDCAST

We have carried out a wave hindcast of the Halloween storm using the winds described above with our first generation ODGP2 model

adapted to the domain in the deep water mode, on a grid of 1/2 degree spacing. This model has been applied over the past decade in a large number of hindcast studies to develop operational and extreme wave criteria. A typical study is described in this conference by Cardone and Ewans (1992).

The hindcast is compared to the measurements of significant wave height and peak spectral period at the offshore buoys off the East Coast in Figure 6, which compares time histories at the same buoys used for Figure 5. We discuss these comparisons in the order 44139, 44137, 44011, 44001 or in order of time of occurrence of maximum winds and sea states.

At 44139, where sea states peaked late on the 29th, the hindcast is in excellent agreement with the measurements, except for a slight lag in the hindcast HS "growth" curve with respect to that measured, an effect typical of this and probably most first and second generation models in situations of very rapid growth. The hindcast peak spectral period (TP) is also generally within 1 second of that measured.

At 44137, located approximately 240 nm southwest, or downwind of 44139, the hindcast simulate the early part of the growth stage on the 29th (we refer to the rapid local increase in wave height loosely as "growth", though local wave responses are actually the combination of advection and growth) but the peak hindcast HS is 3.7 m lower than that measured. While spectra at this buoy have not yet been compared, the deficit in wave energy around the storm peak at 44137 is probably concentrated in the low frequency part of the spectrum, since TP is underpredicted at the storm peak by about 1.7 seconds. It is not possible to partition the reduction of wave energy directionally, because directional wave measurements were not made. The hindcast directional spectrum of the peak sea state at 44137 is distinctly bimodal with about 10% of the total wave variance found in northbound (or crosswind) propagating directions. Some of the deficit of variance in the hindcast spectrum may be associated with underspecification of this southerly swell, especially since this hindcast is in such excellent agreement with peak sea states measured at buoys moored east and west of 44137, in areas not as susceptible to the influence of northerly swell from the southern tropical system.

At the NOAA Georges Bank buoy, 44011, the hindcast time series of HS and TP are found to be in excellent agreement with the measurements. At 44001, excellent agreement is also found including the simulation of the arrival of the long period swell (TP between 18-20 seconds) late on the 30th.

Table 2 compares hindcast and observed peaks of HS and associated TP at 18 buoy and C-MAN measurement sites. Figure 7 gives

scatter plots for HS and TP storm peaks. The mean difference in HS is 0.49m (hindcast lower than measured), and the scatter index is 19%, which is somewhat larger than usually provided by the combination of wind and wave hindcast methodology applied. For TP the mean difference is .43 seconds and scatter index is 22%. Since some of the buoys are located in shallow water and within two model grid distances of the coast, hindcast errors should be lower if only deep water offshore sites are considered. Restricting the comparisons to buoys which are in deep water and at least 60 nm offshore (namely 41001, 41002, 44008, 44011, 44137, 44138, 44139, 44140, 44141). the scatter index is indeed reduced (scatter index of HS of 15%) but the bias is still 1 m due to the underspecification at peak HS at 44137 and 44141). Figure 8 compares hindcast and measured HS and TP for the full time series (three-hourly time steps) at the eight offshore deep water buoys, for the main storm period (29 October - 01 November). The mean differences in HS and TP are exceptionally low at .07m and .22 seconds, respectively. The scatter indices of 18% (HS) and 13% (TP) are also low for time series comparisons.

CONCLUSIONS

1. The time and space evolution of the surface wind field in the Halloween storm can be well described through intensive reanalysis of synoptic data, because Most of the evolution occurred within the enhanced observation array (relative to typical marine areas) associated with the NOAA and AES east coast buoy arrays. The main residual uncertainty concerns the details of the absorption of the remnants of Grace by the extratropical -cyclone.

2. Before use in the analysis the buoy winds have been adjusted for anemometer height and stability, vector average wind speeds have been increased by 5%. and anemometer sampling variability has been attenuated (in part) by smoothing the buoy winds to 3-hourly means. According to our analysis, which assimilated the buoy data, maximum wind speeds in the Halloween storm did not exceed 30 m/sec (1-hour average at 20 m). However, we remain concerned that wind measurements from anemometers mounted at heights near 5 meters on small hull buoys are affected by buoy motion or trough sheltering effects in the extreme sea states generated by this storm. Even small biases, say 5% or so, would lead to at least 10% errors in wave hindcasts in the nearly fully arisen sea states characterizing the highest seas measured.

3. A preliminary hindcast made with an operational first generation spectral wave model provides a generally skillful hindcast of time histories of significant wave height and associated peak spectral period off the east coast. However, the hindcast underspecified the magnitude of the most extreme sea states (HS

greater than 13 m or so) which apparently affected only a small area of the storm near AES buoys 44137 and 44141. Since this area was most susceptible of receiving swell from the seaway generated by the hurricane to the south (in an area where wind errors are larger) it is difficult at this time to attribute the hindcast error at the peak of the storm near 44137 to any particular effect. Further hindcast experiments using a third generation wave model are underway to help resolve this issue.

ACKNOWLEDGEMENTS

This study is supported by Atmospheric Environment Service (Contracts KM 1701-8549 and KM 170-2-8871). under the direction of Val Swail. Oceanweather meteorologists A.T. Cox and M.J. Parsons participated in the synoptic analyses and managed the wind field production.

REFERENCES

Cardone, V. J., A. J. Broccoli, C. V. Greenwood and J. A. Greenwood, 1980: Error characteristics of extratropical storm wind fields specified from historical data. J. Petrol. Tech., 32, 873-880.

Cardone, V. J., 1992: On the structure of the marine wind field in extratropical storms. Preprints of the Third International Workshop on Wave Hindcasting and Forecasting, May 19-22, 1992, Montreal, Quebec, 54-66.

1

Cardone, V. J. and K. C. Ewans, 1992: Validation of the hindcast approach to the specification of wave conditions at the Maui location off the west coast of New Zealand. Preprints of the Third International Workshop on Wave Hindcasting and Forecasting, May 19-22, 1992, Montreal, Quebec, 232-247.

Eid, B. M., C. Morton, E. Dunlop and T. Pierce, 1992: Development of wind and wave climate atlas for the east coast of Canada and the Great Lakes. Preprints of the Third International Workshop on Wave Hindcasting and Forecasting, May 19-22, 1992, Montreal, Quebec, 362-372.

Gilhousen, D. B. 1987: A field evaluation of NDBC moored buoy winds. J. Atmos. Ocean. Tech., 4, 94-104.

Wang, D. and T. Mettlach. 1992: The Halloween storm: data observations from NDBC stations. Preprints of the Third International Workshop on Wave Hindcasting and Forecasting, May 19-22, Montreal, Quebec, 383-400.

Table 1. Hourly observations at AES buoy 44137 (41.2N, 61.1W). Hour is UT, Dirl/D2 is wind direction, SPD1/SPD2 is wind speed (m/s), SWH is significant wave height (m), PER is peak wave period (sec), HMAX is maximum wave height (m), PRESS1/2 is sea level pressure, TAIR is air temperature (deg C.), TSEA is sea temperature (deg C.).

YEAR	MON	DY	HOUR	DIR1	SPD1	DR2	SPD2	SWH	PER	S1MX	S2MX	HMAX	PRESS1	PRESS2	TAIR	TSEA	BUOY#	WATER
1991	Oct	29	2355	359	10.3	30	10.4	2.7	32.0	12.4	12.3	6.3	1003.5	1003.4	15.9	20.2	44137	0
1991	Oct	29	055	355	12.4	24	12.3	3.1	32.0	14.5	14.4	6.0	1002.8	1002.8	15.7	20.2	44137	0
1991	Oct	29	155	358	14.0	26	13.9	3.3	7.4	16.5	16.3	5.7	1002.7	1002.7	14.9	20.2	44137	0
1991	Oct	29	255	2	13.5	30	13.4	3.8	7.4	16.8	16.8	6.7	1002.8	1002.8	14.5	20.2	44137	0
1991	Oct	29	355	3	16.1	31	16.0	4.5	9.5	20.4	20.2	9.5	1002.4	1002.3	13.4	20.3	44137	0
1991	Oct	29	455	10	17.7	38	17.5	5.9	10.7	21.7	20.6	12.0	1002.6	1002.6	12.7	20.3	44137	0
1991	Oct	29	555	4	18.4	32	18.4	6.1	11.1	22.6	21.9	10.9	1003.3	1003.3	11.9	20.4	44137	0
1991	Oct	29	655	6	18.0	36	18.4	7.2	12.2	22.3	21.4	16.4	1003.6	1003.6	11.5	20.4	44137	0
1991	Oct	29	755	11	18.2	43	18.3	7.9	11.6	22.7	22.5	14.9	1003.1	1003.1	11.7	20.5	44137	0
1991	Oct	29	855	9	20.3	43	20.3	8.5	12.8	25.4	24.8	15.6	1003.3	1003.3	11.3	20.7	44137	0
1991	Oct	29	955	17	20.6	50	20.8	8.5	13.5	25.5	24.8	13.4	1003.3	1003.3	11.0	20.7	44137	0
1991	Oct	29	1055	15	20.5	51	20.4	9.7	13.5	25.8	25.9	18.9	1004.0	1004.0	11.0	20.7	44137	0
1991	Oct	29	1155	14	19.7	53	19.5	9.2	13.5	24.9	24.3	21.5	1004.1	1003.9	11.1	20.8	44137	0
1991	Oct	29	1255	17	20.0	58	19.4	9.9	12.8	23.9	24.1	17.7	1004.6	1004.5	10.9	20.8	44137	0
1991	Oct	29	1355	19	18.6	59	18.3	9.4	12.8	24.5	23.5	14.2	1004.2	1004.2	11.6	20.8	44137	0
1991	Oct	29	1555	25	18.9	62	19.0	11.6	15.1	24.1	23.9	20.1	1004.3	1004.3	11.7	20.6	44137	0
1991	Oct	29	1655	31	19.0	65	18.8	10.3	5.1	25.1	24.9	18.1	1003.0	1003.0	12.4	20.5	44137	0
1991	Oct	29	1755	26	19.4	59	19.3	11.5	5.1	26.2	25.3	21.2	1003.1	1003.1	11.9	20.4	44137	0
1991	Oct	29	1855	29	20.7	58	20.5	12.3	16.0	26.8	25.9	17.6	1003.0	1002.9	12.0	20.3	44137	0
1991	Oct	29	1955	30	20.7	59	20.5	12.0	16.0	26.2	25.9	24.6	1002.4	1002.4	12.2	20.2	44137	0
1991	Oct	29	2055	27	21.6	57	21.3	11.8	17.1	28.4	27.7	18.4	1001.9	1001.8	12.5	20.2	44137	0
1991	Oct	29	2155	32	20.6	64	20.7	12.5	17.1	27.4	26.5	22.9	1001.3	1001.3	13.1	20.2	44137	0
1991	Oct	29	2255	44	21.7	76	21.5	13.6	17.1	27.5	27.2	24.2	1000.9	1000.9	13.7	20.2	44137	0
1991	Oct	30	2355	43	21.7	77	21.8	14.5	15.1	29.6	29.2	29.8	1000.8	1000.7	14.2	20.2	44137	0
1991	Oct	30	055	39	22.6	75	22.8	13.3	15.1	29.0	29.0	23.9	999.3	999.3	14.3	20.2	44137	0
1991	Oct	30	155	41	24.3	79	23.8	14.3	17.1	32.7	32.0	26.3	997.1	997.1	14.5	20.2	44137	0
1991	Oct	30	255	41	24.8	80	24.7	15.2	17.1	35.1	33.9	22.4	998.2	998.1	14.6	20.1	44137	0
1991	Oct	30	355	40	23.7	80	23.5	17.4	18.3	32.3	32.0	30.7	996.9	996.9	14.8	20.1	44137	0
1991	Oct	30	455	41	24.3	81	24.0	16.3	16.0	31.4	31.3	29.4	996.3	996.4	14.5	20.0	44137	0
1991	Oct	30	555	41	23.7	82	23.3	17.2	18.3	31.7	31.5	30.6	995.1	995.2	14.4	19.9	44137	0
1991	Oct	30	655	55	24.4	95	23.9	14.7	18.3	34.0	33.8	24.0	994.0	994.0	15.7	19.9	44137	0
1991	Oct	30	755	57	21.6	98	20.9	15.8	16.0	29.3	28.6	24.1	994.2	994.2	16.9	19.9	44137	0
1991	Oct	30	855	77	15.6	121	15.4	15.8	18.3	19.5	19.9	26.4	994.5	994.5	19.2	20.0	44137	0
1991	Oct	30	955	95	13.0	145	12.4	15.2	18.3	16.3	15.9	22.4	995.8	995.9	19.4	20.1	44137	0
1991	Oct	30	1055	108	14.2	158	13.5	14.1	16.0	19.3	18.7	23.3	997.8	997.7	19.5	19.9	44137	0
1991	Oct	30	1155	110	14.1	158	13.4	13.1	18.3	19.8	19.1	24.1	999.0	999.0	19.0	20.1	44137	0
1991	Oct	30	1255	105	17.6	151	16.7	12.4	17.1	22.3	21.5	25.2	999.6	999.5	20.2	20.1	44137	0
1991	Oct	30	1355	119	17.0	164	16.3	12.2	17.1	22.8	22.0	19.6	1001.4	1001.4	21.3	20.3	44137	0
1991	Oct	30	1455	126	17.4	167	16.7	13.3	17.1	23.0	22.0	21.3	1003.3	1003.4	21.4	20.4	44137	0
1991	Oct	30	1555	128	16.5	167	15.8	11.1	17.1	21.2	20.5	18.0	1003.8	1003.8	21.3	20.4	44137	0
1991	Oct	30	1655	138	15.4	173	14.8	11.6	13.5	19.2	18.7	20.0	1005.1	1005.1	21.5	20.3	44137	0
1991	Oct	30	1755	146	13.5	177	13.6	11.4	16.0	17.6	16.4	19.9	1006.7	1006.6	21.6	20.3	44137	0
1991	Oct	30	1855	140	12.6	169	12.1	10.5	13.5	16.3	15.5	18.2	1008.0	1008.0	21.6	20.3	44137	0
1991	Oct	30	1955	139	12.2	168	11.5	10.3	11.6	17.8	17.2	18.9	1009.8	1009.6	21.6	20.2	44137	0
1991	Oct	30	2055	140	11.8	169	11.7	9.4	11.6	15.4	15.3	14.9	1011.2	1011.1	21.1	20.1	44137	0
1991	Oct	30	2155	127	9.1	156	8.8	8.7	13.5	12.1	11.7	15.5	1012.1	1012.0	21.0	19.8	44137	0
1991	Oct	30	2255	131	11.2	164	11.0	8.6	15.1	13.6	13.8	13.6	1013.3	1013.1	21.7	19.7	44137	0
1991	Oct	31	2355	135	11.0	175	10.9	8.0	13.5	14.1	14.2	11.9	1014.6	1014.5	21.6	19.6	44137	0

Table 2. Comparison of hindcast and measured storm peaks at NOAA and AES buoy and C-MAN stations in Halloween storm.

**PEAK TO PEAK COMPARISON
OF
MEASURED VS. HINDCAST (1G WAVE MODEL WITH ENHANCED WINDS)
WAVE HEIGHT AND ASSOCIATED PEAK PERIOD**

BUOY	MEASURED			HINDCAST			ABS. DIFF. (MEAS-HIND)	
	TIME	Hs (m)	Tp (s)	TIME	Hs (m)	Tp (s)	Hs (m)	Tp (s)
41001	3103	7.65	20.00	3014	6.79	14.89	0.86	5.11
41002	3109	7.65	20.00	3011	6.21	12.72	1.44	7.28
44007	3100	6.72	18.57	3107	5.67	14.78	1.05	3.79
44008	3100	9.37	13.05	3100	9.85	18.42	-0.48	-5.37
44009	3112	4.65	13.85	3115	5.87	16.25	-1.22	-2.40
44011	3015	11.57	18.35	3019	11.59	15.78	-0.02	2.57
44012	3106	4.20	17.52	3115	5.31	16.19	-1.11	1.33
44013	3103	8.04	16.70	3107	6.33	15.60	1.71	1.10
44014	3103	7.80	17.52	3118	5.76	16.12	2.04	1.40
44025	3109	4.87	10.05	3110	5.76	16.98	-0.89	-6.93
44137	3006	16.35	17.72	3006	12.64	16.01	3.71	1.71
44138	2918	11.40	13.32	2919	10.57	13.96	0.83	-0.64
44139	2915	9.85	14.65	3006	9.73	13.76	0.12	0.89
44140	2921	7.92	11.75	3003	8.81	13.19	-0.89	-1.44
44141	3003	13.20	15.32	2919	9.70	13.86	3.50	1.46
ALSN6	3109	2.80	12.50	3111	4.38	17.44	-1.58	-4.94
CHLV2	3106	3.93	17.80	3118	5.29	16.30	-1.36	1.50
DSL7	3109	6.37	16.70	3123	5.28	15.71	1.09	0.99

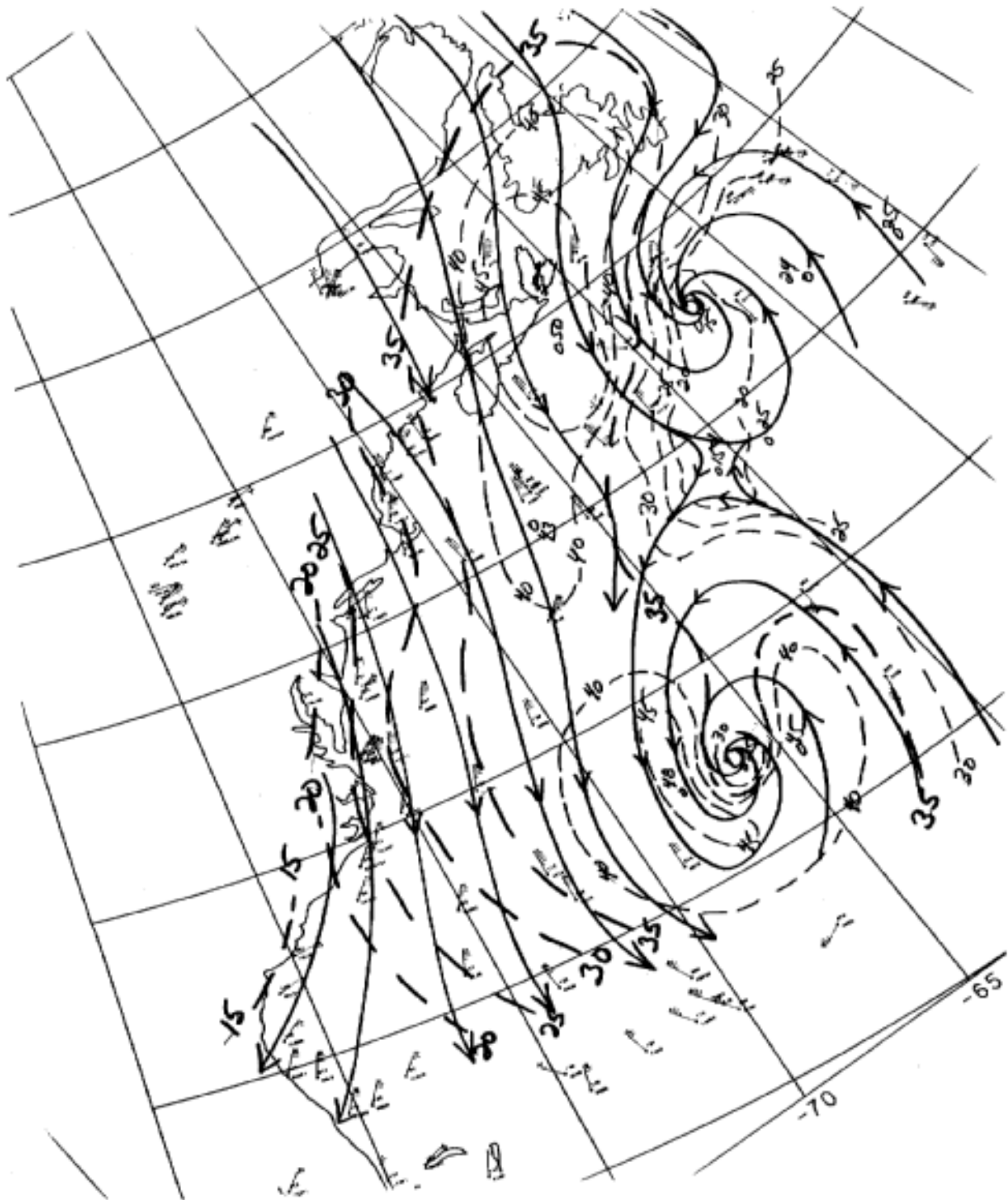


Figure 1. Sample kinematic analysis (00 UT 29 October, 1991). Solid lines are streamlines, dashed lines are isotachs (5 knot intervals). Buoy, C-MAN station and transient ship reports of wind are plotted (knots) after adjustment of speeds to effective neutral 20 m level.

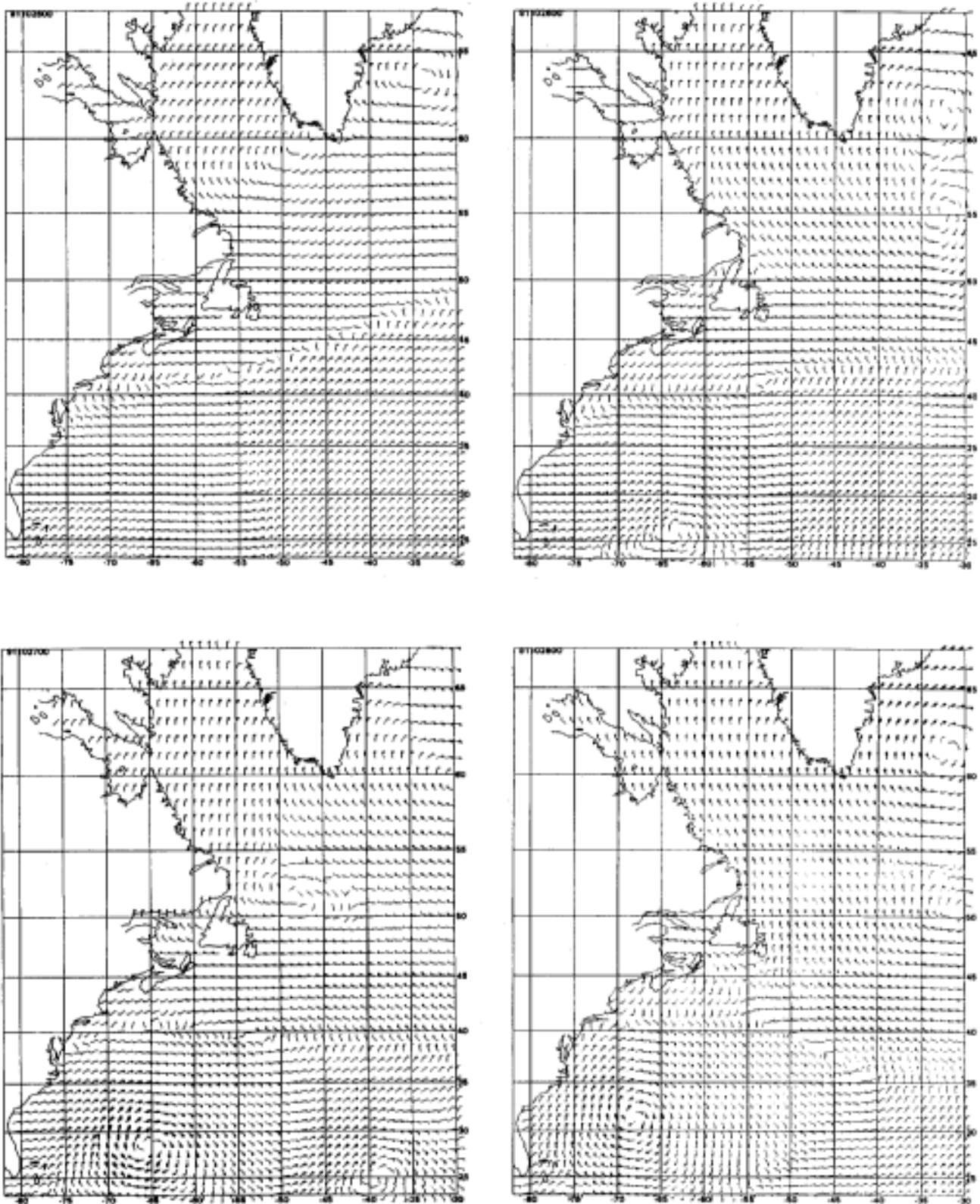
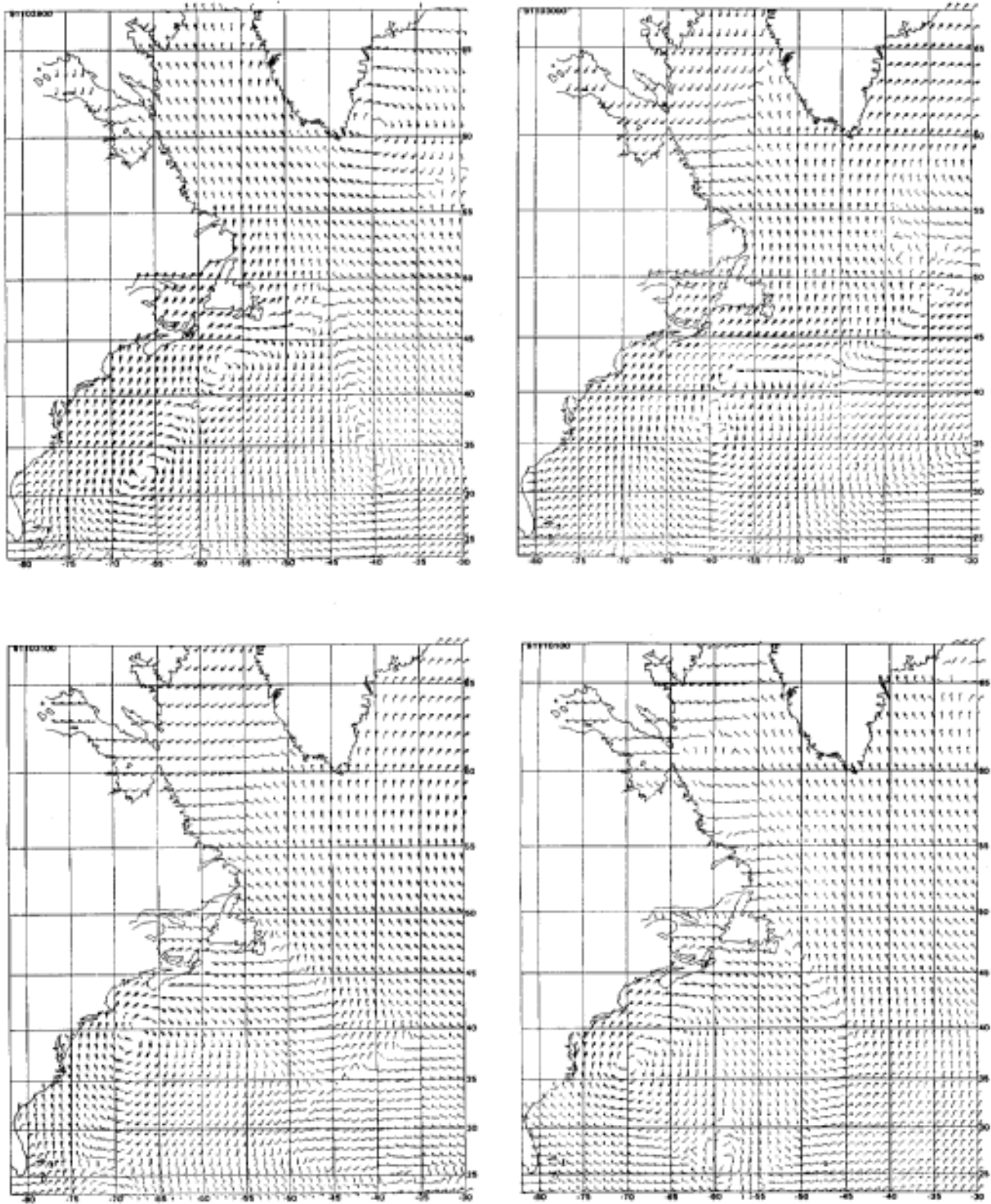


Figure 2. Final analyzed wind fields (20 m) at 24-hourly intervals between 00 UT 25 October and 1 November, 1991.



cont.

Figure 2. Final analyzed wind fields (20 m) at 24-hourly intervals between 00 UT 25 October and 1 November, 1991.

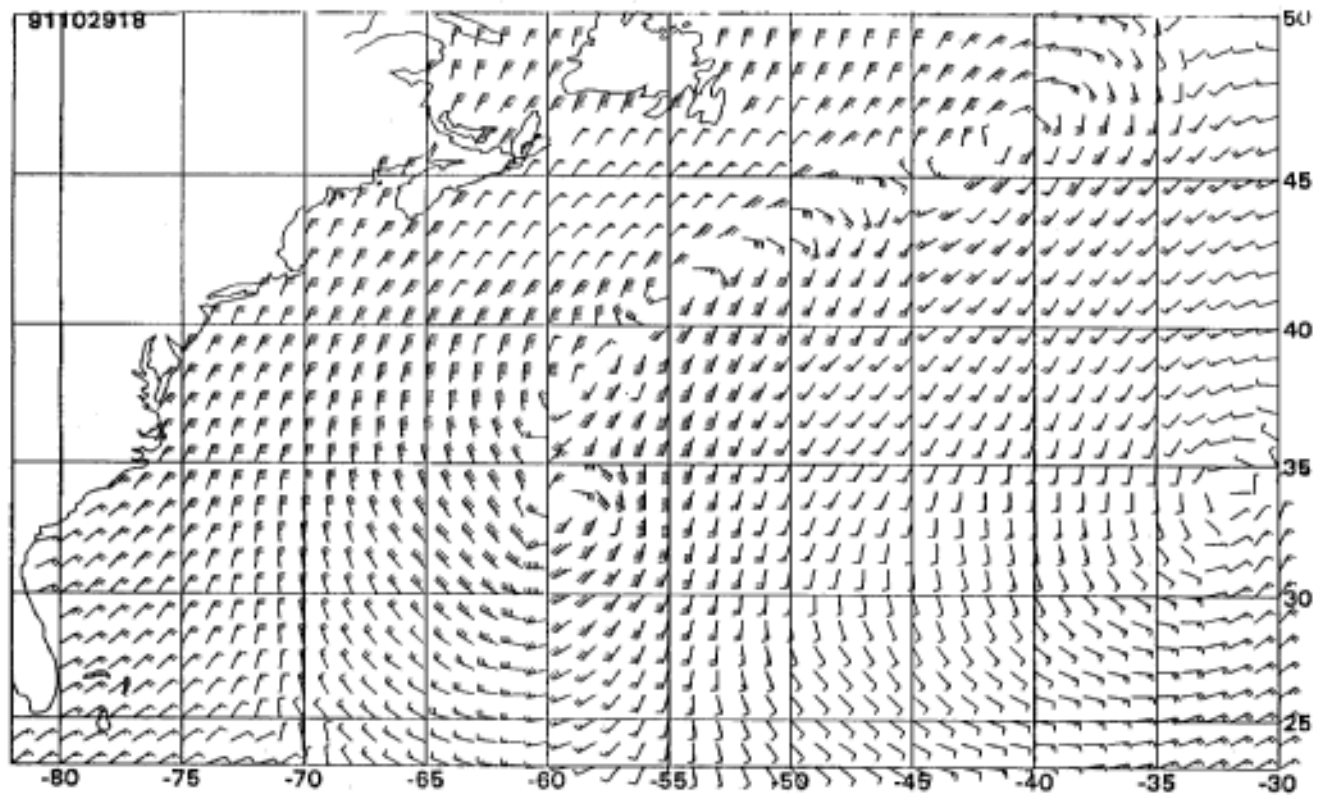
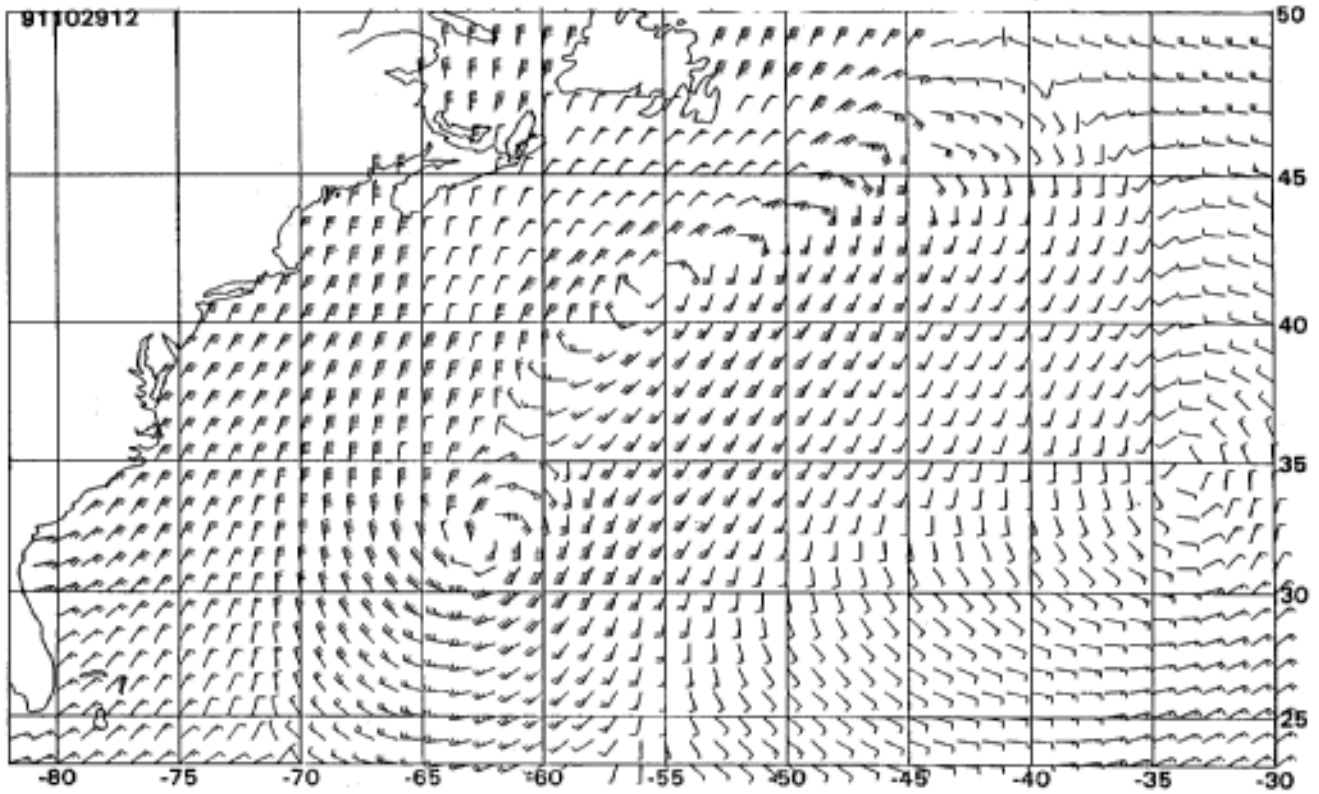


Figure 3. Final analyzed wind fields at 6-hourly intervals between 12 UT 29 October and 06 UT 30 October, 1991.

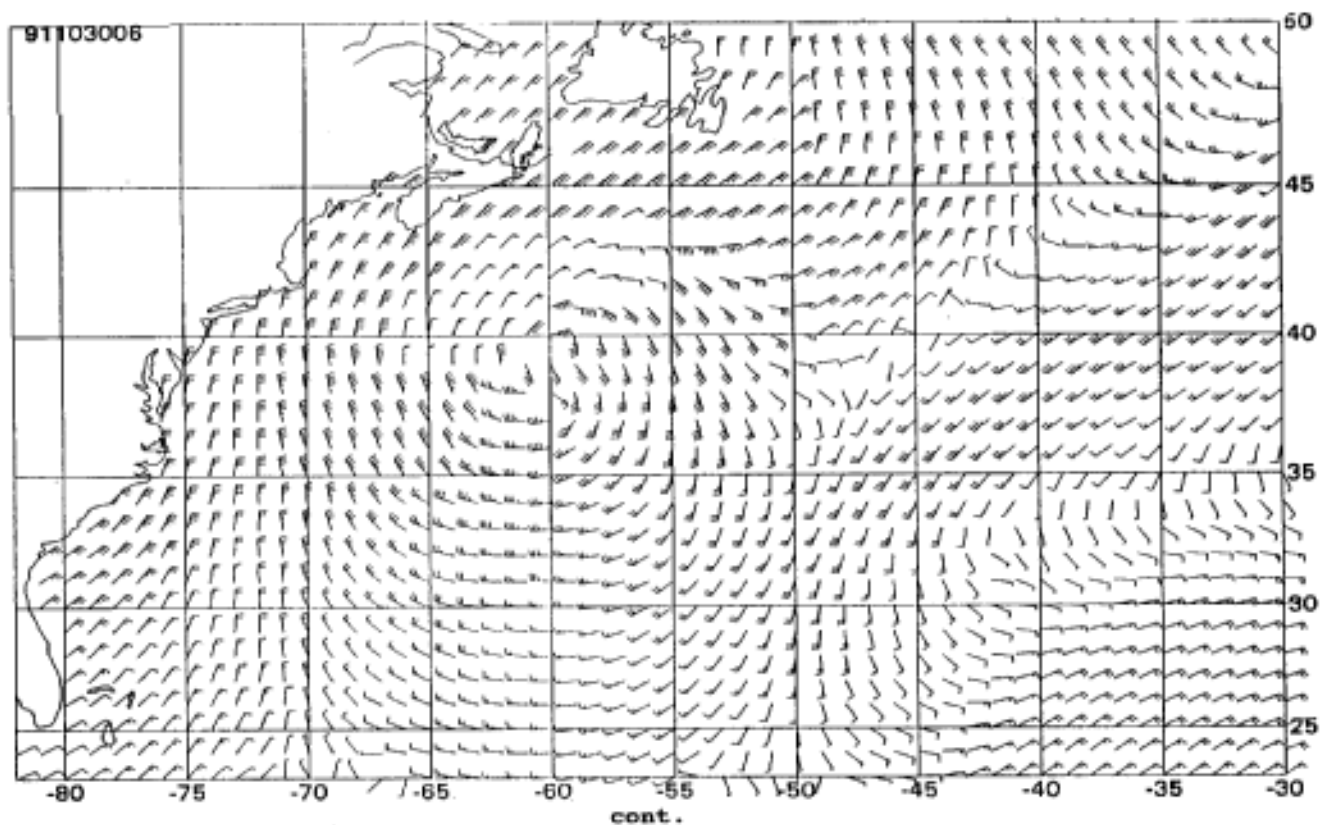
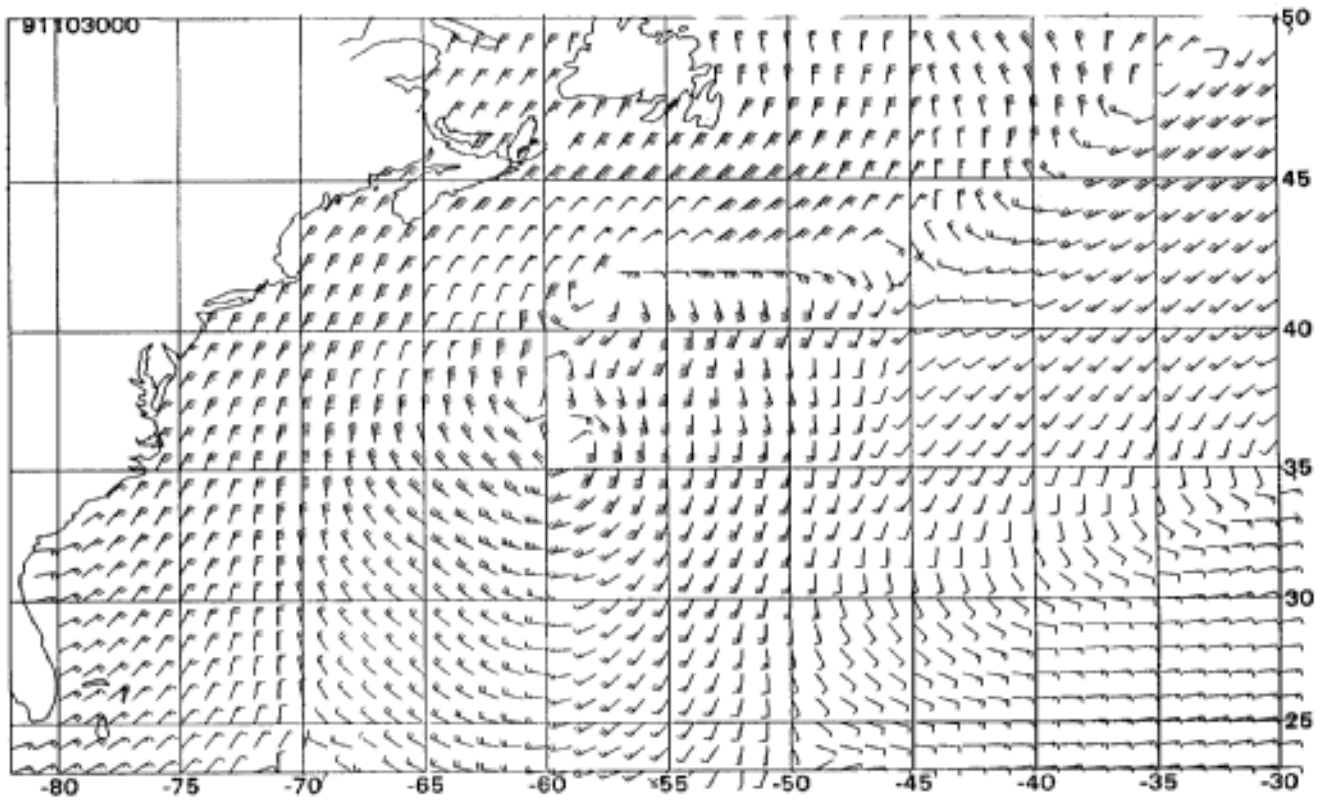


Figure 3. Final analyzed wind fields at 6-hourly intervals between 12 UT 29 October and 06 UT 30 October, 1991.

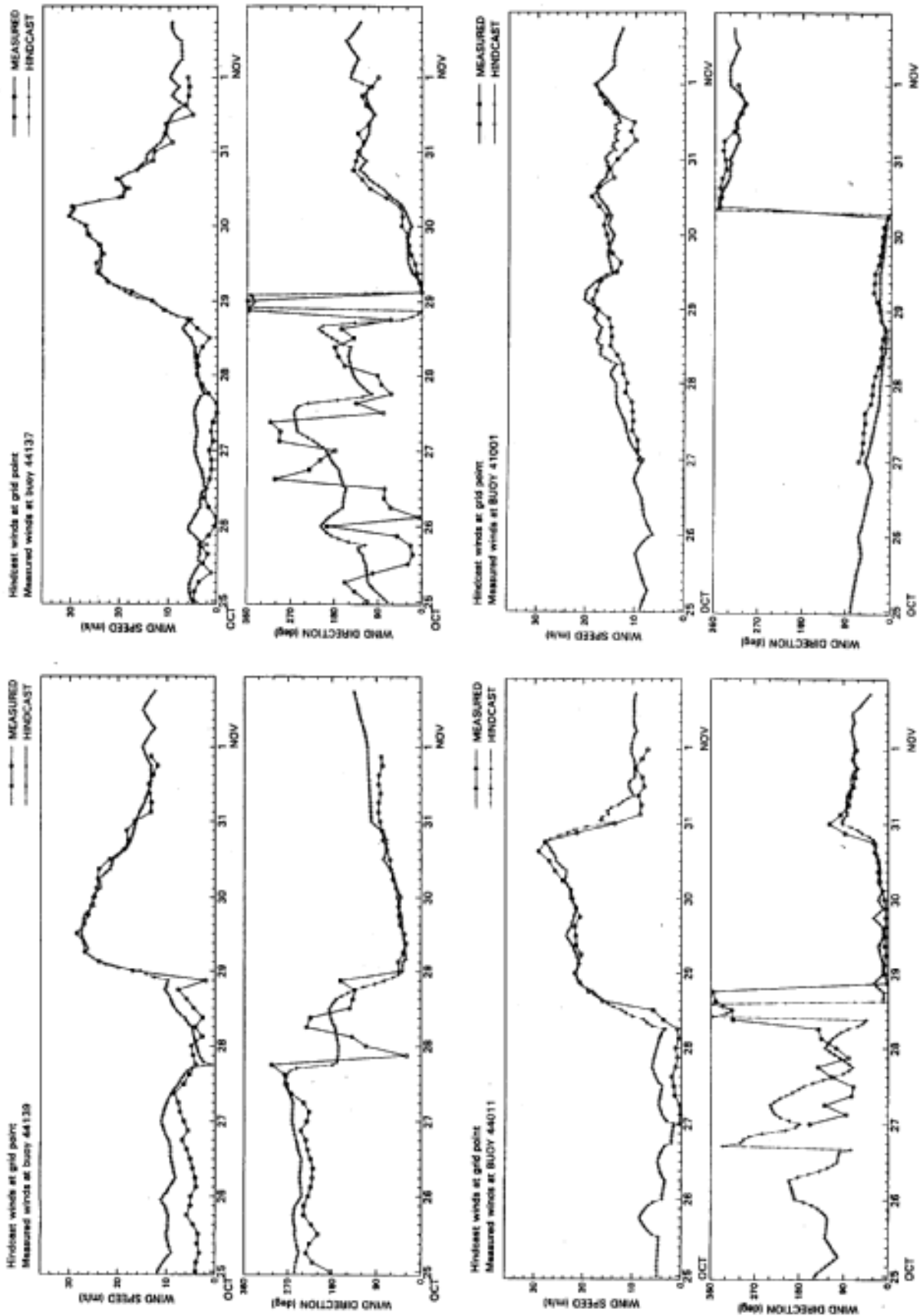
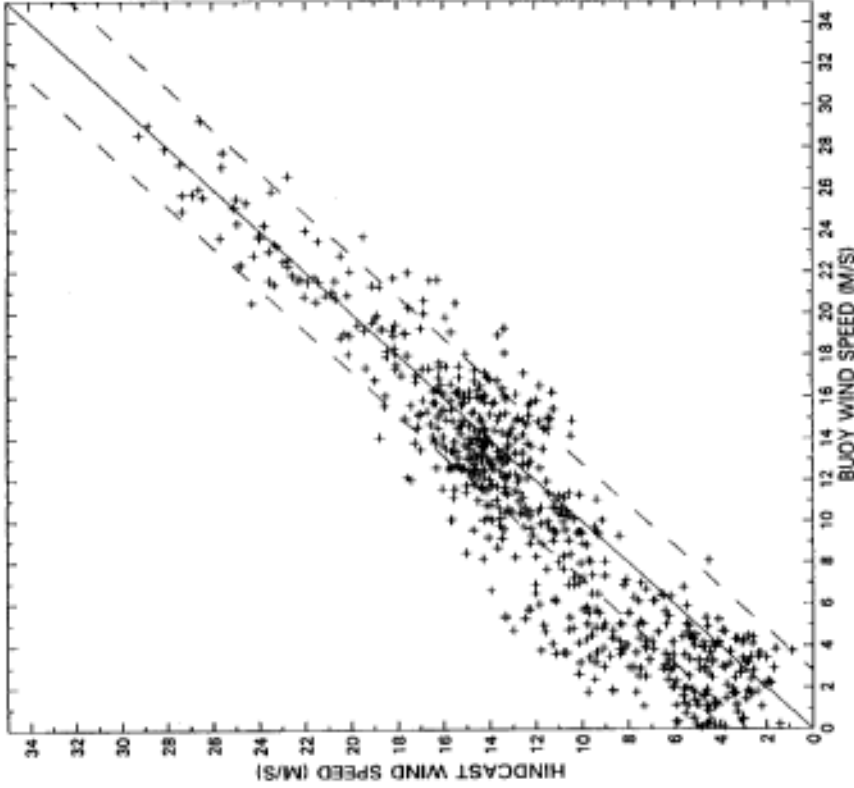


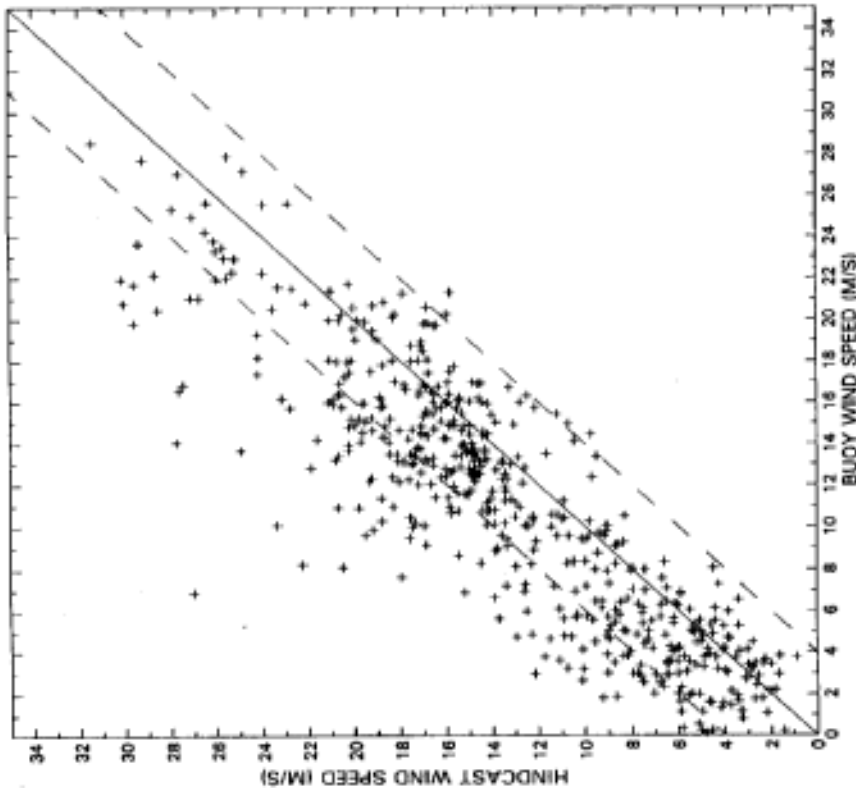
Figure 4. Comparison of time histories of hindcast and measured (adjusted) winds at selected offshore buoys.

HALLOWEEN STORM
91102500 - 91110118
KINEMATIC WINDS VS. 14 BUOYS



Total number of points:	636
Average measurement:	10.93
Average hindcast:	12.16
Mean difference:	-1.23
Root mean square:	2.82
Standard deviation:	2.54
Scatter index:	.23
Ratio:	.30

HALLOWEEN STORM
91102500 - 91110118
PRESTO WINDS VS. ALL [24] BUOYS/CMAN STATIONS



Total number of points:	533
Average measurement:	11.15
Average hindcast:	13.52
Mean difference:	-2.37
Root mean square:	3.98
Standard deviation:	3.20
Scatter index:	.29
Ratio:	.23

Figure 5. Comparison of analyzed and measured winds for (a) planetary boundary layer model and (b) kinematic analysis.

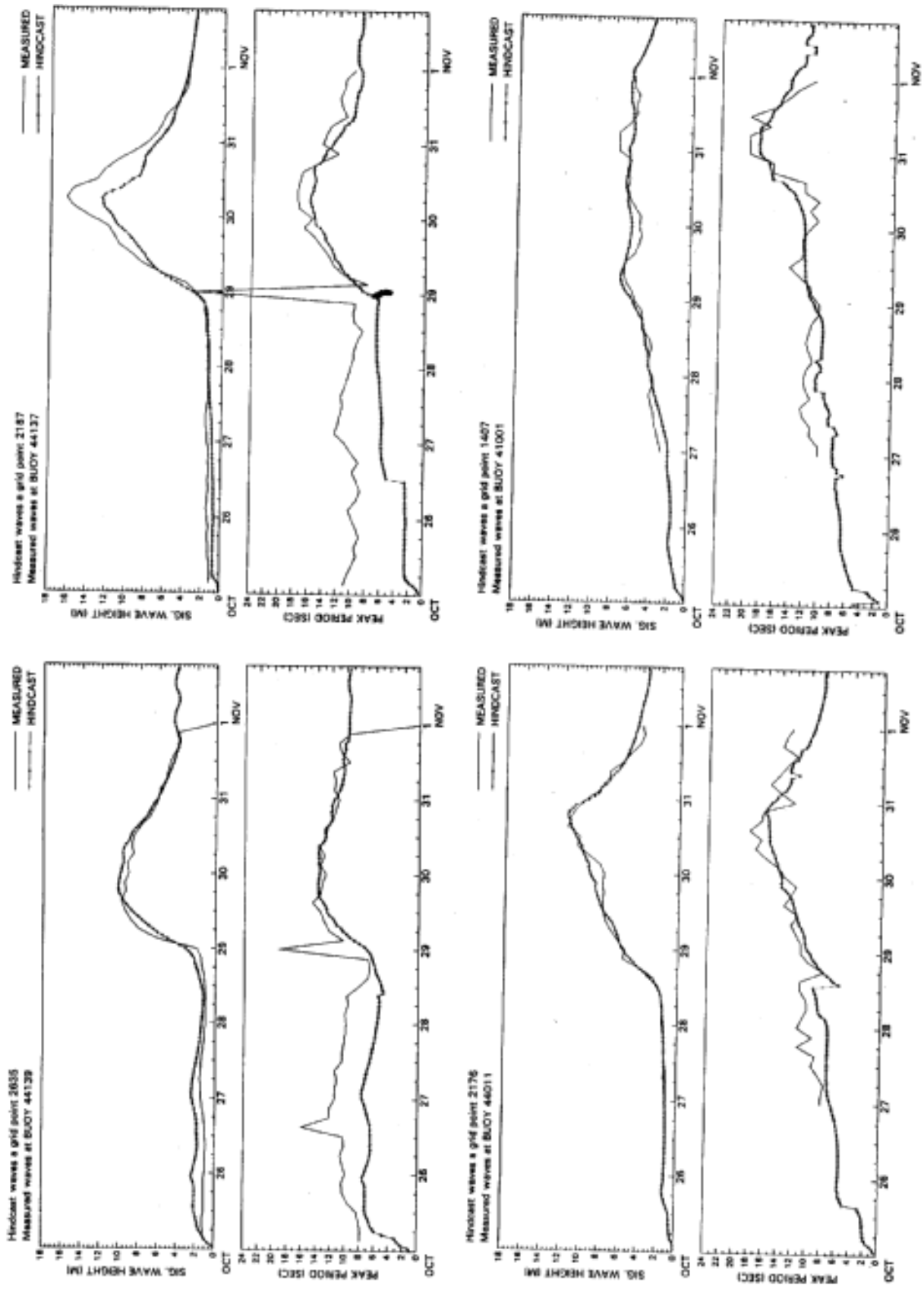
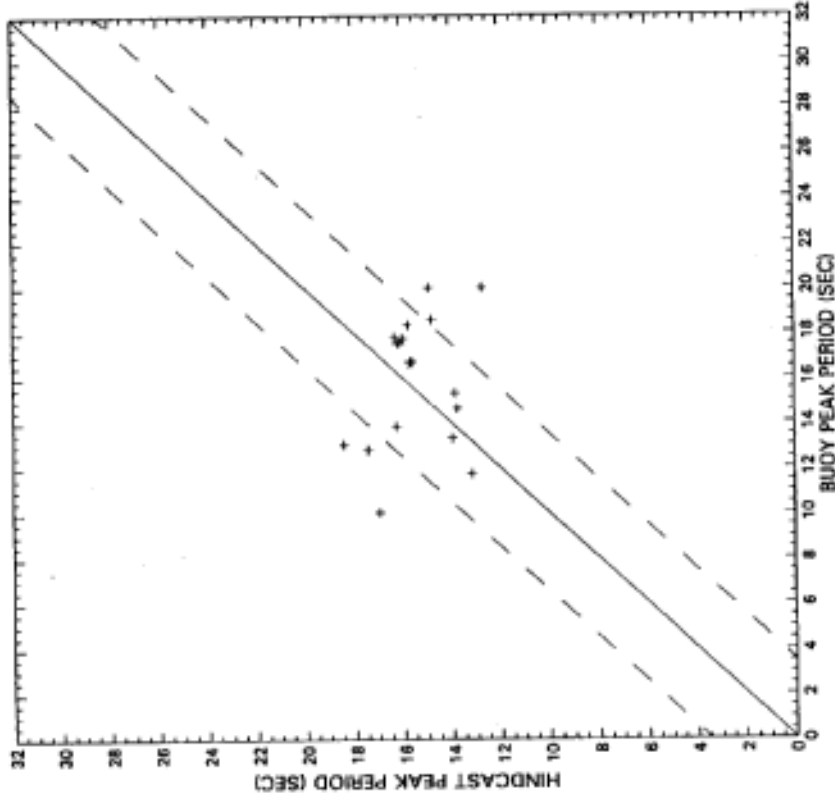


Figure 6. Comparison of time histories of hindcast and measured significant wave height and associated peak spectral period at selected offshore buoys.

HALLOWEEN STORM
ODGP HINDCAST
COMPARISON OF EVENT PEAKS



HALLOWEEN STORM
ODGP HINDCAST
COMPARISON OF EVENT PEAKS

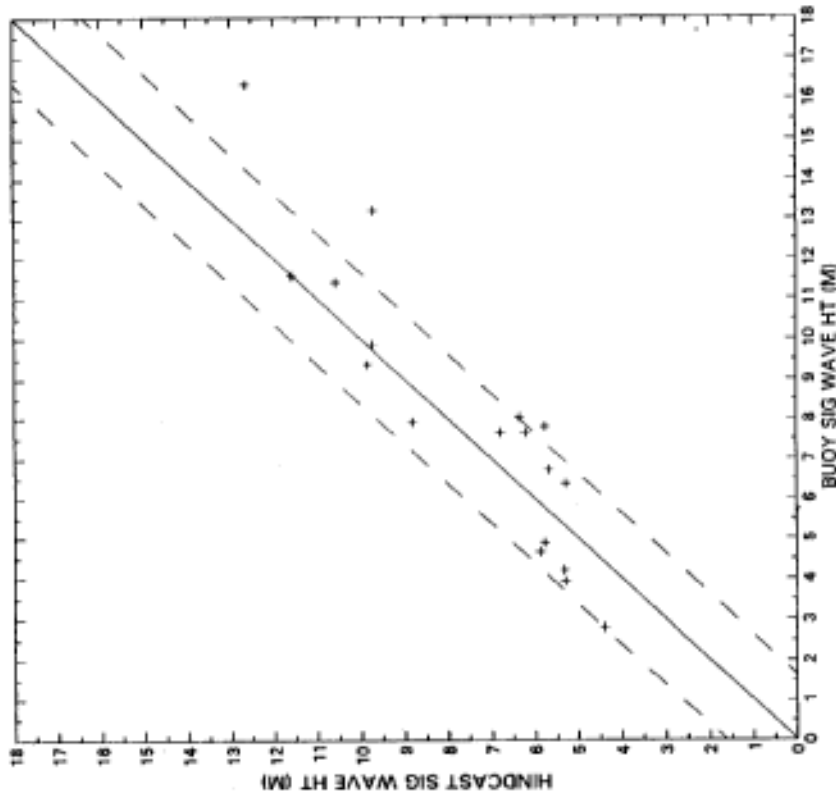


Figure 7. Comparison of hindcast and measured significant wave height and associated peak spectral period at buoy and C-MAN stations, for event peaks only.

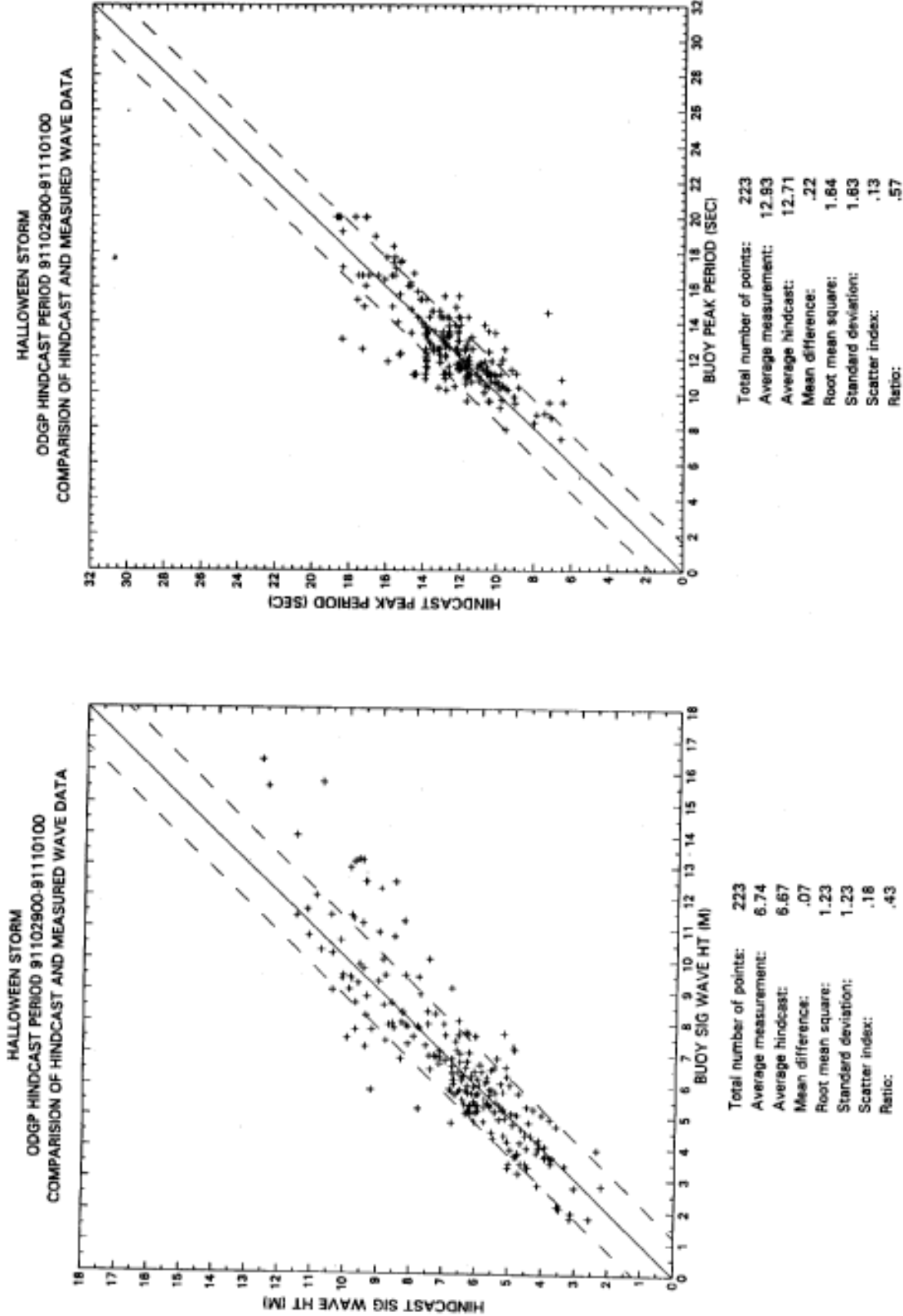


Figure 8. Comparison of hindcast and measured significant wave height and associated spectral peak period at offshore, deep water buoys for time histories at 3-hourly intervals.

**A Possible Interpretation of the Climatology
of the Halloween 1991 East Coast Storm.**

D.T. Resio and M.A. Sager

Florida Institute of Technology, Melbourne, FL.

1. INTRODUCTION

This paper represents a preliminary attempt to the recent "Halloween" Storm of 1991 in a climatological context, A second much more substantial effort to categorize/classify this storm is presently underway with results later this year. Since this storm dramatically recently published design wave criteria over an extensive area of canadian waters, a strong motivation exists for this analysis. Important questions must be answered regarding the risk of encountering such a storm again before existing design criteria can be taken as valid. Although it would be convenient to categorize this storm as an "outlier" and dismiss it from our statistics, it is not readily apparent that such an assumption is justifiable, particularly in light of the lack of information on the overall climatological characteristics of this type of storm.

In typical approaches to offshore risk assessments, it has been a common practice to include all extratropical storms in one category and all tropical storms in another category. It is assumed that this stratification results in two separate homogeneous populations. Resio (1978) showed that may not be a good assumption, since extremal analyses of unstratified extratropical storms can yield results which deviate significantly from analyses of synoptically stratified extratropical storm. Figure 1 shows a plot of maximum storm waves from all storms affecting a site off of Cape Hatteras, North Carolina. Figure 2 show a plot of the same data stratified by the storm tracks shown in Figure 3. In this case the stratified extremal distributions have a different functional form (Fisher-Tippett Type I) than does the combined distribution (Fisher-Tippett Type II). Consequently, extrapolations by the different distributions into longer return intervals diverge from each other.

Resio (1978) also questions the common assumption of temporal homogeneity (climatic stationarity) implicit in typical extremal estimates for structural design and concludes that this assumption may not be sufficiently valid to obtain reliable extremal estimates. Figure 4 provides evidence that, if we take different sub-samples of years from a very long hindcast and perform extremal analyses on these samples, very significant discrepancies can be found among the subsample estimates of wave heights for specific return intervals, In fact, the difference of a factor of about two in these 50-year wave

height estimates (much larger than expected from sampling error) suggests that this is a potentially serious problem in offshore risk assessments. It is t to note that, as discussed in Resio (1978), the primary signal of this variability is not that of a linear trend, but rather one of three- to five-year episodic variations (i.e. short-term climatic variations rather than long-term, secular variations).

Besides storm track location and climatic fluctuations, dynamic arguments suggest that certain large-scale patterns can affect the development of very strong storms, as evidenced in Resio and Hayden's (1975) study of s along the mid-Atlantic coast. In this context, what is the significance of the Halloween storm? Is it truly an outlier or is it just a storm type from a different climatic or synoptic situation than "normally" present?

2. STORM CLIMATOLOGIES

Past studies of cyclonic activity have focussed on storm tracks and frequencies and have not delved very deeply into storm intensities. Thus, for the present study it was necessary to return to a basic data set (synoptic weather charts from 1899-present) and try to determine whether or not the Halloween storm seems to fit within any discernable pattern that is common to a set of storms.

Before proceeding to such an analysis, it was important to decide the specific area within which we will examine storms and the characteristics of storms that should be analyzed. Figure 5 shows an outline of the geographic area within which we analyzed storms. In this case, since we were interested in the wave-generation potential of each storm, the following set of parameters

1. storm intensity
2. storm size
3. storm propagation velocity;
4. storm shape; and
5. storm location.

Of these parameters, the first three tend to be of most to wave-generation potential. The last two are only important in certain circumstances such as when a storm forms into a very elongate form or when it is centered close to the coast. Storm intensity was estimated from the isobaric spacing and available ships' observations. Size was estimated as the average radial distance to the last closed isobar within the region of close isobaric spacing. Storm speed was estimated from successive positions of storm centers.

It should be noted here that we did not include a parameter explicitly related to storm type ("bomb", semi-permanent low, typical of a cyclone family, etc.) since we hoped that eventually this would

"fall out" of our analyses. Hence, we are not, at this stage, eliminating the possibility of synoptic storm types influencing our wave generation potential. In fact, as alluded to previously, it is quite likely that synoptic climatology plays a very role in determining wave climate. For example, the synoptic storm type called a bomb, which is a rapidly intensifying and typically very rapidly moving system, generates very extreme local wave conditions of very high wave steepness. A bomb would not generate long-period waves over a large area as did the Halloween Storm. Consequently, the duration of large wave heights in the Halloween-type of storms is significantly longer than that of the a bomb. This means that the ratio of the individual maximum wave height to the significant wave height will likely be much larger in the Halloween storm. From encounter concepts embodied in extremal statistics, it would seem highly likely that such storms should not be mixed into a single statistical analysis.

3. RESULTS

In the beginning of our search we also concentrated on extratropical storms which began as tropical or had tropical storms injected into them during their life cycle. Although we found that this was not very unusual, we also found that such storms typically did not remain very state. In fact, these storms tended to have characteristics quite similar to all other well developed extratropical cyclones and tended to move rather rapidly off to the northeast if their center read over water. Hence, we suspect that the tropical component of the Halloween Storm is not the primary factor that made it such a remarkable storm in terms of wave generation. This suspicion is further enhanced by the fact that the max wave conditions occurred off the coast of Nova Scotia at a time when the center of Hurricane Grace had not yet combined with the primary circulation center.

Following an iterative process involving many hours of weather map review, we began to characterize patterns in the distribution of storm intensities, storm sizes, and storm motions. In particular, we found that, in contrast to the Halloween storm, the vast majority of storms propagated quite rapidly through our region of interest. The singular exceptions seemed consistently to be storms which were associated with intense blocking highs over the Labrador-Greenland area. Since this was also the synoptic situation occurring in conjunction with the Halloween storm, it was recognized that this large-scale circulation pattern might be crucial to the development of this class of storm. Consequently, we re-analyzed all of the storm period with respect to the existence of such blocking highs.

In our re-analysis of storms, we noted that the occurrence of major storms appeared to be linked to pronounced variations in the zonal index. This is not surprising since one mechanism for the formation of

large blocking highs is the occurrence of a large fluctuation in the zonal index. Specifically, when a high zonal index (a global scale circulation with motions primarily along from west to east) is interrupted and the flow moves into a low zonal index, two phenomena typically occur simultaneously, a large flux of mass toward higher latitudes and the development of large surplus planetary-scale vorticity. Both of these phenomena are very conducive to the formation and development of very strong, nearly stationary extratropical storms.

During our preliminary search, we found four storms which had characteristics that were very similar to those of the Halloween Storm. All of these storms were large, nearly stationary systems which occurred in conjunction with pronounced changes in the zonal index. They all had similar maximum wind speeds (ranging from 55 knots to 65 knots), had similar central pressures 970 mb to 985 mb, and were all of similar shape (nearly circular with a slight northeast eccentricity). They also had similar areas of wind speeds over 40-knots and over 50-knots, as estimated from a rough kinematic analysis of each storm. We anticipate that when the analysis for all storms is completed we will add two or three storms to this list. Storms identified in this phase included December 1919, November 1945, March 1962 (the Ash Wednesday Storm), and February 1969. Even though the Halloween storm is the only storm in this set to move in a retrograde fashion (toward the southwest), this should not create a significant difference in the wave generation potential since all of the storm motions are so slow.

Following the extremal analysis method described in Resio (1985), we can define a spatial envelope of waves for each storm and use these maximum fields to estimate the encounter probability of waves from this class of storm. This has the advantage over point-by-point analysis methods in that it extracts additional information from the spatial patterns in these storms. Recognizing that there are two components to environment data fields, a deterministic component and a random component, one can normalize the wave heights in each storm by the maximum and define a relative wave height pattern around the point of maximum wave height in the storm. Figure 6 shows such a pattern estimated from a hindcast of the Halloween storm. Combining conventional extremal estimation methods with functional forms for the normalized spatial distributions around these maxima provides estimates of the expected extremes at each point in our area of interest.

For this preliminary study, we did not have careful, kinematically-analyzed estimates of entire wind fields as would be required to hindcast this set of storms; however, we can begin to examine the potential for wave generation in these storms at least in

an approximate manner from our rough hindcasts of these storms, based on fairly crude, initial kinematic analyses and a second generation, discrete spectral wave model. Table 1 shows the maximum significant wave heights hindcast for each storm, using this approach. Table 2 gives estimates of the maximum wave heights for selected return intervals. These estimates were obtained via a generalized extreme value analyses using the method of maximum likelihood and represent a measure of expected maximum storm intensities, for the entire region of our analysis. As can be seen from this Table, it appears that the Halloween storm is not truly an outlier. In fact, from this analysis, we expect maximum conditions comparable to the Halloween Storm to occur somewhere in our analysis area about once every 100 years. It should be noted that this is definitely not the same as saying that such a wave height will occur at a particular point once every 100 years. Although the total area analyzed is quite large, most of the maximum storm conditions hindcast in this set of storms occurred in the area south of Nova Scotia. In this preliminary analysis, we will not examine the question of spatial heterogeneity; however, it is apparent that this is an important issue which must be addressed before final estimates of expected wave conditions for specific sub-regions of our analysis area are determined.

Based on these hindcasts with rudimentary wind fields, we can use the method of Resio (1985) to estimate expected extreme wave heights at a specific location. In this context, the encounter of probability of very high waves can be related to the number of occasions that a particular point is to fall within a storm, the relative location of this point to the point of maximum conditions, and the maximum wave height within the storm. Table 3 gives the estimates of wave heights for selected return periods, based on these preliminary hindcasts. These preliminary values are likely to be most valid for the area along the Scotian Shelf south of Nova Scotia. If we take this as a reasonable assumption, it is evident that the 100-year wave heights estimated via this technique are considerably higher than earlier estimates based on methods which have considered all storms mixed together.

4. DISCUSSION

The results of our analyses here should be regarded as quite preliminary; however, one very intriguing issue has been raised here, although perhaps not immediately recognizable as such. This issue relates to the use of single-point estimates of wave conditions for design of fields of structures which extend over a finite area in the ocean. If the design question is simply "Will a particular structure fail?" then a single-point estimate is very relevant. If the design question is "Will any structure in this area fail?" then the

single-point estimate is actually not the a appropriate estimate which should be used. In other words, within a large area we should expect that the 100-year wave height should be exceeded over a small portion much more frequently than once ever 100 years. The spatially-based concept of extremal estimation provides a good method of addressing this problem.

In a sense, the Halloween Storm is not a typical storm at all. The dynamics of this storm were related to violent changes in the large scale circulation pattern combined with an injection of a moderate hurricane into it. The injection of tropical energy came after the time of waves and possibly did not contribute significantly to the maximum waves generated. The question of the role of the tropical energy will be addressed more thoroughly in subsequent analyses; however, at this point we do not think that we can justify ignoring the Halloween storm as an outlier by saying that the combination of a tropical storm with a strong extratropical storm will be extremely rare.

Due to the preliminary nature of this study, the overall accuracy of the hindcasts on which the wave analyses were based is somewhat suspect; therefore, the values in Table 3 should not be given too much credence at present. Based on the results of this preliminary analysis along with results of some previous studies, however, it appears that storms in nature may not be so self-similar that they may be treated as being drawn from a single population. Instead, it appears that a stratification of storms by synoptic climatology is quite warranted. If this is true, conventional extremal methods will not offer usable estimates for very large wave conditions. Since such conditions are the crux of design considerations for of offshore structures, it is very important to pursue this issue of extremal estimation in the future.

5. REFERENCES

- Petrauskus, C. and P.M. Aagard, 1971: Extrapolation of historical storm data for estimating design wave heights. Soc. of Petrol. Engr., V. 11, p 23-35.
- Resio, D.T., 1978: Some aspects of extreme wave prediction related to climatic variations. Offshore Technology Conf., Paper No. 3278, May 8-11, 1978, Houston, TX.
- Resio, D.T., 1985: A new technique for the estimation of extreme wind speeds. International Workshop of Winds and Icing, Halifax, Canada - Proceedings.
- Resio, D.T. and B.P. Hayden, 1975: Recent secular variations in mid-Atlantic extratropical storm climate. J. Appl. Meteorol., V 14, No. 7, p 1223-1234.

TABLE 1

Maximum Values of Significant Wave Height Hindcast
in Five Sample Index-Change Storms

<u>Storm Date</u>	<u>H_{s-max} (metres)</u>
December 1919	14.8
November 1945	15.7
February 1969	13.9
March 1962	15.9
October 1991	16.8

TABLE 2

Estimated Maximum Significant Wave Heights at Any Location
Within a Storm for Selected Return Periods
(Based on GEV analysis of H_{s-max} Data)

<u>Return Period (years)</u>	<u>H_{s-max} (metres)</u>
25	14.6
50	16.1
100	16.8
250	17.3

TABLE 3

Estimated Maximum Significant Wave Heights at a Fixed Location
for Selected Return Periods

<u>Return Period (years)</u>	<u>H_s (metres)</u>
25	12.8
50	13.4
100	14.1
250	14.9

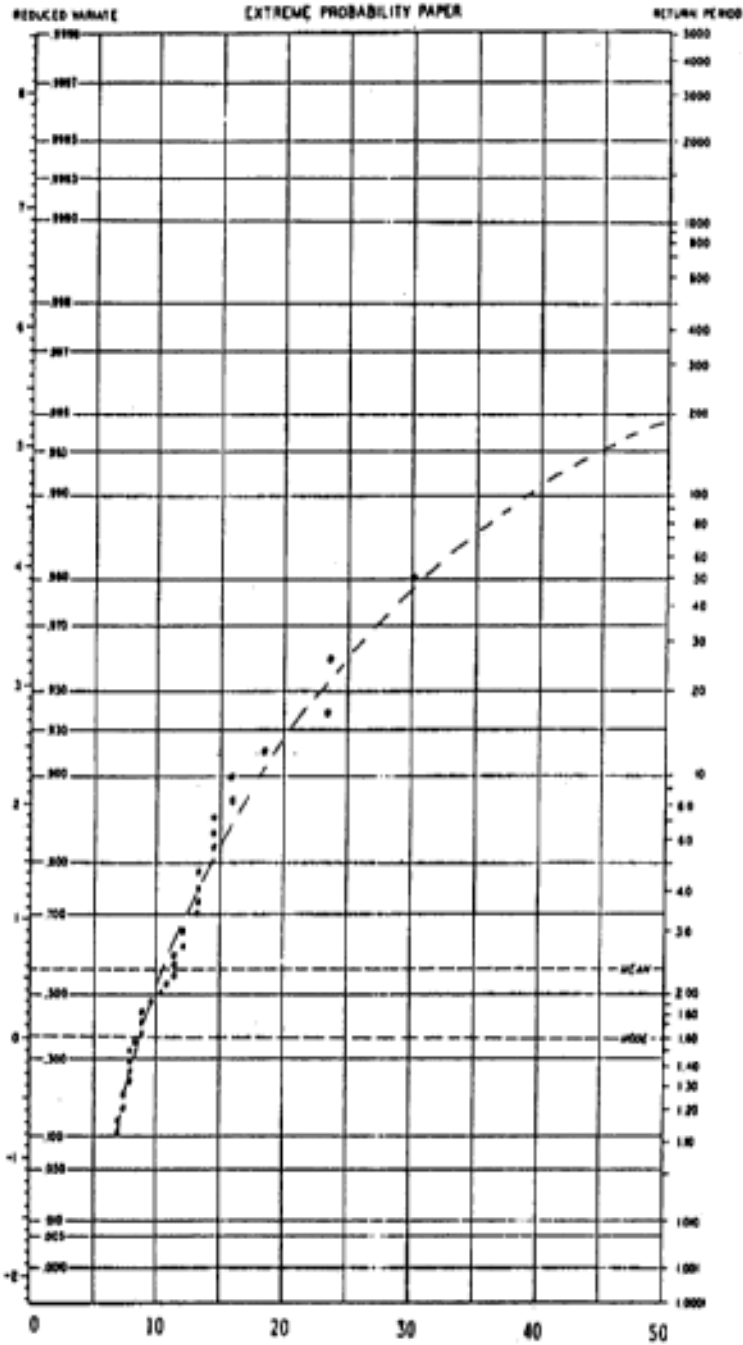


Figure 1. Extremal distribution of unstratified wave heights at a site off of Cape Hatteras, North Carolina based on numerical hindcasts.

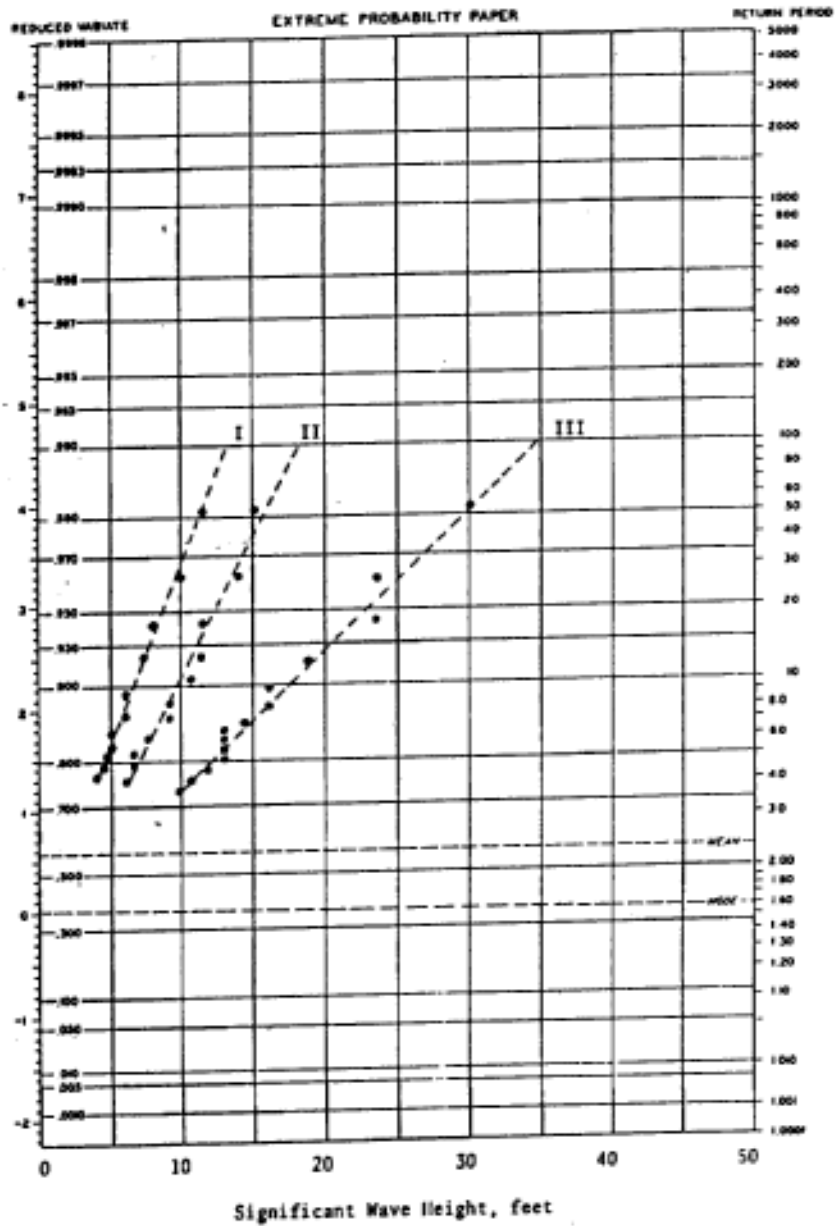


Figure 2. Extremal distributions of stratified wave heights based on same data set shown in Figure 1. Stratification is based on storm tracks given in Figure 3.

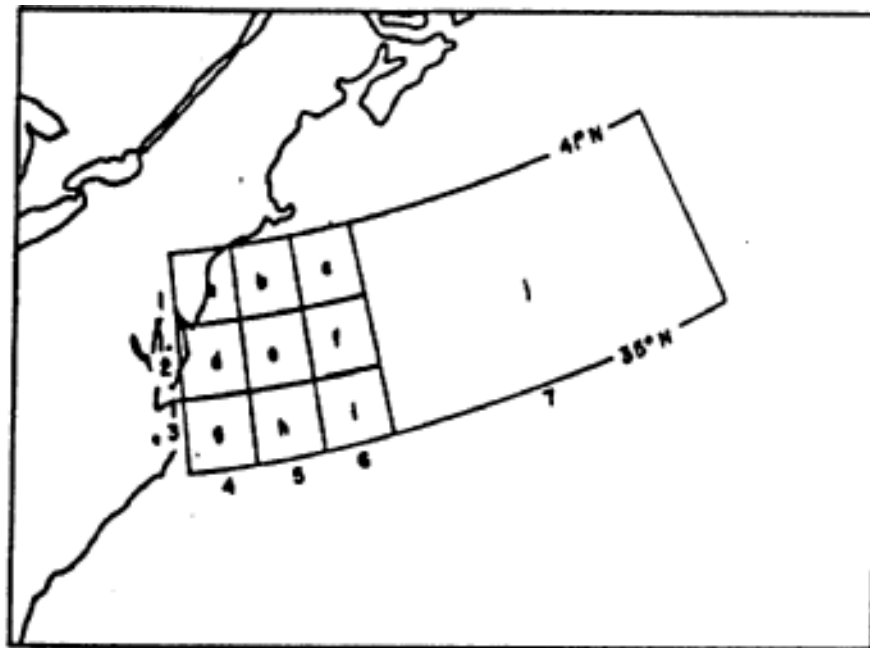


Figure 3. Stratification basis for data shown in Figure 2. Category I includes all storms entering area through line segment 3. Category II includes all storms entering area through line segment 4. Category III includes all storms entering area through line segment 5.

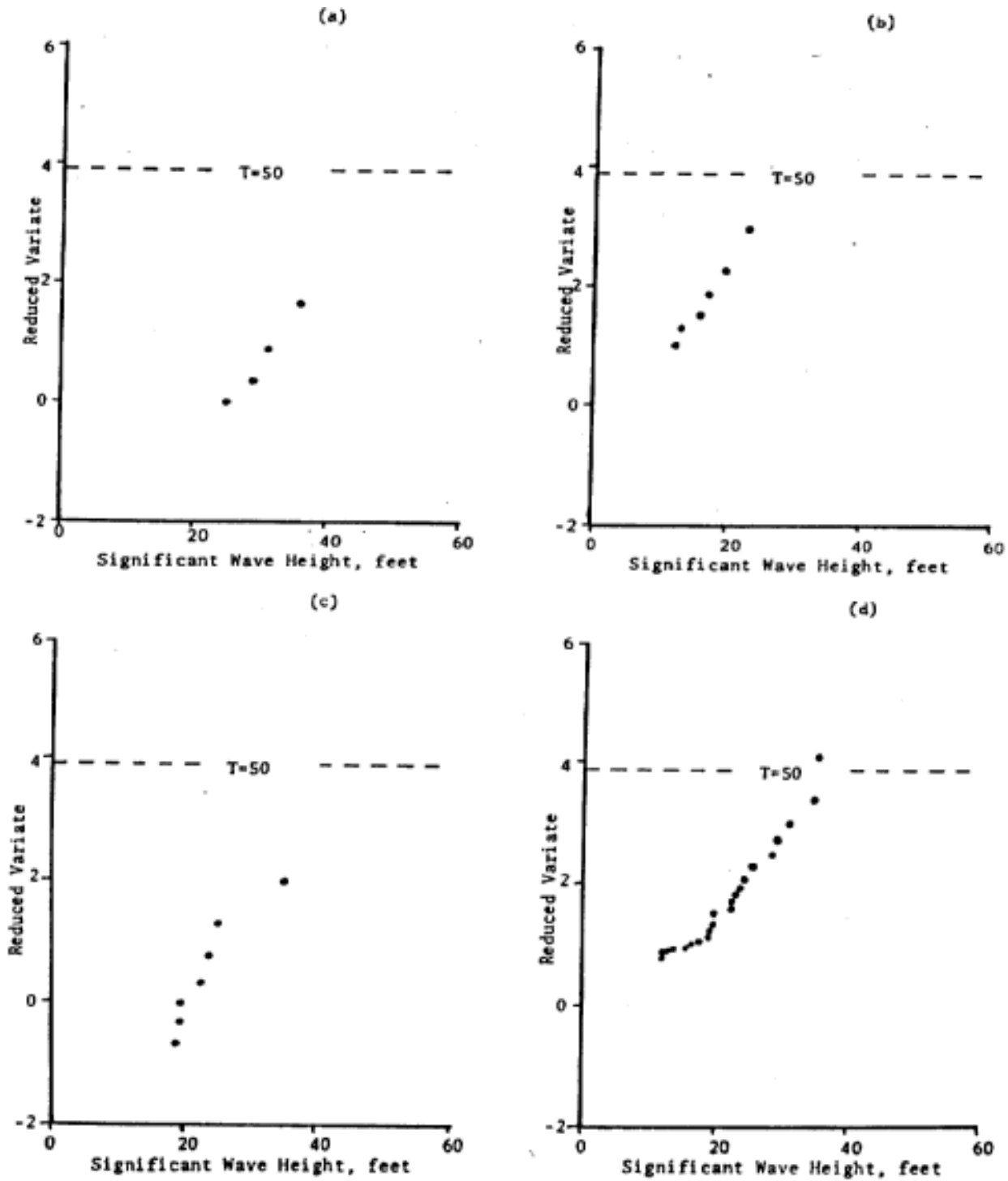


Figure 4. Different distributions of wave heights obtained from different time samples of years in the data of Petrauskus and Aagard (1971).

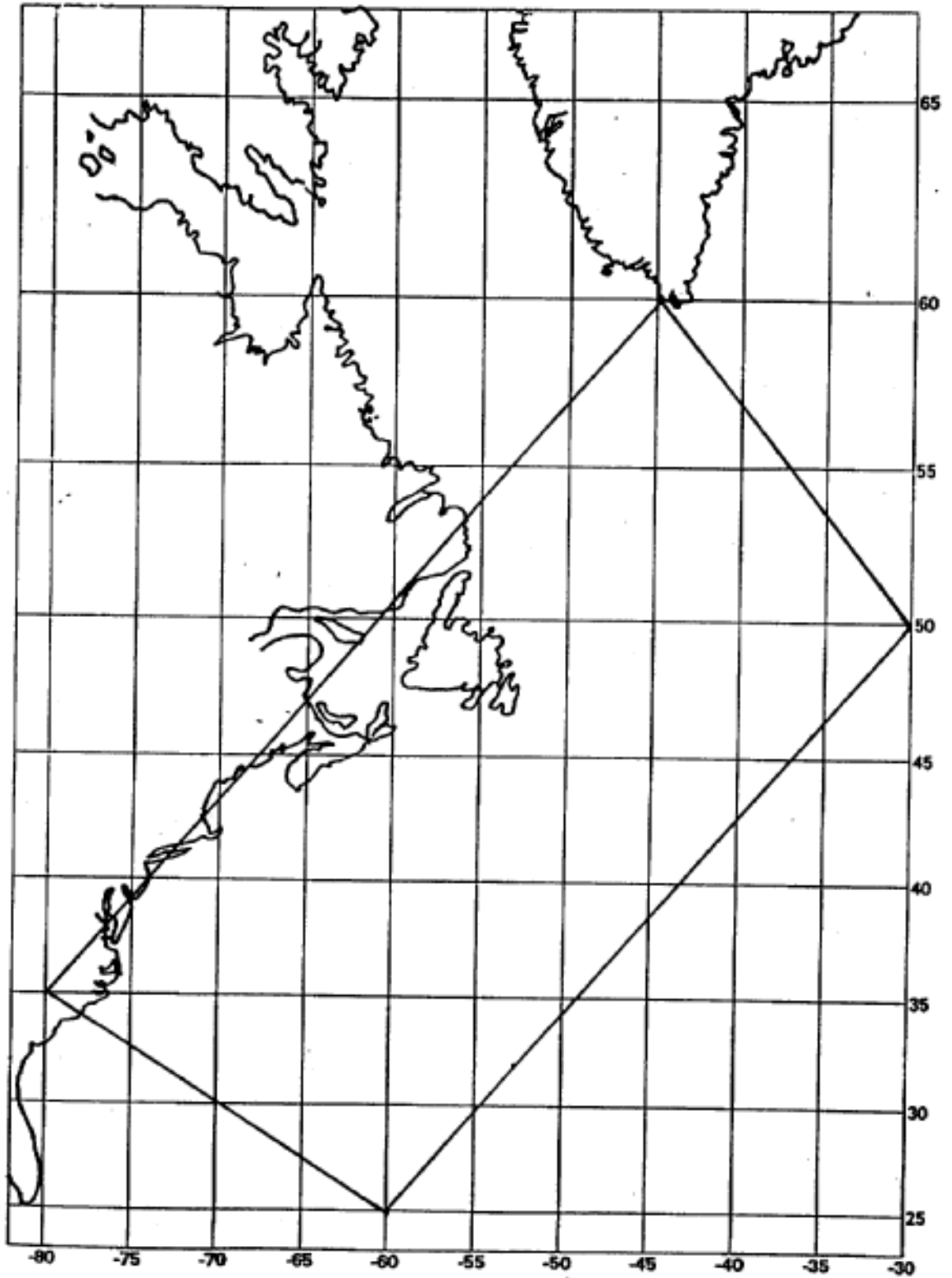


Figure 5. Geographic area included in storm climate analyses.

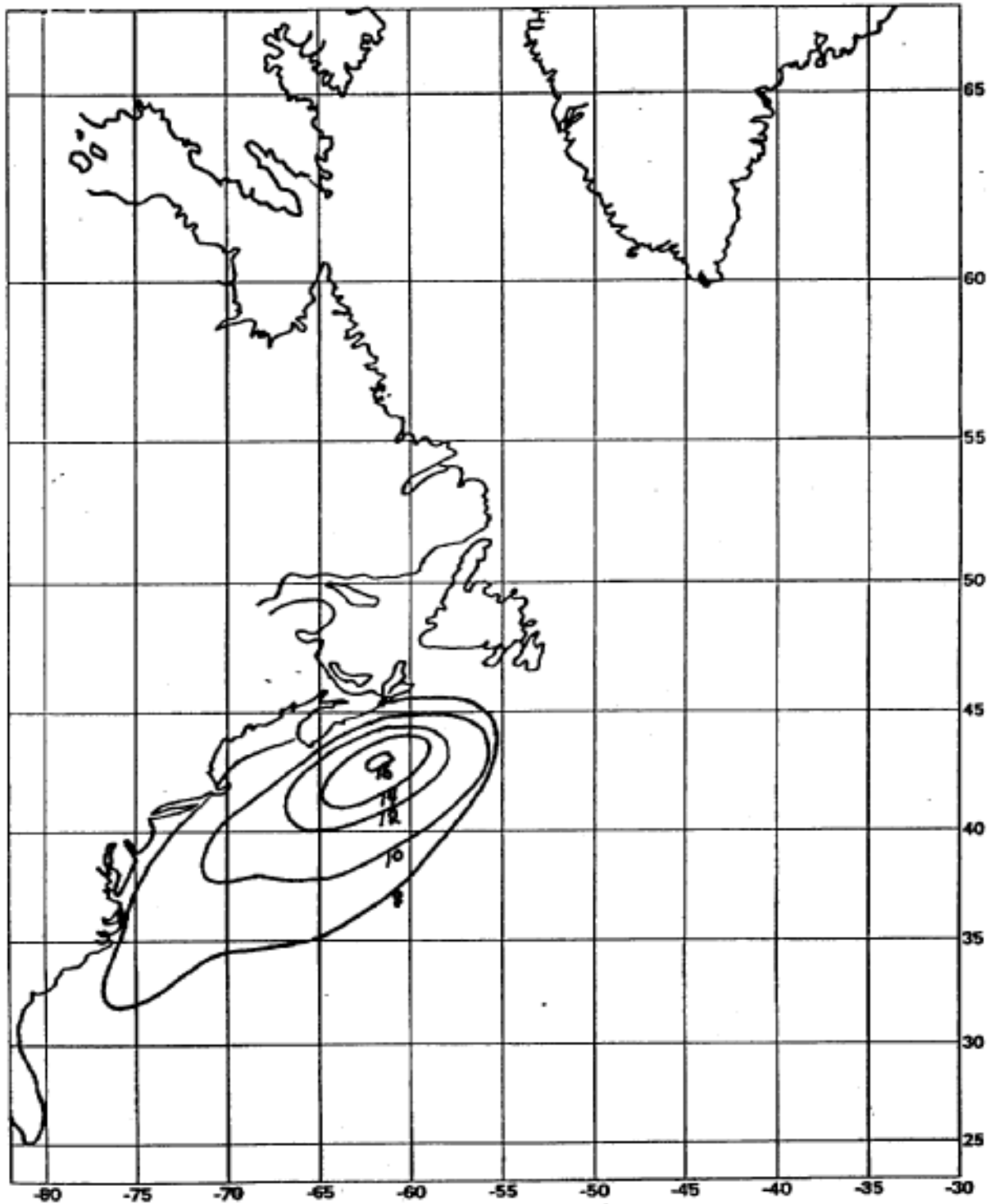


Figure 6. Spatial distribution of significant wave height maxima for Halloween Storm of 1991.

RAPPORTEUR'S SUMMARY REPORT

Peter C. P. Chandler

Institute of Ocean Sciences
Sidney, B.C.**Introduction**

The 3rd International Workshop on Wave Hindcasting and Forecasting was held May 19-22, 1992, at the Bonaventure Hilton Hotel, Montréal, Canada. The purpose of the workshop was to provide a forum to share ideas and information on wave hindcasting and forecasting and to discuss the priorities for future research and development.

The workshop was organized into six main sessions plus a special session on the 1991 Halloween east coast storm, and a poster display. The themes for each of the main six sessions were: wave data analysis, wind modelling, wave modelling, data assimilation, wave hindcasting and wave forecasting.

The atmosphere of the workshop was informal, with each session having ample time available for questions and discussions. Together with the *savoir vivre des Montréalais* the workshop was considered time well spent.

The first part of this report will document the achievements, conclusions and recommendations that were presented and discussed during the workshop sessions. The second part consists of a list of recommendations for future research and development.

Part 1 - Summary of Workshop Sessions

Research into the directional analysis of heave-pitch-roll wave data has led to the development of a corrective scheme for the maximum likelihood method, providing what has been termed the Normalized MLM estimate. For both unimodal and bimodal directional wave spectra the NMLM method is shown to reduce smearing, characteristic of the direct Fourier transform method, and overpredicting the spreading, typical of other MLM methods. Although this approach requires more computing resources than other analysis techniques it should not be considered a constraint given the power of the newer workstations.

The importance and complexity of the interactions between waves and currents was confirmed by separate research carried out at two locations, Lake St. Clair and the Queen Charlotte Islands. Field data show significant modification of the wave field as the surface currents change due to wind and tidal forcing. This research has the potential to further our understanding of the physics of wave-current interactions and the means to better represent it in wave models.

The regional wave models that were presented revealed a diversity of geographical settings that is a tribute to the application of wave modelling. Such locations include: the North Sea, New Zealand waters, the Belgian coast, the U.K. southwest coast, the Mediterranean Sea, the U.S. Atlantic coast, the Iberian Peninsula coast, and Canada's Atlantic, Pacific and Arctic coasts. In addition, wind and wave climate atlases were presented for the east coast of Canada and the Great Lakes.

Departures from the classical description of marine cyclone evolution, prompted by the results of numerical simulations, are being investigated using intensive kinematic analysis of high quality observations from a network of buoys along the east coast of North America. Mesoscale features such as the "bent-back warm front" and the "warm-sector seclusion", not presently included in the wind input to wave models, may account for some of the discrepancies between model results and observations. Further work in this research involves expanding the number of events examined by developing a more efficient evaluation process than the present hand analysis, and assessing the sensitivity of the wave models to the absence of these features in the wind input.

The optimum means of generating wind fields as input to wave models continues to be an active area of research. The *man-machine mix* of kinematic analysis is recognized as providing a superior, but more costly and time consuming, wind field than the *machine only* objective approach. A computerized kinematic analysis (CKA) methodology is being investigated, where the recognition of synoptic scale features and the construction of streamlines is accomplished numerically. Following the steps taken by a meteorologist carrying out a kinematic analysis, the CKA approach is shown to improve upon the objective analysis wind fields by reducing spatially correlated errors and better estimating the maximum winds in storms.

The concept of a generic third generation wave model was presented with a structure consisting of three functional modules: input specification, initialization, and the time steps through the simulation interval. As better numerical solution procedures are discovered, modifications to these modules could be made. As an example, an improvement in the calculation of the nonlinear wave-wave interaction term (S_{nl}) using the two-scale approximation (TSA) could be easily implemented to provide a more accurate representation than the present direct interaction approximation (DIA).

Energy fluxes within the spectrum, specifically in the equilibrium region and the spectral peak region, have been examined for both evolving and fully developed wind waves. Balancing the energy in the wind input (S_{in}), the dissipation (S_{ds}) and the nonlinear transfer

(S_{nl}) terms has been used to compare the energy fluxes and the rate of change of total energy to provide insight into the physics of the evolution of the spectrum.

A second generation wave model which permits integration time steps of two hours while maintaining an accurate representation of the S_{nl} term was described. By altering the time at which S_{nl} is calculated, from the beginning of a time step to some point within the time step, a better balance of the source terms is provided which gives results that compare well with those of a third generation model having time steps of 20 minutes.

Research into the coupling of wave models with boundary layer models and tide-surge models was presented. The complexity of the interactions was made clear with the shortcomings of existing methodologies made more evident than the means by which better results can be achieved.

Use of the adjoint method to assimilate wave height data into the WAM model has been shown to be feasible. Due to the wind-wave coupling in the model, the assimilation of wind data is not required, and the dynamical consistency of winds and waves continues after the assimilation period into a forecast period. The utility of wave data assimilation is shown to depend upon the abundance of data in the model domain. In a wave forecasting mode the assimilation process is shown to minimize the occurrence of a bad prediction. The contribution of wave data assimilation to wave forecasting increases in circumstances where the wind sea component of the spectrum, with its variability on a time scale of about 10 hours, does not dominate the swell component. The effects of assimilation on the modelled wave periods, and whether models are sensitive to the type of data being assimilated, continues to be examined.

The extrapolation of wave data to return periods of 50 to 100 years remains a subject of interest for designers, operators and regulators. Both hindcast and measured data from the Hibernia site off Canada's east coast have been used with several extremal distributions using several fitting methods and evaluated by several goodness-of-fit tests. It has been shown that there is not one distribution or fitting method that can be considered universally applicable. Yet to be resolved are concerns that the maximum events do not always fit the distribution, and that the data may be comprised of more than one statistical population. Also, wave periods continue to be poorly represented in both model wave hindcasts and forecasts, and wave heights tend to be underestimated in the most extreme storms in most areas.

Wave models in a forecasting mode are being used in a growing number of regional applications. Data assimilation and advances in

meteorological input data analysis are shown to improve forecasting ability, particularly over the first 12-24 hours. The interactive graphics editor (INGRED), and its associated system, is being used not only in forecasting, but also to generate the information to form the foundation of a climatological data base.

The Halloween storm of 1991 has been called the most powerful extratropical (nor'easter) storm to hit the Atlantic coast of North America in at least 50 years. The comparison between data collected by direct measurement during the five days of the storm, and wave model output is ongoing. Already it has directed research into the use of synoptic climatology as model input, and into examining more closely what artifacts are present in the data collected in extreme sea states.

Part 2 - Recommendations for Future Research and Development

The Marine Environmental Data Service (MEDS) archive includes directional wave estimates that have been determined using the direct Fourier method, which can be improved using techniques based on the maximum likelihood methods. Before a complete re-analysis of the data base is undertaken, however, further work is required to determine which would provide better results, a standardized analysis method or a knowledge based system capable of using all the methods.

The recognition of the importance of the nonlinear wave-wave interaction term (S_{nl}) in the balance of spectral energy, and the ability to accurately calculate it in wave models, is a key achievement in our understanding of the physics of surface gravity waves. It is now appropriate to advance our understanding of energy dissipation, the S_{ds} term. The specific methodology to accomplish this has yet to be defined but will no doubt require a combination of theoretical analysis, numerical modelling, laboratory experimentation, and the organizational and technical expertise required to carry out a field program.

Concerns have arisen regarding the response of an anemometer mounted on a wave following buoy when exposed to extreme sea states. With vertical excursions of more than 30 m, the difference in the wind measured in the trough of a wave to that at the crest may significantly affect the data used as input to wave models. It is suggested that research carried out in wind tunnels as well as field programs could be used to quantify the implications of this phenomenon.

A consensus was reached among the workshop participants that a clear distinction be made between wave models recommended for research and those for purposes other than research, including operational wave forecasting and hindcasting for design applications. For the latter,

the "newer is better" philosophy should be placed in context with the virtues of consistency and stability that have been acquired with models that have proven themselves over time and a large range of applications.

A novel approach to data collection was proposed that employs a set of aircraft-deployed sensors that are seeded in the path of advancing storms. Similar to the technology used in air-launched XBTs, the idea has the potential to provide mesoscale environmental data on an as-required, and where required, basis.

To some extent wave models are considered to be "working" if they remain numerically stable while producing results that compare reasonably well to output from other models (in a range of situations such as the SWAMP tests). A more comprehensive testing process should be encouraged, involving standardized input and benchmark output, which would permit the evaluation of wave models, or modifications to models, to be more quantitative.

There exists a sense of unfulfilled promise in the usefulness of the satellite data that has become available over the past few years. Accelerated research is recommended to determine whether wave model requirements are better met with satellite-based sensors, or by other means of data collection (including particularly enhanced conventional networks such as buoys).

There also exists a related sense of disappointment over the pace of advances in the area of wind and wave data assimilation into forecast models. Further research incorporating larger volumes of data and increased computer power will hopefully improve the effectiveness of data assimilation schemes.

Research into mesoscale features contained within synoptic scale systems should be a research priority; these features may be responsible for significant increases in wave height in portions of some storms, which in turn would affect wave forecasts and design criteria.

As operational forecasters use interactive systems such as INGRED to prepare wind fields, not only for input to wave models but also directly into a climatological database (and for other applications such as oil spill and ice motion), their understanding of marine meteorology becomes even more critical. It is recommended that in addition to their operational training these forecasters be given every opportunity to develop their understanding of the theoretical aspects of marine meteorology and oceanography.

A strong endorsement was given to holding the *4th International Workshop on Wave Hindcasting and Forecasting* in about three years. The participation by a broad audience of engineers, designers, and regulators as well as researchers and operators should continue to be encouraged.

LIST OF PARTICIPANTS

JUAN C. CARRETERO ALBIACH

Programa de Clima Maritimo M.O.P.T.
Dirreccion General de Puertos y Costas
C/ Vallehermoso 78
28015 Madrid
SPAIN
(34-1) 553 94 94
(34-1) 553 29 74 (fax)

JUAN JOSE CONDE ALDEMIRA

Programa de Clima Maritimo M.O.P.T.
Dirreccion General de Puertos y Costas
C/ Vallehermoso 78
28015 Madrid
SPAIN
(34-1) 553 32 77
(34-1) 553 29 74 (fax)

DOUG BANCROFT

SSO Scientific Services
Meteorology and Oceanography
National Defence Headquarters
Ottawa, Ontario K1A 0K2
CANADA
(613) 996-3658
(613)995-4197 (fax)

RALPH BIGIO

Meteorological and Oceanographic Centre
Building D14, HMC Dockyard
Maritime Command
FMO Halifax, Nova Scotia B3K 2X0
CANADA
(902) 427-6374
(902)427-6381 (fax)

F.P. BRISETTE

Department of Civil Engineering
McMaster University
1280 Main Street West
Hamilton, Ontario L8S 4L7
CANADA

(416) 525-9140
(416) 529-9688 (fax)

ROSS BROWN

Atmospheric Environment Service
LaSalle Academy, Block E
373 Sussex Drive
Ottawa, Ontario K1A 0H3
CANADA
(613) 996-4488
(613) 563-8480 (fax)

JOSEPH BUCKLEY

Department of Physics
Royal Roads Military College
FMO Victoria,
British Columbia VOS 1B0
CANADA
(604) 363-5935
(604) 363-4513 (fax)

M.M. DE LAS HERAS CABALLERO

Programa de Clima Maritimo M.O.P.T.
Dirreccion General de Puertos y Costas
C/ Vallehermoso 78
28015 Madrid
SPAIN
(34-1) 553 94 94
(34-1) 553 29 74 (fax)
presently at:
Royal Netherlands Meteorological Inst.
P.O. Box 201
3730 AE de bilt
NETHERLANDS
(31-30) 206675
(31-30) 210407 (fax)

DON CAMERON

Atmospheric Environment Service
1496 Bedford Highway
Bedford, Nova Scotia B4A 1E5
CANADA

(902) 426-9200
(902) 426-4873 (fax)

VINCENT J. CARDONE

Oceanweather Inc.
5 River Road
Cos Cob, CT 06807
U.S.A.
(203) 661-3091
(203) 661-6809 (fax)

OCTAVE CARON

Société d'énergie de la Baie James
500 boulevard Rene Levesque ouest
Montréal, Québec, H2Z 1Z9
CANADA

(514) 879-6263
(514) 879-4504 (fax)

PETER CHANDLER

Institute of Ocean Sciences
Department of Fisheries and Oceans
P. O. Box 6000
Sidney, British Columbia V8L 4B2
CANADA

(604) 363-6307
(604) 363-6746 (fax)

ZHAN CHENG

National Research Centre for Marine Forecasts
No. 8 Da Hui Si
Hai Dian District
Beijing 100081
CHINA

(861) 831 8882-74
(861) 831 3593 (fax)

ROBERT L. COHEN

Marine Weather Services
Oceanroutes, Inc.
680 West Maude Avenue
Sunnyvale, CA 94086-3518 U.S.A.

(408) 245-3600
(408) 245-5301 (fax)

ROB CROSS

Atmospheric Environment Service
LaSalle Academy, Block E
373 Sussex Drive
Ottawa, Ontario K1A 0H3
CANADA
(613) 996-4248
(613) 996-3289 (fax)

GERARD CROTEAU

Atmospheric Environment Service
Canadian Meteorological Centre
2121 North Service Road
Dorval, Quebec H3P 1J3
CANADA
(514) 421-4618
(514) 421-4639 (fax)

CATRIN DUNLEAVY

Atmospheric Environment
Service
4905 Dufferin Street
Downsview, Ontario M3H 5T4
CANADA

(416) 739-4386
(416) 739-4297 (fax)

PIERRE DUPUIS

Société d'énergie de la Baie James
500 boulevard Rene Levesque ouest
Montréal, Québec, H2Z 1Z9
CANADA

(514) 879-6268
(514) 879-4504 (fax)

BASSEM M. EID

MacLaren Plansearch Ltd.
5657 Spring Garden Road
Suite 200
Halifax, Nova Scotia B3J 3R4
CANADA

(902) 492-4544
(902) 492-4540 (fax)

PAUL FARRAR

Naval Oceanographic Office, Code OPTA
Stennis Space Center, MS 39522-5001
U.S.A.

(601) 688-5177
(601) 688-5605 (fax)

CHARLES P. FOURNIER

Atria Engineering Hydraulics Inc.
6 Gurdwara Road, Suite 200
Ottawa, Ontario K2E 8A3
CANADA

(613) 228-0826
(613) 225-6014 (fax)

CHRIS GRAHAM

Dept. XTS/5, Sarawak Shell Berhad
Locked Bag No. 1, 98009, Miri
Sarawak
MALAYSIA

(60-85) 453498
(60-85) 453532 (fax)

ROSS GRAHAM

Defence Research Establishment Atlantic
9 Grove Street
P.O. Box 1012
Dartmouth, Nova Scotia B2Y 3Z7
CANADA

(902) 426-3100 ext 123
(902) 426-9654 (fax)

J. ARTHUR GREENWOOD

Oceanweather Inc.
5 River Road
Cos Cob, CT 06807
U.S.A.

(203) 661-3092
(203) 661-6809 (fax)

G.Z. GU

Offshore Engineering
Mobil Research and Development Corp.
Post Office Box 819047
Dallas, TX 75381-9047
U.S.A.
(214) 851-8338
(214) 851-8349 (fax)

SVERRE HAVER

Statoil, R&D Dept.
Postuttak
7004 Trondheim
NORWAY
(47-7) 584011
(47-7) 967286 (fax)

RALPH HORNE

Departmental Coordinator, Energy R&D
Office of the Science Advisor,
Environment Canada
241 Blvd. Cite des Jeunes, Block 300
Hull, Quebec K1A 0H3
CANADA
(819) 953-7625
(819) 953-0550 (fax)

JON M. HUBERTZ

CEWES-CR-0
U.S. Army Engineer Waterways Experiment Station
3909 Halls Ferry Road
Vicksburg, MS 39180-6199
U.S.A.
(601) 634-2028
(601) 634-4314 (fax)

VALDIR INNOCENTINI

Instituto Nacional de Pesquisas Espaciais
Av. dos Astronautas 1758
Caixa Postal 515
12201 - Sao Jose dos Campos - SP
BRAZIL
(0123) 41 8977
(0123) 21 9743 (fax)

ANDREW JOHNSON JR.

Naval Oceanographic Office, Code OPTA
Stennis Space Center, MS 39522-5001
U.S.A.

(601) 688-5177
(601) 688-5605 (fax)

ANDREW K. LAING

Marine Research Meteorologist
New Zealand Meteorological Service
P.O. Box 722
Wellington
NEW ZEALAND
(64-4) 4969 351
(64-4) 4735 231 (fax)

ROOP LALBEHARRY

Atmospheric Environment Service
4905 Dufferin Street
Downsview, Ontario M3H 5T4
CANADA
(416) 739-4912
(416) 739-4221 (fax)

SUSAN K. LALLY

Oceanroutes Canada Inc.
271 Brownlow Avenue
Dartmouth, Nova Scotia
B3B 1W6
CANADA

(902) 468-3008
(902) 468-3009 (fax)

OWEN LANGE

Atmospheric Environment Service
1200 - West 73rd Ave.
Vancouver, British Columbia V6P 6H9
CANADA

(604) 664-9000
(604) 664-9005 (fax)

JEAN-MICHEL LEFEVRE

METEO – FRANCE
42 Av Gustave Coriolis
31057 Toulouse Cedex
FRANCE

(33) 61 07 82 95
(33) 61 07 82 32 (fax)

VLADIMIR MAKIN

Royal Netherlands Meteorological Inst.
P.O. Box 201
3730 AE de bilt
NETHERLANDS

(31–30) 206911
(31–30) 210407 (fax)

RICK MARSDEN

Royal Roads Military College
FMO Victoria, B.C. VOS 1B0
CANADA

(604) 363–4533
(604) 363–4513 (fax)

DIANE MASSON

Institute of Ocean Sciences
9860 West Saanich Road
P. O. Box 6000
Sidney, British Columbia
V8L 4B2 CANADA

(604) 363–6521
(604) 363–6746 (fax)

THOMAS H. PEIRCE

Transportation Development Centre
Suite 601, West Tower
200 Rene Levesque Blvd. W.
Montreal, Quebec H2Z 1X4
CANADA

(514) 283–0078
(514) 283–7158 (fax)

PIERRE PELLETIER

Société d'énergie de la Baie James
500 boulevard Rene Levesque ouest
Montréal, Québec,
H2Z 1Z9
CANADA

(514) 879-6269
(514) 879-4504 (fax)

WILLIAM PERRIE

Physical and Chemical Sciences
Bedford Institute of Oceanography
P.O. Box 1006
Dartmouth, Nova Scotia B2Y 4A2
CANADA

(902) 426-3985
(902) 426-7827 (fax)

STUART PORTER

Scientific Services Meteorologist
Atmospheric Environment Service
P.O. Box 9490, Postal Station B
St. John's, Newfoundland A1A 2Y4
CANADA

(709) 772-4695
(709) 772-2593 (fax)

DONALD T. RESIO

Florida Institute of Technology
Dept. of Oceanography and Ocean Engineering
150 West University Blvd.
Melbourne, FL 32901-6988
U.S.A.

(407) 768-8000 ext. 8135
(407) 984-8461 (fax)

KATHRYN J. RESIO

Offshore and Coastal Technologies Inc.
#115 – 7667 N. Wickham Road
Melbourne, FL 32940
U.S.A.

(407) 242–8783
(407) 242–2744 (fax)

IRENE RUBINSTEIN

Earth Observation Laboratory
Institute for Space and Terrestrial Science
4800 Keele Street
Downsview, Ontario M3J 3K1
CANADA
(416) 665–3311
(416) 665–2032 (fax)

KEN SATO

Environment Directorate
National Energy Board
311 – 6th Avenue S.W.
Calgary, Alberta T2P 3H2
CANADA

(403) 299–3675
(403) 292–5503 (fax)

JAGAT H. SHARMA

Amoco Production Co.
P.O. Box 3385
4502 East 41st Street
Tulsa, OK 74102
U.S.A.

(918) 660–4333
(918) 660–4163 (fax)

DONALD SMITH

Marine Technology Support Unit (MATSU)
Culham Laboratory
Abingdon, Oxfordshire
UNITED KINGDOM OX14 3DB

(0235) 463565
(0235) 464207 (fax)

KIM SMITH

Senior Science Advisor, Fossil Fuels
Office of Energy Research & Development, EMR
580 Booth Street, Room 929
Ottawa, Ontario K1A 0E4
CANADA
(613) 995-5299
(613) 995-6146 (fax)

VAL R. SWAIL

Atmospheric Environment Service
4905 Dufferin Street
Downsview, Ontario M3H 5T4
CANADA

(416) 739-4347
(416) 739-4297 (fax)

DAVID SZABO

Offshore Engineering
Mobil Research and Development Corp.
Post Office Box 819047
Dallas, TX 75381-9047
U.S.A.

(214) 851-8347
(214)851-8349 (fax)

IOANNIS K. TSANIS

Department of Civil Engineering
McMaster University
1280 Main Street West
Hamilton, Ontario L8S 4L7
CANADA.

(416) 525-9140
(416)529-9688 (fax)

THACH TRAN VAN

Société d'énergie de la Baie James
500 boulevard Rene Levesque ouest
Montréal, Québec, H2Z 1Z9
CANADA

(514) 879-6266
(514) 879-4504 (fax)

DRIES VAN DEN EYNDE

Instituut voor Hygiene en Epidemiologie
Beheerseenheid Mathematisch Model Noordzee
Gulledelle 100
B-1200 Brussels
BELGIUM

(32-2) 773 21 30
(32-2) 770 69 72 (fax)

C. LINWOOD VINCENT

U.S. Army Corps of Engineers
Coastal Engineering Research Center
3909 Halls Ferry Road
Vicksburg, MS 39180-6199
U.S.A.

(601) 634-2008
(601) 634-4253 (fax)

DAVID WEI-CHI WANG

Computer Sciences Corporation
Data Buoy Support Contract/NDBC
Stennis Space Center, MS 39529
U.S.A.

(601) 688-3046

J. R. WILSON

Marine Environmental Data Service
200 Kent Street, 12th Floor
Ottawa, Ontario K1A 0E6
CANADA

(613) 990-0264
(613) 996-9055 (fax)

LAURENCE J. WILSON

Atmospheric Environment Service
4905 Dufferin Street
Downsview, Ontario M3H 5T4
CANADA

(416) 739-4910
(416) 739-4221 (fax)

LIANGMING WANG

National Research Centre for Marine Forecasts
No. 8 Da Hui Si

Hai Dian District
Beijing 100081
CHINA

presently at:

Physical and Chemical Sciences
Bedford Institute of Oceanography
P.O. Box 1006
Dartmouth, Nova Scotia B2Y 4A2
CANADA

(902) 426-3985
(902)426-7827 (fax)

XIAOMING WU

Proudman Oceanographic Laboratory
Bidston Observatory,
Birkenhead
Merseyside L43 7RA
UNITED KINGDOM

(44-51) 653-8633
(44-51) 653-0269 (fax)

LIST OF PARTICIPANTS

JUAN C. CARRETERO ALBIACH
Programa de Clima Maritimo M.O.P.T.
Dirreccion General de Puertos y Costas
C/ Vallehermoso 78
28015 Madrid
SPAIN

(34-1) 553 94 94
(34-1) 553 29 74 (fax)

JUAN JOSE CONDE ALDEMIRA
Programa de Clima Maritimo M.O.P.T.
Dirreccion General de Puertos y Costas
C/ Vallehermoso 78
28015 Madrid
SPAIN

(34-1) 553 32 77
(34-1) 553 29 74 (fax)

DOUG BANCROFT
SSO Scientific Services
Meteorology and Oceanography
National Defence Headquarters
Ottawa, Ontario K1A 0K2
CANADA

(613) 996-3658
(613) 995-4197 (fax)

RALPH BIGIO
Meteorological and Oceanographic Centre
Building D14, HMC Dockyard
Maritime Command
FMO Halifax, Nova Scotia B3K 2X0
CANADA

(902) 427-6374
(902) 427-6381 (fax)

F.P. BRISETTE
Department of Civil Engineering
McMaster University
1280 Main Street West
Hamilton, Ontario L8S 4L7
CANADA

(416) 525-9140
(416) 529-9688 (fax)

ROSS BROWN
Atmospheric Environment Service
LaSalle Academy, Block E
373 Sussex Drive
Ottawa, Ontario K1A 0H3
CANADA

(613) 996-4488
(613) 563-8480 (fax)

JOSEPH BUCKLEY
Department of Physics
Royal Roads Military College
FMO Victoria, British Columbia V0S 1B0
CANADA

(604) 363-5935
(604) 363-4513 (fax)

M.M. DE LAS HERAS CABALLERO
Programa de Clima Maritimo M.O.P.T.
Dirreccion General de Puertos y Costas
C/ Vallehermoso 78
28015 Madrid
SPAIN

(34-1) 553 94 94
(34-1) 553 29 74 (fax)

presently at:

Royal Netherlands Meteorological Inst.
P.O. Box 201
3730 AE de bilt
NETHERLANDS

(31-30) 206675
(31-30) 210407 (fax)

DON CAMERON
Atmospheric Environment Service
1496 Bedford Highway
Bedford, Nova Scotia B4A 1E5
CANADA

(902) 426-9200
(902) 426-4873 (fax)

LIST OF PARTICIPANTS**VINCENT J. CARDONE**

Oceanweather Inc.
5 River Road
Cos Cob, CT 06807
U.S.A.

(203) 661-3091
(203) 661-6809 (fax)

OCTAVE CARON

Société d'énergie de la Baie James
500 boulevard Rene Levesque ouest
Montréal, Québec, H2Z 1Z9
CANADA

(514) 879-6263
(514) 879-4504 (fax)

PETER CHANDLER

Institute of Ocean Sciences
Department of Fisheries and Oceans
P. O. Box 6000
Sidney, British Columbia V8L 4B2
CANADA

(604) 363-6307
(604) 363-6746 (fax)

ZHAN CHENG

National Research Centre for Marine Forecasts
No. 8 Da Hui Si
Hai Dian District
Beijing 100081
CHINA

(861) 831 8882-74
(861) 831 3593 (fax)

ROBERT L. COHEN

Marine Weather Services
Oceanroutes, Inc.
680 West Maude Avenue
Sunnyvale, CA 94086-3518
U.S.A.

(408) 245-3600
(408) 245-5301 (fax)

ROB CROSS

Atmospheric Environment Service
LaSalle Academy, Block E
373 Sussex Drive
Ottawa, Ontario K1A 0H3
CANADA

(613) 996-4248
(613) 996-3289 (fax)

GERARD CROTEAU

Atmospheric Environment Service
Canadian Meteorological Centre
2121 North Service Road
Dorval, Quebec H3P 1J3
CANADA

(514) 421-4618
(514) 421-4639 (fax)

CATRIN DUNLEAVY

Atmospheric Environment Service
4905 Dufferin Street
Downsview, Ontario M3H 5T4
CANADA

(416) 739-4386
(416) 739-4297 (fax)

PIERRE DUPUIS

Société d'énergie de la Baie James
500 boulevard Rene Levesque ouest
Montréal, Québec, H2Z 1Z9
CANADA

(514) 879-6268
(514) 879-4504 (fax)

BASSEM M. EID

MacLaren Plansearch Ltd.
5657 Spring Garden Road
Suite 200
Halifax, Nova Scotia B3J 3R4
CANADA

(902) 492-4544
(902) 492-4540 (fax)

LIST OF PARTICIPANTS

PAUL FARRAR
Naval Oceanographic Office, Code OPTA
Stennis Space Center, MS 39522-5001
U.S.A.

(601) 688-5177
(601) 688-5605 (fax)

CHARLES P. FOURNIER
Atria Engineering Hydraulics Inc.
6 Gurdwara Road, Suite 200
Ottawa, Ontario K2E 8A3
CANADA

(613) 228-0826
(613) 225-6014 (fax)

CHRIS GRAHAM
Dept. XTS/5, Sarawak Shell Berhad
Locked Bag No. 1, 98009, Miri
Sarawak
MALAYSIA

(60-85) 453498
(60-85) 453532 (fax)

ROSS GRAHAM
Defence Research Establishment Atlantic
9 Grove Street
P.O. Box 1012
Dartmouth, Nova Scotia B2Y 3Z7
CANADA

(902) 426-3100 ext 123
(902) 426-9654 (fax)

J. ARTHUR GREENWOOD
Oceanweather Inc.
5 River Road
Cos Cob, CT 06807
U.S.A.

(203) 661-3092
(203) 661-6809 (fax)

G.Z. GU
Offshore Engineering
Mobil Research and Development Corp.
Post Office Box 819047
Dallas, TX 75381-9047
U.S.A.

(214) 851-8338
(214) 851-8349 (fax)

SVERRE HAVER
Statoil, R&D Dept.
Postuttak
7004 Trondheim
NORWAY

(47-7) 584011
(47-7) 967286 (fax)

RALPH HORNE
Departmental Coordinator, Energy R&D
Office of the Science Advisor, Environment Canada
241 Blvd. Cite des Jeunes, Block 300
Hull, Quebec K1A 0H3
CANADA

(819) 953-7625
(819) 953-0550 (fax)

JON M. HUBERTZ
CEWES-CR-O
U.S. Army Engineer Waterways Experiment Station
3909 Halls Ferry Road
Vicksburg, MS 39180-6199
U.S.A.

(601) 634-2028
(601) 634-4314 (fax)

VALDIR INNOCENTINI
Instituto Nacional de Pesquisas Espaciais
Av. dos Astronautas 1758
Caixa Postal 515
12201 - Sao Jose dos Campos - SP
BRAZIL

(0123) 41 8977
(0123) 21 9743 (fax)

LIST OF PARTICIPANTS

ANDREW JOHNSON JR.
Naval Oceanographic Office, Code OPTA
Stennis Space Center, MS 39522-5001
U.S.A.

(601) 688-5177
(601) 688-5605 (fax)

ANDREW K. LAING
Marine Research Meteorologist
New Zealand Meteorological Service
P.O. Box 722
Wellington
NEW ZEALAND

(64-4) 4969 351
(64-4) 4735 231 (fax)

ROOP LALBEHARRY
Atmospheric Environment Service
4905 Dufferin Street
Downsview, Ontario M3H 5T4
CANADA

(416) 739-4912
(416) 739-4221 (fax)

SUSAN K. LALLY
Oceanroutes Canada Inc.
271 Brownlow Avenue
Dartmouth, Nova Scotia B3B 1W6
CANADA

(902) 468-3008
(902) 468-3009 (fax)

OWEN LANGE
Atmospheric Environment Service
1200 - West 73rd Ave.
Vancouver, British Columbia V6P 6H9
CANADA

(604) 664-9000
(604) 664-9005 (fax)

JEAN-MICHEL LEFEVRE
METEO - FRANCE
42 Av Gustave Coriolis
31057 Toulouse Cedex
FRANCE

(33) 61 07 82 95
(33) 61 07 82 32 (fax)

VLADIMIR MAKIN
Royal Netherlands Meteorological Inst.
P.O. Box 201
3730 AE de bilt
NETHERLANDS

(31-30) 206911
(31-30) 210407 (fax)

RICK MARSDEN
Royal Roads Military College
FMO Victoria, B.C. V0S 1B0
CANADA

(604) 363-4533
(604) 363-4513 (fax)

DIANE MASSON
Institute of Ocean Sciences
9860 West Saanich Road
P. O. Box 6000
Sidney, British Columbia V8L 4B2
CANADA

(604) 363-6521
(604) 363-6746 (fax)

THOMAS H. PEIRCE
Transportation Development Centre
Suite 601, West Tower
200 Rene Levesque Blvd. W.
Montreal, Quebec H2Z 1X4
CANADA

(514) 283-0078
(514) 283-7158 (fax)

LIST OF PARTICIPANTS**PIERRE PELLETIER**

Société d'énergie de la Baie James
500 boulevard Rene Levesque ouest
Montréal, Québec, H2Z 1Z9
CANADA

(514) 879-6269
(514) 879-4504 (fax)

WILLIAM PERRIE

Physical and Chemical Sciences
Bedford Institute of Oceanography
P.O. Box 1006
Dartmouth, Nova Scotia B2Y 4A2
CANADA

(902) 426-3985
(902) 426-7827 (fax)

STUART PORTER

Scientific Services Meteorologist
Atmospheric Environment Service
P.O. Box 9490, Postal Station B
St. John's, Newfoundland A1A 2Y4
CANADA

(709) 772-4695
(709) 772-2593 (fax)

DONALD T. RESIO

Florida Institute of Technology
Dept. of Oceanography and Ocean Engineering
150 West University Blvd.
Melbourne, FL 32901-6988
U.S.A.

(407) 768-8000 ext. 8135
(407) 984-8461 (fax)

KATHRYN J. RESIO

Offshore and Coastal Technologies Inc.
#115 - 7667 N. Wickham Road
Melbourne, FL 32940
U.S.A.

(407) 242-8783
(407) 242-2744 (fax)

IRENE RUBINSTEIN

Earth Observation Laboratory
Institute for Space and Terrestrial Science
4800 Keele Street
Downsview, Ontario M3J 3K1
CANADA

(416) 665-3311
(416) 665-2032 (fax)

KEN SATO

Environment Directorate
National Energy Board
311 - 6th Avenue S.W.
Calgary, Alberta T2P 3H2
CANADA

(403) 299-3675
(403) 292-5503 (fax)

JAGAT H. SHARMA

Amoco Production Co.
P.O. Box 3385
4502 East 41st Street
Tulsa, OK 74102
U.S.A.

(918) 660-4333
(918) 660-4163 (fax)

DONALD SMITH

Marine Technology Support Unit (MATSU)
Culham Laboratory
Abingdon, Oxfordshire
UNITED KINGDOM OX14 3DB

(0235) 463565
(0235) 464207 (fax)

KIM SMITH

Senior Science Advisor, Fossil Fuels
Office of Energy Research & Development, EMR
580 Booth Street, Room 929
Ottawa, Ontario K1A 0E4
CANADA

(613) 995-5299
(613) 995-6146 (fax)

LIST OF PARTICIPANTS

VAL R. SWAIL
Atmospheric Environment Service
4905 Dufferin Street
Downsview, Ontario M3H 5T4
CANADA

(416) 739-4347
(416) 739-4297 (fax)

DAVID SZABO
Offshore Engineering
Mobil Research and Development Corp.
Post Office Box 819047
Dallas, TX 75381-9047
U.S.A.

(214) 851-8347
(214) 851-8349 (fax)

IOANNIS K. TSANIS
Department of Civil Engineering
McMaster University
1280 Main Street West
Hamilton, Ontario L8S 4L7
CANADA.

(416) 525-9140
(416) 529-9688 (fax)

THACH TRAN VAN
Société d'énergie de la Baie James
500 boulevard Rene Levesque ouest
Montréal, Québec, H2Z 1Z9
CANADA

(514) 879-6266
(514) 879-4504 (fax)

DRIES VAN DEN EYNDE
Instituut voor Hygiene en Epidemiologie
Beheerseenheid Mathematisch Model Noordzee
Gulledelle 100
B-1200 Brussels
BELGIUM

(32-2) 773 21 30
(32-2) 770 69 72 (fax)

C. LINWOOD VINCENT
U.S. Army Corps of Engineers
Coastal Engineering Research Center
3909 Halls Ferry Road
Vicksburg, MS 39180-6199
U.S.A.

(601) 634-2008
(601) 634-4253 (fax)

DAVID WEI-CHI WANG
Computer Sciences Corporation
Data Buoy Support Contract/NDBC
Stennis Space Center, MS 39529
U.S.A.

(601) 688-3046

J. R. WILSON
Marine Environmental Data Service
200 Kent Street, 12th Floor
Ottawa, Ontario K1A 0E6
CANADA

(613) 990-0264
(613) 996-9055 (fax)

LAURENCE J. WILSON
Atmospheric Environment Service
4905 Dufferin Street
Downsview, Ontario M3H 5T4
CANADA

(416) 739-4910
(416) 739-4221 (fax)

LIST OF PARTICIPANTS

LIANGMING WANG
National Research Centre for Marine Forecasts
No. 8 Da Hui Si
Hai Dian District
Beijing 100081
CHINA

presently at:

Physical and Chemical Sciences
Bedford Institute of Oceanography
P.O. Box 1006
Dartmouth, Nova Scotia B2Y 4A2
CANADA

(902) 426-3985
(902) 426-7827 (fax)

XIAOMING WU
Proudman Oceanographic Laboratory
Bidston Observatory, Birkenhead
Merseyside L43 7RA
UNITED KINGDOM

(44-51) 653-8633
(44-51) 653-0269 (fax)